ABSTRACT

Title of Dissertation: RELEASE OF ALUMINUM, ARSENIC, CADMIUM, CHROMIUM, COPPER, IRON, LEAD, AND ZINC IN A COAL LEACHATE, AND THEIR REMOVAL FROM SOLUTION UNDERGOING NEUTRALIZATION.

Thomas Lee Tatum, Doctor of Philosophy, 1992

Dissertation directed by: Dr. George R. Helz
Professor, Chemistry

Whole coal contains significant amounts of iron pyrite which is oxidized ultimately to ferric acid sulfate. As a result, trace elements are released from the coal and other minerals in potentially hazardous concentrations.

The purpose of this research was to: 1) study the release and mobility of selected trace elements during the weathering of coal; 2) seek to understand factors controlling solubility of trace elements in a synthetic, acidic leachate undergoing gradual neutralization; and 3) develop a chemical thermodynamic computer model to predict the effects of dilution and neutralization of leachate on trace element mobility and speciation.

Samples collected periodically from a slurry of whole ground coal in water were filtered and analyzed for dissolved sulfate (by ion chromatrography), iron (by flame atomic absorption spectrophotometry), and Al, Zn, Cd, Cu, Cr, Pb, As, and Se (by graphite furnace AAS). Iron, copper, and probably arsenic tracked the production

of sulfate, while aluminum, zinc, chromium, and cadmium concentrations were stable or rose slightly.

A synthetic leachate of ferric sulfate and sulfuric acid was doped with trace levels of Al, Zn, Cu, Cd, Cr, Pb, As, and Se. Slow injection of sodium bicarbonate solution neutralized the stirred system, though hydrolysis of iron buffered the pH near 2.5.

Computer modeling of the sample analyses indicated that sulfate complexes dominated the speciation of iron and the trace elements. The other findings were used to develop a thermodynamic equilibrium model based on the aqueous geochemistry computer model PHREEQE. Iron and sulfate removal were best modeled by the precipitation of $Fe_{16}O_{16}(OH)_{12}(SO_4)_2$. Aluminum solubility was modeled by precipitation of jurbanite below pH 4, of bayerite and basaluminite for pH 4 - 5, and of gibbsite at pH above 5. Chromium, copper, and lead removal was modeled by solid solution formation with the ferric oxyhydroxysulfate precipitates.

Program convergence failures above pH 5 precluded the modeling of zinc and cadmium, but it is hypothesized that their ions are adsorbed onto suspended particles of hydrous ferric oxyhydroxides. The model was tested with our laboratory data, and field data from a creek system contaminated with acid sulfate mine drainage.

RELEASE OF ALUMINUM, ARSENIC, CADMIUM, CHROMIUM, COPPER, IRON, LEAD, AND ZINC IN A COAL LEACHATE, AND THEIR REMOVAL FROM SOLUTION UNDERGOING NEUTRALIZATION

by

Thomas Lee Tatum

Dissertation submitted to the Faculty of the Graduate School
of the University of Maryland in partial fulfillment
of the requirements for the degree of
Doctor of Philosophy
1992

Advisory Committee:

Professor George R. Helz, Chairman/Advisor
Professor Thomas O'Haver
Professor John Tossell
Professor Alice Mignerey
Professor Luke Chang

ACKNOWLEDGMENTS

I wish to express my gratitude to the following:

The Creator - for His marvelous creation, and for enabling me to understand a little bit of it.

My wife, Linda, and children Michelle and Kimberlee - for their encouragement, support, and sacrifice.

My parents, family, and close friends Kathy and Dave Schey, and Brenda and Steve Blackburn - for unfailing concern, prayers, and encouragement.

Dr. George Helz - for advise and motivation.

Dr. Glen Gordon - who believed in me, but died in the last semester of this effort. He is missed.

My dissertation committee - for their patience.

Columbia Union College - for giving me this opportunity and supporting me throughout the endeavor. Especially Dr. Donald Jones, Dr. Robert Wasmer, and Glen Milam.

Maryland Department of Natural Resources, Power Plant Siting Program, and Maryland Water Resources - for supporting various aspects of the project.

My friends in the department, including: Ji Hong Dai, Caroline Purdy, Kostas Daskalakis, Cheri Miller, and librarians Sylvia Evans and Hugh O'Connor.

TABLE OF CONTENTS

LIST OF TABLES

LIST OF FIGURES

CHAPTER 1 INTRODUCTION

Whole coal, as obtained by modern mining methods, may be expected to include a significant amount of non-combustible material. The refuse from the use of coal was estimated to exceed 10^8 tons/yr a decade ago (Schubert and Prodan 1981). Exposure of stored coal and these wastes to the weather often results in leachate and runoff that can seriously degrade the environment.

1.1 COMPOSITION OF COALS

Gluskoter et al. (1977), reported mineral matter associated with whole coal to range from 3.8 to 31.7 percent with mean 15.3%. They also found sulfur to be present in coals in both organic and inorganic combination, with the inorganic sulfur concentrated in the mineral fractions. Iron pyrite (FeS_2) comprises a significant fraction of many coals, often 1 to 15 percent (Nordstrom 1982).

Table 1.1, from Kuhn et al. 1980, identifies the mineral phases that are typically found in coal, and the major and minor constituents commonly associated with them. The trace elements may occur as isomorphic replacements in the minerals, or as exchangeable cations on clays. Kaolinite, illite and expandable clays commonly comprise the major portion of minerals in coal. These

Table 1.1* Elements commonly associated with the principal minerals in coal.+

Mineral Phases	Major Constituents	Trace Constituents
Sulfides		
Pyrite, marcasite	Fe, S	As, Cd, Hg, Ag, Pb,
Sphalerite	Zn, S	Fe, Zn, Cu, Co, Sn,
Galena	Pb, S	Ni, Mo, Se, Ga
Sulfates		
Barite	Ba, S	Sr, Pb, Ca
Gypsum	Ca, S	
Carbonates		
Calcite	Ca	Ba, Sr, Pb, Mn, Ca
Siderite	Fe	Fe, Mg
Ankerite	Ca, Fe	
Dolomite	Ca, Mg	
Phosphates		Rare earths, and
Apatite	Ca, P, F	U, Ce, Mn, Cl, Mg
Silicates		
Quartz	Si	
Zircon	Si, Zr	Hf, Th, P
Tourmaline	Ca, Mg, Fe, B, Al, Si	Li, F
Plagioclase feldspar	Ca, Na, Al, Si	Ba, Sr, Mn, Ti, Fe, Mg
Alkali feldspar	K, Al, Si	Rb, Ba, Sr, Fe, Mg, Ti, Li
Muscovite	K, Al, Si	F, Rb, Cs, Ba, Mg, Fe
Clay Minerals		
Kaolinite	Al, Si	Ti, Mg, Fe, and others
Illite	Al, Si, K	Fe, Mg, Ca, Na, K, Ti, Li,
Montmorillonite	Al, Si, Mg, Fe	V, B, Mn, Cr, Cu, Ni, Rb,
Mixed layer clays	Al, Si, K, Mg, Fe	Cs, Ga, Be, Zn, Se, F, La,
Chlorite	Al, Si, Fe, Mn, Mg	Ba, Sr, Co, and others

* From Kuhn et al. 1980
+ This listing does not rule out the existence of additional associations.

and calcite, pyrite, and quartz are almost ubiquitous in coals of the United States. Eastern coals are more likely to contain iron carbonates; and any iron sulfates are primarily due to the oxidation of pyritic material during storage, (Kuhn et al. 1980).

Among coal solid wastes from Illinois and Montana, Griffin et al. (1980), identified quartz, calcite, kaolinite, and feldspar as common nonferro minerals. The principal iron containing mineral was pyrite, with illite and some ferrous sulfate found to a lesser extent.

Heaton et al. (1982), did a factor analysis on high sulfur coal wastes from two Appalachian coal preparation plants to find what elements and minerals correlate well with each other. The most heavily weighted factor (43%) was a clay factor that included kaolinite, illite, quartz, and the elements: Na, Mg, Al, Si, K, Sc, Ti, V, Cr, Zr, Cs, La, Ce, Eu, Dy, Lu, Hf, and Th. The second most important factor (15.9%) was also primarily a clay fraction representing kaolinite and (non-clay) marcasite and the elements: Al, Co, Ni, Rb, Cs, La, Ce, Eu, Dy, Pb, Th, and U. A third factor represented quartz, illite, and the elements: Mg, Si, K, Zr, Hf. A fourth calcite factor also represented Mg, Ca, Mn, Zr, and Sb. A mixed clay factor included the elements: Sc, V, Co, Ni, Zn, Cs, Ba, and Eu. A pyrite factor included Li, Fe, Cu, As, and Cd. They found the gypsum factor to not

correlate with other elements. Three other factors did not correlate with any particular minerals but did group the elements as follows: Li, Se, Sr, Sb, and V; Na, Mg, Mn, Fe, As, Cd, La, and Lu; Zn, H, Dy, and Eu.

The Illinois State Geological Survey undertook a huge survey of coals from the United States, (Gluskoter et al. 1977). They analyzed 23 whole coal samples from the appalachian coal field of the eastern U.S., 114 samples from the Illinois Basin, and 28 from the western U.S. for the presence of 58 elements. They also determined such parameters of each coal as: moisture content, fixed carbon, heat content (as a fuel), ash content, total sulfur, organic sulfur, pyritic sulfur, and sulfate sulfur. Table 1.2 summarizes their findings for the whole coal samples from the eastern United States. They conclude that As, Cd, Pb, and Zn are among the elements having relatively large concentration ranges; that elemental concentrations tend to be highest in coals from eastern United States and lowest in coals from the west; and that arsenic, chlorine, and selenium are enriched in eastern coals.

Griffin et al. (1980), determined over 60 constituents in coal solid wastes. They found the major elements (concentrations greater than 1000 mg/kg) were Al, Ca, Fe, K, Mg, Na, S, Si, and Ti. The minor elements (concentrations generally between 100 mg/kg and

Table 1.2 Mean analytical values* for 23 whole coal samples from the eastern United States (Appalachian coal fields).

Element	Arithmetic Mean	Geometric Mean	Minimum	Maximum	Standard Deviation	Number Samples
Al	1.7 %	1.6 %	1.1	3.1	0.56	23
C	72. %	72. %	63.	80.	5.3	22
Ca	0.47 %	0.34 %	0.09	2.6	0.51	23
Cl	0.17 %	0.10 %	0.01	0.80	0.21	23
Fe	1.5 %	1.3 %	0.50	2.6	0.69	23
H	4.9 %	4.9 %	4.0	6.0	0.44	22
K	0.25 %	0.21 %	0.06	0.68	0.14	23
Mg	0.06 %	0.05 %	0.02	0.15	0.03	23
N	1.3 %	1.3 %	0.94	1.8	0.27	22
Na	0.04 %	0.03 %	0.01	0.08	0.02	23
O	8.0 %	7.0 %	2.5	18.	4.3	22
Si	2.8 %	2.6 %	1.0	6.3	1.1	23
Ti	0.09 %	0.09 %	0.05	0.16	0.04	23
Or.S	0.92 %	0.82 %	0.35	2.5	0.48	23
Py.S	1.3 %	0.81 %	0.04	2.6	0.91	23
SO_4	0.10 %	0.06 %	0.01	0.42	0.10	22
Tot.S	2.3 %	1.9 %	0.55	5.0	1.3	23

* Notes: Data from Gluskoter et al. 1977.
Or.S is organic sulfur
Py.S is pyritic sulfur

Table 1.2 (continued) Mean Analytical values* for 23 whole coal samples from the eastern United States (Appalachian coal fields).

Element	Arithmetic Mean	Geometric Mean	Minimum	Maximum	Standard Deviation	Number Samples
Ag	0.02	0.02	0.01	0.06	0.01	13
As	25.	15.	1.8	100	27.	23
B	42.	28.	5.0	120	32.	23
Ba	200	170	72.	420	110	14
Be	1.3	1.1	0.23	2.6	0.56	23
Br	12.	8.9	0.71	26	7.6	23
Cd	0.24	0.19	0.10	0.60	0.18	23
Ce	25.	23.	11.	42.	9.1	14
Co	9.8	7.6	1.5	33.	7.8	23
Cr	20.	18.	10.	90.	16.	23
Cs	2.0	1.6	0.40	6.2	1.6	14
Cu	18.	16.	5.1	30.	7.3	23
Dy	2.3	2.0	0.74	3.5	0.94	14
Eu	0.52	0.47	0.16	0.92	0.22	14
F	89.	84.	50.	150	31.	23
Ga	5.7	5.2	2.9	11.	2.6	23
Ge	1.6	0.87	0.10	6.0	1.7	23
Hf	1.2	1.1	0.58	2.2	0.45	14
Hg	0.20	0.17	0.05	0.47	0.12	23
I	1.7	1.4	0.33	4.9	1.1	14
In	0.23	0.22	0.13	0.37	0.08	14
La	15.	14.	6.1	23.	5.3	14

* Notes: Data from Gluskoter et al. 1977.
All quantities are in ug/g.

Table 1.2 (continued) Mean Analytical values* for 23 whole coal samples from the eastern United States (Appalachian coal fields).

Element	Arithmetic Mean	Geometric Mean	Minimum	Maximum	Standard Deviation	Number Samples
Lu	0.22	0.18	0.04	0.40	0.12	14
Mn	18.	12.	2.4	61.	16.	23
Mo	4.6	1.8	0.10	22.	6.3	23
Ni	15.	14.	6.3	28.	5.7	23
P	150	81.	15.	1500	300	23
Pb	5.9	4.7	1.0	18.	4.0	23
Rb	22.	19.	9.0	63.	15.	14
Sb	1.6	1.1	0.25	7.7	1.7	23
Sc	5.1	4.5	1.6	9.3	2.4	14
Se	4.0	3.4	1.1	8.1	2.0	23
Sm	2.6	2.4	0.87	4.3	1.0	14
Sn	2.0	0.97	0.20	8.0	2.4	19
Sr	130	100	28.	550	130	14
Ta	0.33	0.26	0.12	1.1	0.28	14
Tb	0.34	0.28	0.06	0.63	0.17	14
Th	4.5	4.0	1.8	9.0	2.1	14
U	1.5	1.3	0.40	2.9	0.73	14
V	38.	35.	14.	73.	14.	23
W	0.69	0.62	0.22	1.2	0.31	14
Yb	0.83	0.73	0.18	1.4	0.35	14
Zn	25.	19.	2.0	120	24.	23
Zr	45.	41.	8.0	88.	18.	19

* Notes: Data from Gluskoter et al. 1977.
All quantities are in ug/g.

1000 mg/kg) were B, Ba, Ce, Cl, Cr, F, Mn, Sr, Zn, and Zr. Twenty other elements were reported in concentrations less than 100 mg/kg.

Table 1.3 summarizes the data of Kuhn et al. (1980), for the mean concentrations of 45 elements found in raw coals of the eastern United States.

Table 1.3 Mean Elemental Concentrations in Raw Coals from the Eastern United States*

Element	Concentration	Element	Concentration
Al	1.94 ± 0.6%	Mo	6 ± 5
As	10 ± 8	Na	481 ± 248
B	53 ± 42	Ni	12 ± 3
Ba	146 ± 61	P	85 ± 57
Be	0.70 ± 0.2	Pb	8.9 ± 9
Br	11 ± 9	Rb	14 ± 4
Ca	0.62 ± 0.5%	S	2.0 ± 1.7%
Cd	———	Org.S	1.0 ± 0.74%
Ce	21 ± 8	Sb	2.3 ± 2
Co	6.8 ± 6	Sc	4.9 ± 2
Cr	20 ± 7	Se	3.1 ± 2
Cs	1.4 ± 0.6	Si	2.41 ± 0.4%
Cu	22 ± 8	Sm	2.2 ± 0.8
Dy	1.7 ± 0.7	Sr	121 ± 53
Eu	0.4 ± 0.2	Ta	0.37 ± 0.3
Fe	1.0 ± 0.5%	Tb	0.02 ± 0.09
Ga	4.7 ± 2	Th	4.1 ± 2
Hf	1.3 ± 0.4	Ti	0.10 ± 0.04%
K	0.19 ± 0.09%	U	1.2 ± 1
La	13 ± 6	V	48 ± 22
Lu	0.13 ± 0.08	W	0.57 ± 0.4
Mg	0.06 ± 0.05%	Yb	0.58 ± 0.2
Mn	20 ± 10	Zn	29 ± 45

* All values in μg/g unless otherwise noted;
Less than values were not included in the calculation of mean values.
Data from Kuhn et al. 1980.

1.2 WEATHERING OF PYRITE

When exposed to oxygen and moisture, pyrite is oxidized ultimately to ferric iron and sulfuric acid, (Temple and Delchamps 1953, Garrels and Thompson 1960, Kuznetsov et al. 1962, Wangen and Jones 1984). Goldhaber (1983), found rapid oxidation of pyrite to sulfate at the pyrite/water interface, and predicted eventual complete oxidation to sulfate (the thermodynamically stable species in acid solution in equilibrium with excess oxygen). Taylor et al. (1984), used the concentration of sulfate produced in mines as a measure of the amount of pyrite oxidized, commenting that this provides a minimum estimate.

Singer and Stumm (1970), developed a model (Figure 1.1) that summarizes the oxidation of pyrite under

Figure 1.1 Model for the natural weathering (oxidation) of pyrite (from Singer and Stumm, 1970).

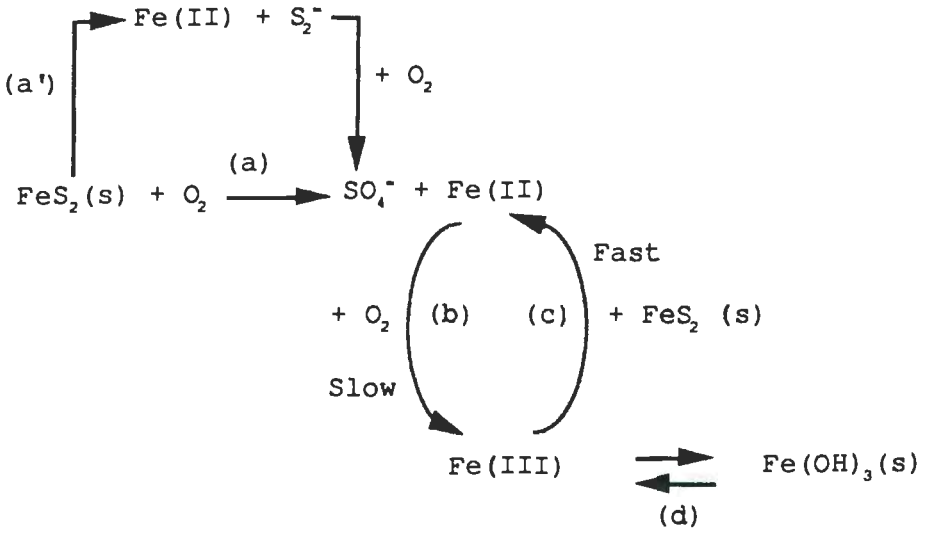

natural weathering conditions. Reaction "a" is the oxidation of FeS_2 to sulfate which releases dissolved Fe(II) and acidity according to the reaction: Eqn.1.1

$$FeS_2 + 3.5(O_2) + H_2O = Fe^{2+} + 2SO_4^{=} + 2H^{+}.$$

Reaction "b" is the oxidation of dissolved Fe(II) to Fe(III) according to the reaction: Eqn.1.2

$$Fe^{2+} + 0.25(O_2) + H^{+} = Fe^{3+} + 0.5H_2O$$

This step is very slow as a purely chemical process in sterile acidic solutions, (Singer and Stumm 1970). (Bacterial catalysis will be discussed below.)

The resulting Fe(III) hydrolyses (reaction "d") releasing more acidity according to the reaction:

$$Fe^{3+} + 3H_2O = Fe(OH)_{3(s)} + 3H^{+} \quad \text{Eqn.1.3}$$

The initial solid precipitate is usually amorphous, but with time is converted to stable FeOOH (goethite), or $K^{+}Fe_3(SO_4)_2(OH)_6$ (jarosite) where sulfate concentration is high.

Reaction "c" shows the attack on pyrite by Fe^{3+} ions that oxidize the sulfide and release acidity (as the Fe^{3+} is itself reduced to Fe^{2+}) according to the reaction:

$$FeS_2 + 14Fe^{3+} + 8H_2O = 15Fe^{2+} + 2SO_4^{=} + 16H^{+} \quad \text{Eqn.1.4}$$

The balanced net reaction for the oxidation of pyrite is:

$$2FeS_2 + 7.5(O_2) + H_2O = 2Fe^{3+} + 4SO_4^{=} + 2H^{+} \quad \text{Eqn.1.5}$$

Thus, each mole of pyrite that undergoes oxidation yields 1 mole of Fe(III), 2 moles of sulfate, and 1 mole of H^{+}.

Also, at pH greater than 2.5, where Fe(III) hydrolyzes, three more moles of hydrogen ions are produced, resulting in lowered solution pH.

Goldhaber (1983) has elucidated a mechanism of pyrite oxidation (which covers steps a,b, and d of the Singer and Stumm model just discussed). Lowson (1982) reviewed proposed mechanisms of ferrous iron oxidation by oxygen to ferric iron.

At pH less than 4.5 the rate of chemical (abiotic) oxidation of Fe^{2+} to Fe^{3+} becomes insignificant, its half life being about 300 days for 5 ppm Fe(II) solution, (Kleinmann et al. 1981). Rather, it is biologically mediated by the bacterium Thiobacillus ferrooxidans. (There have been many studies of the role of T. ferrooxidans in the catalysis of the oxidation of Fe(II) and pyrite: e.g. Temple and Delchamps 1953, Kuznetsov et al. 1962, Silverman 1967, Kleinmann and Crerar 1979, Myerson 1981, Hoffmann et al. 1981, Paciorek et al. 1981, Lazaroff et al. 1982, Taylor et al. 1984). The presence of these microbes, whose optimum activity is between pH 4 and 2 but ceases below pH 1.5, can increase the rate of oxidation of Fe^{2+} by as much as 5 or 6 orders of magnitude.

At pH less than 3.0, Fe^{3+} is the only important oxidizer of pyrite. Garrels and Thompson found that the

rate is limited by adsorption of Fe^{3+} and Fe^{2+} on the pyrite surface.

Taylor et al. (1984) measured the stable isotope ratios for $^{18}O/^{16}O$ and $^{34}S/^{32}S$ in acid mine drainage and estimated the percent contribution of chemical and microbial pathways to pyrite oxidation at pH 2. Their estimates indicate that in aerobic submerged systems, 65% of the pyrite is oxidized by Fe^{3+} and 35% by T. ferro-oxidans. However, in alternating wet and dry systems, (such as exist in coal piles exposed to the weather), only 23% of the oxidation of pyrite is by Fe^{3+} while 77% is by the microbes. Since the bacteria that catalyze the acidity-producing reactions thrive under acid conditions, once acidity is initiated acid production becomes rapid, (Drever 1982).

It should be recognized, however, that the iron-oxidizing bacteria are aerobic, so that gaseous oxygen concentrations of less than 2% by volume are potentially limiting to pyrite oxidation, (Erickson et al. 1984). In mine tailings (and by extension other wastes from coal cleaning and use), the availability of gaseous oxygen and the rate of diffusion of oxygen are the critical factors controlling the rate of acid generation, (Nicholson et al. 1989).

Survey of the literature has revealed the following factors which may affect the rate of oxidation of pyrite:

Bacteria (population, growth factors, and activity)

Catalysts (such as Ni^{2+}, Co^{2+}, Cu^{2+}, Ce(IV), MnO_4^-)

Depletion of mineral phases

Diffusion (of Fe^{3+}, O_2, and reaction products)

Ferrous and ferric ion concentrations

Fe^{3+}/Fe^{2+} ratio (in solution and on active surfaces)

Galvanic protection (by more active sulfides)

Inorganic anion complexes (e.g. of Fe by $SO_4^=$)

Media (dry, moist, submerged, alternating)

Organic compounds (bactericidal and complexing)

Other oxidizing agents (e.g. $Ce(SO_4)_2$)

Oxygen (exchange, partial pressure, and diffusion)

pH (concentrations of both H^+ and OH^- ions)

Surface area (and particle size)

Surface coatings (by organics or precipitates)

Temperature

Gottschlich et al. (1987) summarized the key variables in the rate of oxidation of pyrite to include temperature, particle size, speciation, and O_2/CO_2 profile.

1.3 LEACHING OF TRACE ELEMENTS

There is quite a body of literature on leachates derived from coal, coal storage piles, coal mine tailings, coal cleaning wastes, and end products from the use of coal as fuel (e.g. fly ash and slag). The reader is referred particularly to Anderson et al. 1976, Wachter

and Blackwood 1978, Davis and Boegly, Jr. 1978, 1981a, and 1981b; Griffin et al. 1980, and Heaton et al. 1982.

As a result of the oxidative weathering of coal and the release of acidity, trace elements are released from: a) the pyrite during dissolution, b) the coal itself by leaching, and c) any associated minerals susceptible to acid dissolution or ion exchange, (Kuznetsov et al. 1962, Nordstrom 1982, Heaton et al. 1982). Most trace and minor constituents are found in such minerals as sulfides, sulfates, carbonates, and clays; (see Table 1.1). Some occur as isomorphic replacements or as exchangeable cations on clays, (Kuhn et al. 1980). Pyrite has been reported to serve as a reservoir of S, Fe, As, Se, Br, Cd, and Sb; while the very leachable Co, Ni, Cu, and Zn were associated with mixed-layer clays or dispersed throughout coal wastes, (Heaton et al. 1982).

Griffin et al. (1980), identified important factors controlling the solubility of mineral phases including: pH, redox environment, oxidation states, concentration and speciation of individual inorganic and organic ions and complexes in solution, and total ionic strength. Coward and Horton (1980), identified pH, particle size, flow rate, contact time, and O_2/N_2 as the important variables in the aqueous leaching of heavy metals from soft coal. Davis and Boegly, Jr. (1981a) investigated coal particle size, coal type (eastern or western), and

storage conditions (wet or wet and dry), and found them all to be significant in determining the drainage quality. Griffin et al. (1980), singled out pH as the most important factor affecting the solubility of accessory elements in coal solid wastes; and ranked redox potential as the second most important solubility factor. (See also Garrels and Christ 1965).

Thermochemical solubility modeling has indicated that similar mineral phases control the aqueous solubility of many major, minor, and trace ionic species for solid wastes, (Griffin et al. 1980). Heaton et al. (1982), concluded that important determinants of coal waste leaching behavior are pyrite (which determines the acid generating potential of the waste), calcite (which determines the capacity of the waste to self-neutralize the acids released by oxidation of pyrite), and the clay minerals (which serve as reservoirs for many of the leachable trace elements).

Generalizations regarding component concentrations in coal waste leachates include: a) the highest concentrations of metals are found in the most acidic solutions, with Al, Fe, Mn, and Zn typically the most concentrated; b) sulfate is the dominant anion, and along with Cl, K, and Na, showed no pH dependency in their solubility; and d) Ca, Mn, Pb, and $SO_4^=$ show up repeatedly at concentrations greater than water quality standards over

the entire pH range of 3 - 10; (Griffin et al. 1980). Summarizing the results of a major study of the Leviathan Mine Drainage Basin (California/Nevada), Ball and Nordstrom (1985), stated that the water issuing from the mine area contained mg/L concentrations of As, Cr, Co, Cu, Mn, Ni, Tl, V, and Zn; and from hundreds to thousands of mg/L concentrations of Al, Fe, and SO_4, at pH values as low as 1.8.

Wewerka et al. (1982), tabulated 73 elements released during the continuous leaching of Illinois Basin coal refuse. Griffin et al. (1980) list the concentrations of 57 elements measured in the leachates from coal solid wastes. Their tables include samples collected in the general pH range of 2.5 to 11. Stahl, Jr. and Davis (1984) tested four coals from Illinois, Kentucky, Montana, and Texas in controlled laboratory reactors that simulated rainfall events over a 120 day period. They reported the following ranges for the average value of the runoffs: pH = 2.2 to 7.1, redox potential = -3 to 284 mV, conductivity = 200 to 5833 umhos/cm, turbidity = 5 to 98 (no. of transfer units), ammonia = 0.2 to 1.0 mg/L, nitrate = 0.3 to 27.0 mg/L, organic nitrogen = 9 to 50 mg/L, sulfate = 65 to 7211 mg/L, total organic carbon = 6 to 70 mg/L, inorganic carbon = 2.6 to 21 mg/L, biochemical oxygen demand <5 to 20 mg/L, chemical oxygen demand = 65 to 744 mg/L, and

suspended solids (nonfilterable residue) = 54 to 596 mg/L.

Davis and Boegly, Jr. (1981a) published a table comparing the ranges of data reported in four different studies by other researchers. Table 1.4 (from Wachter and Blackwood 1978), shows the average effluent concentrations for water pollutants from coal storage areas for each major coal region of the United States.

1.4 DRAINAGE DILUTION AND PRECIPITATION

The first precipitates from acidic mine drainage and coal leachates are dominated by Fe(III). Both jarosite and ferric hydroxide have been observed as precipitates in acid mine drainage, forming in surface streams and ponds after discharge; but they are not stable for more than a season due to weathering which decomposes them to goethite, (Nordstrom 1982, Nordstrom et al. 1979, Karathanasis et al. 1988). Brady et al. (1986), found that laboratory precipitates of natrojarosite transformed to Fe-oxides upon aging for 30 days at pH 6.0; and that only ferrihydrite-like materials were produced in solutions with SO_4/Fe ratios greater than 1.5. In the field, they noted that a stream receiving acid-sulfate mine drainage had precipitates consisting primarily of goethite and lesser amounts of ferrihydrite-like materials.

Table 1.4 Average effluent concentrations from coal storage areas.*

Effluent parameter	Appalach'n	Great Plains	Interior Eastern	Interior Western	Western	South-western
Suspended solids	1,521	1,282	1,264	1,853	2,486	1,538
Dissolved solids	259	430	1,136	5,539	1,900	356
Sulfate	66	1,598	648	4,860	240	190
Iron	3.1	1.5	9.1	1,131	8.2	5.5
Manganese	0.03	0.14	0.44	17.9	0.4	0.04
Free silica	12.3	<DL	0.8	86.3	<DL	<DL
Cyanide	<0.001	<DL	0.002	<DL	<DL	<DL
BOD_5	<5.0	<7.5	<DL	<1.2	<2.5	<7.5
COD	1,407	1,324	1,556	1,053	1,826	769
Nitrate	0.12	0.14	0.33	0.09	1.8	0.16
Phosphate	<DL	<DL	<DL	<DL	<DL	<DL
Antimony	2.1	<DL	7.5	10.3	14.0	6.5
Arsenic	23	1.8	4.1	10.1	5.6	4.1
Beryllium	<DL	<DL	<DL	<DL	<DL	<DL
Cadmium	<DL	<DL	<DL	0.05	0.005	<DL
Chromium	<DL	<DL	<DL	0.03	0.04	<DL
Copper	0.02	<DL	<DL	2.2	<DL	0.02
Lead	0.05	0.05	0.06	0.33	0.07	0.05
Nickel	0.06	0.02	0.09	10.2	0.05	0.03
Selenium	23.8	<DL	12.5	25.2	15.0	21.5
Zinc	0.008	0.17	0.14	25.0	0.15	0.04
Mercury	<0.001	0.003	<DL	0.004	0.005	0.002
Chloride	0.33	<DL	<DL	2.3	<DL	<DL
Organic Carbon	251.7	373.2	380.1	90.5	318.4	158.7
pH	6.28	6.93	7.62	2.81	7.24	6.60

* from Wachter and Blackwood, 1978; concentrations are g/m^3.

At pH greater than 5, the concentration of aluminum can be viewed as consistent with the solubility of kaolinite or microcrystalline gibbsite. But in sulfate rich acid mine drainages at pH less than 5, aluminum concentration is consistent with the solubility of a jurbanite-like mineral, (Karathanasis et al. 1988). However, speciation calculations for aluminum in water samples from an acid mine water drainage basin demonstrated a distinct transition from conservative behavior for pH below 4.6 to nonconservative behavior for pH above 4.9. The nonconservative behavior correlated closely with the equilibrium solubility of microcrystalline gibbsite or amorphous aluminum hydroxide, (Nordstrom and Ball 1986).

Chapman et al. (1983), made detailed analysis of the sediments and waters of two acid mine drainage streams. One stream bed had a thick crust of hydrous iron oxide along with substantial quantities of adsorbed silica, sulfate, and aluminum; lesser quantities of arsenic; and small amounts of jarosites. (K^+ and Pb-jarosites and jurbanite were supersaturated for all sites.) Saturation index calculations for the second stream indicated that $Fe(OH)_3$, $Al(OH)_3$, and $Cu_2(OH)_2CO3$ should be precipitating; a prediction supported by the down stream loss of the elements. Changes in pH and the concentrations of Cu, Zn, Cd, and Mn could usually be accounted for by dilution alone.

Adsorption and coprecipitation have long been thought to control the accumulation and distribution of many trace elements in natural waters and soils, (Jenne 1977, Wangen et al. 1982, Wangen and Jones 1984). It has been observed that Fe^{2+}, Mn^{2+}, Mg^{2+}, and Zn^{2+} are lost from solutions at pH values below their OH^- solubility limits, indicating that they are being scavenged from solution by adsorption, (Jenke et al. 1983). Adsorption of metal ions on oxide surfaces is pH dependent. (See Davis and Leckie 1978, Benjamin and Leckie 1981, Buffle 1988, and Dzombak and Morel 1990.)

Griffin et al. (1980), hypothesized that removal of trace metals such as Cd, Co, Cr, Cu, Ni, Pb, and Zn from slurry pond leachates may be controlled by adsorption on or coprecipitation with iron, manganese, and aluminum oxides and hydroxides. They commented that this could continue as long as the solid phase was continually replenished by formation of new metal oxides. The chemical nature and generally high specific surface area of iron oxides in particles and as coatings on other particles make them efficient sinks for anions such as phosphate, molybdate, and silicate, as well as trace elements like Cu, Pb, V, Zn, Co, Cr, and Ni, (Schwertmann and Taylor 1977). Iron from mine waters was found to be transported predominantly in the particulate phase in Carnon River waters (south west England), and virtually

all of the dissolved iron precipitated in estuarine waters. Dissolved concentrations of Cu, Zn, and As appeared to be regulated by sorptive processes particularly with Fe oxyhydroxides in both fresh and saline waters, (Johnson and Thornton 1987).

Fillipek et al. (1987), investigated the interaction of acid mine drainage with creek waters and sediments. They found that acid mine drainage had acidified large volumes of water and added high concentrations of dissolved heavy metals to a creek draining rocks of low acid-neutralizing capacity. During mixing of the acid sulfate stream waters with an almost equal volume of dilute uncontaminated water, Cu, Zn, Mn, and Al remained in solution rather than precipitating or adsorbing onto solid phases. They found that arsenic was almost completely scavenged from solution within a short distance from the sulfide sources; and that relative sorption of cations decreased with decreasing water pH.

In a report on recent work investigating the neutralization of synthetic acid leachates from coal using solutions of $NaHCO_3$, Valette-Silver and Helz (1989) found: no losses of Al, Cu, Cr, and Be below pH 2.5; filterable iron disappeared rapidly between pH 2.5 and 3.5; filterable Al and Cr were removed above pH 4; and Cu and Be were not quantitatively removed until higher pH values were reached. They concluded that the contamina-

tion of surface water near coal piles would be confined to the near-field unless the leachate overcomes the neutralizing capacity of the receiving waters. In experiments diluting the synthetic leachates with river water or estuarine water, they found dilutions of approximately 500:1 necessary to reach pH's that brought about the removal of the toxic metals. They noted that precipitation of the iron contained in the leachate facilitated removal of the metals by adsorption onto the oxyhydroxide. Reduced acidity in solution affects surface charge, and thus trace element adsorption onto solid surfaces. (See Davis et al. 1978.)

1.5 ENVIRONMENTAL HAZARDS OF COAL DRAINAGE

The thermodynamic activity of the uncomplexed ion is probably the single most important factor affecting the biological availability of solute trace elements. The biological importance of solid forms of trace elements may be mainly due to their regulation of equilibrium solute concentrations in the water by sorption-desorption and dissolution-precipitation reactions, (Jenne and Luoma 1977). Certainly accumulation in the aquatic food chain of toxic substances from coal drainage can pose serious environmental hazards. Forstner and Wittmann (1979) summarized catastrophic episodes of metal poisonings by Hg, Cd, Pb, Cu, and Cr. Table 1.5, from their book,

shows a classification of elements according to toxicity and availability in the environment.

Table 1.5 Toxicity and availability of elements.

Noncritical			Toxic but v.insoluble or v.rare		Very toxic and relatively accessible		
Na	C	F	Ti	Ga	Be	As	Au
K	P	Li	Hf	La	Co	Se	Hg
Mg	Fe	Rb	Zr	Os	Ni	Te	Tl
Ca	S	Sr	W	Rh	Cu	Pd	Pb
H	Cl	Al	Nb	Ir	Zn	Ag	Sb
O	Br	Si	Ta	Ru	Sn	Cd	Bi
N			Re	Ba		Pt	

Trace concentration of metals such as Pb, As, Cu, or Al, when leached from coal and its associated mineral matter, may be toxic to plants, fish, wildlife, and aquatic insects, (Davis and Boegly, Jr. 1981b). Arsenic, cadmium, and selenium from coal pile and coal waste effluents could cause potential biological problems in the aquatic environment, (Hall, Jr. and Burton 1982). Wewerka, et al. (1982), identified Al, As, Be, Cd, Co, Cu, Fe, Mn, Ni, Pb, Se, and Zn as trace elements being released from Illinois Basin coal cleaning wastes in potentially hazardous concentrations. Bioassay studies with leachates from Illinois coal solid wastes led to the conclusions: a) approximately one-half of the leachates were acutely toxic to young fathead minnow fry; b) the degree of a leachate's toxicity and the amount of dilution necessary to ensure survival of the minnows

during a 96-hour bioassay was largely a function of the pH and total ion concentration of the leachate, (Griffin et al. 1980).

Table 1.6, (from Wachter and Blackwood, 1978), compares runoff concentration from coal storage areas to hazardous concentration for twelve elements that have been considered inorganic pollutants.

Table 1.6 Coal storage runoff concentrations compared to hazardous concentrations.*

Effluent	Runoff+, g/m^3	Hazardous#, g/m^3	C_R/C_H ratio
Arsenic	0.001	0.05	0.02
Beryllium	<DL	0.011	----
Cadmium	$2x10^{-7}$	0.01	0.00002
Chromium	$4x10^{-7}$	0.05	0.000008
Copper	$<7x10^{-6}$	1.0	0.000007
Cyanides	$7x10^{-7}$	0.005	0.00014
Lead	$6x10^{-6}$	0.05	0.00012
Mercury	$1x10^{-7}$	0.002	0.00005
Nickel	$4x10^{-5}$	0.0013	0.031
Selenium	0.002	0.01	0.2
Silver	<DL	0.05	----
Zinc	$7x10^{-5}$	5.0	0.000014

* From Wachter and Blackwood 1978.

+ The runoff concentration was calculated from the source concentrations of their "representative" (105,000 ton) coal stockpile, diluted by the average runoff volume from the storage facility drainage basin (610 m^3/hr).

\# Also note that the hazardous concentrations were taken from the USEPA water quality criteria published July, 1976. They were estimated from LD_{50} oral/rat values, and (supposedly) represent the maximum concentration that would have no effect on human health.

Torrey (1978) summarized the results of about 200 bioassays on the toxicity of As, Ba, Cd, Cl, Cr, Cu, Fe, Pb, Mn, Hg, Ni, Se, and Zn to aquatic biota. Portions of that work are included in Table 1.7.

An early article on stream quality in Appalachia reported that nearly 200 of 318 sites assessed did not meet drinking-water standards, due mainly to excessive concentrations of solutes commonly associated with coal mine waters, (Biesecker and George 1966). More recently, Swift (1982), studied the effects of coal pile runoff on a stream in Allegany County, Maryland. Coal pile leachate had high concentrations of Fe, SO_4, Mn, Al, and Zn, and pH's from 1.4 to 3.1. The author cites dilution as the reason the creek waters had much lower concentrations of sulfate and metals, and a pH of about 7. He also found much lower macroinvertebrate population densities at all sites downstream from coal storage areas than were found upstream.

Table 1.7 Toxicity of selected trace elements to aquatic biota.*

Organism	Dosage, mg/L	Remarks
Arsenic		
Gen'l Aquatic organisms	1.1 - 45	Lethal, arsenite
Daphnia magna	2.85	LC_{50} = 3 wk
	0.52	16% reproductive impairment
Oncorhynchus gorbuscha	5.0	Lethal, 10 days
O. keta	8.4	LC_{50} = 48 hr
Trout	7.6	Tolerated 30 days
Trout	5.0	Tolerated 24 hr
Alburnus alburnus	2.2	Lethal, 72 hr
	1.1 - 1.6	Tolerated 11 days
Cyprinus carpio	3.1	Lethal, 4 - 6 days
	2.2	Tolerated 13 days
Minnows	11.6	Lethal, 36 hr
	60	Lethal, 16 hr
	29	LC_{50} = 48 hr
	15	Tolerated 96 hr
Lucioperca sp.	1.1 - 2.2	Lethal, 48 hr
	0.7 - 1.1	Tolerated 11 days
Barium		
Daphnia magna	14.5	LC_{50} = 48 hr
	13.5	LC_{50} = 3 wk
	5.8	LC_{50}, 50% reproductive impairment
	8.9	LC_{50}, 50% reproductive impairment
Stickleback	400	Lethal concen. limit
Cadmium		
Ephemerella subvaria	2.0	LC_{50} = 96 hr
Daphnia magna	0.005	LC_{50} = 3 wk
	0.0017	LC_{50} = 3 wk, 16% reproduct. impairmt.
Eurypanopeus depressus	4.9	LC_{50} = 72 hr
	11.0	LC_{100}
Pimephales promelas	0.029	LC_{50} = 30 days
Fish (general)	0.029-73.5	LC_{50} = 96 hr
Lepomis macrochirus	80	LC_{50} = 11 mo, adults
	1.94	LC_{50} = 96 hr, fry
L. cyanellus	2.84	LC_{50} = 96 hr, fry
Carassius auratus	2.34	LC_{50} = 96 hr, fry

* from Torrey 1978.

Table 1.7 continued: Toxicity of selected trace elements to aquatic biota.*

Organism	Dosage, mg/L	Remarks
Cadmium, cont.		
Poecilia reticulata	1.27	LC_{50} = 96 hr, fry
Lepomis gibbosus	1.5	LC_{50} = 96 hr, fry
Cyprinus carpio	0.24	LC_{50} = 96 hr, fry
Anguilla rostrata	0.82	LC_{50} = 96 hr, fry
Roccus americanus	8.4	LC_{50} = 96 hr, fry
R. saxatilis	1.1	LC_{50} = 96 hr, fry
Fundulus diaphanus	0.11	LC_{50} = 96 hr, fry
Chlorine		
White sucker	1.0	Lethal 30 to 60 min, residual chlorine
Rainbow trout	0.014-0.029	TL_{50} = 96 hr
Fathead minnow	0.05 - 0.16	TL_{50} = 96 hr
Brook trout	0.02	Lethal
Brown trout	0.02	Lethal
Daphnia magna	0.014	Lethal
Gammarus pseudolimnaeus	0.014	Lethal
Crayfish	0.78	TL_{50} = 7 days
Snails	0.78	TL_{50} = 7 days
Chromium		
Daphnia magna	<1.2	Threshold immobilization, 64 hr
	0.33	16% reproductive impairment, 3 wk
	0.60	50% reproductive impairment, 3 wk
Acroneuria lycorias	32	LC_{50} = 7 days
Ephemerella subvaria	16	LC_{50} = 96 hr
Hydropsyche betteri	32	LC_{50} = 7 days
Hexagenia (nymphs)	8.6	Mortality, 96 hr
Lepomis macrochirus	71.9	LC_{50} = 96 hr, Cr^{+++}
Fathead minnow	64.7	LC_{50} = 96 hr, Cr^{+++}
	2.0	Reproductive impairment, 10 mo.
Carassius auratus	37.5	LC_{50} = 96 hr
Lebistes reticulatus	30.0	LC_{50} = 96 hr
Brook trout	0.40	Reproductive impairment, 2 yr
	50.0	TLm = 96 hr

* from Torrey 1978.

Table 1.7 continued: Toxicity of selected trace elements to aquatic biota.*

Organism	Dosage, mg/L	Remarks
Chromium, cont.		
Rainbow trout	0.40	Reproductive impairment, 2 yr
	69.0	TLm = 96 hr
Largemouth bass	195	TLm = 48 hr
	94	TLm = 80 hr
Copper		
Daphnia magna	0.022	LC_{50}, 16% repro. impairment, 3 wk
	0.035	LC_{50}. 50% repro. impairment, 3 wk
Acroneuria lycorias	8.3	LC_{50} = 96 hr
Ephemerella subvaria	0.32	LC_{50} = 48 hr
Hydropsyche betteri	32	LC_{50} = 14 days
Orconectes rusticus	3	LC_{50} = 96 hr
Campeloma decisum	1.7	LC_{50} = 96 hr
Physa integra	0.039	LC_{50} = 96 hr
Gammarus pseudolimnaeus	0.020	LC_{50} = 96 hr
Pimephales promelas	0.023	LC_{50} = 96 hr
	0.018	Reproductive impairment, 10 mo.
	0.075	LC_{50} = 96 hr
Lepomis macrochirus	0.66	LC_{50} = 96 hr
Carassium auratus	0.036	LC_{50} = 96 hr
Lebistes reticulatus	0.036	LC_{50} = 96 hr
Salvelinus fontinalis	0.10	LC_{50} = 96 hr
	0.03	43% survival of adults, 8 months
Ictalurus nebulosus	0.18	LC_{50} = 96 hr
Sockeye and pink salmon	0.025	Mortality, retarded development
Rainbow trout	0.037	Reduced egg and fry survival
Steelhead	0.03	Fry mortality, 96 hr
Lake trout	0.111	Reduced egg and fry survival
Brown trout	0.037	Reduced egg and fry survival

* from Torrey 1978.

Table 1.7 continued: Toxicity of selected trace elements to aquatic biota.*

	Organism	Dosage, mg/L	Remarks
Iron			
	Daphnia magna	5.2	Reproductive impairment, 3 wk
		5.9	LC_{50} = 3 wk
		4.4	16% reproductive impairment, 3 wk
	Gammarids	3.0	Reproductive impairment, 4 months
	Caddisflies	25.0	Reduced emergence, 2 months
	Acroneuria lycorias	16.0	LC_{50} = 9 days
	Ephemerella subvaria	0.32	LC_{50} = 96 hr
	Hydropsyche betteri	16.0	LC_{50} = 9 days
	Fathead minnow	50.0	Mortality, 5 months
	Brook trout	12.0	Reduced growth 37 wk
Lead			
	Daphnia magna	0.45	LC_{50} = 48 hr
		1 - 0.3	LC_{50} = 3 wk
	Acroneuria lycorias	64.0	LC_{50} = 14 days
	Ephemerella subvaria	16.0	LC_{50} = 7 days
	Hydropsyche betteri	32.0	LC_{50} = 7 days
	Pimephales promelas	5.6	LC_{50} = 96 hr
	Lepomis macrohirus	23.8	LC_{50} = 96 hr
	Carassius auratus	31.4	LC_{50} = 96 hr
	Lebistes reticulatus	20.6	LC_{50} = 96 hr
	Coho salmon	0.3	Fry mortality, 96 hr
	Chinook salmon	1.0	Fry mortality, 96 hr
	Steelhead	0.6	Fry mortality, 96 hr
	Brook trout	0.5	Fry mortality, 3 wk
	Fathead minnow	5.58	LC_{50} = 96 hr
Manganese			
	Daphnia magna	5.20	Reproductive impairment, 3 wk
		5.7	LC_{50} = 3 wk
		4.1	16% reproductive impairment, 3 wk
	Anguilla japonica	4.1	Lethal
Mercury			
	Macrocystis pyrifera	50	50% photosynthesis reduction, 4 days
	Phytoplankton	100	Complete inactivation, 4 days

* from Torrey 1978.

Table 1.7 continued: Toxicity of selected trace elements to aquatic biota.*

Organism	Dosage, mg/L	Remarks
Mercury, cont.		
Nitzschia delicatissima	0.1	Reduced growth and photosynthesis
Daphnia magna	0.13	LC_{50} = 3 wk
	6.7	50% reproductive impairment, 3 wk
	3.4	10% reproductive impairment, 3 wk
	5.0	LC_{50} = 48 hr
Nickel		
Daphnia magna	0.51	LC_{50} = 48 hr
	0.13	50% reproductive impairment, 3 wk
	0.03	16% reproductive impairment, 3 wk
Acroneuria lycorias	33.5	LC_{50} = 96 hr
Ephemerella subvaria	4.0	LC_{50} = 96 hr
Hydropsyche betteri	64.0	LC_{50} > 14 days
Pimephales promelas	4.58	LC_{50} = 96 hr
Lepomis macrochirus	5.18	LC_{50} = 96 hr
Carassius auratus	9.82	LC_{50} = 96 hr
Lebistes reticulatus	4.45	LC_{50} = 96 hr
Rainbow trout	32	LC_{50} = 48 hr
Zinc		
Daphnia magna	0.10	LC_{50} = 48 hr
	0.158	LC_{50} = 3 wk
	0.07	16% reproductive impairment, 3 wk
	0.102	50% reproductive impairment, 3 wk
Acroneuria lycorias	32	LC_{50} = 14 days
Ephemerella subvaria	16	LC_{50} = 10 days
Hydropsyche betteri	32	LC_{50} = 11 days
Pimephales promelas	0.96	LC_{50} = 96 hr
Lepomis macrochirus	6.44	LC_{50} = 96 hr
Carassius reticulatus	1.27	LC_{50} = 96 hr
Coho salmon	0.14	Fry mortality, 96 hr
Chinook salmon	0.30	Fry mortality, 96 hr
Steelhead	0.30	Fry mortality, 96 hr
Rainbow trout	4.6	LC_{50} = 5 days

Note: LC_{50} is the lethal concen. to 50% of a population.
TL_{50} is the tolerance limit for 50% of population.
TLm is the median tolerance limit.

* from Torrey 1978.

CHAPTER 2 METHODS

2.1 BATCH OXIDATION OF SLURRY OF WHOLE COAL

2.1.1 Introduction

A study of the release of selected elements during the oxidation of whole coal was undertaken. A sample of whole coal was ground and slurried in water in contact with air. Samples were withdrawn periodically and filtered. The pH of each filtrate was measured before its acidification and storage. The solids were washed with a magnesium chloride ion-exchange solution, which was also filtered and acidified and stored. Analyses for dissolved sulfate, iron, aluminum, zinc, cadmium, copper, chromium, lead, arsenic, and selenium were performed later.

2.1.2 Coal Sample

Several kilograms of coal from the Leslie Mine in Osceola Mills, Centre County, Pennsylvania, were obtained from the Potomac Electric Power Company, Chalk Point Generating Station, (Aquasco, Maryland) by N. J. Fendinger, (then a University of Maryland graduate student engaged in research on coal at the Center for Environmental and Estuarine Studies, Chesapeake Biological Laboratory, Solomons, Md). After being mined, the coal was crushed, washed to reduce sulfur and ash content, and

shipped by coal train to PEPCO's Aquasco facility where it was stored outside; (Fendinger et al. 1989, and private communication). Our sample was obtained approximately one month after the coal was mined. It was scooped from the coal pile into a large, heavy-duty, plastic bag. After transport back to the laboratory, it was refrigerated at 7 to 8 degrees Celsius for short-term storage.

About five kilograms of the coal, in small batches, were ground to powder with a mortar and pestle and then dried for two hours at sixty degrees Celsius with occasional stirring in a forced-air oven. The individual batches were thoroughly mixed before being placed in a large desiccator over Drierite, (anhydrous calcium sulfate), for long-term storage.

2.1.3 Characterization of the Coal

Chemical characterization of this coal is summarized in Table 2.1. The metals data have been published by Helz et al. 1987, and were obtained by DC plasma emission spectroscopy and atomic absorption spectroscopy. Specifically, aluminum and beryllium were determined by DCP and the rest of the metals mainly by AAS. The rest of the data are from Fendinger et al. 1989. Total carbon, hydrogen, and nitrogen were determined using a Perkin-Elmer model 240B elemental analyzer. Penniman and Brown

(Baltimore, Maryland), determined sulfur using ASTM method D-4239-C, and the ash content using ASTM method D-3174-B2. The trace organic materials were operationally defined and determined in duplicate 2 g samples of the coal by extraction during sonication in dichloromethane, fractionation on silica gel, and characterization by gas chromatography and GC/MS. (See Fendinger et al. 1989).

Table 2.1 Chemical characterization of coal sample.*

Substance	Concentration, (w/w)
Major Components, %	
C	69.0
H	4.76
N	1.16
S	3.38
Ash	14.8
Al	2.42
Fe	1.87
Minor Components, mg/g	
K	2.8
Na	2.3
Ca	1.19
Mg	1.09
Trace Components, ug/g	
Cu	39.7
Zn	35.3
Mn	28.5
Cd	4.2
Be	2.9
Organic Material, ug/g	
Total Aliphatic Hydrocarbons	29.85
Total Aromatic Hydrocarbons	62.40
Polynuclear Aromatic Hydrocarbons	3.34

* Adapted from Helz et al. 1987, and Fendinger et al. 1989.

Comparison of Table 2.1 with Tables 1.2 and 1.3 reveals that the concentration of most of the elements

determined in this coal are within a range of about +/- one standard deviation of averages previously reported for whole coals from the eastern United States. The exceptions include copper, beryllium, sodium, and cadmium. The total sulfur content of this coal, 3.38%, is approximately one standard deviation above the means reported by Gluskoter et al. 1977, but well within the range of values they reported, (0.55 through 5.0%). Among the other major components, aluminum (2.42%) and iron (1.87%) are also approximately one standard deviation above the mean values for Eastern coals. For further comparison, Table 2.2 shows the mean concentrations of sulfur, aluminum, and iron reported for Illinois Basin and Western coals by Gluskoter et al. 1977, and Kuhn et al. 1980.

Table 2.2 Mean S, Al, and Fe concentrations in Illinois Basin and Western coals.

	Sulfur	Aluminum	Iron
Illinois Basin	3.5 ± 1.1%	1.2 ± 0.4%	2.0 ± 0.6% *
	3.9 ± 1.4%	1.3 ± 0.3%	2.0 ± 0.9% +
Western	0.73±0.33%	0.94±0.56%	0.51±0.24% *
	0.73±0.2 %	1.06±0.4 %	0.43±0.1 % +

* Gluskoter et al. 1977
\+ Kuhn et al. 1980

Note that this sample of an Eastern coal contains sulfur and iron concentrations only a little below the averages

for Illinois Basin coals, but its aluminum content is about twice their typical concentration.

The copper concentration in this coal is about twice the reported averages, but could easily be attributed to a localized enrichment of $CuFeS_2$, (chalcopyrite, a mineral commonly found in Eastern coals) in the sample of coal analyzed. The concentration of cadmium in this coal appears to be about seven times the average for 23 Eastern coals reported by Gluskoter et al. 1977, (see Table 1.2). This may also be due to a localized enrichment of sulfide minerals, since cadmium is typically found in association with zinc, and sphalerite (ZnS) is commonly found among the sulfide minerals associated with coal, (see Table 1.1).

Beryllium is listed in Table 1.1 as a trace constituent of the clay minerals. Its concentration in this coal is two to four times the average concentrations shown in Tables 1.2 and 1.3. However, Wachter and Blackwood (1978) reported Be in Appalachian coals to average 0.0025 percent, which is ten times the level found in this sample.

The sodium concentration in this coal is five to six times the averages presented in Tables 1.2 and 1.3 for Eastern coals. Sodium is a major constituent of albite ($NaAlSi_3O_8$) and other minerals in the alkali feldspar series, (Phillips and Griffen 1981). The very high

concentration of sodium found in this coal could be attributed to a non-representative sample having a significant amount of a sodium-substituted silicate mineral; or it could be due to contamination of the sample with sodium.

X-ray diffraction was used to analyze a sample of the coal for mineral components that might be present in significant quantities. A few grams of the previously ground coal were ground again under acetone with an agate mortar and pestle. A few drops of the resultant slurry were applied to a clean glass slide and air dried. The slide was mounted in a Philips X-ray Diffractometer with XRG 3100 X-ray Generator and APD 3720 Diffractometer Controller. A program was employed which used CuKα radiation (lambda = 1.5418 angstroms) and scanned the range 15° - 55° at 2° per minute. The uncertainty in the angle measurement is less than 0.5° and typically +/- 0.01°. The instrument provided signal processing and a digital printout of the peak location (2 theta), the calculated interplanar distance (d), and peak intensity in arbitrary units.

Table 2.3 shows the results obtained from the X-ray diffraction analysis and tentative peak assignments (as discussed below). The entries without values for peak intensity are additional peaks that were visually identi-

fied as appearing to rise to approximately two times the average background noise or higher.

Table 2.3 X-ray diffraction peaks of coal sample.*

Interplanar Distance (angstroms)	Relative Peak Intensity	Tentative Peak Assignment
5.89		
4.8853	84	
4.4759	107	Illite
4.3500	116	
4.2535	122	Quartz
3.7665	133	
3.5823	150	Kaolinite
3.53		
3.3434	160	Quartz & Illite(?)
3.18		
3.0680	121	
3.0009	130	Alunite
2.8981	115	Alunite
2.8628	86	
2.84		
2.69		Pyrite(?)
2.68		
2.6497	93	
2.5852	84	
2.57		
2.50		Kaolinite(?)
2.46		Quartz(?)
2.42		Pyrite(?) & Illite(?)
2.34		
2.30		Alunite
1.96		
1.90		
1.7755	80	
1.76		Alunite

* Entries with no listed Relative Peak Intensity were visually identified as rising about two times the average background noise or higher.

It should be noted that components comprising less than 5% of a sample typically do not provide adequate

signal strength to produce definite peaks. In addition, components with reduced crystallinity give rise to peaks that are poorly resolved or indistinguishable from the background noise.

Table 2.4 lists the five major X-ray diffraction peaks in the approximate range of the analysis (and in order of relative peak intensity) for minerals suspected of being present in the coal. Comparison of Table 2.3 with Table 2.4 shows that the single strongest peak (d=3.3434) matches the principal peak used to identify quartz. The second most important quartz peak is also prominent in the analysis. The remaining major quartz peaks are relatively weak and were identifiable in our analysis barely if at all. The second strongest peak identified (d=3.5823) corresponds closely to the principal kaolinite peak within the range analyzed. However the second kaolinite peak is off scale, the third matches the experimental data poorly, and the remaining two peaks were weak or unidentifiable. The principal illite peak (d=4.48) can be paired with the fairly strong peak at d=4.4759. The second most important illite peak, if present, is probably masked by the principal quartz peak. The third illite peak was unidentifiable in these results, the fourth was off scale, and the fifth was very small, at best.

Table 2.4 X-ray diffraction peaks for selected minerals.*

Quartz (#5-490)+	Alunite (#14-136)	Kaolinite (#14-164)	Illite (#9-343)	Pyrite (#6-710)	Calcite (#24-27)
3.343 (100)	2.99 (100)	3.579 (80)	4.48 (90)	1.633 (100)	3.030 (100)
4.26 (35)	2.89 (100)	1.620 (70)	3.33 (90)	2.71 (85)	1.8726 (34)
1.182 (17)	1.757 (88)	4.366 (60)	2.61 (60)	2.423 (65)	3.852 (29)
2.458 (12)	2.293 (80)	4.186 (45)	1.53 (60)	2.2118 (50)	2.094 (27)
2.282 (12)	1.926 (70)	2.495 (45)	2.42 (40)	1.9155 (40)	2.284 (18)

* Expressed as interplanar distance (d), in angstroms.

+ American Society for Testing and Materials (ASTM) Powder Diffraction File reference number.

Note: Numbers in parentheses indicate relative peak intensity.

Thus, among the major silicate minerals commonly found with eastern U.S. coals, quartz was rather strongly indicated by its two principal peaks, and kaolinite and illite were suggested, but their presence could not be confirmed in the whole coal.

Comparison of the principal pyrite peaks with the data reveals that the most important peak was off scale, the next two were very weak, and the last two could not be recognized. For calcite, none of the major peaks were identifiable. These results are due in part to the coal being washed to reduce its mineral and ash content prior to being used as a fuel. Also, the bulk of the coal itself dilutes any mineral phases still present, and weakens the signals obtained by X-ray diffraction.

The presence of alunite is strongly suggested by the occurrence of its four strongest peaks. It is considered likely that this phase is the result of the initial oxidation of pyritic sulfur to sulfate ions, which then crystallize with aluminum ions from any soluble alumino-silicate phases.

A careful and systematic Hanawalt search of the ASTM Powder Diffraction File data failed to reveal any other mineral phases as being present in the sample of whole coal analyzed. However, other researchers (Means et al. 1987) investigating another sample of coal from

Figure 2.1 X-ray diffraction pattern obtained from low temperature ash of the coal by microwave-excited oxygen.*

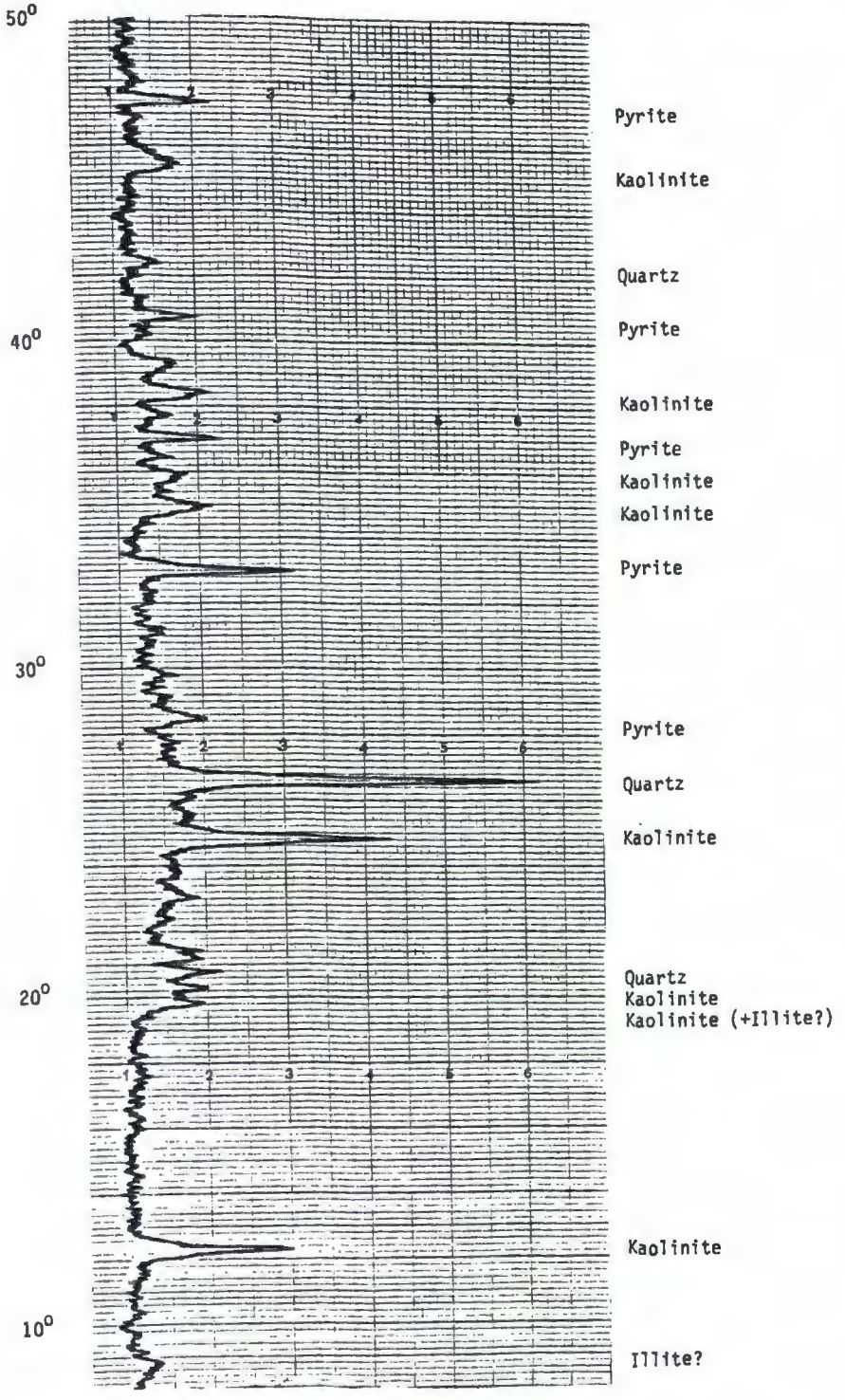

* Means et al. 1987, (including peak assignments).

the same shipment, prepared a low temperature ash in microwave-excited oxygen. (Removal of the bulk carbon phase effectively concentrates the mineral phases and results in stronger signals.) The X-ray diffraction pattern they obtained is shown in Figure 2.1, along with the peak assignments that they made. The evidence for the presence of quartz, kaolinite, and pyrite is stronger, and the presence of illite is again suggested. However, there is not support for the presence of alunite.

2.1.4 Set-up for Batch Oxidation

A five liter boiling flask was cleaned and soaked in one percent nitric acid and thoroughly rinsed with distilled water that had been deionized by a Millipore Milli-Q water purification system, (subsequently referred to as Milli-Q water). A 4.00 liter volume of Milli-Q water was added to the flask and aerated with breathing grade compressed air while being stirred by a direct-drive mechanical stirrer using a polyethylene-coated propeller and shaft.

Three hours later, the pH of the initial water system was determined to be 5.66, using an Orion Research model 701A digital pH meter with glass combination electrode calibrated with standard commercial buffer solutions of pH 4.00 and 7.00. About 55 mL of water was

withdrawn for the first ("blank") sample and handled as described later under "sampling routine".

Ground coal was removed from its desiccator in small quantities, and reground with mortar and pestle to obtain a fine free-flowing consistency. A 1038 gram mass of this powdered, whole coal was added to the vigorously stirred reaction flask. A 205 mL volume of Milli-Q water was added to the system to bring the initial ratio of coal to water to be 1:4 (mass:volume).

Aeration of the slurry was discontinued after the first night with the assumption that constant contact of the atmosphere with the vigorously stirred system would maintain air-saturation of the slurry.

2.1.5 Sampling Routine

Periodically, a 50-60 mL sample was withdrawn from the actively stirred slurry through a glass tube by a large plastic syringe, (Becton-Dickinson 60 cc Luer-Lok tip). To remove bulk solids, each sample was vacuum filtered through an 11.0 cm disc of Whatman Qualitative Filter Paper #1, using a Buchner filtration apparatus. The filtrate was caught directly in a large test tube and transferred to a 50 mL beaker.

In order to remove fine particles and colloids from the filtrate, a second large syringe was used to force the suspension through a Millipore Swinex 47 mm filter

having a 0.45 μm pore size filter disc. The final filtrate was caught in a clean, glass container that would be used for storage.

The pH of each sample was determined using the Orion pH system calibrated with commercial pH buffer solution standards (pH values 7.00, 4.00, and 2.00) shortly before each sample solution was measured.

An ion-exchange wash consisting of 50. mL of 1.00 molar magnesium chloride was passed repeatedly through the solids retained in the Buchner funnel in order to facilitate equilibration of the solution with the solids and surfaces. This wash solution was passed through the same steps (using the same glassware, second syringe, and Millipore filter) as the original sample solution, in order that it might gather up any ions that may have been adsorbed onto the equipment surfaces.

Both final solutions (sample and wash) were acidified to 0.2% (vol/vol) nitric acid using the concentrated reagent. They were each stored in a dry, acid-prewashed glass container that was sealed using a Parafilm membrane.

2.2 NEUTRALIZATION TITRATION OF SYNTHETIC SOLUTION WITH SODIUM BICARBONATE

2.2.1 Introduction

In order to simulate the neutralization of acid-drainage from weathering coal piles, a synthetic solution of ferric sulfate and sulfuric acid was formulated to approximate the composition found during the Batch Oxidation experiment. This was doped with trace levels of Al, Zn, Cu, Cd, Cr, Pb, As, and Se.

Neutralization was accomplished by titration in segments using a slow, steady injection of sodium bicarbonate solution into the stirred open system. Each base-injection period was followed by an equilibration period before a sample was withdrawn and stored for later analysis of iron and trace-element composition.

2.2.2 Synthetic Solution Composition

The ratio of sulfate to iron in solution found during the last half of the Batch Oxidation experiment was approximately 1.55 to 1. In order to imitate that composition, a 3.5 liter volume of Milli-Q water was placed in a clean (acid-soaked, Milli-Q water rinsed, and dried) four liter beaker and acidified with 17 mL of 3.69 molar sulfuric acid. To this was added 69.9 grams of powdered ferric sulphate hydrate (72.0% minimum iron(III)

sulfate), which dissolved with mechanical stirring within one hour.

The solution was loosely covered and stirred overnight in contact with air. The next day, aluminum and selected trace elements were added as follows: 0.315 grams of aluminum sulfate eighteen hydrate; 7.0 mL of 1000. ppm zinc (from reagent grade powdered metal) in 1% hydrochloric acid; 3.5 mL of 1000. ppm copper (from reagent grade powdered metal) in 5% nitric acid; 3.5 mL of 998.4 ppm cadmium (from reagent grade metal turnings) in 1% hydrochloric acid; 3.5 mL of 1000. ppm chromium (from reagent grade K_2CrO_4) in Milli-Q water; 3.5 mL of 1000. ppm lead (from reagent grade anhydrous $Pb(NO_3)_2$) in 1% nitric acid; 3.5 mL of 1000. ppm arsenic (from reagent grade As_2O_3 that was dissolved in 20 w/v % KOH, neutralized with 20 v/v % H_2SO_4, and then with 0.1 M NaOH, and diluted with Milli-Q water); 3.5 mL of 1020 ppm selenium (from reagent grade powdered selenium, dissolved in con HNO_3 and slowly evaporated dry with heat, redissolved with water and heat evaporated dry three more times, and finally taken up in 10% hydrochloric acid). The final solution volume was approximately 3.54 liters having the overall composition given in Table 2.5.

Table 2.5 Composition of synthetic coal leachate

0.05 molar iron(III) sulfate
0.018 molar sulfuric acid
0.0016 molar hydrochloric acid
0.001 molar nitric acid
7.2 ppm aluminum
3.5 ppm potassium
2.0 ppm zinc
1.0 ppm in each of Cu, Cd, Cr, Pb, As, and Se.
0.2 ppm sodium

2.2.3 Base Titrant

Sodium bicarbonate was chosen to be the base titrant for gradual neutralization, because a fairly concentrated solution could be used (to minimize dilution volume) and its pH would be nearly neutral (8.3). In contrast, a one molar solution of sodium hydroxide should have pH nearly 14, and would be expected to precipitate amorphous ferric hydroxide when injected into the acidic solution of ferric iron.

A 2.00 liter volume of 1.20 molar base titrant was prepared by dissolving 201.6 grams of sodium bicarbonate in Milli-Q water.

2.2.4 Apparatus

A Masterflex Peristaltic Pump with head number 7013.20 was used to pump the base titrant through Tygon tubing at flow rates ranging from 1.86 mL/min down to 0.65 mL/min. The flow rate was checked before and after each titration segment, and the volume dispensed was

estimated by the product of average flow rate and elapsed time. In addition, the volume of titrant removed from its reservoir during each titration interval was noted. The average of these two values was taken to be the total volume of sodium bicarbonate solution injected into the reaction vessel during each titration episode. The data is summarized in Table 2.6.

Table 2.6 Estimated, observed, and average volumes of dispensed sodium bicarbonate titrant.

Estimated*	Observed+	Average
140.9 mL		140.9 mL
138.4		138.4
81.1	82.5 mL	81.8
116.4	120.	118.2
100.3	97.	98.7
123.0	120.	121.5
104.0	101.3	102.7
25.2	23.5	24.4
18.3	17.7	18.0
18.5	18.0	18.2
19.5	19.0	19.3
20.7	20.0	20.4

* Product of average flow rate and elapsed time.
+ Difference of initial and final reservoir volumes.

The titrant was delivered into the region of apparently maximum turbulence of the vigorously stirred synthetic solution through a Teflon capillary tube jacketed in a glass tube (for structural rigidity). Highly turbulent stirring was achieved by using two direct-drive mechanical stirrers with polyethylene-coated propellers and shafts, (see Figure 2.2). The solution was restrain-

ed from "boiling" out of the four liter reaction vessel by a Plexiglas lid, (see Figure 2.3). Fixed vanes that extended approximately one quarter of the way down into the solution thwarted the creation of a central vortex and allowed much higher stirrer speeds to be used.

The solution, though covered to minimize fall-in of contaminants and splash-out of contents, was always open to the air. During periods of titration the stirring speed was turned up so high that air was drawn into the solution by small vortexes, and instantly dispersed throughout the vessel. Thus the system was kept aerated and the carbon dioxide neutralization product was allowed to escape readily from solution.

Figure 2.2 Reaction vessel for neutralization titration.

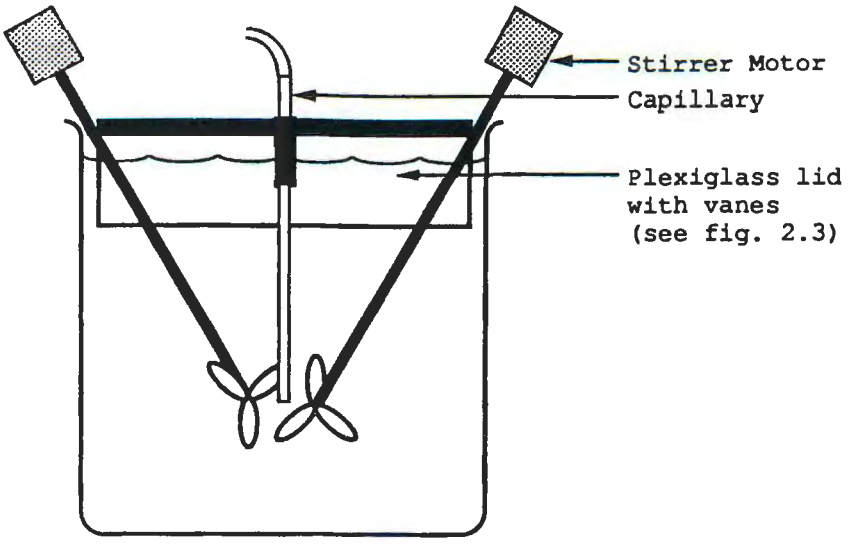

Figure 2.3 Lid for reaction vessel.

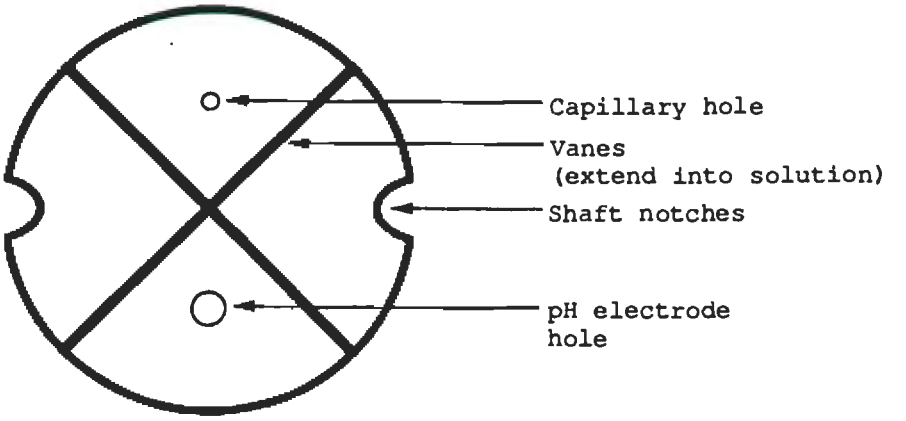

2.2.5 pH Monitoring and System Equilibration

The pH response of the system during and after each titration period was monitored as follows. An Orion Research model 701A digital pH meter with glass combination electrode was calibrated using commercial buffer solution standards of pH 7.00, 4.00, and 2.00. The electrode was rinsed, suspended in the stirred reaction solution, and the initial pH of the system recorded.

In order to avoid pushing the neutralization reaction too far during any one segment, the pH was noted every one to ten minutes throughout each injection period. The titration was stopped by removing the capillary injector if the pH of the system had risen more than one pH unit from its initial value.

Following each titration segment, the pH was monitored for an additional fifteen to thirty minutes while the system was still being vigorously stirred. This allowed the observation of pH drift or relaxation as the system began to equilibrate.

Within an hour after each titration segment, the rate of stirring was reduced below the point where air was drawn into the mixture. The pH electrode was removed and the reaction vessel covered to minimize evaporation and contamination.

At least twenty hours were allowed for the moderately stirred system to equilibrate internally and with the

atmosphere before being sampled, (with the exception of sample number 2 which was collected at pH 2 while the system still appeared to be a true solution).

2.2.6 Sampling Routine and Storage

Samples were withdrawn from deep within the continuously well-stirred system using a glass tube and large plastic syringe, (Becton-Dickinson 60 cc Luer-Lok). The sample suspension was forced through a Millipore Swinex 47 mm filter having a 0.45 um pore size filter disc. The filtrate was caught in an acid prewashed, Milli-Q water rinsed, and dried, glass sample bottle that would be used for storage.

The pH of each sample was determined using the same Orion Research pH meter and glass combination electrode that would be used to monitor reaction pH during the subsequent titration period. The system was calibrated just before use with commercial pH buffer solution standards of pH 7.00, 4.00, and 2.00.

Shortly after the pH of each filtered sample was measured, it was acidified to 0.2% (vol/vol) nitric acid using the concentrated reagent. The sample bottles were sealed using a Parafilm membrane.

2.3 ANALYSIS OF SAMPLES

2.3.1 Introduction

The sample solutions from the Batch Oxidation experiment were analyzed by flame atomic absorption spectroscopy for iron, and by ion chromatography for sulfate. Graphite furnace atomic absorption spectroscopy was used to determine aluminum, cadmium, chromium, copper, lead, and zinc in the solution samples from both the Batch Oxidation and the Titration experiments. Cation Exchange was used to remove interfering cations from these same sample solutions prior to determination of arsenic and selenium, also by graphite furnace atomic absorption spectroscopy.

2.3.2 Ion Chromatography

A Dionex QIC ion chromatograph was used for the separation, detection, and measurement of sulfate in diluted sample solutions from the Batch Oxidation experiment. Our system was configured with adjustable pump-stoke capacity, heavy-walled Teflon-tube pulse damper, 3-passage injection valve with replaceable sample-loops of various capacity, guard and separator columns, ion suppressor, and conductivity cell detector.

The pump stroke was set to provide a flow rate of about 2 mL/min and a 50 μL sample loop was used on the injection valve. The Dionex-recommended HPIC-AG1 ION PAC column was used as guard column. It was found that a second, newer AG1 column gave adequate separation of sulfate from the other anions in our samples, and halved the retention time of the usual DIONEX ION PAC HPIC-S1 Anion Separator analytical column.

The fiber-type counter-flowing ion suppressor used 0.25 normal sulfuric acid as suppressor regenerant. The conductivity cell output was internally amplified and transformed into a 0-1 volt signal which we used to drive the pen of a Bioanalytical Systems RYT strip chart recorder.

The ion suppressor was bypassed and the system was flushed to rejuvenate the columns as follows:

10-15 min with Milli-Q water,
10-15 min with 0.1 molar sodium hydroxide,
about 10 min with Milli-Q water,
about 10 min with 0.1 molar sodium carbonate,
finally, about 2 min with Milli-Q water.

The ion suppressor column was hooked up again and the normal sodium bicarbonate/sodium carbonate eluent (mobile phase used to elute the analytes from a chromatographic column) was pumped through for over an hour to re-equili-

brate the entire system and establish the baseline conductivity.

Short-term shutdown of the system, for up to a few days, was done simply by turning off the pump, recorder, and system electronics. For long-term shutdown, the guard and separator columns were flushed and stored with 0.1 molar sodium hydroxide. The rest of the system was flushed thoroughly with Milli-Q water and turned off.

Preparation of Solutions

The eluent used for the determination of sulfate in our samples was a solution containing 0.003 molar sodium bicarbonate and 0.0024 molar sodium carbonate. We prepared 4.0 liter batches of this buffer system using 1.01 grams of reagent grade sodium bicarbonate and 1.02 grams of reagent grade sodium carbonate in Milli-Q water.

The 0.025 normal sulfuric acid ion-suppressor column regenerant was prepared by diluting 2.45 mL of concentrated sulfuric acid to 3.5 liters with Milli-Q water.

The diluent used for both standards and samples was 0.2% (vol/vol) hydrochloric acid prepared by diluting 4.0 mL of reagent grade concentrated hydrochloric acid to 2000.mL with Milli-Q water.

The 1000.ppm stock solution of sulfate standard was prepared by dissolving 1.4790 grams of reagent sodium sulfate in 1.000 liter of the 0.2% (vol/vol) hydrochloric

acid diluent. Working standards (0.10, 0.20, 0.50, 0.80, and 1.0 ppm) were prepared by serial dilution of the stock standard such that each final solution was 0.02% (vol/vol) hydrochloric acid (to avoid swamping the columns and detector with chloride ions).

The original samples (acidified to 0.2% HNO_3 for storage) were diluted 100-fold with 0.2% (vol/vol) hydrochloric acid, then 100-fold with 0.02% (vol/vol) hydrochloric acid, and if necessary, 2-5 fold with 0.02% (vol/vol) hydrochloric acid in order to avoid swamping the system with either chloride or nitrate anions.

Injection Routine

After the baseline stabilized, 4 mL of sample or standard were pushed through the sample loop using a 5 mL plastic syringe (Becton-Dickinson). Immediately the injection valve was used to load a reproducible volume onto the columns. Within a few seconds the water band reached the detector. When the recorder traced the conductivity dip the injection valve was returned to the "load" position. The sample loop was then rinsed with 2.5 mL of Milli-Q water, and again at the emergence of the sulfate peak (about 12 minutes) with 1.5 mL of Milli-Q water. The baseline was re-established in about two more minutes.

Analysis of Standards and Interpretation of Sample Data

The standards were run before and after each set of ten to fifteen samples. Signal amplification and recorder range were selected so as to use 1 - 95% of the chart paper width, and thus minimize the uncertainty of measuring peak heights.

The data for all the standards measured during a given session were plotted as peak height versus sulfate concentration (see Figure 2.4). The least-squares fit regression line was calculated and used to interpret the sample peak height data in terms of sulfate concentration.

Figure 2.4 Calibration curve for the determination of sulfate in the Batch Oxidation filtrates by ion chromatography.

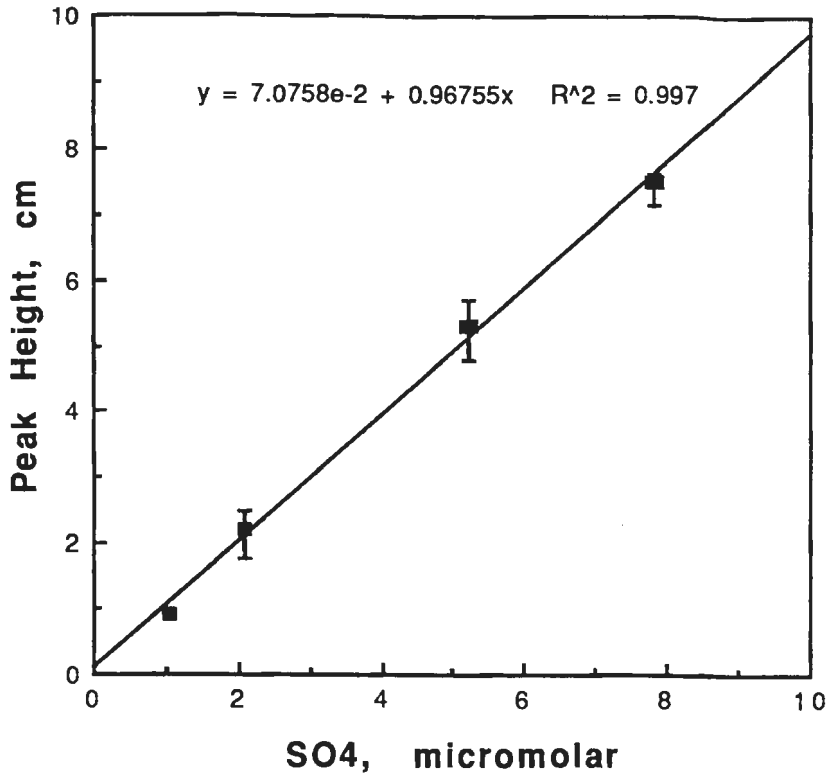

Notes: The standards were run before, during, and after the analysis of samples. Each point represents the average of the 2 - 4 separate analyses of a given standard solution. The vertical bars indicate the range of values obtained for that standard. The uncertainty of the concentration of each standard is not greater than the width of the symbols used to plot the data.

The line is the least-squares regression line fit to all the data points. The equation of the line was used to interpret the peak height of each sample in terms of sulfate concentration.

2.3.3 Flame Atomic Absorption Spectroscopy

Samples and diluted samples from the Batch Oxidation experiment (both filtrates and washes), and the Titration experiment, were analyzed by flame atomic absorption spectroscopy (FAAS). The instrument used was a Perkin-Elmer model 360 Atomic Absorption Spectrophotometer equipped with a deuterium arc continuum source background corrector and electronic signal integration.

I used the 372.0 nm iron line obtained from an iron single element hollow cathode source lamp driven usually with a filament current of 12 ma, (recommended range: 9-14 ma). The monochromator slits were set at the normal 0.2 nm. A four inch air-acetylene laminar flow burner head was used. The source and burner positions, as well as the nebulizer and monochromator settings, were all optimized after the instrument was warmed up for at least twenty minutes and before samples or standards were run.

The sample and standard solutions all had a matrix of 0.2% (vol/vol) nitric acid. Generally, five replicate three-second integrations were made of each solution and averaged. Multiple (7-17, but typically about 8) standards were made up spanning the useful analytical range of 1 - 100 or 200 ppm iron. These were run before and after each set of samples being analyzed.

The averaged data for the standards measured in a given session were plotted as absorbance seconds vs iron

concentration (see Figure 2.5). The least-squares fit regression line was calculated and used to interpret the sample absorbance data in terms of iron concentration.

Figure 2.5 Calibration curve for iron by flame atomic absorption spectroscopy.

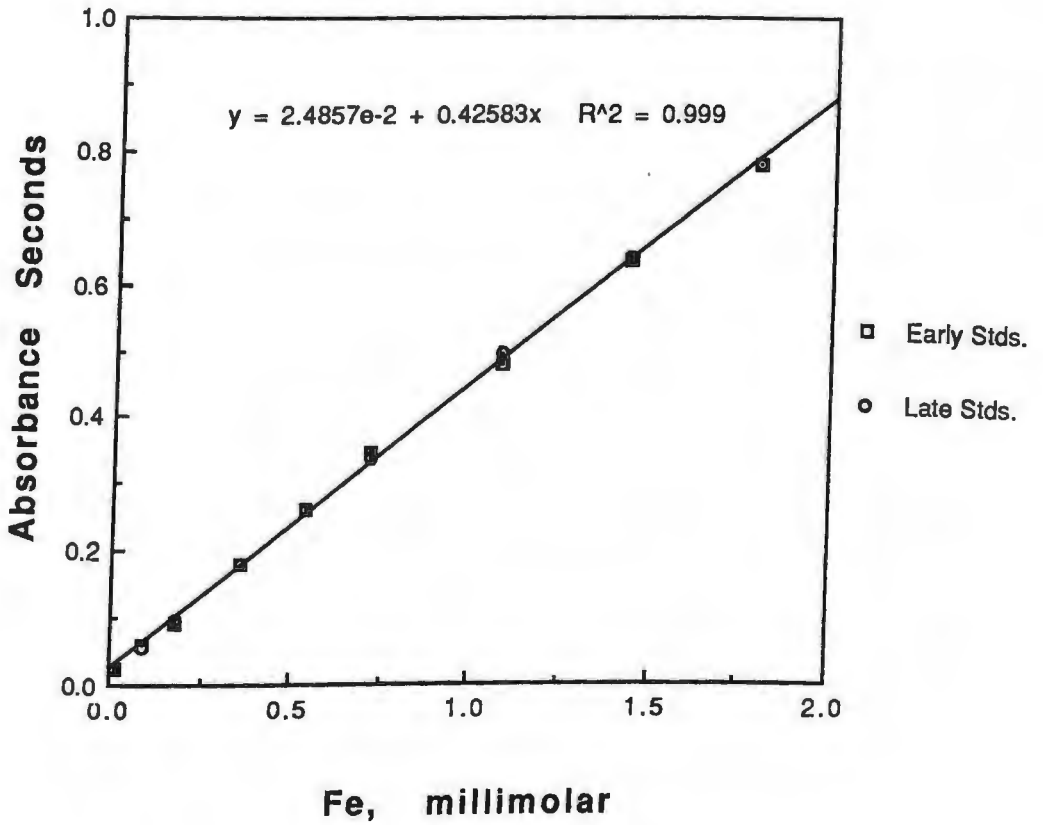

Notes: Standard solutions were run before ("Early Stds") and after ("Late Stds") the analysis of samples. Each point represents the average of four repli cate three-second integrations in the analysis of a standard.

The line is the least-squares regression line fit to the points plotted. The equation of the line was used to interpret the averaged absorbance of each sample in terms of iron concentration.

2.3.4 Interference avoidance and minimization in GFAAS analysis of arsenic and selenium.

Arsenic and selenium analyses by graphite furnace atomic absorption spectroscopy (GFAAS) suffer from severe background absorption and interferences by accompanying ions in solution. Welz and Schlemmer (1986) attributed the excessive background absorption to large amounts of matrix metals being volatilized during analyte atomization. Riley (1982) noted spectral interferences of iron for selenium and of aluminum for arsenic. Bauslaugh et al. (1984) noted interferences due to molecular absorption by phosphorous dimers formed during the decomposition of phosphates. (See also Fernandez and Giddings 1982.)

Interferences with arsenic signals by many matrix species including Na^+, K^+, Mg^{2+}, Ca^{2+}, Fe^{3+}, Cl^-, SO_4^{2-}, PO_4^{3-}, and MoO_4^{2-} have been noted. At least thirty-eight metals have been found to interfere with selenium signals (Henn 1975, 1977) as well as matrix acids including hydrochloric, sulfuric, and nitric (Tsalev 1984). Cation exchange has been used to remove metals from solutions of arsenic and selenium (Henn 1975).

In acidic, oxygenated waters, arsenic exists as $H_2AsO_4^-$, and below pH 2 as H_3AsO_4. Similarly, selenium should exist as SeO_4^{2-} at pH greater than 2, and as $HSeO_4^-$ at pH less than 1.75. Thus, cation-exchange was used to

remove many interferents before graphite furnace atomic absorption spectroscopy of arsenic and selenium. Matrix modifiers and pre-coating the graphite tubes and L'Vov platforms were used to minimize anion effects, (see Henn 1975, 1977).

Cation-exchange solution clean-up:

BIO-RAD cation exchange resin AG50W-X16, H^+ form, 200-400 mesh, with resin capacity 2.4 meq/mL, was soaked overnight in Milli-Q water and used to pack small columns. The slurried resin was poured into each Kontes Flex-Column a few milliliters at a time, and allowed to settle while the excess water drained down to the top of the resin bed. Subsequent additions of slurry were used to create a packed 7-8 cm resin bed in the 10 cm columns.

Smaller 0.7 cm diameter columns had a dead volume of about one milliliter and a calculated capacity of about 6.5 milliequivalents. The total cationic load in our filtrates was estimated to be 0.11 - 0.12 meq/mL; and that of our magnesium chloride wash solutions diluted ten-fold was estimated to be 0.18 - 0.20 meq/mL. Thus, a maximum of 54 mL of filtrate, or 32 mL of 1:10 diluted wash sample solutions could be cation exchanged.

Larger 1.0 cm diameter columns had a dead volume of about two milliliters and a calculated capacity of about 13 milliequivalents. Thus a maximum of 110 mL of fil-

trate, or 65 mL of 1:10 diluted wash sample solution could be cation exchanged.

Each sample solution (whether filtrate or wash) was diluted ten-fold with 0.2% (vol/vol) Ultrex nitric acid in Milli-Q water and placed in a 60 cc plastic (Becton-Dickinson Luer-Lok) syringe barrel. This sample reservoir was gravity fed vertically through about three feet of Tygon tubing and a cation exchange resin packed column.

Three successive 3-5 mL portions of effluent were collected as column washes and used to rinse the acid-washed collection vials. The remaining effluent was collected directly in the vials, which were subsequently sealed for storage.

The diluted filtrate solutions, having a high concentration of dissolved iron, produced a very dark band on the resin column, which only travelled 1/10 - 1/6 of the column length, even when two samples were passed through the column.

The diluted magnesium chloride wash solutions, having lower dissolved iron, but very high (about 0.1 molar) magnesium ion concentration, produced a slightly darkish band on the resin column, which travelled approximately 1/5 of the column length with just one sample passing through the column. All of the collected effluents were clear and appeared colorless.

2.3.5 Graphite Furnace Atomic Absorption Spectroscopy

Samples and diluted samples from the Batch Oxidation experiment (both filtrates and washes), and from the Titration experiment were analyzed by GFAAS for aluminum, cadmium, chromium, copper, iron, lead, zinc, arsenic, and selenium. The instrument used was a programmable Perkin-Elmer HGA-300 Graphite Tube Furnace fitted to a Perkin-Elmer model 2380 Atomic Absorption Spectrophotometer equipped with a deuterium arc source background corrector and electronic signal integration. A Perkin-Elmer model AS-40 programmable Autosampler was used to inject all blanks, standards, samples, and matrix modifiers into the graphite furnace tubes, which were pyrocoated and fitted with massive pyrographic carbon L'Vov platforms.

Set-up and Program Optimization

For each analysis of each element a single-element hollow cathode lamp source was used and the spectrophotometer optimized for maximum sensitivity (in terms of: source and furnace positions, monochromator wavelength and slit settings, and electronic peak area integration of absorbance).

Preliminary investigations of each element in the sample matrix were performed to determine the optimal matrix modification and temperature program to use to obtain maximum sensitivity, linearity, and reproducibil-

ity while minimizing interferences. Parameters optimized for analysis of (usually) twenty microliter samples acidified to 0.2% (vol/vol) with Ultrex nitric acid included:

type and amount of matrix modifier,
drying temperature ramp and time,
thermal pretreatment temperature ramp and time,
atomization temperature and time,
absorbance signal integration time, and
graphite tube purging temperature and time.

A series of typically 8-12 standards in 0.2% (vol/vol) Ultrex nitric acid was run for each element and plotted as absorbance-seconds versus concentration to estimate the sensitivity and range of linearity for each element under the selected conditions of analysis.

See Appendix A for specific conditions of the graphite furnace AAS analyses.

Analytical Scheme

The general analytical scheme adopted for the graphite furnace atomic absorption analysis for each element of interest was to:

1) Analyze all samples (diluted with 0.2% Ultrex nitric acid if necessary) using the optimal instrument parameters and matrix modification, as previously determined.

2) Interpret the data using a calibration curve based on 4-6 simple standards in 0.2% (vol/vol) Ultrex nitric acid and spread over the range of reasonable linearity obtained by our method. This revealed the range, trends, and approximate concentration of each analyte in our samples.

3) Re-analyze approximately every third sample by the method of standard additions of known analyte to four or five aliquots of each sample. These data were interpreted by extrapolation back to zero absorbance (baseline corrected) to establish the concentration of each analyte in a subset of our samples which spanned the ranges of sample collection time and analyte concentration in our experiments.

Analysis Routine

The typical routine followed for the analysis of a set of samples started with instrument warm-up while working-standard solutions were made by serial dilution with 0.2% (vol/vol) Ultrex nitric acid of a 1000. ppm stock standard solution of the appropriate element. Final tune-up of the instrument for optimal performance was followed by "analyzing" the diluent (0.2% Ultrex nitric acid) plus matrix modifier solution to establish the baseline absorbance level.

For small sample-sets, the standards were run first, followed by the samples, and often ending with one or two check-standards. For the average set of samples, the standards were run before and after, in order to establish instrument response over the duration of the analyses. For large sample sets, the standards were run about mid-day, as well as before and after the samples, for the same reason.

During each set of analyses, the reagent blank (0.2% Ultrex nitric acid plus matrix modifier solution) was run after every few samples or standards, in order to monitor the baseline absorbance signal.

Calibration Curves, Uncertainty, Limits of Detection, and Limits of Quantitation

On the following pages are presented the calibration curves of the elements analyzed by atomic absorption methods. The absolute uncertainty associated with each point is plotted using error bars. The uncertainty of the concentrations of the calibration standards (abscissa) was derived using propagation of errors analysis, as follows.

The uncertainty of each weighing and dilution procedure used in the preparation of one of the higher concentration working standards, and the uncertainty of its introduction into the graphite furnace, were estimated

and included in the calculation of overall uncertainty for that standard solution. For example, to estimate the uncertainty of concentration of a 100 ppm working standard:

Weighing and dissolving 1.0000 g of pure, dry metal:	±0.02%
Diluting to 1000.0 mL for the stock standard:	±0.06%
Diluting 5.00 mL to 500.0 mL to reach 10 ppm solution:	±0.5%
Diluting 5.00 mL to 500.0 mL to obtain 100 ppb standard:	±0.5%
Autopipetting 20 μL into the graphite furnace:	±1.0%

The overall relative uncertainty of these combined operations is the square root of the sum of the squares of the individual relative uncertainties, (Harris 1991), which is ±1.23% in this case.

The absolute uncertainty associated with a given standard is the product of its nominal concentration times its relative uncertainty. For the above example this gives ±1.23 ppb, and results in the expression 100.0 ± 1.2 ppb for the concentration of that standard. The calculated uncertainty was applied to each standard and plotted using horizontal error bars.

The uncertainty of the magnitude of the signal for each standard is indicated by the vertical error bars. They show the range of values obtained from the same standard as measured at different times. The central point plotted is the average of the separate measurements, and was used in the least squares fit of a regres-

sion line to the standards. The equation of the line and its goodness of fit (R^2) are included near the top of each plot. (Note that the error bars will not be visible in those cases where the range of uncertainty is smaller than the space covered by the graph symbol.)

Table 2.7 (which is presented just before the set of calibration curves) lists limits of detection (LOD) and limits of quantitation (LOQ) from the literature and from this work for the trace elements included in this study. Also listed are the dilution factors from each analysis, and the resulting LOD and LOQ of each element in the original undiluted samples. The limit of detection in each case was operationally defined to be that concentration of analyte which produced a signal at least two times the (locally) averaged baseline signal. The limit of quantitation in each case was obtained by multiplying the LOD by a factor of five, thus estimating the LOQ to be approximately 10 times the average baseline signal.

The LOD for zinc exceeds the published range by a factor of at least 10. It is believed that the high baseline zinc signals obtained were due to contamination. Also, the relatively noisy individual readings presented by the GFAAS instrument exacerbated the problem. These factors account in large part for the poor detection limits obtained for this element.

Table 2.7 Limits of detection and quantitation for the analyses of trace elements by Flame AAS and Graphite Furnace AAS.

Element	Slavin (1984) LOD (μM)	ASTM (1985) LOD (μM)	Dilute Solutions[2] LOD (μM)	Dilute Solutions[2] LOQ (μM)	Dilution Factors	Original Samples[1] LOD (μM)	Original Samples[1] LOQ (μM)
Al	0.0074	0.11					
BO/F[3]			0.04	0.2	1000	40	200
BO/W[4]			0.04	0.2	1000	40	200
Titn[5]			0.04	0.2	100	4	20
As	0.0134	0.013					
BO/F			0.1	0.5	10	1	5
BO/W			0.1	0.6	10	1	6
Titn			0.06	0.3	10	0.6	3
Cd	0.00013	0.0009					
BO/F			0.0005	0.0025	10	0.005	0.025
BO/W			0.0005	0.0025	10	0.005	0.025
Titn			0.001	0.005	10	0.01	0.05
Cr	0.00096	0.019					
BO/F			0.04	0.2	10	0.4	2
BO/W			0.08	0.4	10	0.8	4
Titn			0.06	0.3	10	0.6	3

Notes:
1. Original Samples were undiluted, but too concentrated for analysis.
2. Dilute Solutions were analyzed after serial dilution from the Original Samples by the Dilution Factor tabulated.
3. BO/F represents the Batch Oxidation filtrate samples.
4. BO/W represents the Batch Oxidation $MgCL_2$ wash samples.
5. Titn represents the neutralization Titration samples.

(continued on next page)

Table 2.7 (continued) Limits of detection and quantitation.

Element	Slavin (1984) LOD (μM)	ASTM (1985) LOD (μM)	Dilute Solutions[2] LOD (μM)	Dilute Solutions[2] LOQ (μM)	Dilution Factors	Original Samples[1] LOD (μM)	Original Samples[1] LOQ (μM)
Cu	0.0008	0.016					
BO/F[3]			0.016	0.08	100	1.6	8
BO/W[4]			0.008	0.04	100	0.8	4
Titn[5]			0.008	0.04	100	0.8	4
Fe (FAAS)	2						
BO/F			10	50	100	1000	5000
BO/W			10	50	10	100	500
(GFAAS)	0.0018	0.018					
Titn			0.018	0.09	100,000	1800	9000
Pb	0.0012	0.0048					
BO/F			0.003	0.015	10	0.03	0.15
BO/W			0.003	0.015	10	0.03	0.15
Titn			0.006	0.03	10	0.06	0.3
Se	0.019	0.025					
BO/F			0.2	0.9	10	2	9
BO/W			0.08	0.4	10	0.8	4
Titn			0.05	0.25	10	0.5	2.5
Zn	0.00008	0.0008					
BO/F			0.0016	0.008	1000	1.6	8
BO/W			0.016	0.08	100	1.6	8
Titn			0.02	0.1	100	2.	10

Notes:
1. Original Samples were undiluted, but too concentrated for analysis.
2. Dilute Solutions were analyzed after serial dilution from the Original Samples by the Dilution Factor tabulated.
3. BO/F represents the Batch Oxidation filtrate samples.
4. BO/W represents the Batch Oxidation $MgCL_2$ wash samples.
5. Titn represents the neutralization Titration samples.

Figure 2.6 Calibration curve for the determination of aluminum in the batch oxidation filtrates by graphite furnace AAS.

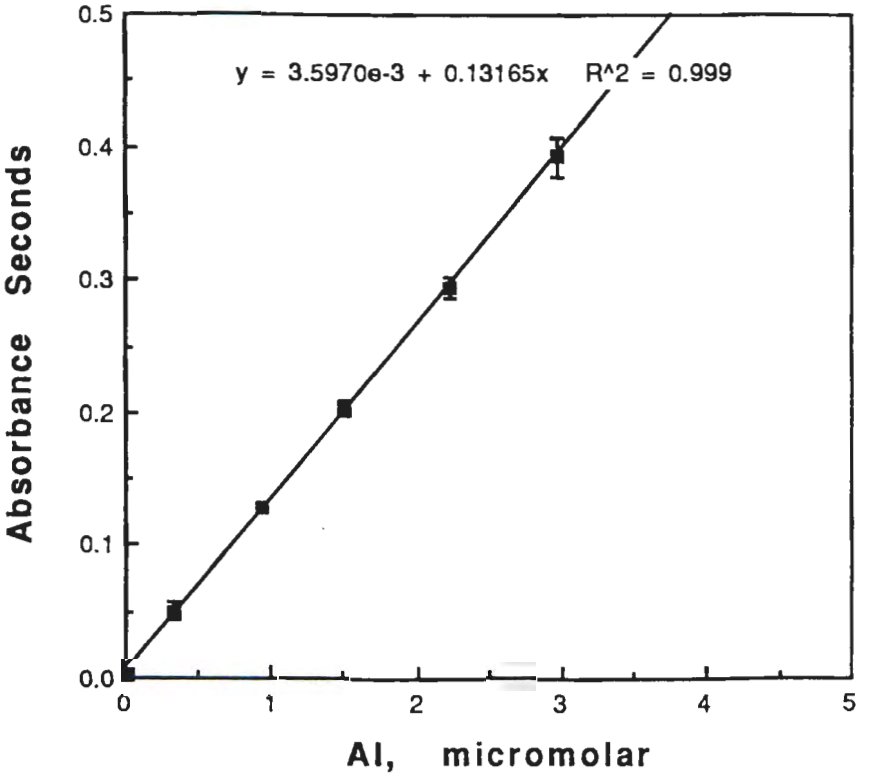

Figure 2.7 Calibration curve for the determination of aluminum in the batch oxidation washes by graphite furnace AAS.

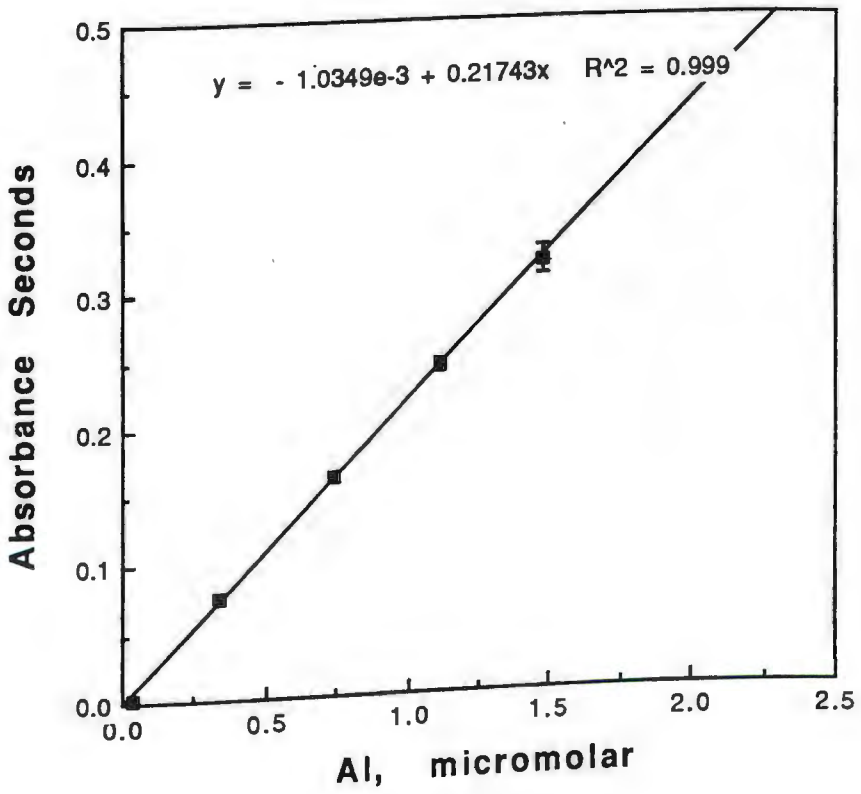

Figure 2.8 Calibration curve for the determination of aluminum in the neutralization titration by graphite furnace AAS.

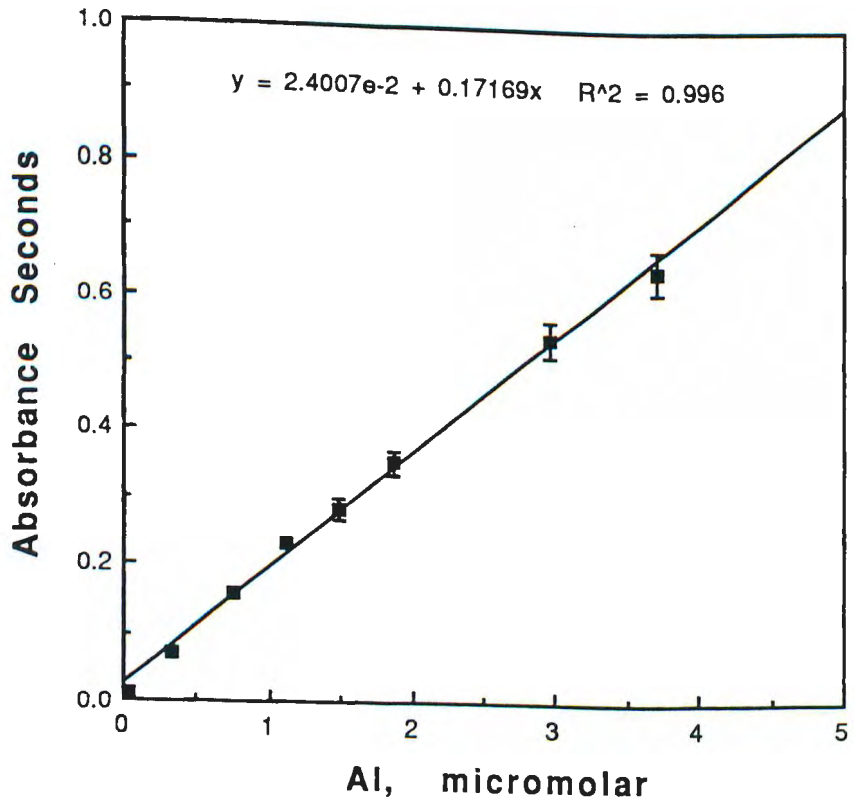

Figure 2.9 Calibration curve for the determination of arsenic in the batch oxidation filtrates by graphite furnace AAS.

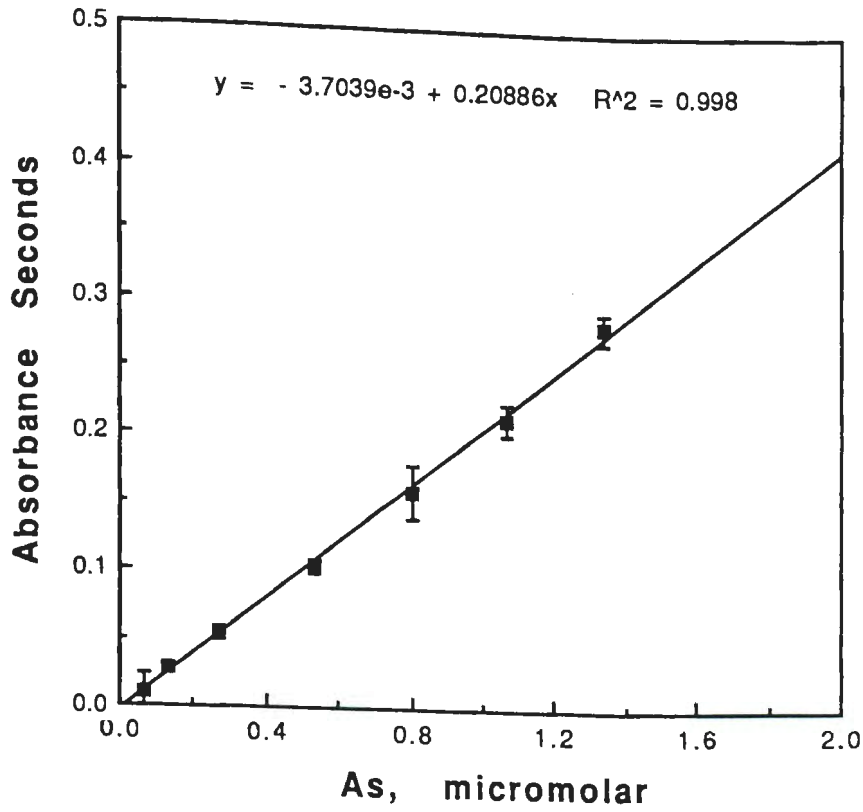

Figure 2.10 Calibration curve for the determination of arsenic in the batch oxidation washes by graphite furnace AAS.

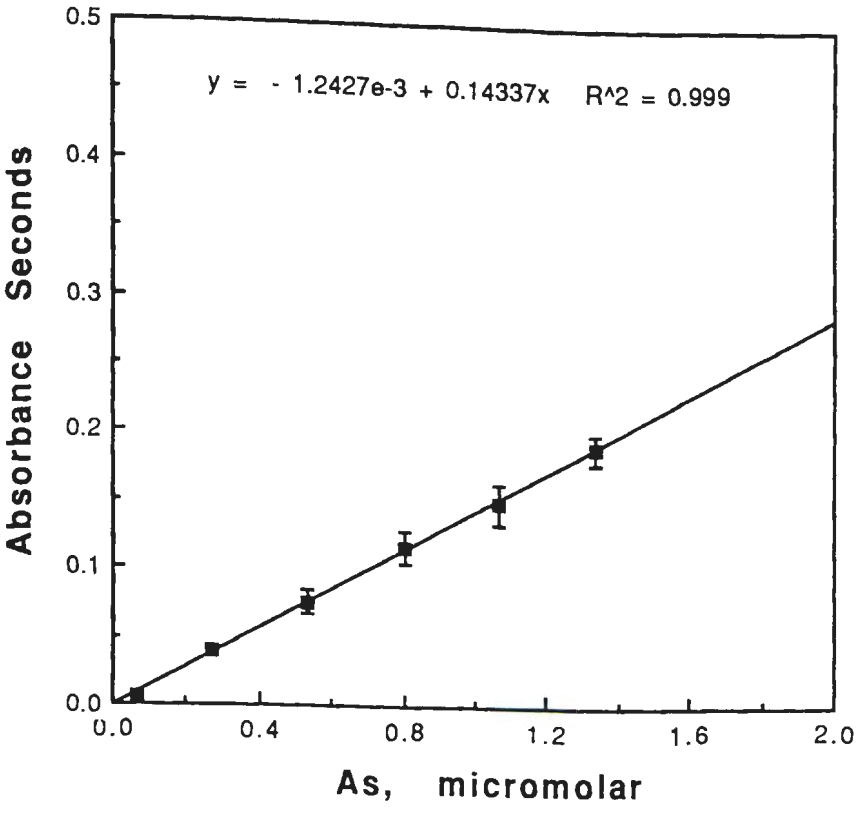

Figure 2.11 Calibration curve for the determination of arsenic in the neutralization titration by graphite furnace AAS.

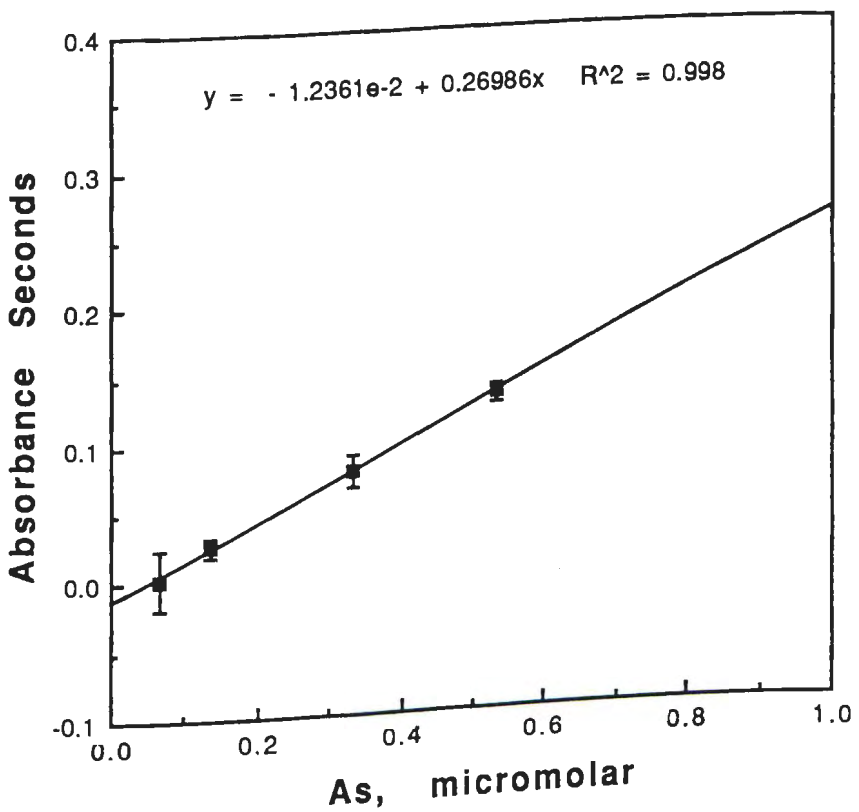

Figure 2.12 Calibration curve for the determination of cadmium in the batch oxidation filtrates by graphite furnace AAS.

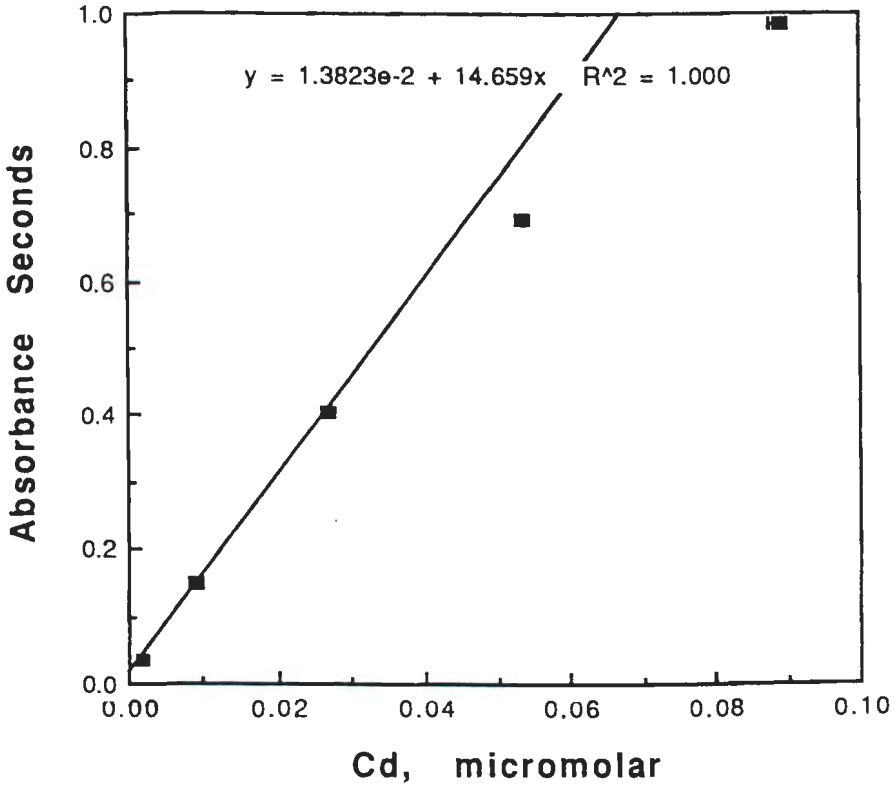

Note: The regression line was fit to only the first three points to avoid the curvature apparent at the higher concentrations. The sample concentrations fell within the apparently linear range.

Figure 2.13 Calibration curve for the determination of cadmium in the batch oxidation washes by graphite furnace AAS.

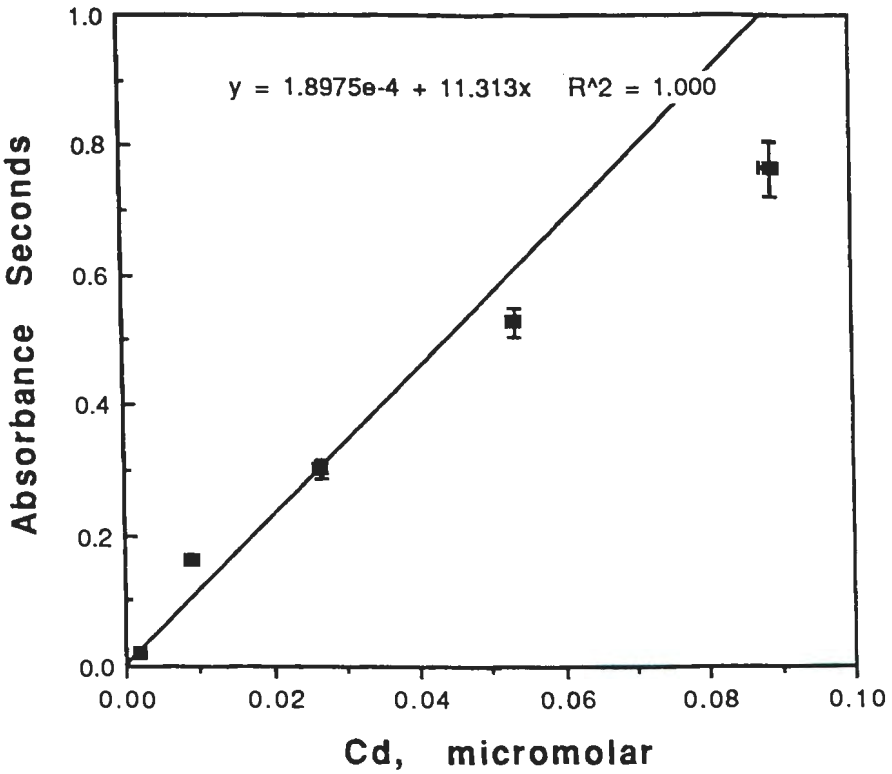

Note: The regression line was fit to only the first and third points, ignoring the erroneous second point, and to avoid the curvature apparent at the higher concentrations.

Figure 2.14 Calibration curve for the determination of cadmium in the neutralization titration by graphite furnace AAS.

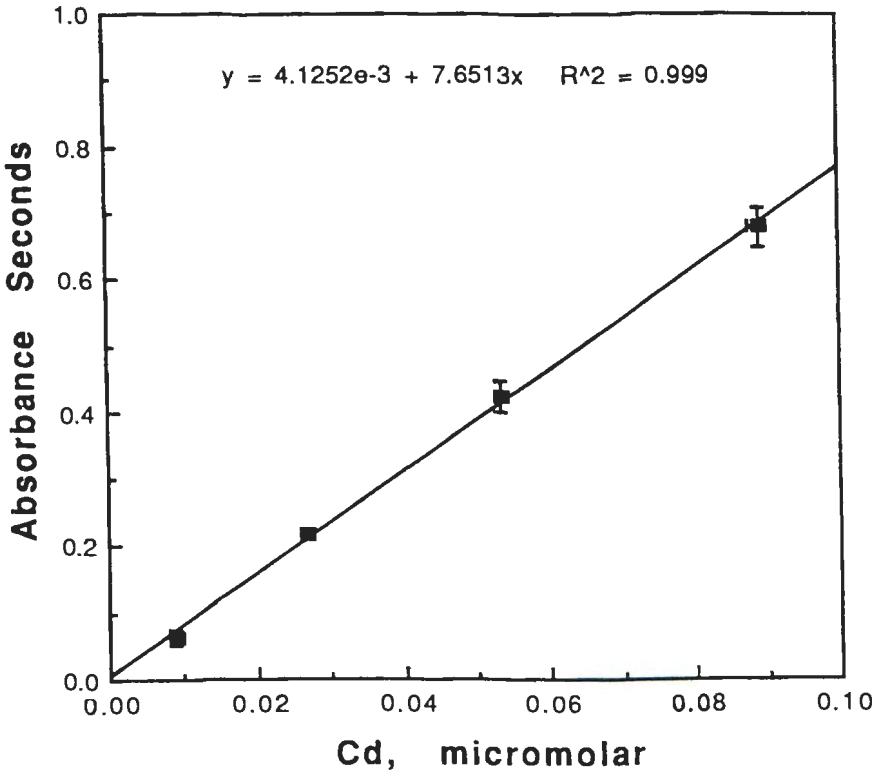

Figure 2.15 Calibration curve for the determination of chromium in the batch oxidation filtrates by graphite furnace AAS.

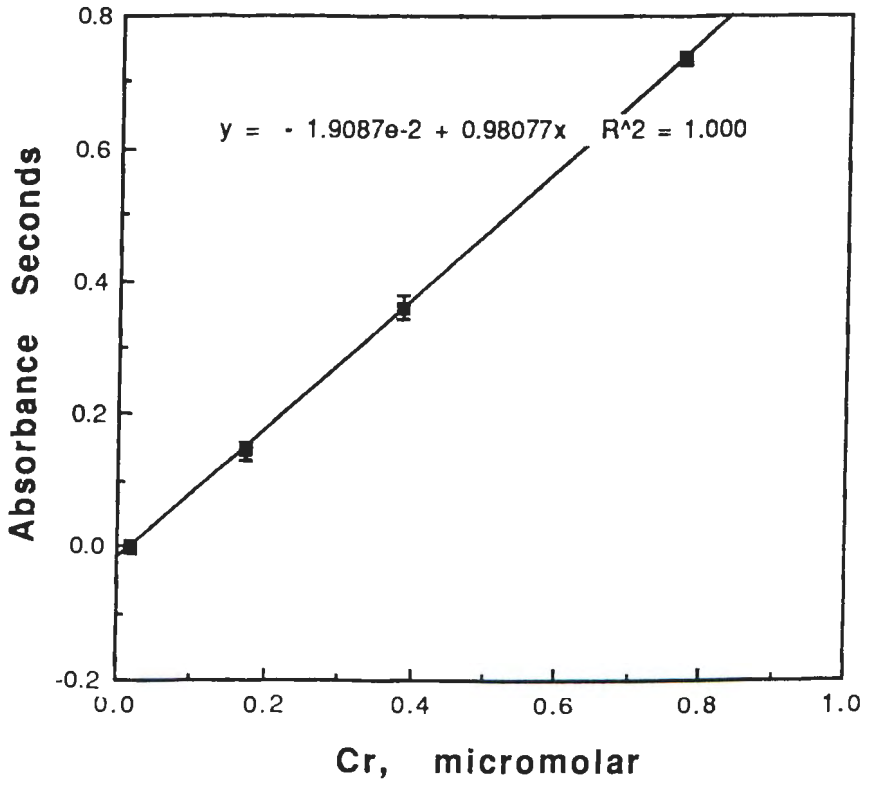

Figure 2.16 Calibration curve for the determination of chromium in the batch oxidation washes by graphite furnace AAS.

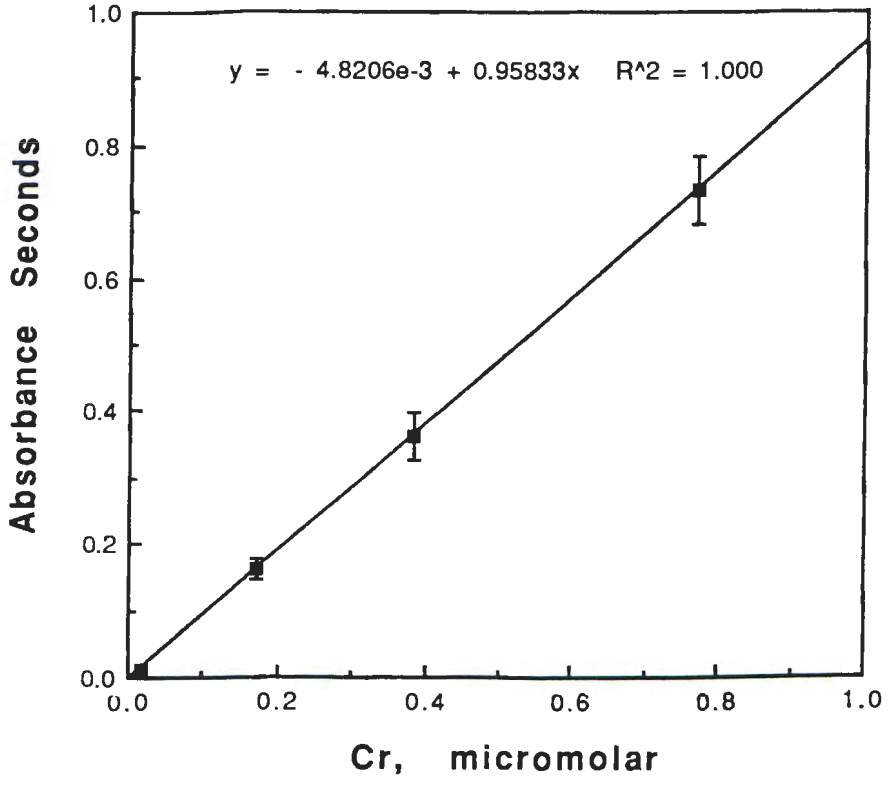

Figure 2.17 Calibration curve for the determination of chromium in the neutralization titration by graphite furnace AAS.

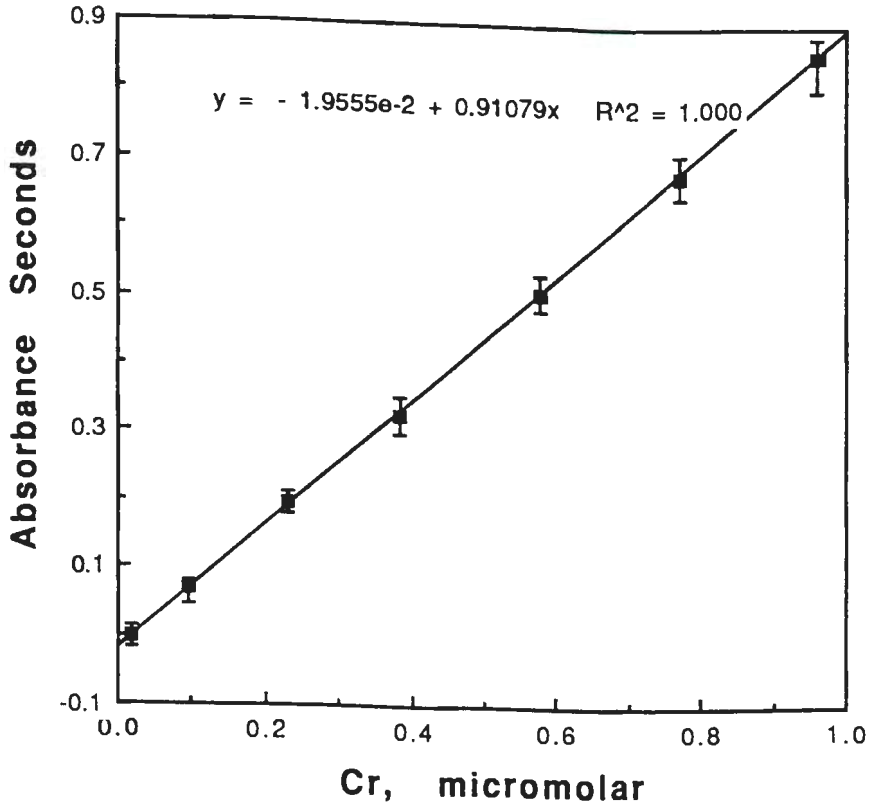

Figure 2.18 Calibration curve for the determination of copper in the batch oxidation filtrates by graphite furnace AAS.

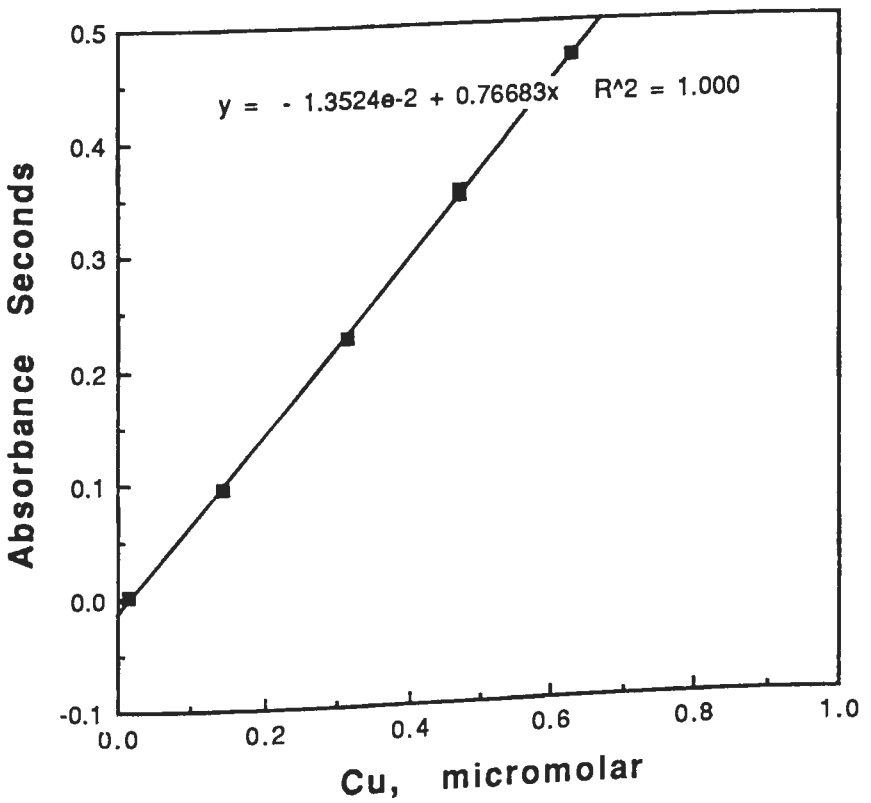

Figure 2.19 Calibration curve for the determination of copper in the batch oxidation washes by graphite furnace AAS.

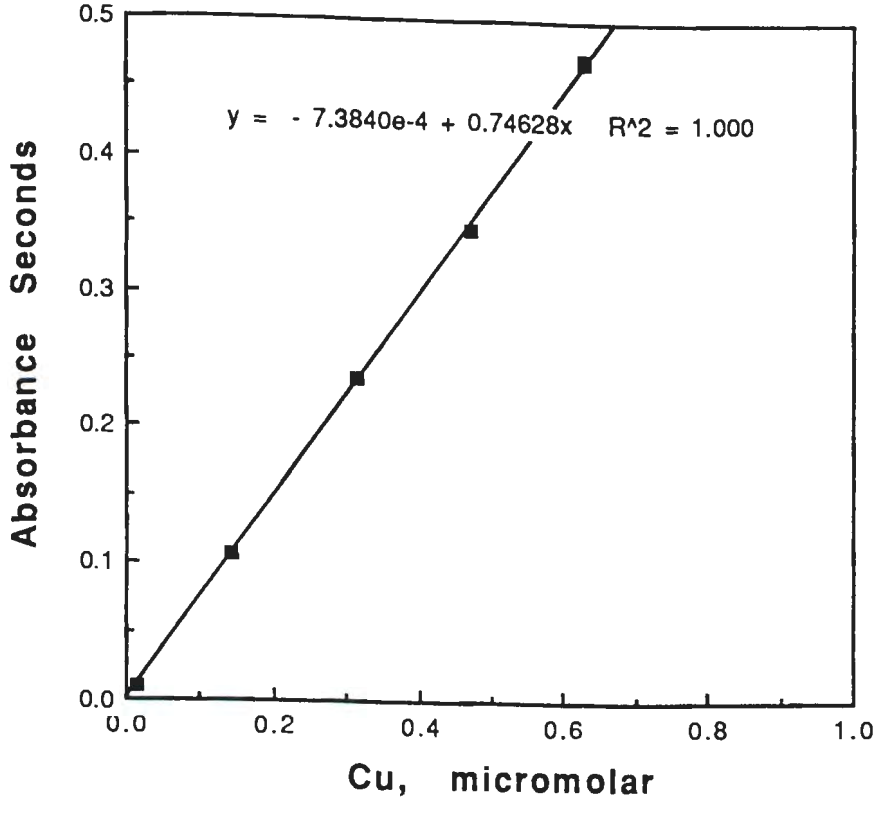

Figure 2.20 Calibration curve for the determination of copper in the neutralization titration by graphite furnace AAS.

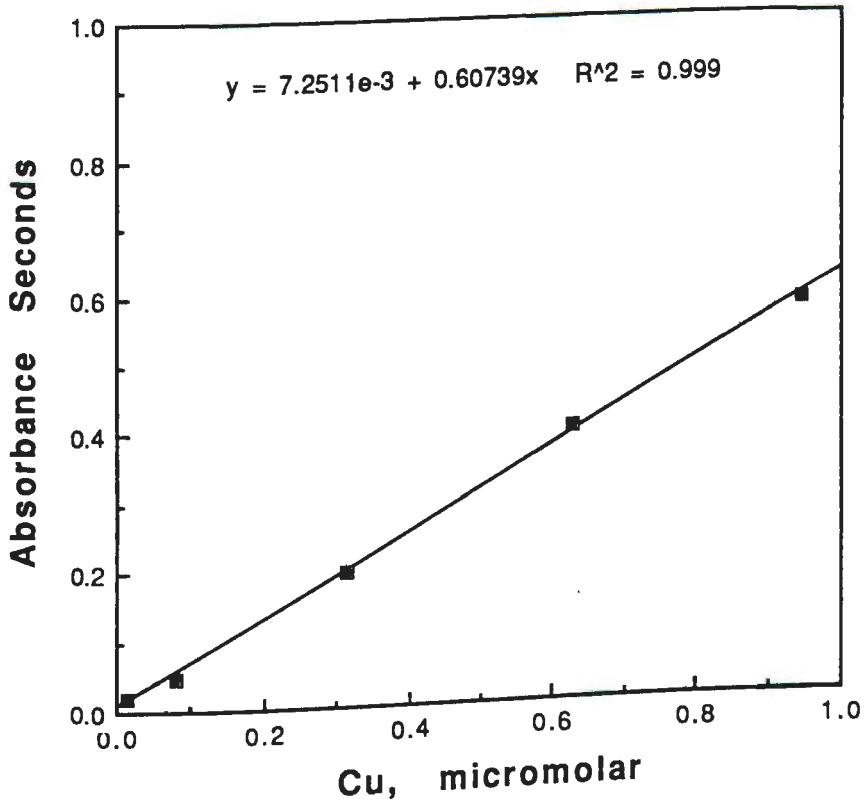

Figure 2.21 Calibration curve for the determination of iron in the batch oxidation filtrates by graphite furnace AAS.

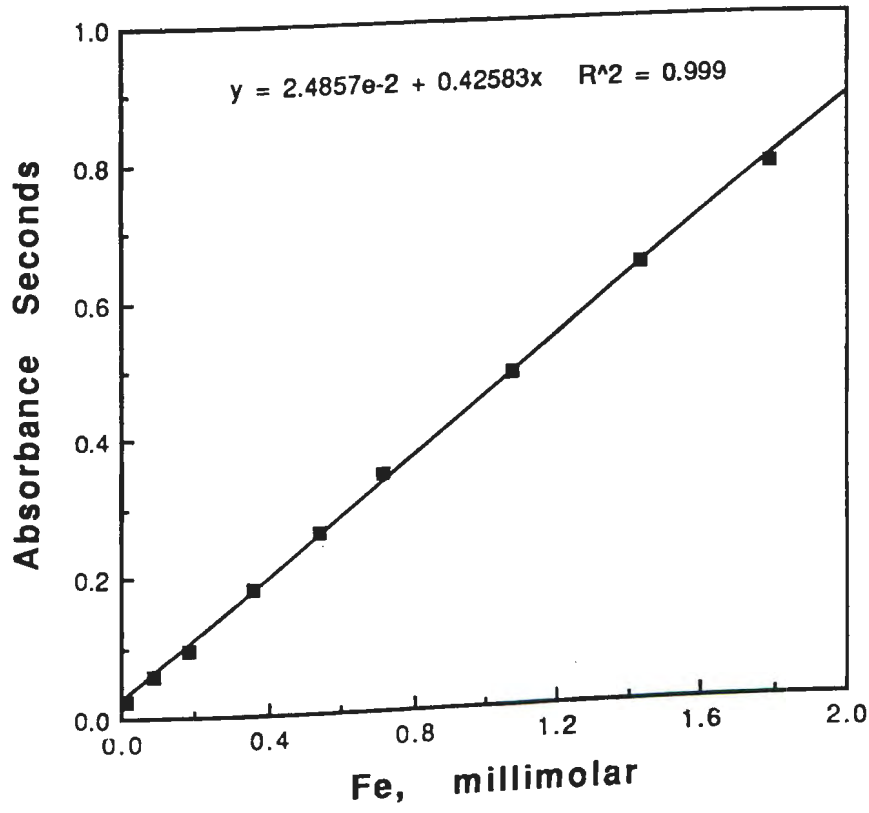

Figure 2.22 Calibration curve for the determination of iron in the batch oxidation washes by graphite furnace AAS.

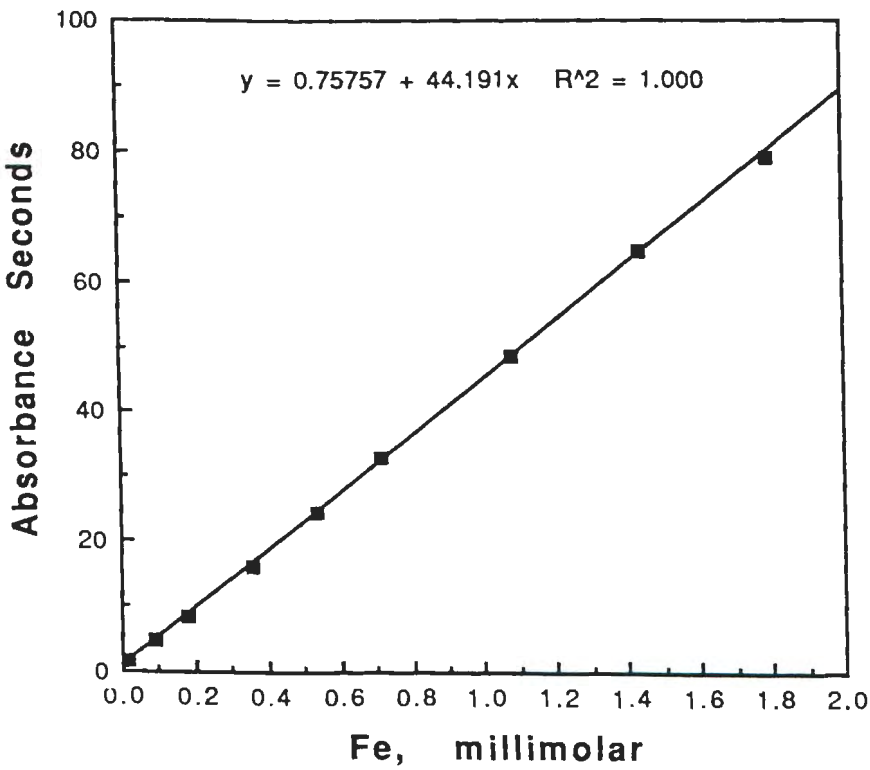

Figure 2.23 Calibration curve for the determination of iron in the neutralization titration by graphite furnace AAS.

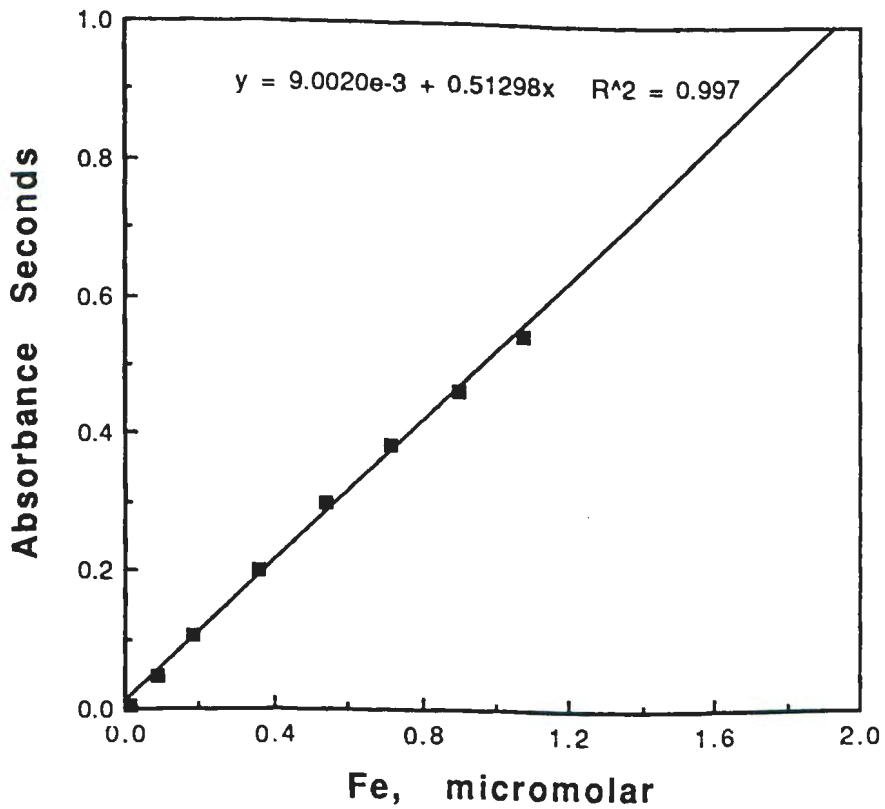

Figure 2.24 Calibration curve for the determination of lead in the batch oxidation filtrates by graphite furnace AAS.

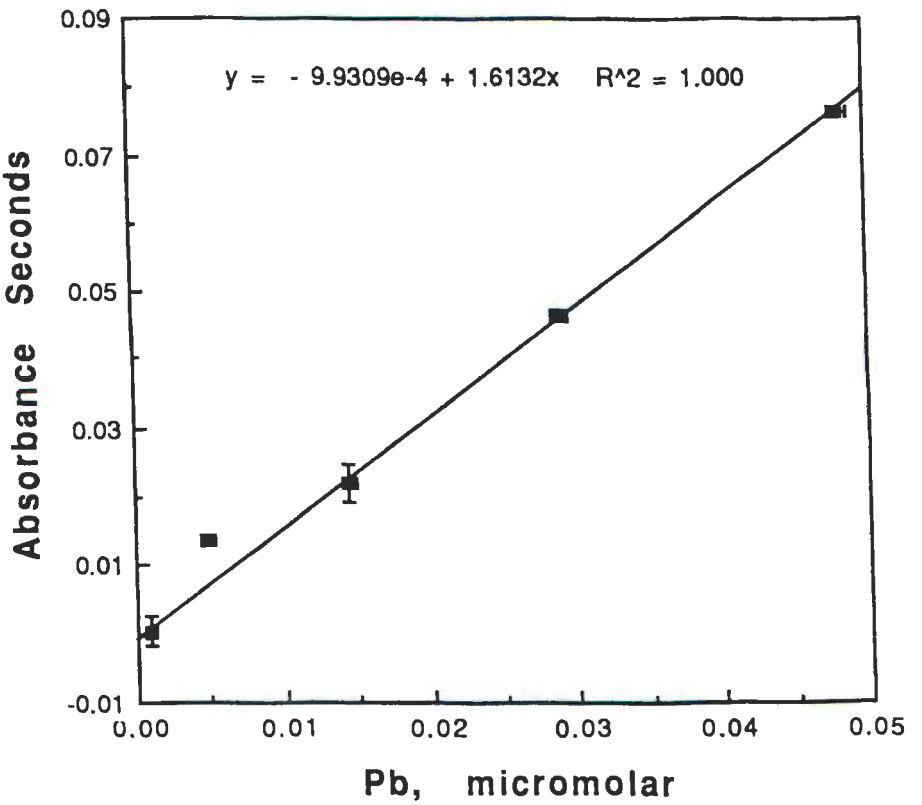

Note: The 0.005 μM standard was not included in the regression line fit. It appears to be erroneous.

Figure 2.25 Calibration curve for the determination of lead in the batch oxidation washes by graphite furnace AAS.

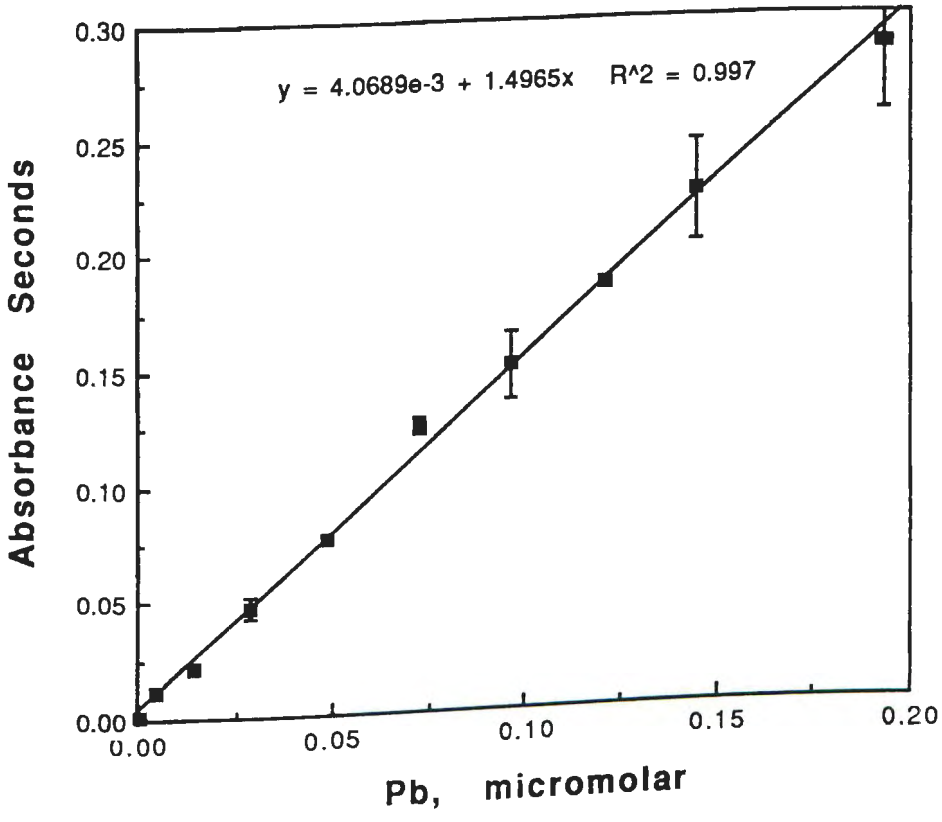

Figure 2.26 Calibration curve for the determination of lead in the neutralization titration by graphite furnace AAS.

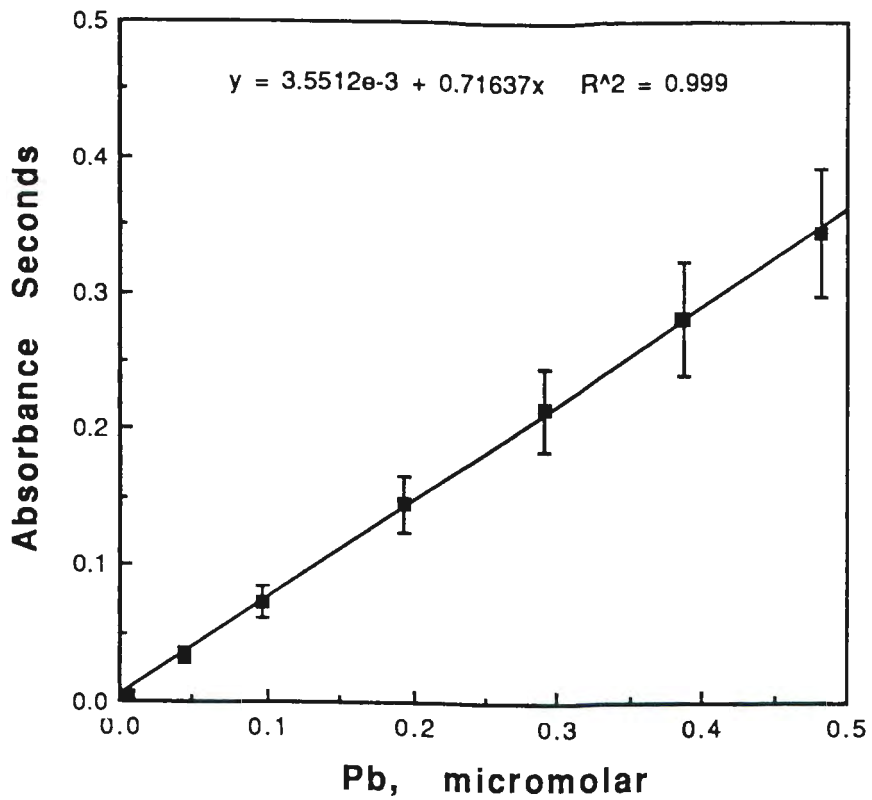

Figure 2.27 Calibration curve for the determination of selenium in the batch oxidation filtrates by graphite furnace AAS.

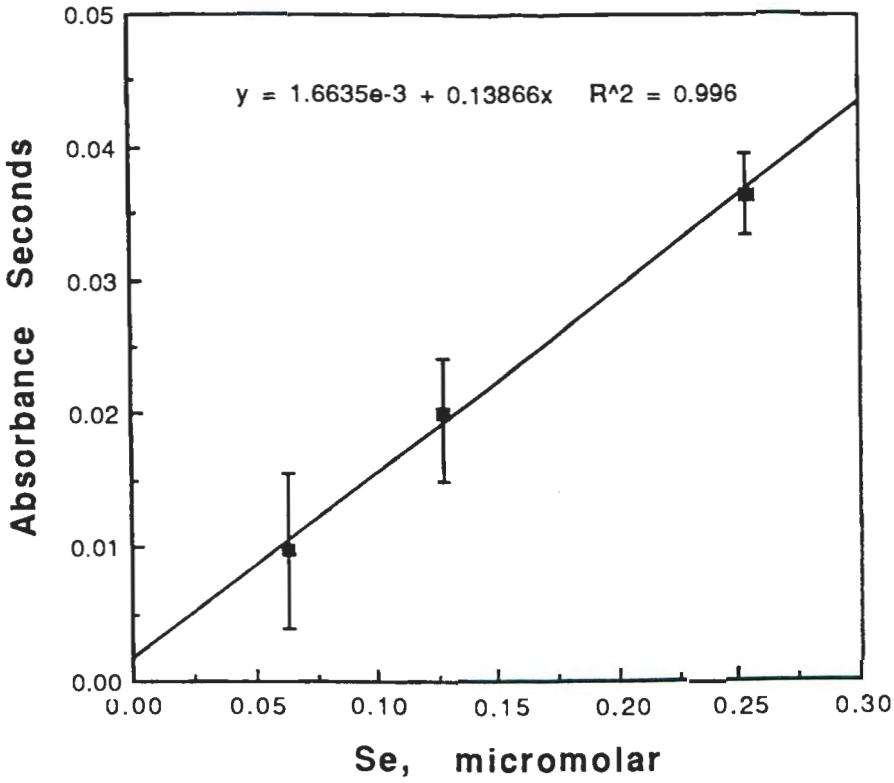

Figure 2.28 Calibration curve for the determination of selenium in the batch oxidation washes by graphite furnace AAS.

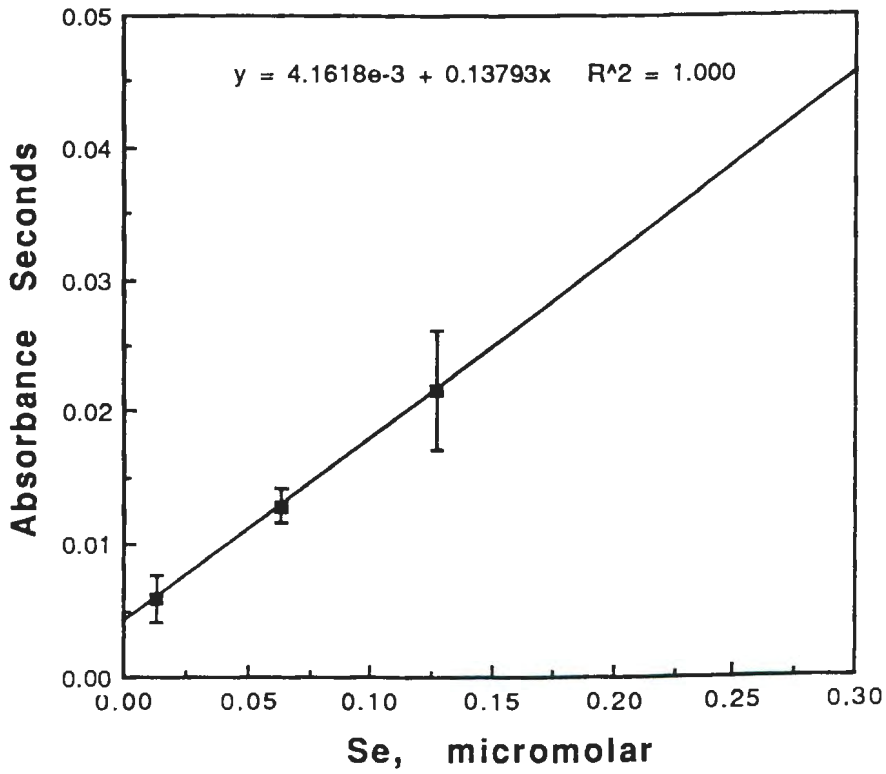

Figure 2.29 Calibration curve for the determination of selenium in the neutralization titration by graphite furnace AAS.

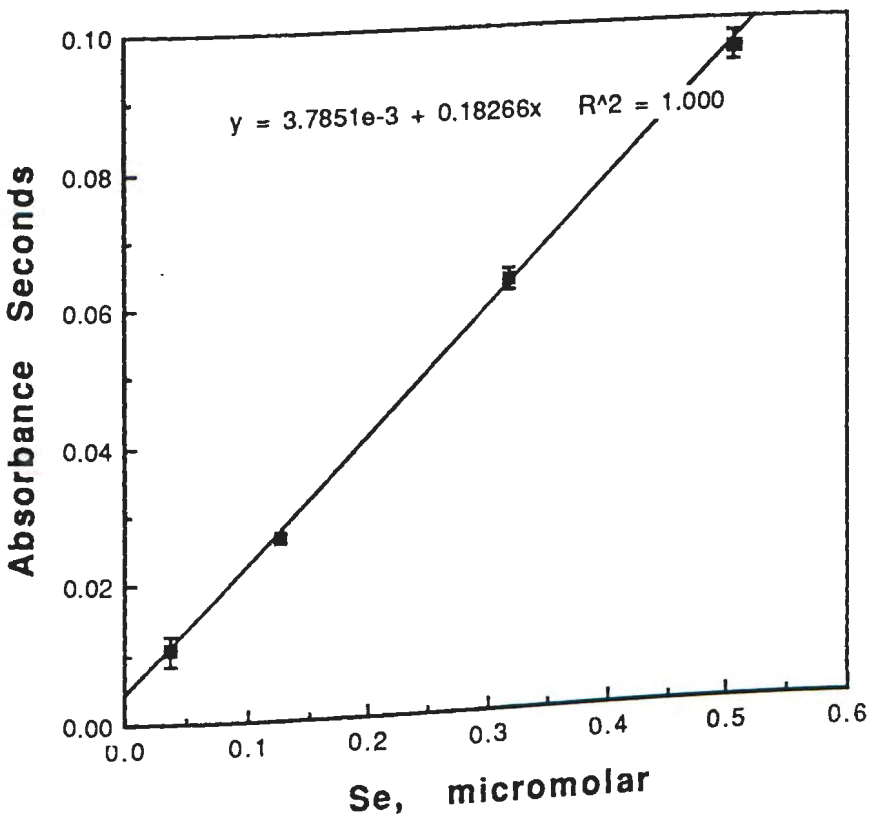

Figure 2.30 Calibration curve for the determination of zinc in the batch oxidation filtrates by graphite furnace AAS.

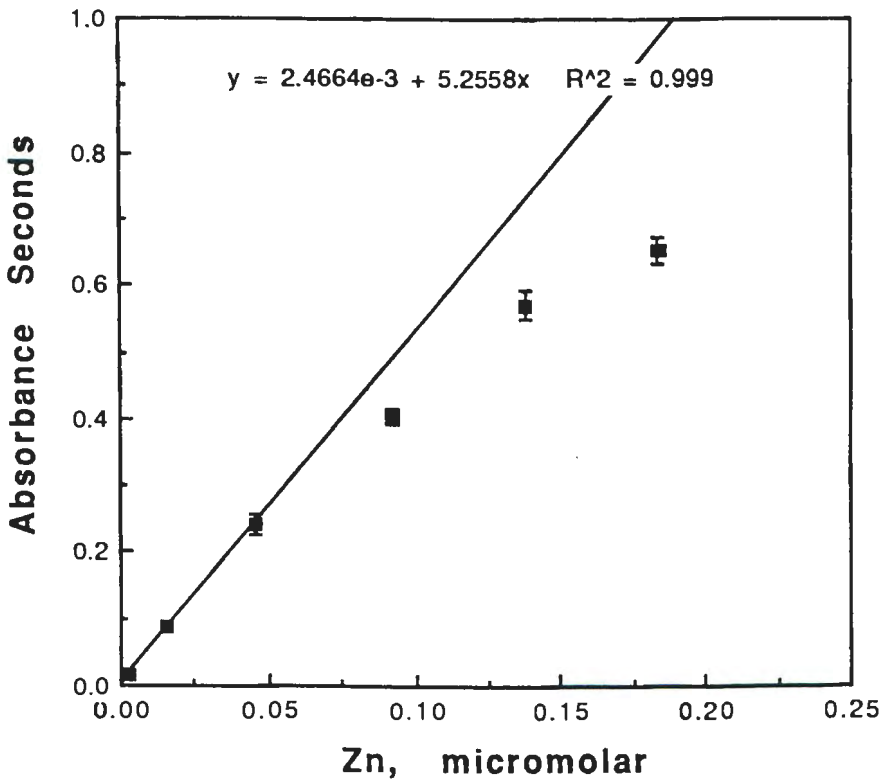

Note: The regression line was fit to only the first three points to avoid the curvature apparent at the higher concentrations. The sample concentrations fell within the apparently linear range.

Figure 2.31 Calibration curve for the determination of zinc in the batch oxidation washes by graphite furnace AAS.

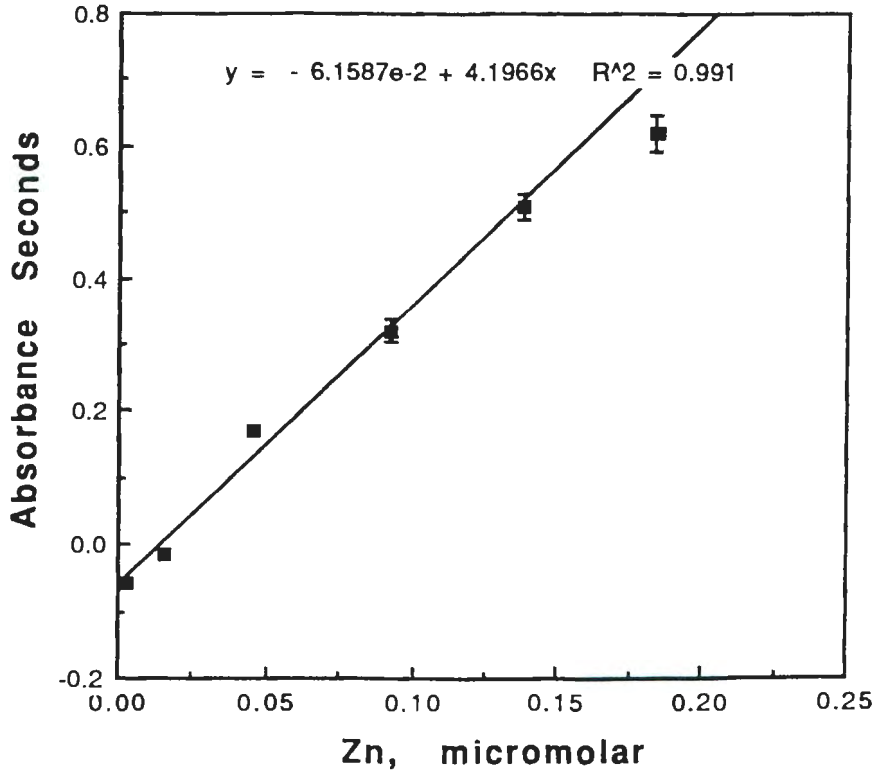

Note: The regression line was fit to only the first 5 points to avoid the curvature that is apparent at the highest concentration. The sample concentrations fell within the apparently linear range.

Figure 2.32 Calibration curve for the determination of zinc in the neutralization titration by graphite furnace AAS.

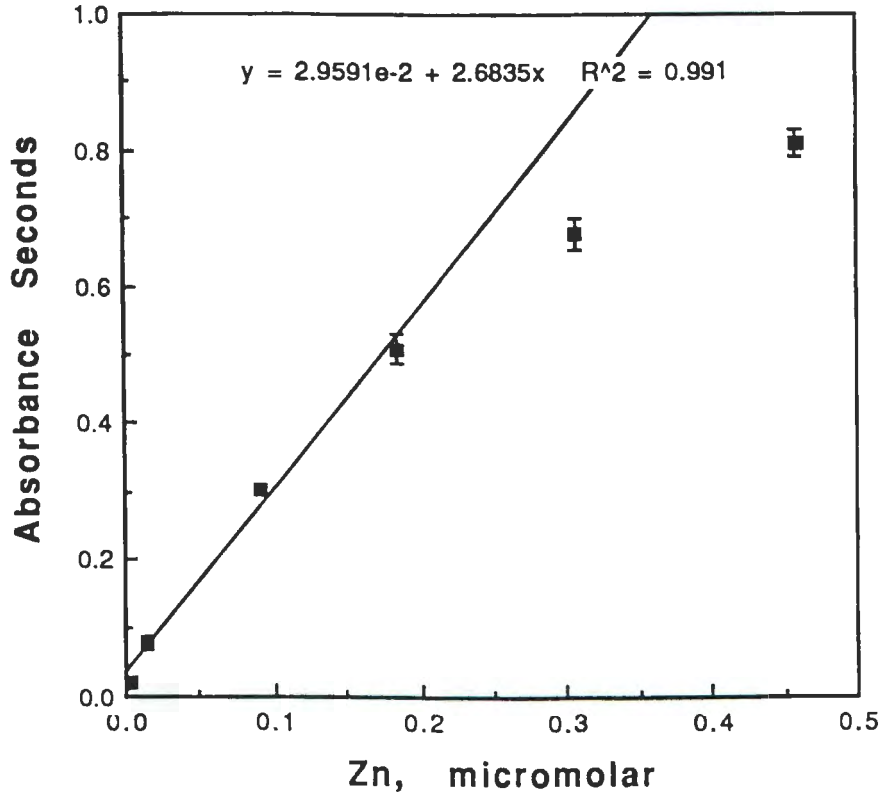

Note: The regression line was fit to only the second, third, and fourth points to avoid the curvature apparent at the higher concentrations. The sample concentrations fell within the linear range.

CHAPTER 3 RESULTS

3.1 RESULTS OF BATCH OXIDATION OF SLURRY OF WHOLE COAL

During this experiment, samples were withdrawn from the slurry every day during the first week, then every two or three days through the second month, and then every three or four days during the third month. The final sample was taken seventy days after the slurry oxidation was initiated.

Table 3.1 lists the data obtained from the filtrate samples for the major dissolved inorganic constituents measured: hydrogen ions as pH, sulfate, iron, and aluminum.

Table 3.2 lists the data obtained from the magnesium chloride wash samples for the major dissolved inorganic constituents measured: sulfate, iron, and aluminum. The pH of each wash sample was not determined; however, the pH of the 1.0 molar wash solution measured 4.56 after being processed through the sampling routine.

Table 3.3 lists the data obtained from the filtrate samples analyzed for the dissolved minor and trace inorganic constituents: arsenic, cadmium, chromium, copper, lead, selenium, and zinc. All these data are reported in micromolar units, which show zinc and copper to be notably more abundant in these slurry filtrate samples than are the other trace elements.

Table 3.1 Major dissolved inorganics measured in Batch Oxidation filtrates.

Date	Day	pH	Tot.SO_4 (mM)	Tot.Fe (mM)	Tot.Al (mM)
Jan 20	0	*5.66 #4.26	<0.001	0.01±.01	<0.004
Jan 21	1	2.50	12.	9.	3.5
Jan 22	2	2.56	15.	10.	
Jan 23	3	2.48	18.5	11.	
Jan 24	4	2.57	16.5	11.	3.3
Jan 27	7	2.54	18.5	12.	4.1
Jan 29	9	2.595	19.	11.	
Jan 31	11	2.535	20.	12.	2.6
Feb 3	14	2.32	22.5	12.	2.7
Feb 5	16	2.195	30.	16.	2.8
Feb 7	18	2.20	36.	21.	2.5
Feb 10	21	2.13	44.	26.	2.5
Feb 12	23	2.11	47.	29.	
Feb 14	25	2.12	51.5	31.	
Feb 17	28	2.095	58.5	34.	2.5
Feb 20	31	2.04	71.	39.	
Feb 24	35	2.04	73.	44.	2.9
Feb 28	39	2.04	73.5	45.	
Mar 3	42	1.99	79.	51.	3.1
Mar 7	46	2.00	85.	54.	
Mar 10	49	1.975	91.	58.	4.7
Mar 14	53	1.96	93.5	62.	
Mar 17	56	1.93	98.	63.	3.4
Mar 21	60	1.94	100±2	68.	
Mar 31	70	1.89±.02	115±5	75±1	3.6

* pH of milli-Q water measured in reaction vessel.
# pH of water after processing through sampling routine.

Table 3.2 Major dissolved inorganics measured in Batch Oxidation washes.

Date	Day	Tot.Fe (mM)	Tot.Al (mM)
Jan 20	0	0.06±.03	
Jan 21	1	1.6	
Jan 22	2	1.9	0.61
Jan 23	3	1.7	
Jan 24	4	2.2	
Jan 27	7	1.8	
Jan 29	9	1.9	0.67
Jan 31	11	2.0	
Feb 3	14	2.3	
Feb 5	16	2.7	0.68
Feb 7	18	3.5	
Feb 10	21	4.1	0.68
Feb 12	23	5.0	0.57
Feb 14	25	5.6	
Feb 17	28	5.9	
Feb 20	31	6.3	0.61
Feb 24	35	7.2	
Feb 28	39	6.4	0.70
Mar 3	42	8.9	0.70
Mar 7	46	9.8	0.71
Mar 10	49	9.65	
Mar 14	53	8.9	
Mar 17	56	11.4	
Mar 21	60	12.3	0.71
Mar 31	70	13.1	0.78

Note: The concentrations are millimoles of analyte per liter of 1.0 M $MgCl_2$ wash solution; but, by experimental design, they also represent millimoles of analyte per liter of slurry.

Table 3.3 Minor and trace dissolved inorganics in Batch Oxidation filtrates.

Day	As (μM)	Cd (μM)	Cr (μM)	Cu (μM)	Pb (μM)	Se (μM)	Zn (μM)
0	0.6	<0.002	0.1+	<0.07	<0.03	<1.7	<0.8
1	1.5+	0.18	1.0+	19.8	0.1+	<1.7	80.
2							
3							
4	1.*	0.19	<0.4	20.5	0.19	<1.7	68.
7	1.*	0.20	1.1+	20.7	<0.03	<1.7	81.
9							
11	1.*	0.22	1.2+	23.2	0.03*	<1.7	71.
14	2.+	0.22	1.2+	28.1	0.03*	<1.7	20
16	3.+	0.23	1.2+	31.9	0.08+	<1.7	82.
18	3.+	0.24	1.7+	36.1	0.04*	<1.7	82.
21	4.5+	0.24	1.8+	36.9	0.04*	<1.7	85.
23							
25							
28	7.7	0.26	2.0	43.9	0.03*	<1.7	88.
31							
35	1.5+	0.28	2.1	55.5	0.03*	<1.7	92.
39							
42	7.0	0.28	2.1	50.6	0.04*	<1.7	89.
46							
49	5.9	0.30	2.7	55.2	0.07+	<1.7	86.
53							
56	1.5+	0.32	2.3	57.7	0.14	<1.7	91.
60							
70	1.5+	0.36	2.6	63.0	0.17	<1.7	101.

* Approximately equal to the limit of detection for this analysis. (See Table 2.7 for LOD and LOQ.)
+ Less than the limit of quantitation, but greater than the limit of detection for this analysis.

Table 3.4 lists the data obtained from the magnesium chloride wash samples analyzed for the same dissolved minor and trace inorganic constituents: arsenic, cadmium, chromium, copper, lead, selenium, and zinc. All these data are also reported in micromolar units. Again,

zinc and to a lesser extent copper, are seen to be notably more abundant in these magnesium chloride wash samples than are the other trace elements.

Table 3.4 Minor and trace dissolved inorganics in Batch Oxidation washes.

Day	As (μM)	Cd (μM)	Cr (μM)	Cu (μM)	Pb (μM)	Se# (μM)	Zn (μM)
0	14-15	<0.001	1.7+	1.1	<0.01	0.7	3.
1	1.*	0.03	1.6+	3.+	0.2	<0.76	19.
7	<1.	0.01+	1.8+	3.5+	0.1+	<0.76	19.
9							
11	<1.					<0.76	
14	1.*	0.01+	2.6+	5.4	0.1+	<0.76*	22.
16							
18	1.5+	0.02+		6.3	0.1+	<0.76	21.
21		0.01+	2.4+	7.3	0.1+		24.
23	2.5+					<0.76	
25							
28	3.+	0.02+	2.2+	8.3	0.1+	<0.76	21.
31							
35	5.+	0.02+	2.5+	8.6	<0.03	<0.76	21.
39							
42	5.+	0.02+	2.5+	10.5	0.9	1.0+	24.
56	7.2	0.02+	2.4+	12.9	1.8	1.0+	26.
60							
70	8.8	0.02+	2.3+	14.0	1.8	0.8*	26.

Not corrected by standard additions since the signals were near the detection limit.
* Approximately equal to the limit of detection for this analysis. (See Table 2.7 for LOD and LOQ.)
+ Less than the limit of quantitation, but greater than the limit of detection for this analysis.

Note: The concentrations are micromoles of analyte per liter of 1.0 M $MgCl_2$ wash solution; but, by experimental design, they also represent micromoles of analyte per liter of slurry.

3.2 RESULTS OF $NaHCO_3$ TITRATION OF SYNTHETIC SOLUTIONS

During the titration of the synthetic acid - sulfate - ferric iron solution doped with selected trace elements, samples were withdrawn only after an equilibration period of approximately twenty hours or longer following each titration segment. Table 3.5 lists the data obtained from these samples for the major dissolved constituents measured: hydrogen ions as pH, iron, and aluminum.

Table 3.5 Major dissolved constituents measured in Titration experiment filtrates.

Sample Number	pH	Tot.Fe (mM)	Tot.Al (mM)
1	1.575	100.	0.56
2	1.97	99.	0.39
3	2.44	96.	0.37
4	2.295	71.	0.38
5	2.36	55.	0.38
6	2.305	37.	0.40
7	2.475	13.	0.48
8	2.875	1.1*	0.59
9	3.515	<0.1	0.24
10	3.90	<0.01	0.14
11	4.83	<0.01	0.13
12	5.745	<0.01	0.12
13	5.55	<0.01	0.13

* Approximately equal to the limit of detection for this analysis. (See Table 2.7 for LOD and LOQ.)

Table 3.6 lists the data obtained from the titration samples for the dissolved minor and trace constituents: arsenic, cadmium, chromium, copper, lead, selenium, and zinc. All these data are reported in micromolar units.

Table 3.6 Minor and trace dissolved constituents in Titration filtrates.

Sample Number	As (μM)	Cd (μM)	Cr (μM)	Cu (μM)	Pb (μM)	Se (μM)	Zn (μM)
1	1.2	9.2	22.	15.1	4.7	2.7	28.
2	1.+	8.5	21.	14.6	2.6	2.+	24.
3	1.+	7.9	21.	14.1	3.9	2.6	24.
4	1.+	7.8	17.	13.5	4.0	1.+	26.
5	0.9+	8.0	18.	14.0	3.6	0.8+	31.
6	0.9+	8.3	17.	15.0	0.5	<0.5	36.
7	0.7*	7.7	14.	13.7	0.1+	<0.5	32.
8	0.9+	7.5	10.	13.7	0.1+	<0.5	33.
9	0.8+	8.4	2.9+	9.7	<0.06*	<0.5	28.
10	0.7*	8.5	1.4+	2.9+	<0.06	<0.5	25.
11	0.6*	8.5	<0.6*	<0.8*	0.1+	<0.5	17.
12	0.7*	6.3	<0.6	<0.8	0.1+	<0.5	4.+
13	0.7*	5.0	<0.6	<0.8	0.07*	<0.5	3.+

* Approximately equal to the limit of detection for this analysis. (See Table 2.7 for LOD and LOQ.)
\+ Less than the limit of quantitation, but greater than the limit of detection for this analysis.

CHAPTER 4 DISCUSSION

4.1 OXIDATION OF WHOLE COAL

The primary objective of this first experiment was reconnaissance of a natural oxidation of a slurry of ground whole Eastern (U.S.A.) coal in water saturated with air. We wanted to observe the time of release and build-up of selected inorganic components in the filtrates, as well as determine their total concentration in this most mobile fraction of the system.

4.1.1 Reaction Progress

The filtrates from this experiment were found to be oxidized and acidic from the beginning. The first sample, taken one day after the coal was slurried, had a pH of 2.50 and iron and sulfate concentrations of 9 and 12 mM, respectively. The immediate release of these oxidation products indicates that the coal had weathered to some extent before being used in this experiment.

Figure 4.1 shows that the system pH hovered around 2.5 for at least the first 11 days. Comparison with Figure 4.2 shows that during this same period the filterable iron concentration plateaued, but the sulfate concentration rose gradually. This indicates that oxidation of presumably pyritic material was proceeding slowly and releasing sulfate. The cogenerated acidity must have

Figure 4.1 pH of the batch oxidation samples as a function of time.

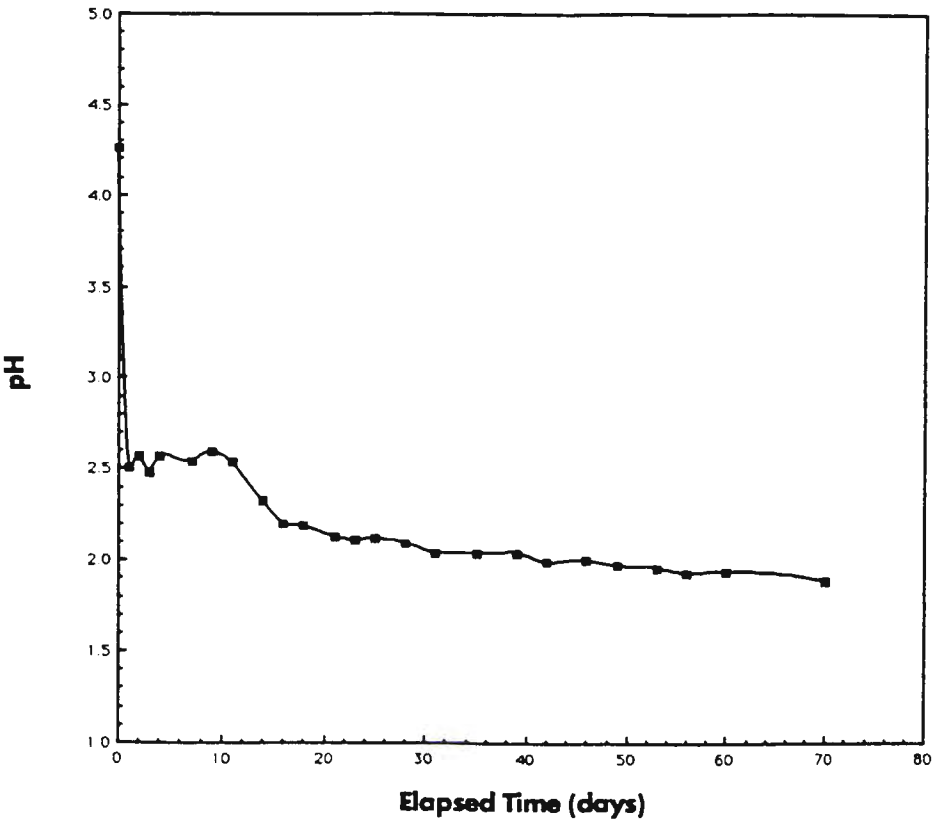

Figure 4.2 Accumulation of total filterable sulfate and iron in the batch filtrates, and of iron in the magnesium chloride wash solutions.

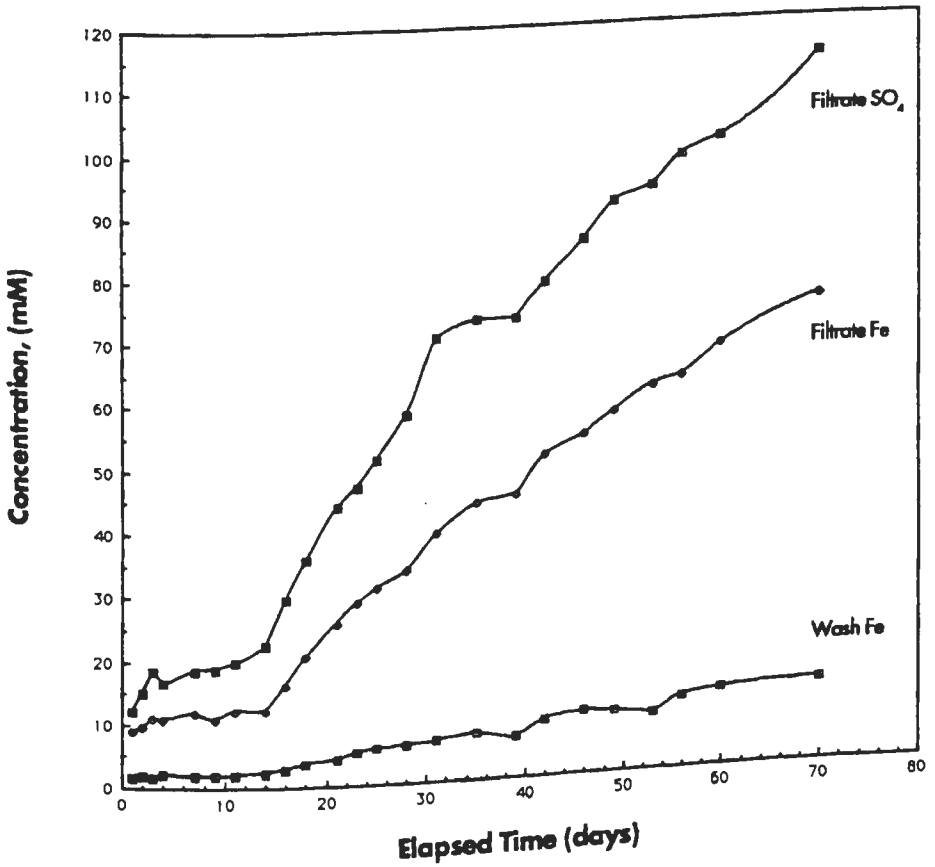

been neutralized by alkaline substances present initially in the coal. The presence of alkalinity in general, and solid carbonates in particular, has been cited as important in controlling the buildup and release of acidity in mine materials associated with pyrite (Kleinmann et al. 1981, Olem 1982, Wangen & Jones 1984). Carbonate minerals such as calcite and siderite are found associated with coals from the Eastern United States, (Kuhn et al. 1980). The extreme dependence of iron solubility on pH accounts for the constant concentration of iron in solution during this period of buffered pH.

After day 11 the pH of the samples dropped rapidly signalling the exhaustion of the alkaline components of the system. Highly insoluble ferric hydroxides become soluble below pH 3 (Langmuir and Whittemore 1971, McAndrew et al. 1975, Dousma and de Bruyn 1976, Kleinmann 1981). Further, the resultant aqueous ferric iron oxidizes iron pyrite directly according to the overall reaction:

Eqn. 4.1

$$FeS_2 + 14Fe^{3+} + 8H_2O = 15Fe^{2+} + 2SO_4^{=} + 16H^{+}$$

This catalytic cycle of pyrite oxidation is completed by the regeneration of Fe^{3+} from Fe^{2+} by the autotrophic bacteria Thiobacillus ferrooxidans. Thus, the rate of oxidation is greatly accelerated by the fall of pH below 2.5 in the presence of T. ferrooxidans. (See Temple and Delchamps 1953, Garrels and Thompson 1960, Kuznetsov et

al. 1962, Silverman 1967, Kleinman et al. 1981, and Nordstrom 1982.)

On day 14 a slight jump in sulfate concentration was seen, and by day 16 both sulfate and iron concentrations had increased significantly. Thereafter, they built up rapidly in the filtrates in a ratio that approaches the stoichiometry of $Fe_2(SO_4)_3$. The molar ratio of sulfate to iron in the filtrates is shown in Figure 4.3. From early in the experiment the ratio was less than 2, the theoretical ratio of SO_4 to Fe(III) that should result from the oxidation of pyrite according to equation 1.5.

Weathering of the coal would have commenced as soon as it was mined and exposed to air and moisture. The initial oxidation products would be sulfate and, at pH's greater than 3, highly insoluble ferric hydroxides; (see Figure 1.1). Prior to our receipt of the coal, it had been processed to reduce sulfur and ash content, then shipped in open coal cars and stored outside. Thus, it is probable that a reservoir of insoluble iron accumulated while the soluble sulfate and cogenerated acidity were flushed from the system.

During our experiment, the oxidation of pyrite would have generated SO_4 and Fe(III) in a 2:1 ratio; but as soon as the pH fell to 2.5 and below, the gradual dissolution of the reservoir of ferric hydroxides apparently

Figure 4.3 Ratio of the molar concentrations of sulfate to iron in the batch oxidation filtrates.

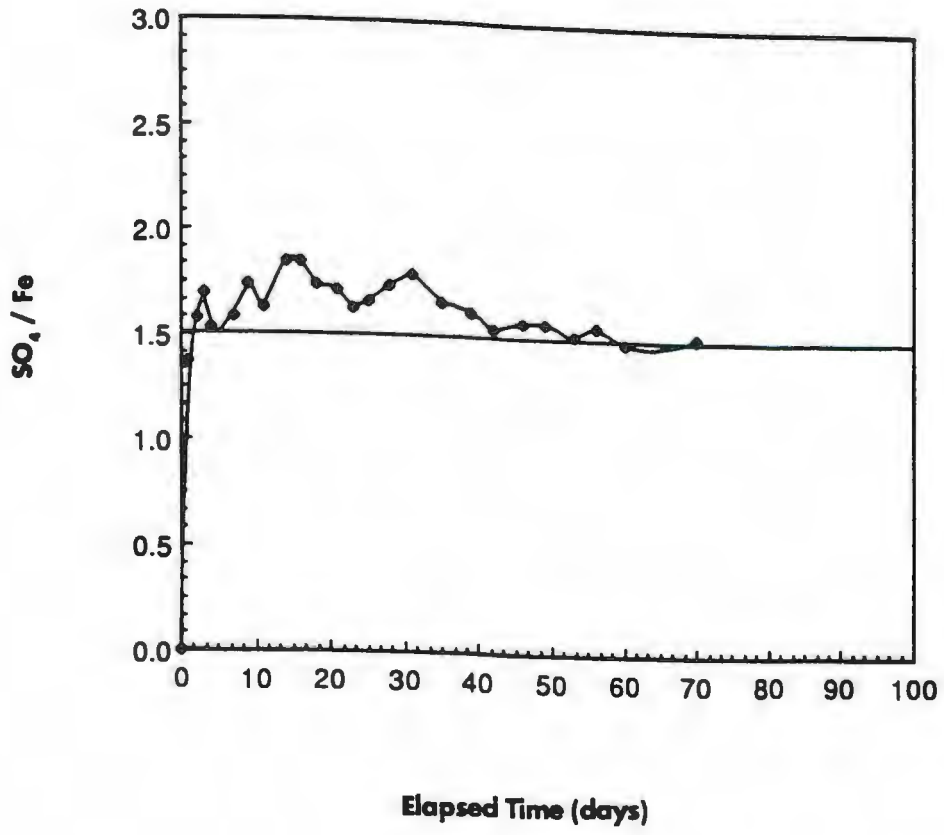

reduced the ratio at which sulfate and iron accumulated in solution.

The causes for the "hump" in the sulfate plot (Figure 4.2) and the dips in the plot of iron in the magnesium chloride washes are unknown. The relatively low concentrations found in the sample from day 39 are due to a procedural error in which the filtrate was diluted by a small but unknown amount. Apparently the error also affected the wash sample.

The iron in the magnesium chloride wash samples appears to follow the iron levels in the filtrates but at a fraction of their concentration. The ratio of iron in the washes to iron in the filtrates averaged very close to 0.17 throughout the experiment. An estimate of the volume of filtrate retained by the captured solids and by the filter systems themselves and its subsequent inclusion in the wash solution accounts for a roughly 17 percent carryover. This is assumed to be the source of the iron in the wash samples, rather than adsorbed iron that was desorbed by the ion exchange wash solution.

Figure 4.4 is a logarithmic plot of the total micromolar concentration of each analyte measured in the filtrates versus the elapsed time in days between when the coal was slurried and when the sample was taken. It shows the relative concentrations of each analyte and allows for comparison between analytes of their respec-

Figure 4.4 Logarithmic plot of the total micromolar concentration of each analyte in the batch oxidation filtrates as a function of elapsed time in days.

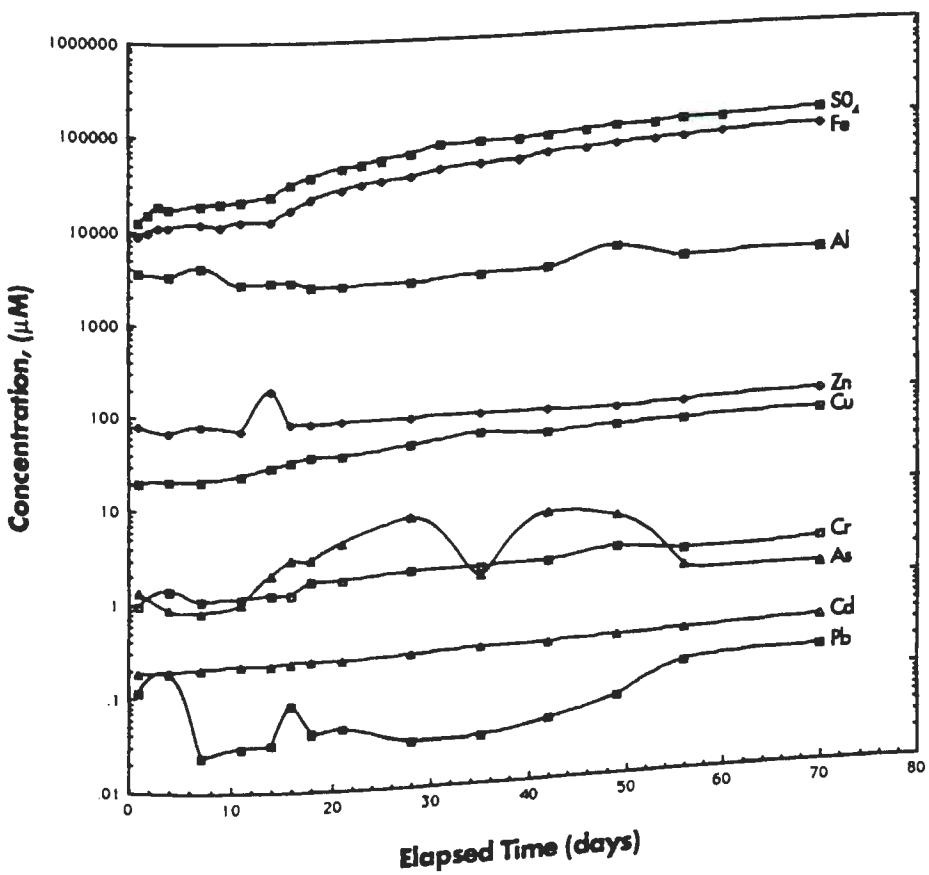

tive time of release and rate of build-up in the filterable portion of the samples. Figure 4.5 is a similar logarithmic plot of the total micromolar concentration of each analyte measured in the 1.0 molar magnesium chloride wash of the filter cake of each sample. (Recall that each wash solution was poured repeatedly through the still-wet solids and otherwise undisturbed apparatus that had just been used to handle the filtrate, in an effort to collect species that may have sorbed onto surfaces of the apparatus.)

Clearly sulfate and iron are dominant in the filtrates, with iron closely tracking the release and build-up of sulfate. Iron is presented as being the major dissolved inorganic substance in the washes; though the wash solution was 1.0 molar magnesium chloride, and sulfate was not measured in the washes because the high concentration of chloride swamped the ion chromatograph. In both media aluminum is a minor constituent whose concentration is from 0.5 to 1.5 orders of magnitude below that of iron. The concentrations of the trace elements are orders of magnitude lower, but their relative order is substantially the same in both media. Although the arsenic and chromium curves cross, in both plots arsenic is dominant in most of the samples. Cadmium and lead clearly exchange positions as the analyte of lowest concentration measured. (However, in both the

Figure 4.5 Logarithmic plot of the total micromolar concentration of each analyte in the 1.0 molar magnesium chloride wash (of the filter cake of each sample from the batch oxidation) as a function of time in days.

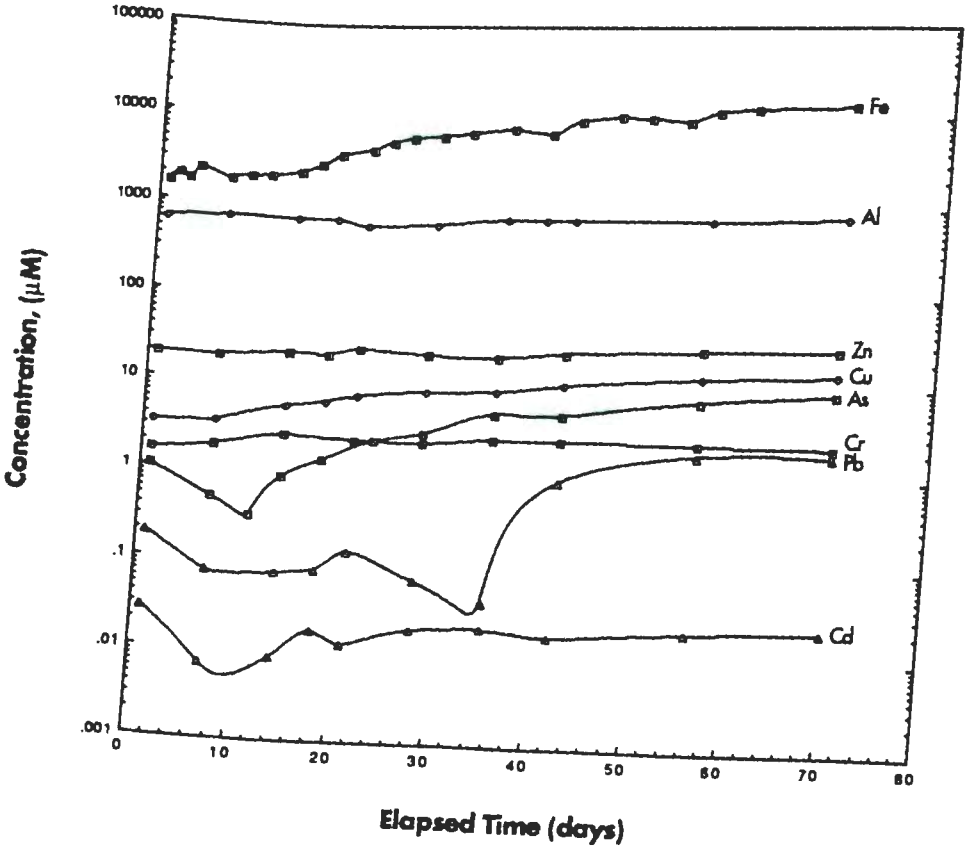

analysis of the filtrates and the analysis of the washes, most of the lead values were below the limit of quantitation; see Tables 3.3 and 3.4.)

4.1.2 Trace Elements

Figures 4.6 through 4.12 are individual plots for each analyte of their total concentration as found in both filtrate and wash samples. These minor and trace constituents will be discussed in the order of their average concentration in the filtrates.

The results for aluminum are plotted in Figure 4.6. Aluminum in the filtrates ranged from 2.5 to 3.6 mM and averaged about 3 mM, ignoring the values from days 7 and 49 which appear to be erroneous. Significant aluminum contamination can be introduced into the samples as dust. (This is particularly likely here since the sample tray of the AS-40 autosampler was of aluminum that had oxidized to some extent.) The apparently lower concentrations in the samples collected between days 10 and 30 are unexplained except as perhaps experimental, sampling, handling, and analytical variation; although they appear to be systematic rather than random. Aluminum in the washes ranged from 0.61 through 0.78 mM and averaged almost 0.70 mM. The value from day 21 is too low because

Figure 4.6 Aluminum in filtrates and washes of the batch oxidation as a function of elapsed time.

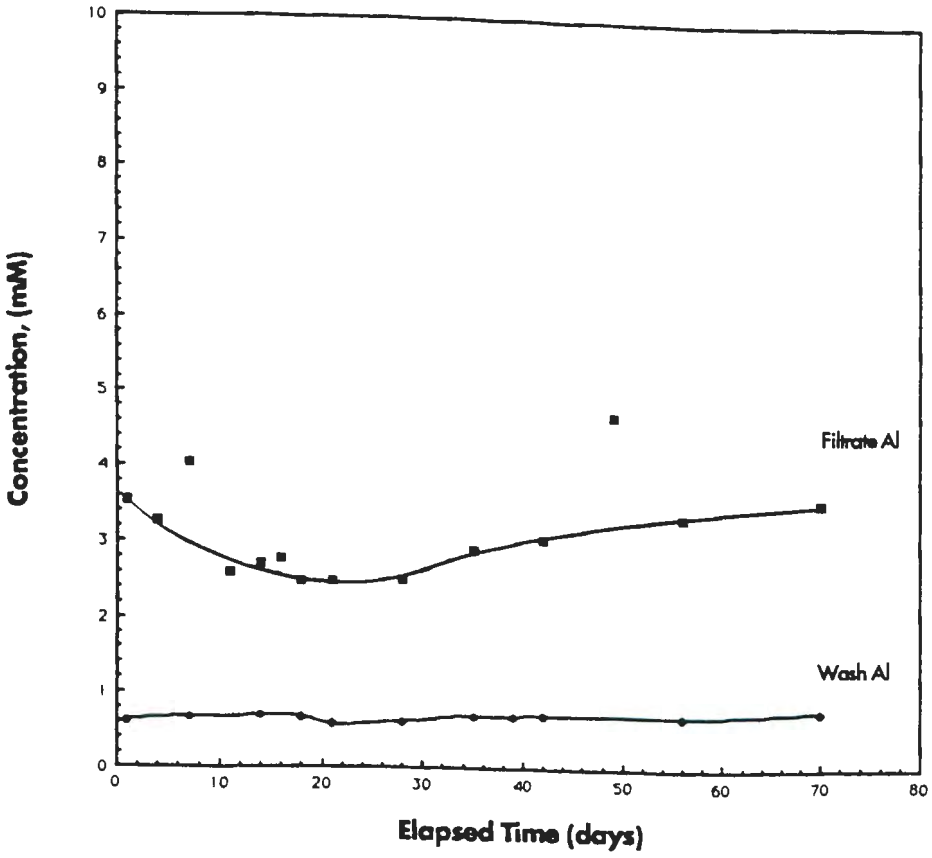

Notes: Concentrations are millimolar. The smooth curve for filtrate aluminum was drawn ignoring the values from days 7 and 49, which appear to be erroneous. The curve for wash aluminum is interpolated between points.

of a procedural error that resulted in little or no carryover of the filtrate liquid into the wash sample.

Neither aluminum in the filtrates or the washes tracked iron; but rather in both cases aluminum concentrations were relatively constant throughout the experiment. The ratio of aluminum in the washes to that in the filtrates was 0.17 for days 1 through 6, which matches the average ratio of iron in the washes to that found in the filtrates. Throughout the rest of the experiment, the aluminum ratio varies from 0.26 to 0.21, which is caused by the systematic variation of the filtrate values. These observations suggest that the solubility of aluminum in coal leachates is not controlled significantly by the extent of oxidation of the coal, by pH changes in the range 2.6 to 1.9, or by ion-exchange with relatively high concentrations of magnesium and chloride ions. The most likely source of the aluminum is the kaolinite and illite and any alunite in the coal.

Silicate and clay minerals are commonly found associated with coals. Aluminum is a major constituent of many of these minerals. Heaton et al. 1982, reported a strong positive correlation between aluminum in Eastern coal waste samples and kaolinite, illite, and quartz components of those wastes. Helz et al. 1987, postulated a trace aluminum phase that was highly soluble in acid and quickly depleted, with the remainder of the aluminum

in the system relatively resistant to acid leaching. A system including some alunite as well as kaolinite and illite could account for observations like those.

Zinc does not appear to track iron build-up in the filtrates, (Compare Figure 4.7 with Figure 4.2). The range of zinc concentration in the filtrates was from 68 to 101 micromolar, with an average of about 84 μM. Its range in the washes was from 19 to 26 μM with an average of about 22 μM. In both sets of data the variation is rather random. The ratio of zinc in the washes to that in the filtrates varies rather systematically from 0.235 to 0.27, which shows the magnesium chloride washes to be slightly enriched in zinc compared to the filtrates (relative to the 0.17 ratio of iron in the washes to that in the filtrates). An important source of zinc could be sphalerite, ZnS. Also, zinc may be rather steadily leaching from some clay mineral. Kuhn et al. 1980, reported zinc to be a trace constituent of mixed layer clays.

Figure 4.7 Zinc in filtrates and washes of the batch oxidation as a function of elapsed time.

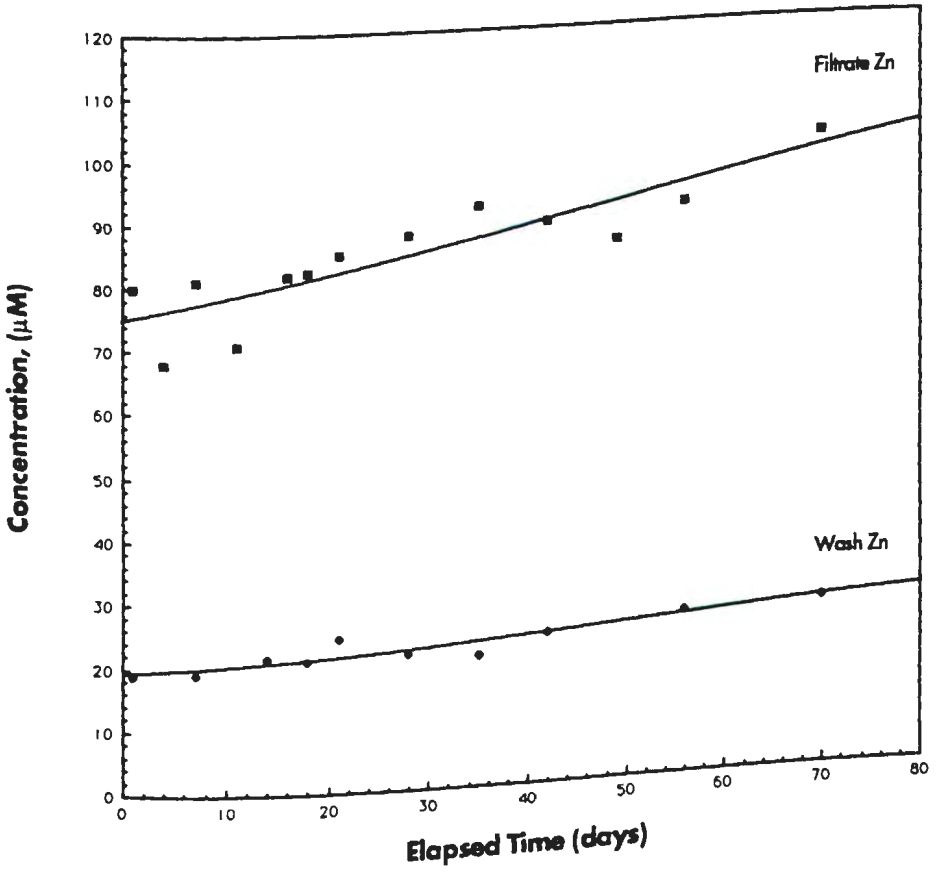

Notes: Concentrations are micromolar. The lines are least squares fits to each set of data.

Figure 4.8 shows the plots of copper in the filtrates and washes. The shape of the upper curve strongly suggests that copper tracks the release of iron in this system. The initial plateau before day 10, the steep rise in concentration after day 10, and the gradual decline in slope as the oxidation progresses, all closely resemble those of iron and sulfate in these samples. The range of copper concentrations in the filtrates was from about 20 to 63 micromolar, with an average of almost 39 μm. The unusually high value for day 35 is thought to be erroneous. Copper concentrations in the washes also track the iron concentrations in the washes. The range of copper in these samples was from 1 to 14 micromolar, with an average of almost 7.5 μM. The ratio of copper in the washes to that in the filtrates varies rather steadily from 0.164 to 0.223, which is not significantly different from the average of 0.17 found for iron. These observations strongly suggest that copper is found as a sulfide such as chalcopyrite associated with the pyritic material of the coal, and that it is released as the sulfidic material is oxidized. This relationship has also been proposed by Helz et al. 1987.

Figure 4.8 Copper in filtrates and washes of the batch oxidation as a function of elapsed time.

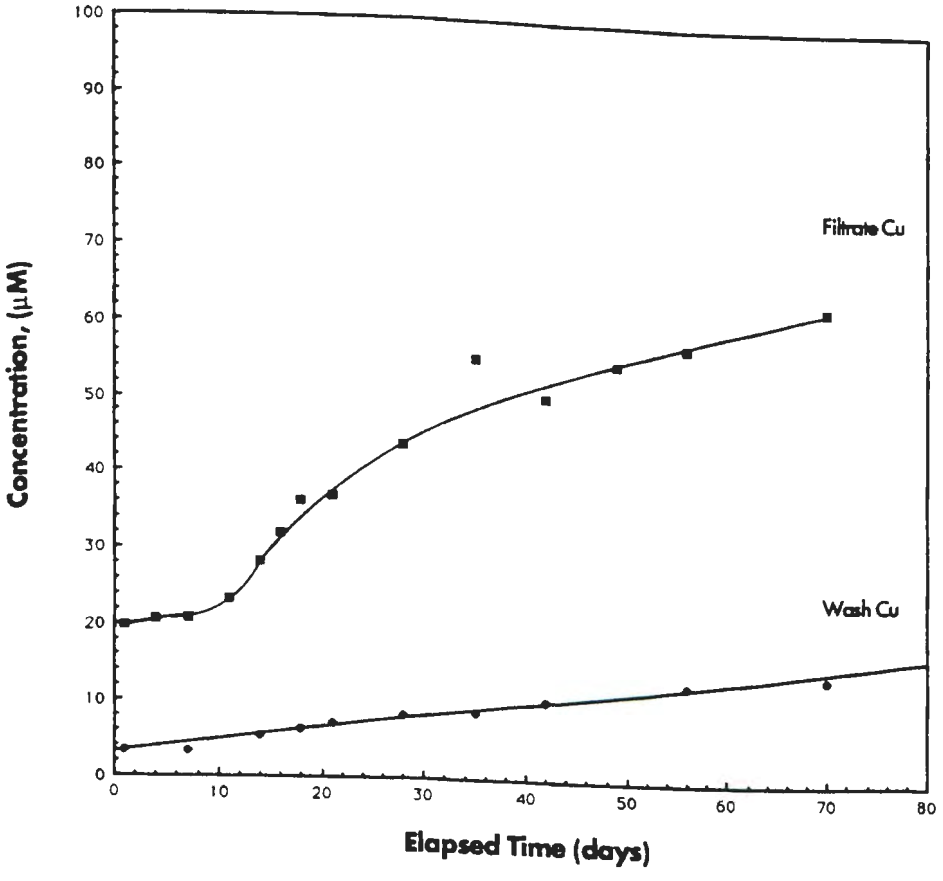

Notes: Concentrations are micromolar. The smooth curve for filtrate copper was drawn largely ignoring the values from days 18, 35, and 42. The line for wash copper is a least squares fit to the set of data points.

Figure 4.9 is a plot of the arsenic data for both filtrates and washes. In both cases, the values below one micromolar were below the limit of detection for these analyses. The appearance of trends in the data are attributed to averaging the results of repetitive measurements of the samples and to the reproducibility of aliquots injected by the AS-40 Autosampler into the graphite furnace. The range of values obtained for arsenic in the filtrates was from about 1 to 8 micromolar, with an average of about 3 μM. The data for the first half of the experiment vaguely resembles that of iron, which started with a low plateau, then rose quickly in concentration after day 10, and tended toward leveling off after the first half of the experiment. The plot of arsenic in the washes also vaguely resembles that of iron, which didn't start to rise until after day 10, and then rose rather steadily throughout the rest of the experiment. The range of arsenic concentrations in these solutions was from 1 to almost 9 micromolar, and averaged just over 3 μM. The ratio of arsenic in the washes to that in the filtrates is near 0.5 through day 28, after which it rises rapidly reaching a value of almost 6 as the filtrate levels of arsenic decline. A comparison of these ratios to the average ratio of 0.17 for iron in these samples indicates that arsenic is always relatively enriched in the washes, and that it is concentrated

Figure 4.9 Arsenic in filtrates and washes of the batch oxidation as a function of elapsed time.

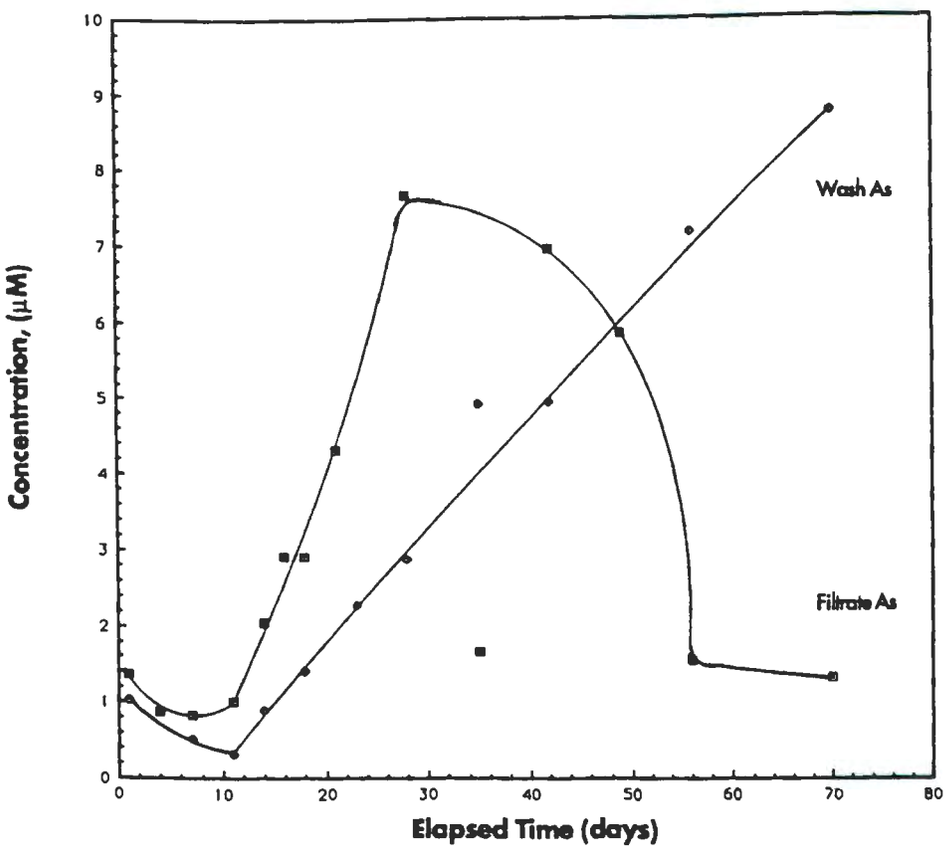

Notes: Concentrations are micromolar, with the limit of detection about 1 μM. Both curves are "eyeball" fits drawn to reflect the data points except for the values obtained on day 35, which appear to be erroneous.

rather strongly into the washes when the level of arsenic in the filtrates falls off. This suggests that later in the process of this batch oxidation of whole coal, arsenic tends to be adsorbed onto non-filterable particles when in the acidic leachates, and exchangeable and soluble when the filter cake is washed by the neutral magnesium chloride solution.

These observations may be explained by assuming that arsenic is a trace constituent of the sulfide minerals commonly found with coal (see Kuhn et al. 1980), and that its release is controlled by the oxidation of pyrite and these minerals. Heaton et al. 1982, reported a very strong correlation between arsenic and the pyrite-containing component of Eastern coal waste samples. The later decline of arsenic in the filtrates and concentration into the washes occurred after day 28 in this experiment, which was when the pH fell to 2.1 and below. This coincides with the calculated pH at which arsenate ions in solution shift from $H_2AsO_4^-$ to the neutral species H_3AsO_4. It is possible that this neutral species is adsorbed from solution onto particles that are largely retained during filtration, and that they are subject to ion exchange back into solution by neutral, 1.0 molar magnesium chloride. (Note, the speciation of arsenic and iron will be discussed further in the later section on computer modelling of synthetic acidic leachates.)

The chromium data are plotted in Figure 4.10. Both curves are second order polynomial least-squares fits to the data points. Chromium in the filtrates ranged from 1.0 to 2.6 micromolar and averaged 1.7 μM, while chromium in the washes ranged from 1.6 to 2.6 μM and averaged almost 2.3 μM. Throughout most of the samples, chromium was found to be more concentrated in the washes. But the curves cross when the pH was measured to be 1.93, and at the lower pH of the last sample the concentration of chromium in the filtrates was higher. The ratio of chromium in the washes to that in the filtrates declined from about 1.7 to 0.9 over the course of the experiment. Compared to the average value of 0.17 for iron, chromium is relatively enriched in the wash solutions, although less so as the pH of the system decreases.

In this system with large amounts of iron and organic material available, it is assumed that all of the mobile chromium exists as chromium(III). Bartlett and James 1988, compared the speciation and mobility of chromium(III) in soils and found its behavior best described by analogy with aluminum. Kuhn et al. 1980, list chromium as being a trace constituent of clay minerals among the principal minerals found in coals. Heaton et al. 1982, reported chromium in Eastern coal waste samples to correlate most strongly with illite, followed by quartz and kaolinite, and to lesser extent with mixed

Figure 4.10 Chromium in filtrates and washes of the batch oxidation as a function of time.

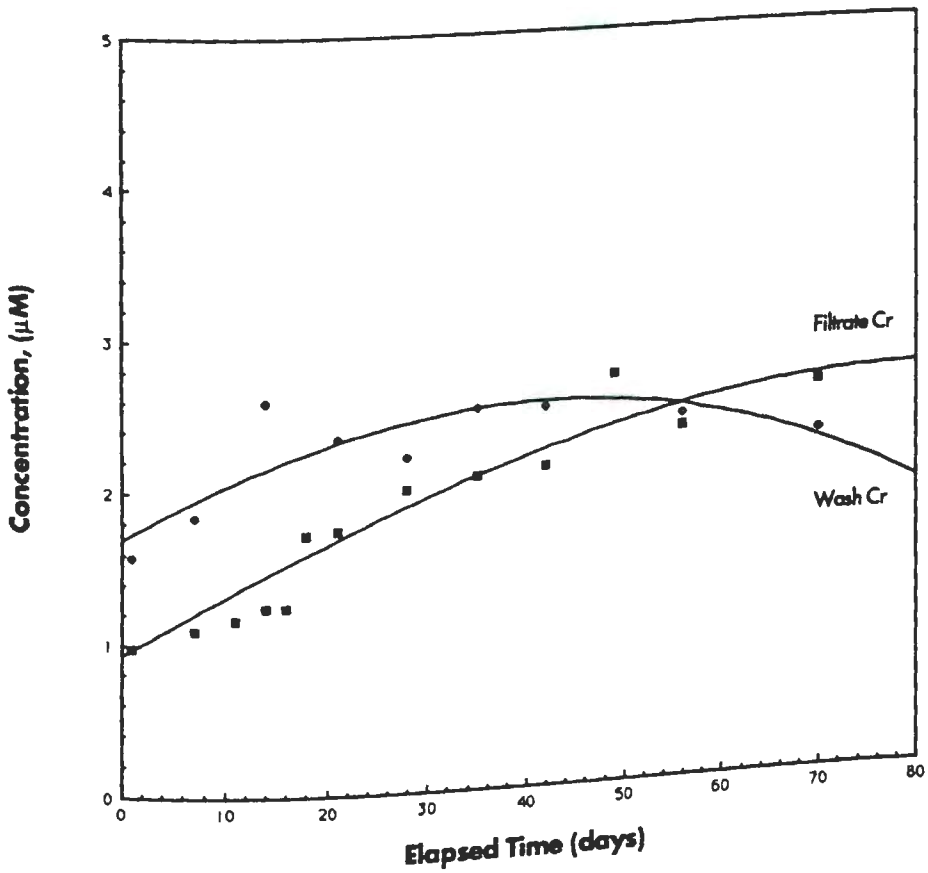

Notes: Concentrations are micromolar. Both curves are least squares fits of second order polynomials to each set of data points.

clay and gypsum. The results of this experiment do not show chromium tracking aluminum closely; however, like aluminum, the chromium concentrations in the first samples were not much different from the highest concentrations found, nor did they change much over the course of the experiment. Therefore it seems likely that the source of chromium in this system was silicate and clay minerals with chromium as a trace constituent that was leachable and exchangeable to a limited extent.

Figure 4.11 is a plot of the cadmium data. Its concentration in the filtrates increased steadily from about 0.18 to 0.36 micromolar, and averaged 0.25 μM. Cadmium concentrations in the washes were very close to the average 0.02 μM throughout, though it should be noted that in all these samples the signals obtained were between the limit of detection and the limit of quantitation for the analyses. The ratio of cadmium in the washes to that in the filtrates varied from 0.04 to 0.06, with the exception of day 2 when the questionable value of 0.15 was found. Thus cadmium is found significantly enriched in the filtrates, compared to the average ratio of iron in these samples.

Kuhn et al. 1980, listed cadmium as a trace constituent of the sulfide mineral phase, and Heaton et al. 1982, reported positive correlations for cadmium with

Figure 4.11 Cadmium in filtrates and washes of the batch oxidation as a function of elapsed time.

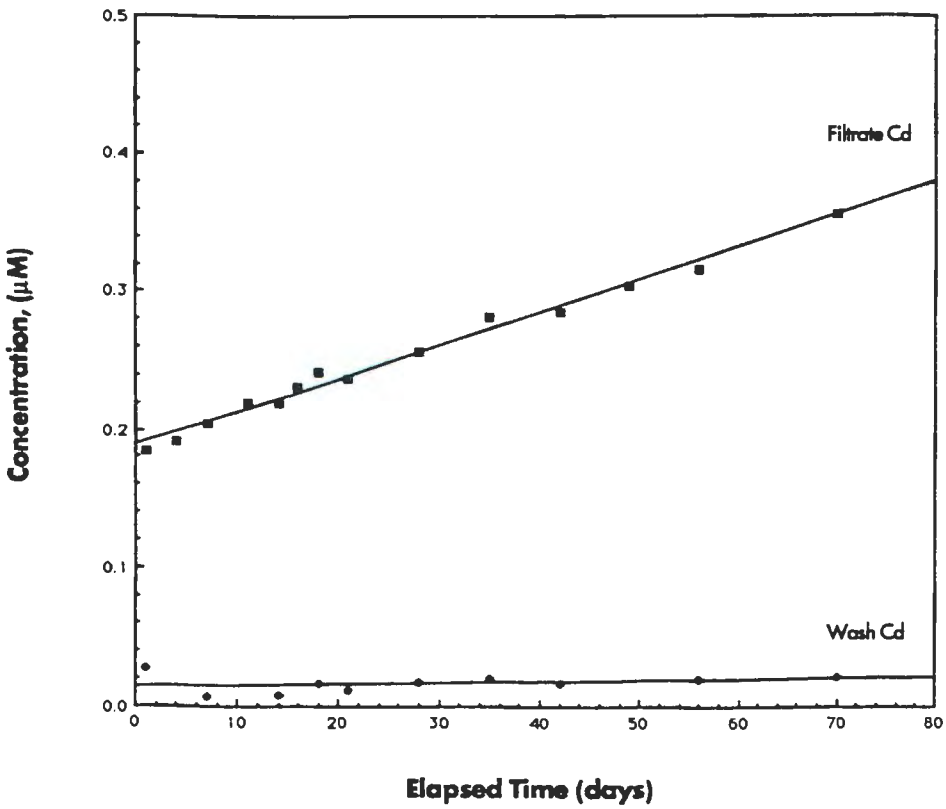

Notes: Concentrations are micromolar. The lines are least squares fits to each set of data.

only pyrite and carbon among the components of Eastern coal waste samples. In our samples, the cadmium levels are at least five orders of magnitude below those of iron and sulfate, and don't reflect the features of their plots.

The data for lead are plotted in Figure 4.12. Only the highest 2 or 3 concentrations found in each set of samples were at or above the limit of quantitation for the analyses. Lead in the filtrates ranged from the limit of detection (about 0.03 μM) to almost 0.2 μM. Lead in the washes also ranged from the limit of detection to approximately 1.8 μM. Because of the large uncertainty of the data, distribution ratios are not meaningful, though inspection of the plot suggests that toward the end of the experiment lead was highly enriched in the washes as compared to the filtrates. However, lead is listed as one of the trace impurities of the reagent magnesium chloride used to make the wash solution. Calculation of the maximum lead impurity concentration in the washes, based on the lot analysis reported on the reagent bottle, indicates that this source may account for all the lead in the wash samples.

Lead does not appear to track either iron or aluminum in this system. About all that can be noted that may be significant, is the increase of lead measured in the

Figure 4.12 Lead in filtrates and washes of the batch oxidation as a function of elapsed time.

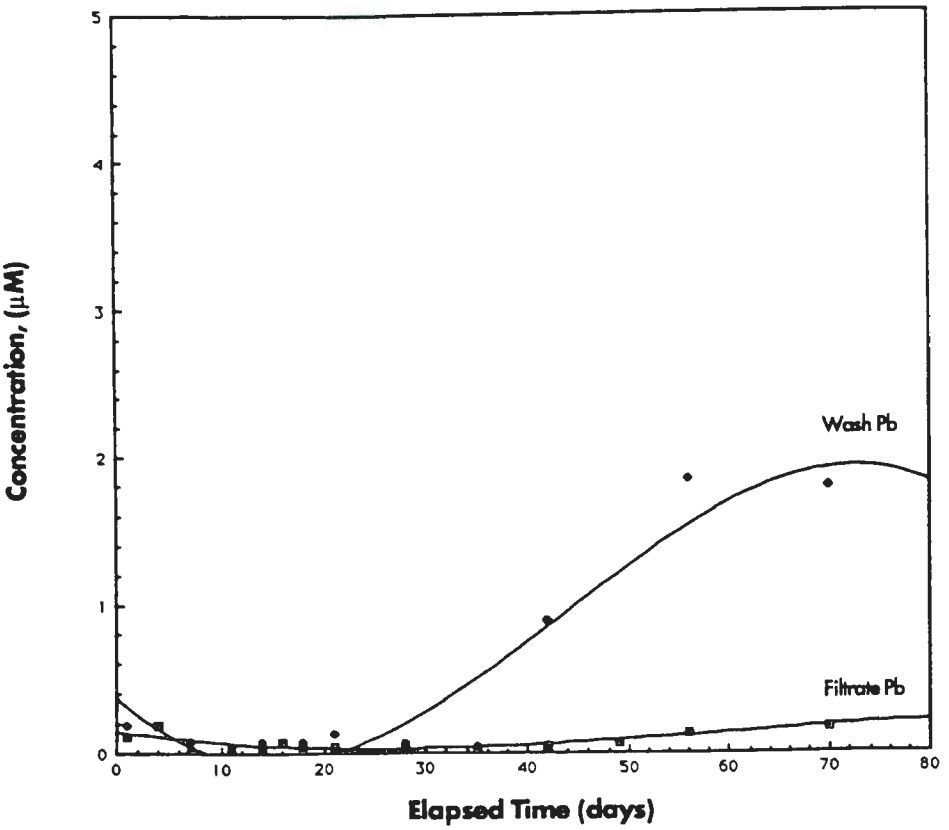

Notes: Concentrations are micromolar. The curve for filtrate lead is the least squares fit of a second order polynomial to the data. The curve for wash lead is the least squares fit of a third order polynomial to the data.

filtrates of pH less than 2, (which is observed in the washes as well, despite the doubt as to its source). Kuhn et al. 1980, listed lead as being a trace constituent of sulfides, sulfates, and carbonate minerals found in coals. Heaton et al. 1982, reported lead in Eastern coal wastes to correlate best with kaolinite and marcasite, less well with illite, quartz, and gypsum, and weakly with mixed clay.

4.2 COMPUTER MODEL DEVELOPMENT

4.2.1 PHREEQE Aqueous Geochemical Model

Computer modeling is an important tool for obtaining a thorough picture of the chemistry of this system and the interaction of its components. Among the more important computer models of aqueous systems that have seen continued development and use, WATEQ was first developed in the early seventies by Truesdell and Jones, (1973). It is designed for modeling major and trace element species activities in natural waters (rain, ground, river, lake, and even ocean and low temperature hydrothermal waters). It uses temperature, pH, total concentrations of analytes, alkalinity, and redox potential (Eh). It calculates chemical speciation and reports individual ion activities, equilibrium pressures of certain gases, and the degree of saturation of the solution with respect to many solid phases.

The ion-interaction models have been developed principally by Pitzer, Harvie, and Reardon to model brines and electrolytes at high concentrations. They use empirical data to account for complexing and ion-pair formation, but they have not been designed to model redox reactions.

Plummer and Parkhurst first developed PHREEQE about 1980. It models geochemical reactions based on an ion-

pairing aqueous model which is external to the computer code and completely user-definable. It can calculate the chemical speciation of solutions in equilibrium with multiple phases. It can simulate the mixing of solutions or the addition of reactants. It can also calculate pH, redox potential, and mass transfer as a function of reaction progress. It has been found to work well for solution ionic strengths up through that of seawater.

The most important single factor in obtaining reliable results from a computer model is the mathematical model which is used to describe the system being studied. D. K. Nordstrom, J. W. Ball, and E. A. Jenne have done major work on the collection, evaluation, selection, and generation of self-consistent, best-available thermodynamic data and/or equilibrium constants for use in the data bases of these and other geochemical modeling programs. Starting from their recent publications (Nordstrom et al. 1989, Parkhurst 1989, and PHREEQE documentation that accompanies the program, (Plummer and Tisaranni 1990), the database that pertains to the elements, dissolved species and complexes, gases, and solids has been carefully checked. Other major sources used to check the existing database and to obtain thermodynamic and/or equilibrium constants for additional species to be incorporated into the model include: Smith and Martell,

1989 and 1982, Bard, et al. (IUPAC, 1985), Wagman et al. (NBS, 1982), Turner et al. 1981. Some individual species were found in the literature and incorporated into the database (see Appendix B). Woods and Garrels 1985, was found useful for cross-checking that thermodynamic data used in a calculation in the literature was in reasonable agreement with the major compilations of selected values.

The only major additions to the PHREEQE database were the elements arsenic and chromium and their redox, speciation, and mineral phase equilibria. The sources of the data for these and other individual additions and modifications to the database are given in Appendix B.

Input that was required by PHREEQE in order to model a given sample, and the source of the values used, included:

pH = as measured in each filtered sample.

Temperature = 25°C

pE = an estimate of solution redox potential, we used the equation used by the program:

$$pE = \{\log(P_{O2}) - 4pH + 83.1\}/4 \qquad \text{Eqn. 4.2}$$

Density of solution = 1.0175 for first sample, 1.01825 as the average density of the partially titrated samples.

Dissolved elements = total millimolar concentration of each one added or measured.

Gases (identity and partial pressure of each gas with which the solution was equilibrated): air O_2 = 0.21 atm.

air CO_2 = 3.3×10^{-4} atm.

Solids (identity of each solid phase with which the solution was to be equilibrated)

Charge-balance method and species if desired, (see later discussion).

Also included as part of the database was a list of selected non-aqueous phases to be monitored by the calculation of saturation indices.

The computer outputs included: reiteration of the input data and parameters, mass transfer to or from non-aqueous phases during the equilibration step, total molality of each element being modeled, a summary of solution descriptors (including pH, pE, activity of water, ionic strength, temperature, net electrical imbalance, and total alkalinity), a table of the calculated distribution of the major and important species of each element modeled (listing their molality, activity, and activity coefficient), and a list of saturation indices for non-aqueous phases being modeled.

4.2.2 General Problems

The PHREEQE chemical model discussed above ignores kinetic factors. It assumes that there are no kinetic hindrances to achieving equilibrium, and calculates complete systemic equilibration at each step of a simulation. This assumption works acceptably well for many applications of the program, but can result in profound errors when the system being modeled is not in fact at equilibrium.

Iron in unoxidized coal exists primarily in the form of pyrite and marcasite. Exposure to air and moisture brings about oxidation of the FeS_2 and release of ferric iron and sulfate. The complete oxidation of the pyritic material may take months or years, depending on environmental and chemical factors. Helz et al. 1987, noted that the production of sulfate in laboratory experiments with coal did not approach completion in a 60 - 90 day period. Thus, a natural system of whole coal exposed to weathering is expected to have significant concentrations of both ferrous and ferric iron, limited of course by the solubility of each at the pH of their microenvironment.

PHREEQE calculates the redox distribution of iron in equilibrium with the redox potential of solution, which is determined by pH and the partial pressure of dissolved oxygen. In air-saturated aqueous solutions of low pH, the calculated pE is high (ranging from 15 to 19 in our

simulations). The resultant ratio of ferric to ferrous iron was predicted to be on the order of 10^6 at pH 1.6, 10^5 at pH 2.5, 10^4 at pH 3.9, and 10^2 at pH 5.6. Thus, PHREEQE would not be expected to accurately model the iron redox state in a coal suspension undergoing oxidation. (However, it should still give a reasonable picture of the species distribution within a specific oxidation state. That is, even though the Fe(II)/Fe(III) ratio is unreliable, the $Fe^{3+}/FeOH^{2+}$ ratio should be realistic.)

Our synthetic coal leachate was intended to represent a fully oxidized effluent from some well-exposed and weathered coal. Sulfuric acid and iron(III) sulfate were the sources for the iron and sulfur in the synthetic solution; and it was left exposed to air and kept well stirred throughout the experiment so that air saturation would be maintained. Thus, PHREEQE is expected to present a good model of the iron redox state and speciation in samples from this neutralization reaction.

Net imbalance between total positive and total negative charges in solution can be used as a gross indicator of the adequacy of the solution analysis. That is, a charge imbalance of greater than 20% should be investigated as to its source(s). It may indicate omission of some important substance in the analysis, or

significant errors in the analysis, or large systematic errors in the concentrations of components that are estimated. It could also arise from typographical errors during data entry, or from inclusion of non-charge balanced reaction equations in the chemical model.

PHREEQE has options that allow the user to: 1) calculate and report the charge imbalance and hold it constant throughout the calculations; 2) adjust solution pH to obtain electroneutrality (which allows the program to calculate pH changes of solution due to hydrolysis or other proton producing/consuming processes); and 3) adjust the total concentration of some specified anion and/or cation to balance the net charge, and then hold that balance throughout subsequent calculations (e.g. adjust Na^+ or Cl^- in a seawater simulation).

Most of the samples from the neutralization experiment exhibited significant charge imbalance. The early samples had excessive positive charge, and the amount in excess tended to decrease as the neutralization progressed and iron was removed from solution by hydrolysis and precipitation. This can be explained by the incomplete removal of fully hydrolyzed iron from solution during filtration. During hydrolysis, each Fe^{3+} ion is replaced by three H^+ ions according to the net reaction:

$$Fe^{3+} + 3H_2O = 3H^+ + Fe(OH)_3 \qquad \text{Eqn. 4.3}$$

Thus, the total positive charge in solution is conserved, and the other product, being neutral, has a net charge per iron atom of zero. Removal of this neutral entity from solution by precipitation and filtration does not affect the charge balance.

Spiro et al. 1966, reported that hydrolysis of ferric nitrate with bicarbonate produces solutions that contain a discrete high polymeric component having an average molecular weight of approximately 1.4×10^5. Polymer size and composition were found to be nearly independent of degree of hydrolysis between 1.0 and 2.0 base equivalents per mole of iron(III). Electron microscopy revealed isolated spheres mostly of about 70 angstroms diameter and ranging up to about 90 angstroms. The authors further reported that formation of these particles was rapid, but dissolution was very slow. In fact, they were stable indefinitely if isolated, otherwise ferric hydroxide precipitated in a few days. Brady et al. 1968, also reported formation of 70 angstrom spheres during the hydrolysis of iron(III). Dousma and deBruyn 1976, outlined four steps in the hydrolysis-precipitation of iron(III):

1) Hydrolysis to monomers and dimers;
2) Reversible rapid growth to small polymers (approximately 40 angstroms);

3) Formation of slowly reacting large polymers (200 to 500 angstroms);

4) Precipitation of a solid phase.

Nominally 0.45 μm millipore filters should catch most particles that are greater than 500 nm; but that is at least ten times the size of even the largest particles cited above. Thus, significant amounts of fully hydrolyzed, uncharged, precipitated iron can be collected in filtrates as colloidal particles. These filtrates are physically constrained to be charge balanced. In our experiments, the pH of each filtrate was measured at this point, before the sample was acidified and stored. But the added acid would be expected to dissolve any colloidal iron during the storage period. Thus, at the time of analysis there could be significantly more dissolved iron in solution than there was when the sample was collected. (Even colloidal iron reaching the atomic absorption atomizer could be decomposed and contribute positive error to the analysis.) This excess iron is believed to be the source of the excess positive charge in acidic filtrates containing appreciable iron.

Later samples, collected after the bulk of iron had been removed from solution by precipitation, tended to exhibit small excesses of negative charge. This was thought to be due to the assumption, built into the

original PHREEQE chemical model by default, that sulfate was conserved in solution during the precipitation of iron, which left solution as pure $Fe(OH)_3$. Lazaroff et - al. 1982, in a study of amorphous sediments produced by bacterial oxidation of ferrous ions in acid solution, obtained infrared spectral evidence for outer-sphere coordination of Fe(III) by sulfate ions. Khoe and Robins 1989, investigated the hydrolysis and polymerization of iron(III) in the presence of sulfate. They suggested that sulfate is incorporated in the structure of the polymer formed; and they gave the empirical formula for the polymer as $Fe(OH)_{2.4}(SO_4)_{0.3}$. Bigham et al. 1990, identified a poorly crystallized oxyhydroxysulfate of iron as the primary component of precipitates from sulfate-rich mine waters having pH values in the range of 2.5 to 4.0. They determined it to have sulfate occupying both surface and tunnel sites; and they gave the formula as $Fe_{16}O_{16}(OH)_{12}(SO_4)_2$ but ranging to $Fe_{16}O_{16}(OH)_{10}(SO_4)_3$.

The data for three of the samples were examined to estimate the contribution of the major substances to charge uncertainty. Sample 2 was collected at pH 1.97 before visible precipitates had formed in solution. The major contributors of charge in solution were iron, sulfate, hydrogen, and sodium ions (in that order of importance). The estimated uncertainty of each component

concentration in terms of equivalents per liter, summed over the above major components, totaled about $7x10^{-2}$ equivalents per liter. PHREEQE calculated the net charge imbalance of the sample to be $+5x10^{-2}$ Eq/L. Sample 7 was the middle one collected; its pH was 2.47, and only about 14 percent of the original iron remained in solution. The major contributors of charge in this solution were sulfate, sodium, iron, and hydrogen ions (in that order). The sum of their estimated uncertainties was approximately $8x10^{-2}$ equivalents per liter; and PHREEQE calculated the net charge imbalance to be $+3.6x10^{-3}$ Eq/L.

Sample 12 was collected at pH 5.74, after the iron concentration in the filtrate had dropped below the limit of quantitation. The major contributors of charge in this solution were sulfate and sodium ions (in that order) with iron and hydrogen ions about five orders of magnitude lower. The total estimated uncertainty was not more than $12x10^{-2}$ Eq/L; and PHREEQE calculated the net charge imbalance to be approximately $+2x10^{-2}$ Eq/L. Thus the computer calculated charge imbalance of the solutions was less than the estimated limit of uncertainty in the data being used by the program.

An effort was made to adjust the input data for each sample to compensate for the systematic errors discussed

above and render the data a more realistic description of the true solution conditions.

It was assumed that all the precipitated iron had taken some sulfate out of solution with it, either incorporated into the structure or adsorbed onto the surface of the solid. Estimation of the amount of sulfate removed by formation of an iron precipitate having the formula $Fe(OH)_{2.4}(SO_4)_{0.3}$, given by Khoe and Robins 1989, resulted in overcorrection of the excess negative charge in the later samples by a factor of about 2. But use of $Fe_{16}O_{16}(OH)_{12}(SO_4)_2$, the first formula given (and preferred) by Bigham et al. 1990, brought the later solution compositions nearly into charge balance.

Final charge balance in samples 8 through 13 was achieved by slight adjustments in total sodium and total sulfate simultaneously. These components had been introduced into solution separately (sulfate at the outset as ferric sulfate and sulfuric acid, sodium in the sodium bicarbonate titrant), and their total concentration in each sample had been estimated separately. No indication was found that either sodium or sulfate concentrations were more likely to be in error. It was realized that adjustment of just one or the other would affect the total dissolved solids and the ionic strength of solution, as well as impact on the speciation of all components involving that ion.

Thus, equal equivalents of sodium and sulfate were added and removed simultaneously in a series of successive approximations that led to essential charge balance for each of the samples. The resulting average change of sodium was 0.4% of total Na, and the average change of sulfate was 0.4% of total SO_4. These were well within the uncertainty of the estimated total concentrations of these components; and the small changes involved produced negligible effects on the calculated speciation of the solutions affected.

In the early samples where excess positive charge was judged to stem from colloidal iron in the filtrates being redissolved during storage, the total iron input was reduced manually until charge balance was obtained at the measured pH. (See Figures 4.30 and 4.31). The reductions necessary ranged from about 7.25% to 26.7% of the measured filterable iron. The larger adjustments were required for samples 3 through 6. Presumably the first two samples had not hydrolyzed sufficiently to form significant amounts of larger iron polycations and colloidal polymers. By the time sample 7 was collected, most of the iron had been removed from solution by hydrolysis-precipitation and flocculation to particles large enough to be caught by the filters. Thus it is supposed

that little colloidal iron existed to pass into the filtrate.

An average iron reduction of 19.7% was necessary to achieve charge balance in samples 1 through 7. This can be interpreted to mean that approximately one fifth of the filterable iron had in effect a net charge per iron atom of zero.

The Saturation Index of each non-aqueous phase being monitored by PHREEQE is calculated using the formula:

SI = log(Ion Activity Product / K) Eqn. 4.4

Thus, the Saturation Index for a mineral expresses the extent to which the solution is over- or under-saturated with respect to the equilibrium constant for the solubility of that mineral.

Some fluctuation was noted in the SI values reported by PHREEQE. A correlation analysis was made between SI and the variables involved in its calculation for minerals of interest which appeared to be near saturation in multiple solutions. Of the iron(III) hydroxides, only $Fe(OH)_3$(soil) was ever reported within one log unit of saturation; and its SI fluctuated about zero by as much as one log unit. The correlation analysis revealed that the variations of pH from sample to sample were the major cause of variation in the Ion Activity Product, and therefore accounted for the fluctuations in SI. Similar-

ly for jurbanite, $Al(OH)SO_4$, correlation analysis revealed that variations of pH from sample to sample were the major cause of variation in the Ion Activity Product. The second most important contributor to fluctuation in the Saturation Index for jurbanite was changes in the activity of Al^{3+}; and of least impact were changes in the activity of $SO_4^{=}$.

4.2.3 Relatively Inert Components

The components of solution during the neutralization reaction that were present in concentrations well above those of the trace elements being analyzed were:

sulfate from ferric sulfate and sulfuric acid, initially 0.170 molar;

sodium from the sodium bicarbonate titrant, increased from 0.0 to 0.326 molar;

chloride and nitrate that were matrix ions of the trace element spikes, averaged 1.5 mM and 0.9 mM, respectively.

These were judged to be relatively inert, as compared to the chemistry of iron during neutralization reactions. The matrix composition of the first sample was estimated from the initial formulation of the system. For the rest of the samples, running total concentrations of the matrix components were estimated assuming their conservation in solution, and taking into account sample removal,

titrant addition, and evaporative losses from the system during the three weeks duration of this experiment. Of course, the total sulfate and total sodium concentrations were eventually adjusted slightly to obtain charge balance, as has been discussed.

4.2.4 Specific Problems

Iron

Because of the results indicating a large imbalance of positive and negative charge in the modeled solutions, thermodynamic data was sought for larger iron polycations. (These have been assumed or postulated in numerous articles; i.e. Schneider and Schwyn 1987, Hong-Xiao and Stumm 1987, Dousma et al. 1979, Dousma and de Bruyn 1976, 1978, and 1979, Buffle and Nembrini 1977, and Rengasamy and Oades 1977.) Computer assisted search of the literature enabled me to find only one iron polycation beyond $Fe_3(OH)_4^{5+}$ that had been characterized to the extent of an equilibrium value. Ciavatta and Grimaldi (1975) reported log(B) = -46.1 for:

$$12Fe^{3+} + 34H_2O = Fe_{12}(OH)_{34}^{2+} + 34H^+ \qquad \text{Eqn. 4.5}$$

In the absence of a literature value for $Fe_4(OH)_6^{6+}$, the (log K) vs (No. of iron atoms) for the series: Fe^{3+}, $Fe_2(OH)_2^{4+}$, $Fe_3(OH)_4^{5+}$ was extrapolated (Figure 4.13) to obtain an estimate for the log(K) of formation for the next member of the series, $Fe_4(OH)_6^{6+}$. The value obtained

Figure 4.13 Extrapolation of Fe(III)-hydroxy species log K's to obtain an estimate of the log(K) for $Fe_4(OH)_6^{6+}$.

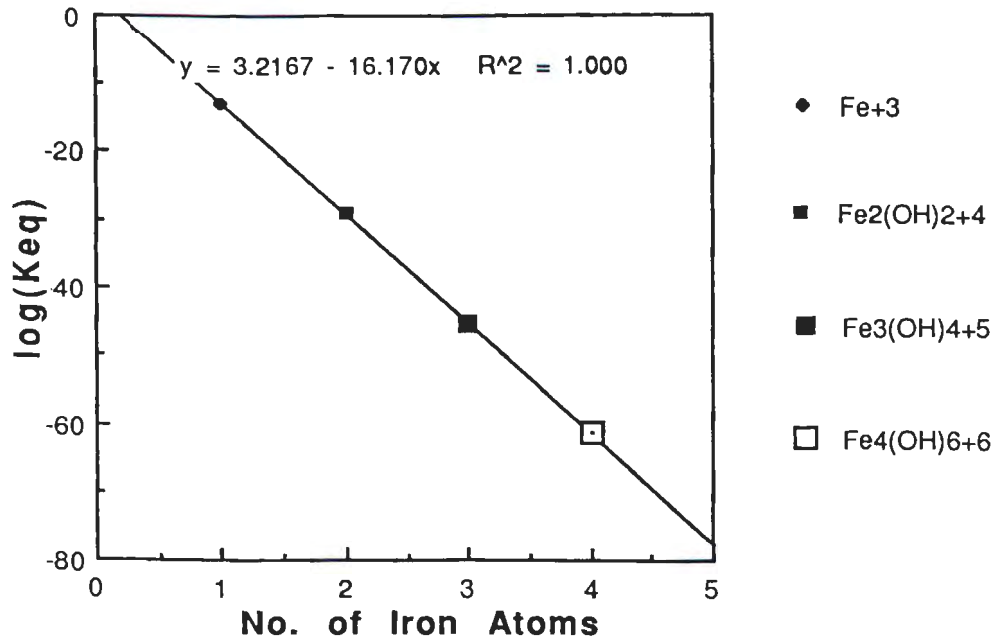

was -61.46 for the reaction:

$$4Fe^{2+} + 6H_2O = Fe_4(OH)_6^{6+} + 6H^+ + 4e^- \qquad \text{Eqn. 4.6}$$

which was incorporated into the PHREEQE database. Further extrapolation of the series led to an asymptotic approach to a value of -16.17 for the (log K)/(Fe atom) of formation of a polycation having one million Fe atoms. This value lies between the corresponding log(K) of formation for goethite (-14.02) and amorphous ferric hydroxide (-17.91) according to the following reactions:

$$Fe^{2+} + 2H_2O = FeO(OH)_{(goethite)} + 3H^+ + 1e^- \qquad \text{Eqn. 4.7}$$

$$Fe^{2+} + 3H_2O = Fe(OH)_{3(am)} + 3H^+ + 1e^- \qquad \text{Eqn. 4.8}$$

Subsequent computer modeling of samples from the neutralization titration never revealed either $Fe_4(OH)_6^{6+}$ or $Fe_{12}(OH)_{34}^{2+}$ to be of importance among the iron species considered in our calculations.

Jarosites

Special attention was given to the selection of equilibrium constants to be used to model the jarosites. Numerous authors have commented on the apparent contradictions that jarosite forms readily in the environment, yet many solutions are found to be supersaturated with respect to jarosite by orders of magnitude, which implies failure to equilibrate. (See for example: Nordstrom et al. 1979, Bladh 1982, Chapman et al. 1983, Helz et al. 1987, Karathanasis et al. 1988, and Alpers and Brimhall

1989.) In addition, there is a wide range of data reported for the Gibbs free energy of formation and/or solubility of jarosite. Brown 1970, determined the Gibbs free energy of K-jarosite to lie between -3276 +/- 84 kJ/mol and -3192 +/- 25 kJ/mol. Zotov et al. 1973, reported -790.1 +/- 1.0 kcal/mole, which corresponds to -3306 kJ/mole. Vlek et al. 1974, determined a value of -791.2 kcal/mole, which corresponds to -3310 kJ/mole. Kashkay et al. 1975, determined a value of -788.64 +/- 1.0 kcal/mole, which corresponds to -3300. kJ/mole.

Bladh 1982, reported ambiguities in earlier calculations as a result of the wide range of published values of thermodynamic data, and recalculated the log(K) for jarosite to be -7.12 for the reaction: Eqn. 4.9

$$KFe_3(OH)_6(SO_4)_2 + 6H^+ = K^+ + 3Fe^{3+} + 2SO_4^{=} + 6H_2O$$

which corresponds to a Gibbs free energy value for K-jarosite of -3275 kJ/mole (Alpers et al. 1989). This value would make jarosite more than five orders of magnitude more soluble than the widely used log(K) value of -12.5 (as in Lindsay 1979). However, Alpers et al. 1989, found Bladh's value to be inconsistent with their results, and recommended the use of the values of Kashkay et al. 1975, as the best available internally consistent set of data for the three end-member jarosites (K^+, H_3O^+, and Na^+ - jarosites).

Thus, the values used in PHREEQE for the log(K) of the pure jarosites (for reactions of the type of equation 4.9) were: jarosite, -9.21; carphosiderite (hydronium-jarosite), -5.39; and natrojarosite, -5.28. In addition, the work of Alpers et al. 1989, recommended a Gibbs free energy of -3293.5 +/- 2.1 kJ/mol for a jarosite solid solution of composition $K_{.77}Na_{.03}(H_3O)_{.20}Fe_3(OH)_6(SO_4)_2$. This value was not used because of the absence of potassium in the solutions to be modeled. However, their work did allow the estimation of a Gibbs free energy value of -3239 kJ/mole for a pseudo-binary H_3O^+-Na^+-jarosite with formula $(H_3O)_{.75}Na_{.25}Fe_3(OH)_6(SO_4)_2$, and this value was incorporated into the PHREEQE database.

Soil-Iron

Lindsay 1979, noted that soils generally maintain an iron(III) activity slightly below that of amorphous ferric hydroxide. He defined $Fe(OH)_{3(soil)}$ or soil-Fe to be an amorphous phase having a greater degree of structural order than freshly precipitated am-$Fe(OH)_3$. Log(K) = 2.70 was assigned to the reaction:

$$Fe(OH)_{3(soil)} + 3H^+ = Fe^{3+} + 3H_2O \qquad \text{Eqn. 4.10}$$

This value was incorporated into the PHREEQE database and will be seen to be of significance in the modeling of our solutions.

Silica

Similarly, the Pyrex glass of the reaction vessel is intermediate in solubility between amorphous and crystalline SiO_2. Equilibrium with silica glass was defined by adding the following reaction:

$$SiO_2 \cdot H_2O_{(glass)} + H_2O = H_4SiO_4^\circ \qquad \text{Eqn. 4.11}$$

for which log(K) = -3.018, (based on Summer, 1990 database supplied with PHREEQE, and Nordstrom, 1989).

Aluminum

Baes and Mesmer 1976, summarized the aluminum hydrolysis products and recommended that a value of -98.73 be used for the log(K) of formation of $Al_{13}O_4(OH)_{24}^{7+}$. Based on work by Brown with Sylva, Batley, and Ellis, 1985, log(B) = -107.41 for the reaction:

$$13Al^{3+} + 32H_2O = Al_{13}(OH)_{32}^{7+} + 32H^+ \qquad \text{Eqn. 4.12}$$

This was also incorporated into the database for PHREEQE, and was shown to be of importance in the speciation of aluminum in the two least acidic samples modeled, those of pH 5.55 and 5.75.

Jurbanite proves to be of some importance in the calculations. Its log(K) of -3.8 was obtained from Karathanasis et al. 1988 for the reaction:

$$AlOHSO_{4(jurbanite)} + H^+ = Al^{3+} + SO_4^{2-} + H_2O \qquad \text{Eqn. 4.13}$$

Nordstrom 1982b, listed several possible solid phases that might control aluminum solubility in natural waters, including alunogen ($Al_2(SO_4)_3 \cdot 17H_2O$), jurbanite ($AlOHSO_4 \cdot 5H_2O$), basaluminite ($Al_4(OH)_{10}SO_4 \cdot 5H_2O$), alunite ($KAl_3(OH)_6(SO_4)_2$), and gibbsite ($\gamma$-$Al(OH)_3$). He concluded that jurbanite is stable at low pH up to at least pH 4 in the presence of 10^{-2} molar sulfate, that alunite is stable between jurbanite and gibbsite (pH 3.3 through 5.7 depending on sulfate concentration), and that gibbsite is the most stable phase at higher pH. He noted that basaluminite shows a solubility pattern similar to gibbsite and alunite, and that it forms most readily, but is metastable over the entire pH range. Later, studying water from acid mine water drainage basins, Nordstrom and Ball 1986, found aluminum to be conserved in samples at pH less than 4.6, and non-conserved at pH greater than 4.9. The loss of aluminum correlated most closely to the formation of amorphous or microcrystalline $Al(OH)_3$.

Karathanasis et al. 1988, in a study of surface waters of acid mine watersheds, concluded that high levels of dissolved aluminum (in solutions with pH up to 4.2 or even 5) were limited by the solubility of a jurbanite-like mineral. They interpreted the absence of jurbanite X-ray diffraction peaks to suggest the presence of an amorphous form, or of a mineral stoichiometrically similar to jurbanite. Aluminum in samples with pH 5 or

more could be interpreted as obeying the solubility of microcrystalline gibbsite.

The best fit to our data was obtained using the following reactions to model aluminum concentrations as being controlled by jurbanite (log(K) = -3.8) up to pH 3.9, then by bayerite (log(K) = +8.41) up to pH 4.8, then by basaluminite (log(K) = +22.4) up to pH 5.0, and thereafter by micro-crystalline gibbsite (log(K) = +9.35).

$$AlOHSO_{4(cr)} + 1H^{+} = 1Al^{3+} + 1SO_4^{=} + 1H_2O \qquad \text{Eqn. 4.14}$$

$$\alpha\text{-}Al(OH)_3 + 3H^{+} = 1Al^{3+} + 3H_2O \qquad \text{Eqn. 4.15}$$

$$Al_4(OH)_{10}SO_{4(cr)} + 10H^{+} = 4Al^{3+} + 1SO_4^{=} + 10H_2O \qquad \text{Eqn. 4.16}$$

$$\gamma\text{-}Al(OH)_{3(Bcr)} + 3H^{+} = 1Al^{3+} + 3H_2O \qquad \text{Eqn. 4.17}$$

(The fit may be seen in section 4.3, Figure 4.19.)

Chromium

K_2CrO_4 was used in the formulation of the fully oxidized synthetic leachate, as well as fully oxidized forms of all the other components; and the system was kept well oxygenated throughout the experiment. Assuming equilibrium of dissolved chromium with dissolved oxygen in an acid-sulfate system, PHREEQE predicts that Cr(III) species predominate below pH 2.5, and that Cr(VI) species predominate above pH 2.5.

However, a principal objective of this work is to develope a computer model that can be used to predict the

mobility of trace elements in a leachate that is undergoing dilution and/or neutralization. In a coal leachate, especially if in contact with reduced mineral and organic material, chromium would be expected to exist only as Cr(III).

The work of Rai et al. 1987, and of Sass and Rai 1987, was used to model the removal of chromium from solution by coprecipitation with iron. They derived the following composition-dependent solubility equation which can be used to model aqueous chromium concentrations in equilibrium with $Cr_XFe_{1-X}(OH)_3$ for X less than or equal to 0.69 and for pH between 2 and 6.

$$\log(CrOH^{2+}) = \qquad \text{Eqn. 4.18}$$

$$-2pH + 4.18 + 0.28(1-X)^2 - 1.79(1-X)^3 + \log(X)$$

This equation was imbedded in the PHREEQE program code and solved at each iteration of the program for X. The resulting mole fraction was used to calculate the amount of chromium coprecipitating with each mass transfer of iron out of solution, as well as the amount of Fe(III) replaced in the precipitating solid and therefore retained in solution. This approach was used because it linked the coprecipitation of chromium with iron after Sass and Rai 1987, as well as preserving the coprecipitation of sulfate with iron after Bigham et al. 1990.

The model thus developed was first used to simulate the removal of chromium from our synthetic leachate

solution during neutralization by sodium bicarbonate. The calculated results roughly approximated our experimental data. Adjustment of the constant in the Sass and Rai equation corresponded to adjustment of the log(K) of the solubility of amorphous $Cr(OH)_3$ used in their derivation. The best simulation of our chromium data was obtained using +3.64 for the constant in their equation, which corresponds to a pure chromium(III) hydroxide phase that would be 0.54 log units more stable than the amorphous form assumed in the Sass and Rai derivation. Rai et al. (1987) obtained log(K) < 9.35 for the reaction:

$$Cr(OH)_{3(s)} + 3H^{+} = Cr^{3+} + 3H_2O \qquad \text{Eqn. 4.19}$$

This differs by almost three orders of magnitude from the value of 12.0 adopted by Baes and Mesmer 1976, and supported by the thermodynamic values published in the NBS and IUPAC compilations (Wagman et al. 1982, and Bard et al. 1985, respectively). Thus, we consider our adjustment of the equilibrium constant to be within the range of uncertainty of the appropriate stability constant for the pure solid phase.

Copper

The results from both the batch oxidation of coal and the neutralization titration of synthetic coal leachate suggest that the chemistry of copper is related to that of iron in these systems. The work of Frimmel and Geywitz 1987, suggest the removal of 3 micromolar copper by coprecipitation with ferric hydroxide (from solutions containing 0.1 millimolar total iron) to occur in the pH range 5 to 7. It was decided to model the removal of copper from solution during neutralization as the coprecipitation of copper with iron, similar to the above model for chromium. The derivation that follows is patterned after Sass and Rai 1987.

Cu^{2+} is a major species of copper in solution over the pH range of interest (1.6 to 5.6), (see Baes and Mesmer 1976). $Cu(OH)_{2(c)}$ is the most soluble of the solid phases likely to control copper solubility in this system, (see Lindsay 1979). According to Bard et al. 1985, log(K) = +8.6 for the reaction:

$$Cu(OH)_{2(s)} + 2H^{+} = Cu^{2+} + 2H_2O \qquad \text{Eqn. 4.20}$$

For this reaction the equilibrium constant expression may be written, (using { } to denote the activity of the enclosed substance) as: Eqn. 4.21

$$\log(K) = \log\{Cu^{2+}\} + 2\log\{H_2O\} - 2\log\{H^{+}\} - \log\{Cu(OH)_2\}$$

which may be rewritten as:

$$\log(K) + \log\{Cu(OH)_2\} = \log\{Cu^{2+}\} + 2\log\{H_2O\} + 2pH \qquad \text{Eqn. 4.22}$$

where $\{Cu(OH)_2\}$ represents the activity of $Cu(OH)_2$ in the solid solution that precipitates, and for which:

$$\log\{Cu(OH)_2\} = \log(K_x) - \log(K) \qquad \text{Eqn. 4.23}$$

where K_x is composition dependent and related to the mole fraction, X, of $Cu(OH)_2$ in the precipitate. (Note that when $Cu(OH)_2$ is pure, its standard state, its mole fraction is 1.0 and its activity is 1.0, by definition for pure solids. Thus, $\log\{Cu(OH)_2\} = 0.0$ and the above equation becomes: $\log(K_x) = \log(K)$. Also note that as the mole fraction of $Cu(OH)_2$ becomes less than 1.0, its activity in the solid solution becomes less than 1.0; and thus $\log\{Cu(OH)_2\}$ becomes less than zero. But since $\log(K)$ is fixed, then $\log(K_x)$ must also decrease.) Thus:

$$\log(K_x) = \log(K) + \log\{Cu(OH)_2\} \qquad \text{Eqn. 4.24}$$

Combining equations 4.22 and 4.24 gives:

$$\log(K_x) = \log\{Cu^{2+}\} + 2\log\{H_2O\} + 2pH \qquad \text{Eqn. 4.25}$$

Now, to evaluate $\log(K_x)$ I used the values for each of the other variables in equation 4.25 that were calculated by PHREEQE in the original processing of sample solutions of the neutralization titration in the pH range where copper was thought to be coprecipitating with iron. The results are listed in column 2 of Table 4.1. Column 3 of the same table lists the values for $\log\{Cu(OH)_2\}$ calculated using equation 4.23.

Table 4.1 Estimated and derived quantities in the development of a relation for the coprecipitation of copper with iron during neutralization of acid solution.

pH	$\log(K_x)$	$\log\{Cu(OH)_2\}$	$X_{Cu(OH)2}$	$\log(Y_{Cu(OH)2})$
2.8743	-0.1564	-8.7564	0.000063	-4.5548
3.145	0.324	-8.276	0.000285	-4.7310
3.400	0.764	-7.836	0.04552	-6.4942
3.5146	0.9632	-7.6368	0.088706	-6.5848
3.650	1.044	-7.556	0.21846	-6.8954
3.750	1.094	-7.506	0.25085	-6.9054
3.8984	1.1848	-7.4152	0.3072	-6.9026
4.400	1.849	-6.751	0.44764	-6.4019
5.643	3.54	-5.06	0.6713	-4.8869
pure $Cu(OH)_2$	8.6	0.0000	1.0000	0.0000

The mole fraction of $Cu(OH)_2$ precipitating with iron at each selected point in the neutralization titration was estimated to be the increment of copper removed from solution within +/- 0.005 pH units of that point, divided by the sum of the increments of copper and iron removed from solution over the same pH range. These estimates are listed in column 4 of Table 4.1. Column 5 lists the activity coefficient of $Cu(OH)_2$ in the solid solution at each selected point. These were based on:

$$\{Cu(OH)_2\} = X \cdot Y_{Cu(OH)2} \qquad \text{Eqn. 4.26}$$

and were calculated by:

$$\log(Y_{Cu(OH)2}) = \log\{Cu(OH)_2\} - \log(X) \qquad \text{Eqn. 4.27}$$

Figure 4.14 is a plot of the calculated log activity coefficients of $Cu(OH)_2$ in the solid solution precipitates versus one minus the mole fraction of $Cu(OH)_2$ in the precipitates. The least squares fit of a second order polynomial to the data produced the relation given below, for which $R^2 = 0.954$. Eqn. 4.28

$$\log(Y_{Cu(OH)2}) = 0.1310 - 20.99(1-X) + 15.61(1-X)^2$$

Combining equations 4.20 and 4.25 we obtain:

$$\log(K) + \log(Y_{Cu(OH)2}) + \log(X) = \log\{Cu^{2+}\} + 2\log\{H_2O\} + 2pH \quad \text{Eqn. 4.29}$$

And combining equations 4.28 and 4.29 we obtain:

$$\log(K) + 0.1310 - 20.99(1-X) + 15.61(1-X)^2 + \log(X) = \log\{Cu^{2+}\} + 2\log\{H_2O\} + 2pH \quad \text{Eqn. 4.30}$$

which can be rearranged to the form given below:

$$0 = \log\{Cu^{2+}\} + 2\log\{H_2O\} + 2pH - \log(K) - 0.1310 + 20.99(1-X) - 15.61(1-X)^2 - \log(X) \quad \text{Eqn. 4.31}$$

All except the last three terms in this equation are constants, or are available from the calculations after each iteration of the PHREEQE equation solving subroutines. These values were summed within the program, so that equation 4.31 collapsed into the form: Eqn. 4.32

$$0 = \text{CONSTANTS} + 20.99(1-X) - 15.61(1-X)^2 - \log(X)$$

This was solved at the end of each PHREEQE iteration by a method of successive bisections between 0.0 and 1.0 that

Figure 4.14 Logarithmic plot of the activity coefficient of $Cu(OH)_2$ in solid solution with $Fe(OH)_3$ as a function of the mole fraction of $Cu(OH)_2$ in the solid solution.

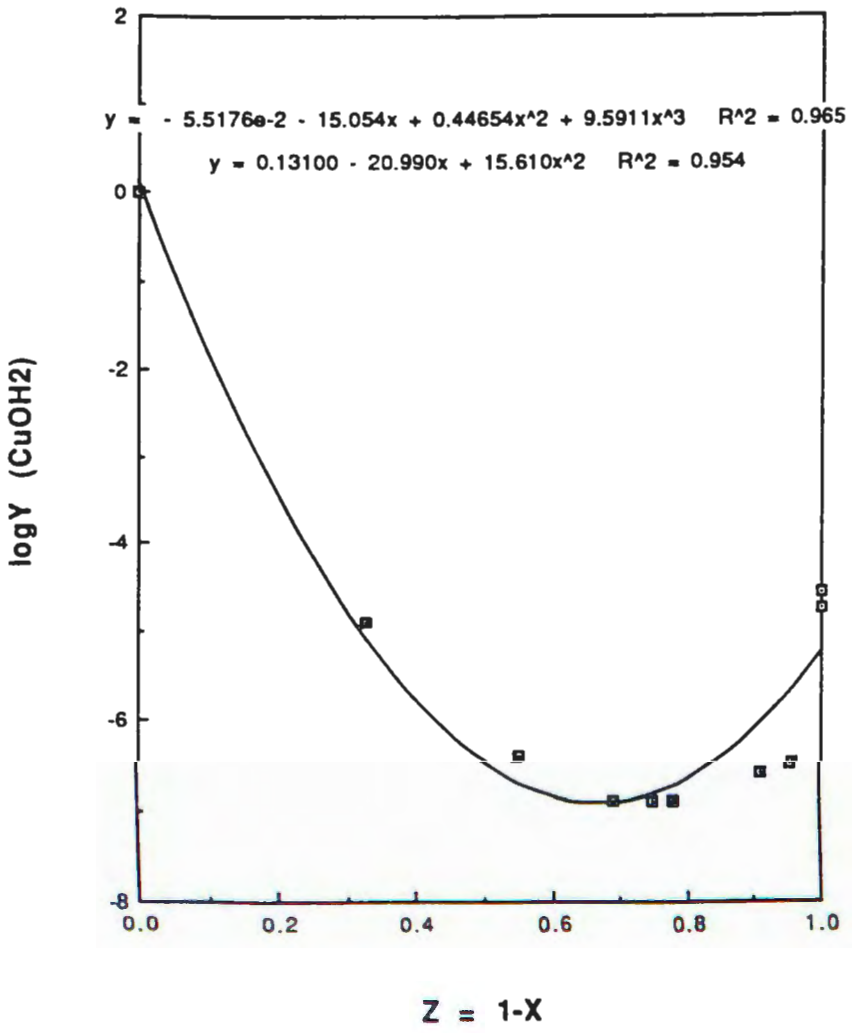

Note: Both second and third order least-squares polynomial fits to the data were calculated (after Sass and Rai 1987), and are shown. The curve plotted is from the second order fit, which gave the best computational results, and was used in the derivation.

approached the value of X which would make equation 4.29 true (neither positive nor negative). Thus we obtained the mole fraction of copper that should be coprecipitated with iron at each adjustment made by PHREEQE of the total iron in solution. This allowed the modelling of a fractional coprecipitation of copper with iron such that each increment of iron precipitated from solution resulted in the removal of an amount of copper appropriate to the immediate solution conditions, (including pH, total elemental concentrations, and state of complexation/speciation).

Specifically, for each mole of $Fe_{16}O_{16}(OH)_{12}(SO_4)_2$ that PHREEQE calculated should be precipitated from solution, 16X/(1-X/3) moles of copper were coprecipitated and (2/3)*16X/(1-X/3) moles of iron were redissolved. The included adjustments were necessary in order to achieve the desired composition of the precipitate and preserve charge balance within the system (without disturbing the amount of each anion removed and/or the calculated pH of the system during the simulated precipitation).

Use of the above model to simulate the removal of copper from the synthetic leachate solution during neutralization by sodium bicarbonate gave calculated results that roughly approximated the experimental data. (The goodness of fit may be seen in Figure 4.21, in section 4.3) Adjustment of the value used for the log(K) of the

solubility of solid $Cu(OH)_2$ from +8.6 to +9.2 produced the best simulation of my copper data. This corresponds to a pure copper(II) hydroxide phase that would be 0.6 log units more soluble than the crystalline form used in the above derivation, which suggests a microcrystalline form of the solid.

Lead

Comparison of the lead data from the neutralization titration experiment with the literature (see later discussion in section 4.4.2) revealed no satisfactory mechanism by which to model the possible controls and removal mechanisms for lead. In view of the above successes in modeling the removal of chromium and copper from solution as coprecipitation with a ferric oxyhydroxysulfate, it was decided to try the same approach to model the lead chemistry, (after the method of Sass and Rai 1987). The derivation of a function for lead and its implementation in PHREEQE were the same as described above for copper. Key assumptions, relations, and calculated data are summarized below.

Pb^{2+} is a major species of lead in solution over the pH range of interest, (see Baes and Mesmer 1976). $Pb(OH)_{2(cr)}$ is more soluble than anglesite, ($PbSO_4$), in this pH range, (see Lindsay 1979). The hydroxide was chosen

as the most likely of the solid phases to control lead solubility during coprecipitation with iron oxyhydroxy-sulfate. For the reaction below, log(K) = +8.15, (based on Lindsay 1979, and the NBS tables, Wagman et al. 1982).

$$Pb(OH)_{2(s)} + 2H^+ = Pb^{2+} + 2H_2O \qquad \text{Eqn. 4.33}$$

For this reaction the equilibrium constant expression may be written (using { } to denote the activity of the enclosed substance) as: Eqn. 4.34

$$\log(K) = \log\{Pb^{2+}\} + 2\log\{H_2O\} - 2\log\{H^+\} - \log\{Pb(OH)_2\}$$

where $\{Pb(OH)_2\}$ represents the activity of $Pb(OH)_2$ in the solid solution that precipitates, and for which:

$$\log\{Pb(OH)_2\} = \log(K_x) - \log(K) \qquad \text{Eqn. 4.35}$$

where K_x is composition dependent and related to the mole fraction, X, of $Pb(OH)_2$ in the precipitate. Combining equations 4.34 and 4.35 gives:

$$\log(K_x) = \log\{Pb^{2+}\} + 2\log\{H_2O\} + 2pH \qquad \text{Eqn. 4.36}$$

$Log(K_x)$ was evaluated using this equation and results calculated by PHREEQE in the original processing of sample solutions of the neutralization titration in the pH range where lead was thought to be coprecipitating with iron. The results are listed in column 2 of Table 4.2. Column 3 of the same table lists the values for $\log\{Pb(OH)_2\}$ calculated using equation 4.35.

The mole fraction of $Pb(OH)_2$ precipitating with iron at each selected point in the neutralization titration

Table 4.2 Estimated and derived quantities in the development of a relation for the coprecipitation of lead with iron during neutralization of acid solution.

pH	$\log(K_x)$	$\log\{Pb(OH)_2\}$	$X_{Pb(OH)2}$	$\log)Y_{Pb(OH)2})$
1.575	-3.178	-11.328	0.0002596	-7.7422
1.973	-2.483	-10.633	0.0001974	-6.9283
2.3505	-3.283	-11.433	0.0000135	-6.5632
2.4005	-3.2655	-11.4155	0.0000455	-7.0733
3.5146	-1.4468	-9.5968	0.0000983	-5.5894
3.8984	-0.7142	-8.8642	0.0008047	-5.7699
4.400	0.268	-7.8820	0.0057096	-5.6386
4.8275	1.1065	-7.0435	0.005625	-4.7936
5.6483	2.7439	-5.4061	0.06732	-4.2342
pure $Pb(OH)_2$	8.15	0.0000	1.0000	0.0000

was estimated to be the increment of lead removed from solution within +/- 0.005 pH units of that point, divided by the sum of the increments of lead and iron removed over the same pH range. These estimates are listed in column 4 of Table 4.2. Column 5 lists the activity coefficient of $Pb(OH)_2$ in the solid solution at each selected point. These were calculated by the relation:

$$\log(Y_{Pb(OH)2}) = \log\{Pb(OH)_2\} - \log(X) \qquad \text{Eqn. 4.37}$$

Figure 4.15 is a plot of the calculated log activity coefficients of $Pb(OH)_2$ in the solid solution precipitates versus the log of the mole fraction of $Pb(OH)_2$ in the precipitates. The least squares fit of a third order polynomial to the data produced the relation:

$$\log(Y_{Pb(OH)2}) = -0.13927 + \qquad \text{Eqn. 4.38}$$

$$3.8129[\log(X)] + 0.73110[\log(X)]^2 + 0.046105[\log(X)]^3$$

for which $R^2 = 0.906$.

Figure 4.15 Logarithmic plot of the activity coefficient of $Pb(OH)_2$ in solid solution with $Fe(OH)_3$ as a function of the mole fraction of $Pb(OH)_2$ in the solid solution.

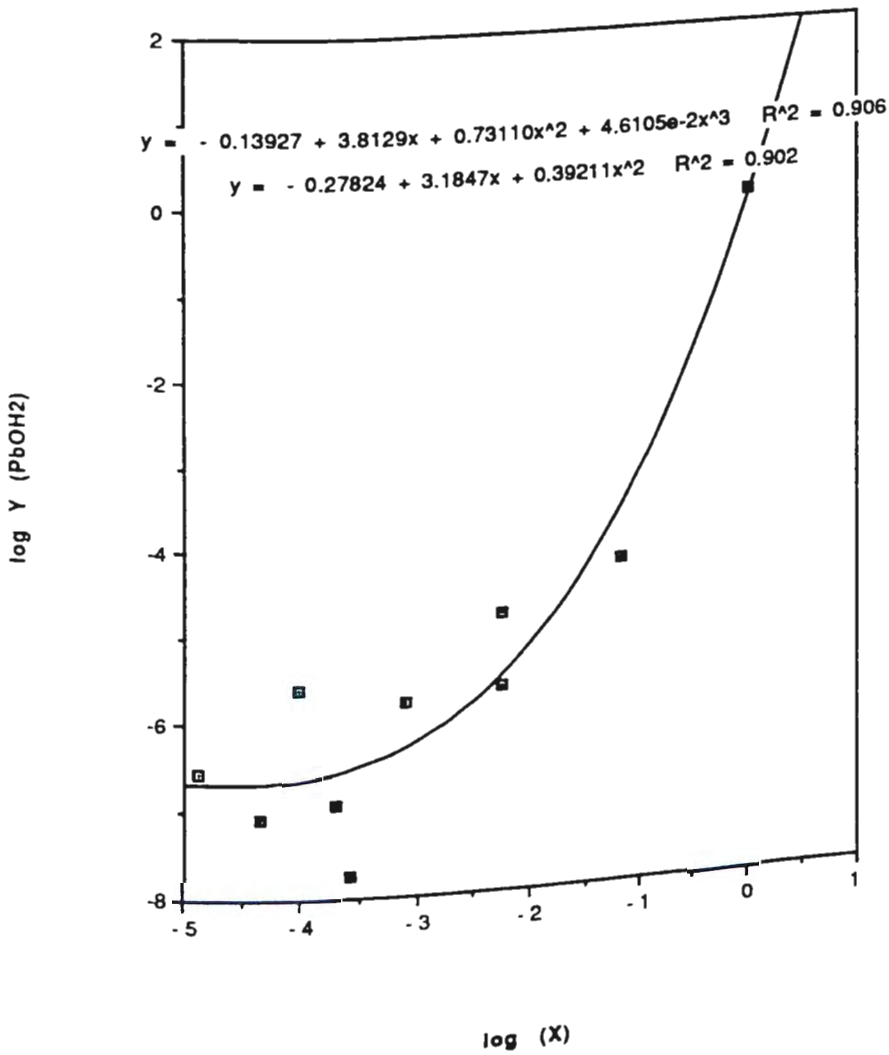

Note: Both second and third order least-squares polynomial fits to the data were calculated (after Sass and Rai 1987), and are shown. The curve plotted is from the third order fit, which was used in the derivation.

Combining equations 4.35, 4.36, 4.37, and substituting the pH function gives: Eqn. 4.39

$$\log(K) + \log(Y_{Pb(OH)2}) = \log\{Pb^{2+}\} + 2\log\{H_2O\} + 2pH - \log(X)$$

And combining equations 4.38 and 4.39 gives: Eqn. 4.40

$$\log(K) -0.13927 + 3.8129[\log(X)] + 0.73110[\log(X)]^2 + 0.046105[\log(X)]^3 = \log\{Pb^{2+}\} + 2\log\{H_2O\} + 2pH - \log(X)$$

which can be rearranged to equation 4.41, below:

$$0 = \log\{Pb^{2+}\} + 2\log\{H_2O\} + 2pH - \log(K) + 0.13927 - 4.8129[\log(X)] - 0.73110[\log(X)]^2 - 0.046105[\log(X)]^3 \quad \text{Eqn.4.41}$$

All except the last three terms in this equation are constants, or are available from the calculations after each iteration of PHREEQE. These values were summed within the program, so that equation 4.41 collapsed to the form:

$$0 = \text{CONSTANTS} - 4.8129[\log(X)] - 0.73110[\log(X)]^2 - 0.046105[\log(X)]^3 \quad \text{Eqn. 4.42}$$

The last equation was solved for X at the end of each PHREEQE iteration by a method of successive bisections between zero and one. Thus I obtained the mole fraction of lead that should be coprecipitated with iron at each adjustment made by PHREEQE of the total iron in solution. This was used to model the fractional coprecipitation of lead with iron. Specifically, for each mole of $Fe_{16}O_{16}(OH)_{12}(SO_4)_2$ that PHREEQE calculated should be precipitated from solution, 16X/(1-X/3) moles of lead were coprecipitated and (2/3)*16X/(1-X/3) moles of iron

were redissolved. This achieved the desired composition of the precipitate and preserved charge balance within the system.

Use of this model to simulate the removal of lead from the synthetic leachate during neutralization gave calculated results that roughly approximated the experimental data. (The goodness of fit may be seen in Figure 4.22 in section 4.3) Adjustment of the value used for the log(K) of the solubility of solid $Pb(OH)_2$ from +8.15 to +9.08 produced the best simulation of my lead data. This corresponds to a pure lead(II) hydroxide phase that would be 0.93 log units more soluble than the crystalline form assumed in the above derivation, which suggests a microcrystalline form of the solid.

4.2.5 Trace Elements Not Modeled

Zinc

The data of Kinniburgh and Jackson 1982, indicate that at pH about 5.1, hydrous ferric oxide will adsorb 50% of zinc. Frimmel and Geywitz 1987, evaluated differential pulse polarography for recording the coprecipitation with ferric hydroxide of 3 micromolar metal ions from solutions 0.1 millimolar in total iron. Their data suggest the removal of zinc in the pH range 5.5 through 9.5. The failure of the PHREEQE equation solving sub-

routines to converge beyond pH 5 precluded useful modeling of the zinc data.

Cadmium

Inspection of the cadmium data in the neutralization titration (Table 3.6) shows that cadmium was largely conserved in solution until after pH 4.8. This agrees with adsorption on hydrous ferric oxide in the pH range of 4.5 or 5 through 7 or 7.5, as in Dzombak and Morel 1990. The data of Frimmel and Geywitz suggest the removal of 3 micromolar cadmium by coprecipitation with ferric hydroxide to occur in the pH range of 6 to 9.5. As with zinc, this also could not be modeled due to convergence problems of the computer program PHREEQE beyond pH 5.

Arsenic

The arsenic data from the leachate neutralization are plotted and discussed in section 4.4.2. No suitable basis was found with which to model the removal of arsenic from acidic leachates containing high levels of total iron and sulfate during neutralization.

Selenium

The selenium data are unreliable, (as is clear from Table 3.6), and no attempt was made to model selenium.

4.3 TEST AND EVALUATION OF THE MODEL

4.3.1 Simulation of Synthetic Leachate Neutralization

The PHREEQE geochemical program, as adapted and developed to model the loss of iron, sulfate, aluminum, chromium, copper, and lead during the neutralization of acidic leachates, was tested first as to its ability to simulate the results of our neutralization titration experiment. The initial input for the simulation was: an option card specifying the type of problem to be solved, (model an initial solution and simulate equilibration with other phases and reaction with an added reagent); the data describing the first sample of the titration experiment, (which was taken before any base titrant was added); specifications for other phases with which the system was to be equilibrated, (O_2 and CO_2 from the air, the silica glass of the reaction vessel, and eventually solid precipitates that should form); special phases to be monitored with respect to saturation index, (such as soil-$Fe(OH)_3$ as defined by Lindsay 1979); and specification of the neutralization reaction to be used, (addition of sodium bicarbonate). The simulation was set up to proceed in steps that would predict the concentrations of all elements defined to be in the system at the pH of samples taken during the laboratory neutralization.

Table 4.3 summarizes the experimental data and the results of the computer simulation as the common logarithm of the total molal concentration of each element of interest. An overview of the results of the entire simulation is given in Figure 4.16, which is a plot of the log total molal concentration of each element versus pH. This plot allows comparison of the relative concentrations of the elements, the timing of their respective removal processes in terms of pH, and the relative shape, steepness, and extent of their concentration changes. The calculations were terminated just beyond pH 5 due to the failure of the PHREEQE equation solving subroutines to achieve convergence to a set of simultaneous solutions for all the equilibria involved in the expanded model that has been developed based on the PHREEQE program code.

Figure 4.17 shows both the observed and simulated iron data versus pH. The fluctuations of the experimental pH data between pH 2.25 and 2.5 are due to incomplete equilibration of the system between titration and sampling events, as will be discussed in section 4.4.1 The divergence of the data sets after pH 4.83 is thought to be due to the use of an erroneous iron concentration for the last point plotted, (a value was assumed because the actual solution concentration was below the detection

Table 4.3 Neutralization Titration: Data and Simulation Results *

	Sodium		Sulfate		Iron		Aluminum	
pH	est	sim	est	sim	obs	sim	obs	sim
1.575	0.000	0.000	-0.769	-0.769	-1.059	-1.059	-3.253	-3.396
1.973	-1.321	-1.355	-0.787	-0.769	-1.088	-1.059	-3.413	-3.396
2.077		-1.288		-0.769		-1.059		-3.396
2.300	-0.820	-0.687	-0.824	-0.786	-1.400	-1.468	-3.400	-3.396
2.361	-0.807	-0.633	-0.832	-0.789	-1.388	-1.605	-3.422	-3.396
2.440	-1.034	-0.586	-0.802	-0.792	-1.149	-1.795	-3.430	-3.396
2.474	-0.639	-0.571	-0.854	-0.793	-1.909	-1.880	-3.317	-3.396
2.874	-0.582	-0.508	-0.869	-0.797	-2.963	-2.932	-3.226	-3.396
3.019		-0.503		-0.798		-3.320		-3.396
3.290		-0.499		-0.798		-4.039		-3.396
3.515	-0.566	-0.497	-0.867	-0.798	-4.428	-4.611	-3.627	-3.619
3.750		-0.496		-0.798		-5.143		-3.851
3.898	-0.539	-0.495	-0.842	-0.798	-5.431	-5.413	-3.846	-3.997
4.828	-0.533	-0.495	-0.837	-0.798	-6.087	-6.089	-3.885	-3.870
5.000		-0.494		-0.799		-6.168		

* Notes: All concentrations are log(molality)
est = estimated concentrations
sim = simulation results
obs = observed concentrations

*Table 4.3 (continued) Neutralization Titration: Data and Simulation Results**

	Chromium		Copper		Lead	
pH	obs	sim	obs	sim	obs	sim
1.575	-4.654	-4.654	-4.819	-4.819	-5.326	-5.375
1.973	-4.680	-4.654	-4.834	-4.819	-5.576	-5.375
2.077		-4.654		-4.819		-5.375
2.300	-4.770	-4.704	-4.845	-4.833	-5.740	-5.643
2.361	-4.749	-4.714	-4.853	-4.835	-5.445	-5.687
2.440	-4.672		-4.850		-5.413	
2.474	-4.856	-4.737	-4.861	-4.840	-7.082	-5.785
2.874	-5.016	-4.970	-4.862	-4.867	-6.875	-6.653
3.019		-5.030		-4.871		-6.733
3.290		-5.299		-4.882		-6.920
3.515	-5.539	-5.454	-5.011	-4.887	-7.267	-6.983
3.750						
3.898	-5.852	-5.761	-5.542	-5.343	-7.404	-7.052
4.828	-6.295	-6.690	-6.168	-6.357	-7.004	-7.150
5.000		-7.101		-6.751		-7.169

* Notes: All concentrations are log(molality)
est = estimated concentrations
sim = simulation results
obs = observed concentrations

Figure 4.16 Logarithmic plot of sulfate and trace element concentrations from the neutralization titration simulation versus pH.

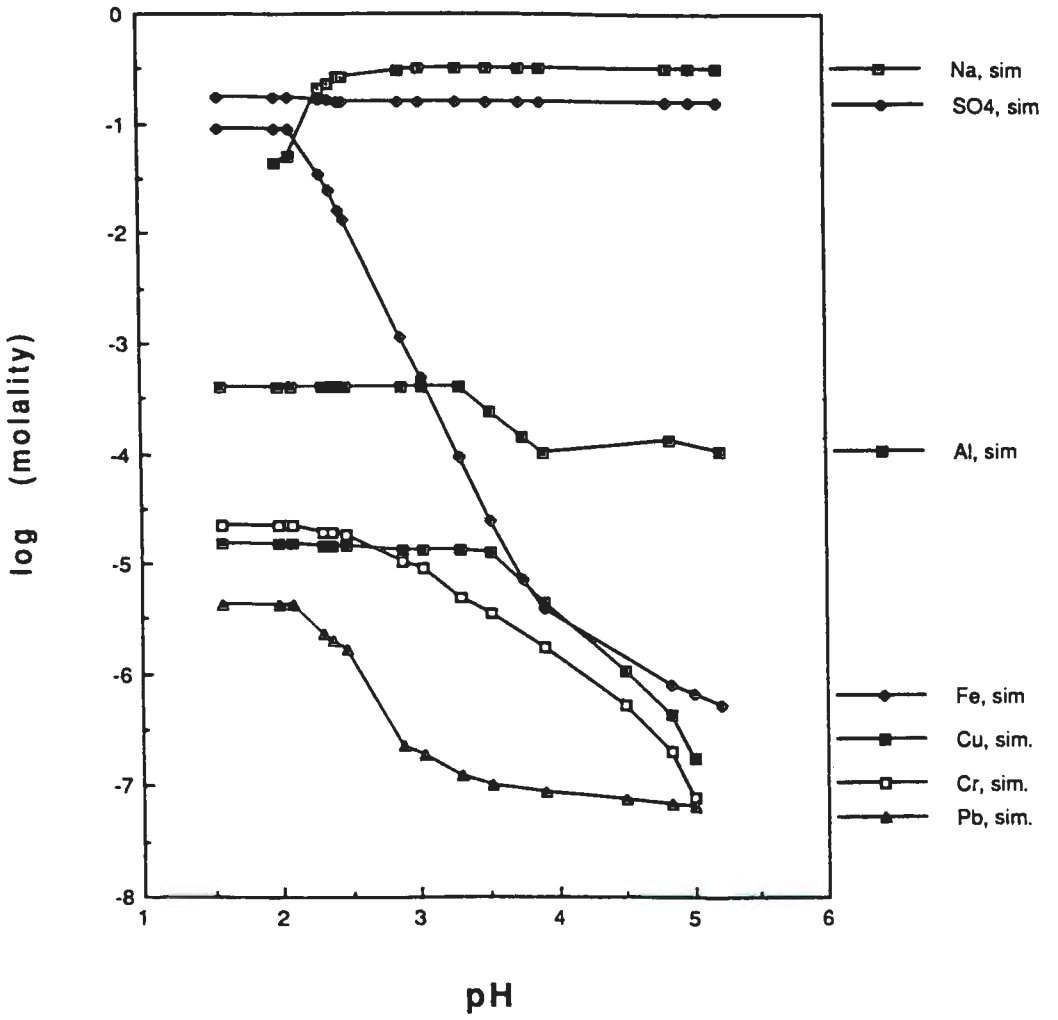

Note: Concentrations are log(molal).

Figure 4.17 Logarithmic plot of observed and simulated iron concentrations in the neutralization titration as a function of pH.

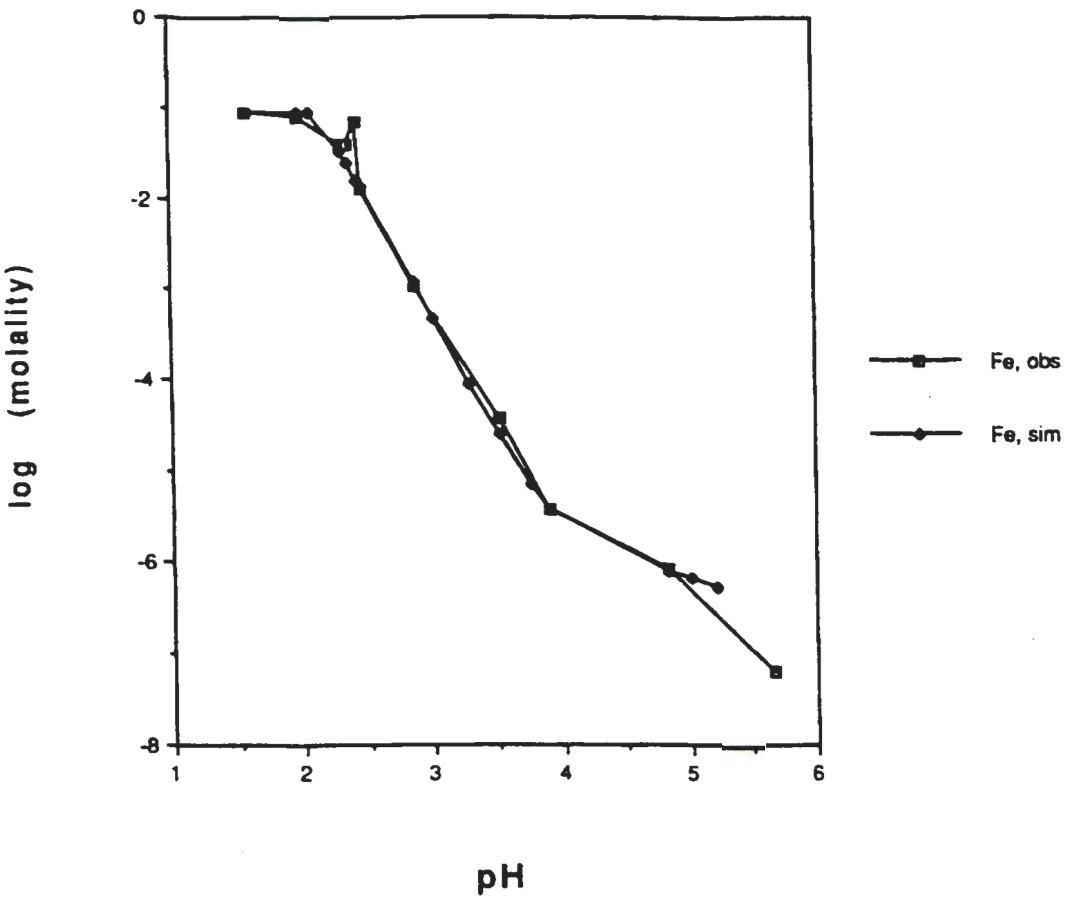

Note: The final "observed" iron value was not measured, but was arbitrarily selected as a value that allowed the computer simulation to achieve convergence past pH = 5.

limit). The simulation results past pH 5 are thought to be a better estimate of the actual iron concentration remaining in solution.

Sodium and sulfate data, both observed and simulated, are superimposed on the iron data in Figure 4.18. No sodium or titrant had been added to the first sample, so its concentration was assumed to be zero and not plotted. Thereafter, the experimental sodium was calculated based on the added sodium bicarbonate titrant. In the pH 2.25 to 2.5 range, the sodium fluctuations mirror those of the iron data: when less sodium has been added, more iron is still in solution. This indicates that the pH measured in these solutions was inappropriate (due to incomplete equilibration of the system) rather than that the iron data are erroneous.

Sodium bicarbonate neutralizes acidic solutions according to the reaction:

$$1NaHCO_3 + 1H^+ = 1Na^+ + 1CO_2 + 1H_2O \qquad \text{Eqn. 4.43}$$

PHREEQE does not keep a mass balance for hydrogen, and so does not accept hydrogen as a reagent input. Throughout the simulation, the addition of base was modeled as $Na(CO_3)_{0.5}$ reacting with hydrogen ions as follows:

$$1Na(CO_3)_{0.5} + 1H^+ = 1Na^+ + 0.5CO_2 + 0.5H_2O \qquad \text{Eqn. 4.44}$$

Figure 4.18 Logarithmic plot of observed and simulation concentrations of sodium, sulfate, and iron in the neutralization titration versus pH.

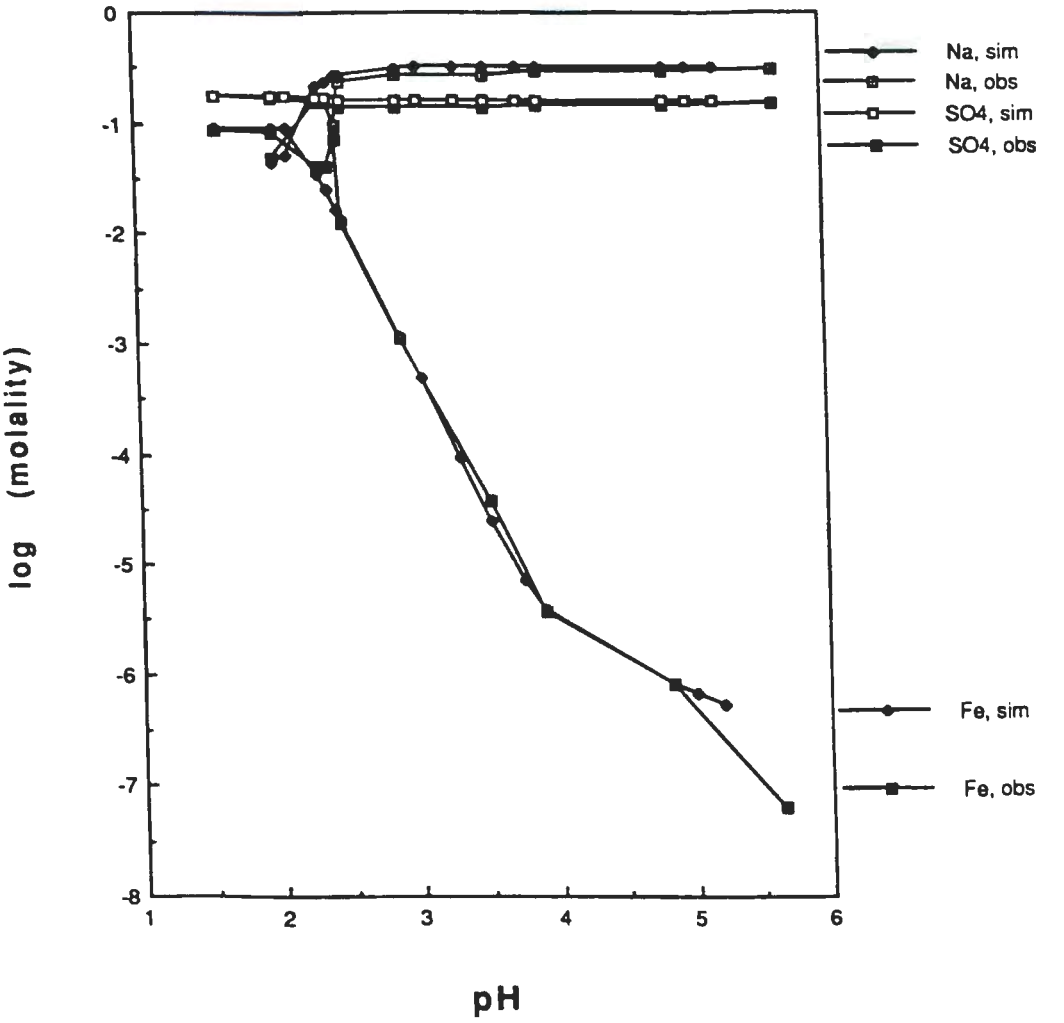

Notes: Concentrations are log(molal). See text for discussion of sodium and iron fluctuations in the pH range between 2.25 and 2.50.

Thus, each molecule of added base neutralized one hydrogen ion, which was replaced in solution by one sodium ion, just as in equation 4.43. The carbon dioxide produced in each case was equilibrated with the atmosphere, so that the solution concentrations were not a function of the CO_2 produced by the reactions. The greater amount of water produced in the laboratory reaction was offset by evaporation from the system, so that the production of less water in the simulation was deemed to be acceptable. Throughout the simulation, the total sodium concentration was just that accumulated in the system during the neutralization (according to equation 4.44) as necessary to reach each target pH.

No simulation was attempted for the effects of sample removal and dilution by added titrant, which explains those instances where the simulation results run slightly higher than the laboratory results, such as for sodium and sulfate. The removal of sulfate from solution during the precipitation of $Fe_{16}O_{16}(OH)_{12}(SO_4)_2$ is theoretically less than 10 percent of the initial total sulfate, and the effects are barely noticeable.

The aluminum data, both observed and simulated, are superimposed on that of iron in Figure 4.19. The fluctuations in the simulation points for aluminum relative to

Figure 4.19 Logarithmic plot of observed and simulation concentrations of aluminum and iron in the neutralization titration versus pH.

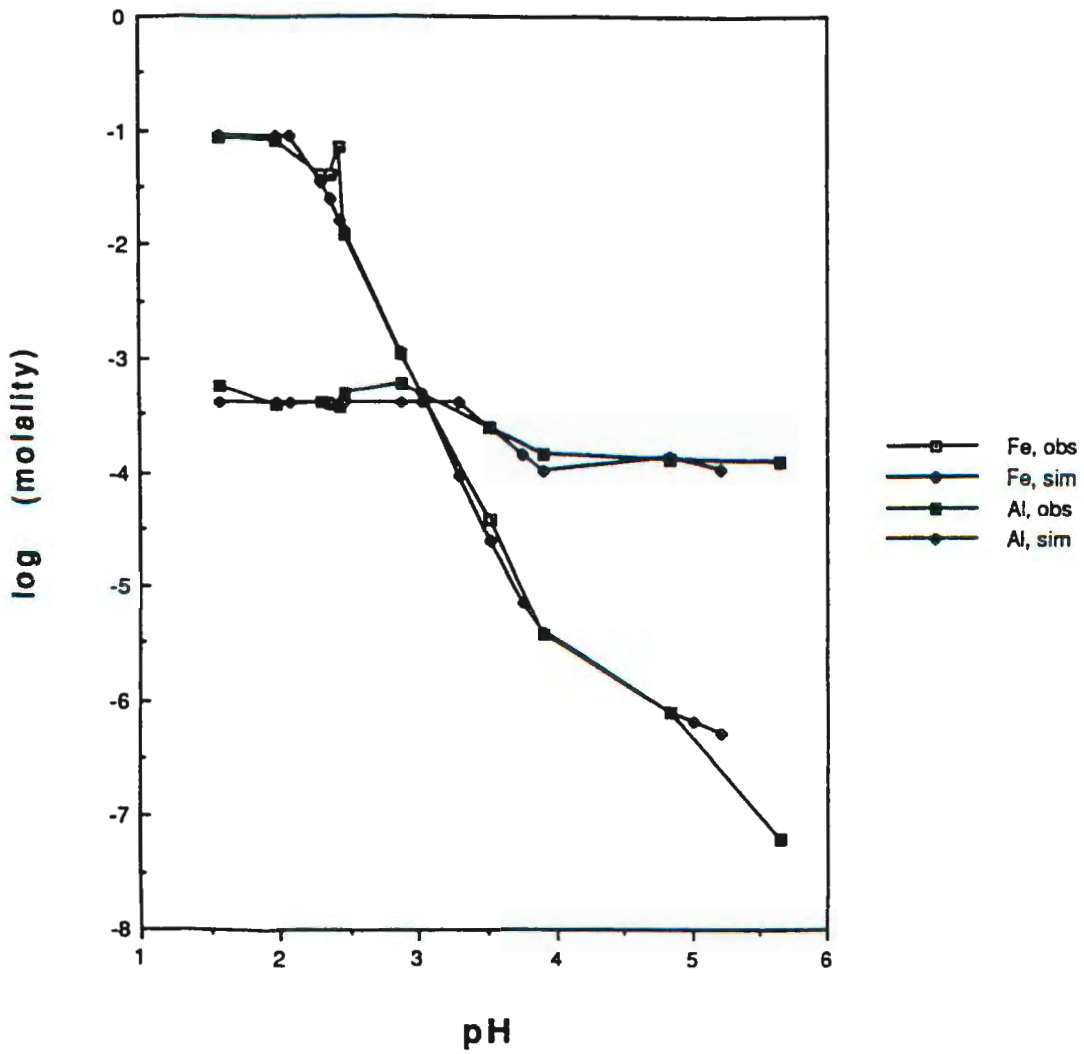

the observed concentrations are due to the series of different pure stable phases used to model the removal of aluminum between pH 3.5 and 5. (See section 4.2.4). Small adjustments of the log(K) of each compound could be made such that the curve would be smoothed and approximate the laboratory data better.

Figure 4.20 presents the observed and simulated data for chromium superimposed on that of iron. The smoothness of the curve and the goodness of fit are due largely to the excellent work of Sass and Rai 1987, developing their mathematical model for the coprecipitation of chromium with ferric iron. The middle portion of the curve accounts for the removal of chromium from solution before saturation with respect to pure crystalline $Cr(OH)_3$. The downward turn about pH 5 corresponds to a shift from formation of the chromium-and-iron hydroxide solid solution to the precipitation of pure chromium(III) hydroxide. Decreasing log(K) for solid $Cr(OH)_3$ improves the fit at lower pH, but accentuates the divergence of the simulation from the experimental above pH 4. Conversely, increasing log(K) improves the fit above pH 4, but worsens the fit at lower pH.

Figure 4.20 Logarithmic plot of observed and simulation concentrations of chromium and iron in the neutralization titration versus pH.

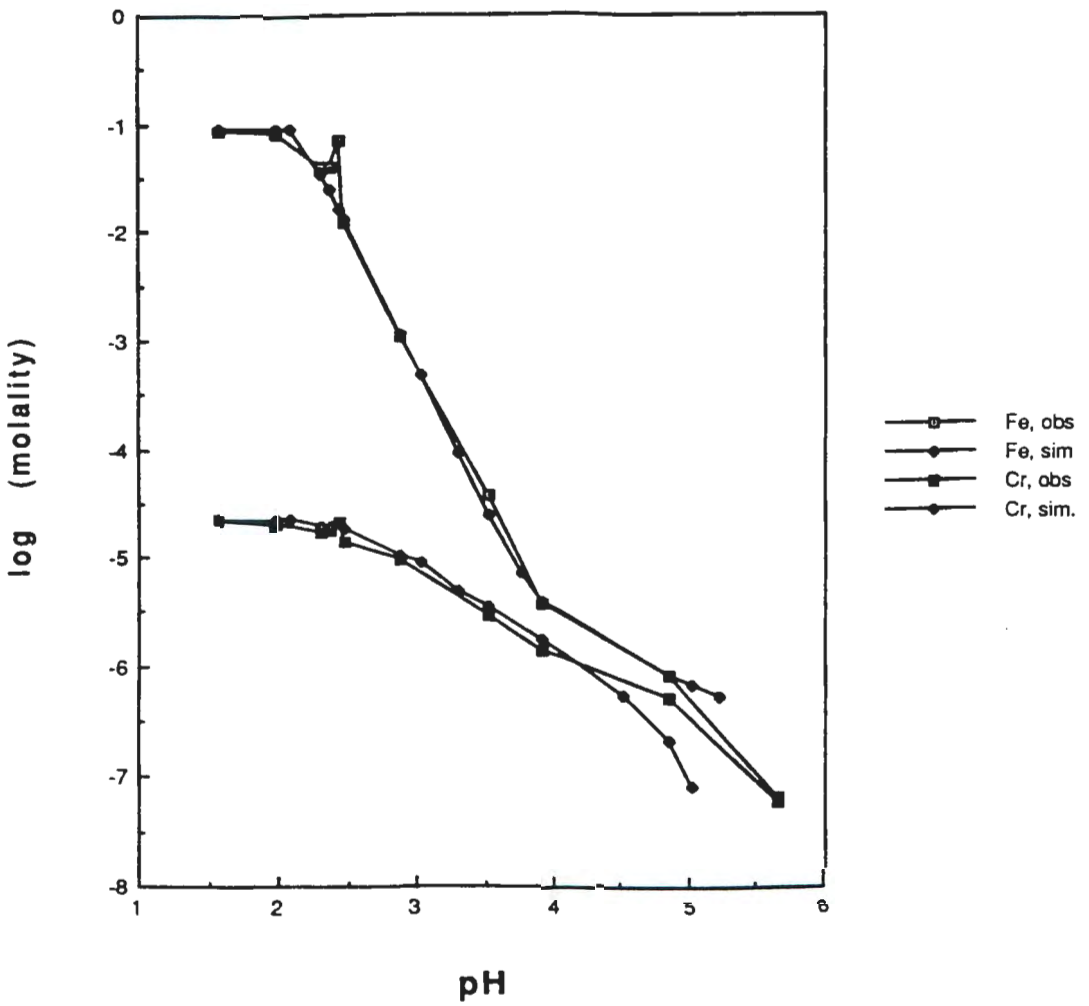

The laboratory and simulation data for copper are plotted in Figure 4.21 with the iron data. The simulation data run higher than the experimental data for copper due partly to the omission of modeling the effects of sample withdrawal and dilution by titrant. Smaller log(K) for the pure copper(II) hydroxide solubility improved the earlier fit, and also increased the divergence of the two data sets after about pH 4.5; while-larger log(K) improved the later fit but worsened the fit between pH 2.5 and 4.5. The middle portion of the curve describes the removal of copper from solution by coprecipitation with iron before saturation is reached with respect to pure, solid copper(II) hydroxide. Of course, early removal of some copper delays the system from reaching saturation until a higher pH. Eventually, at higher pH, the unprecipitated iron concentration is so depleted that it ceases to be an important removal mechanism for copper by coprecipitation. But saturation with respect to pure copper(II) hydroxide results in a shift to formation of the pure solid, and the simulation curve turns noticeably downward to adopt the slope of copper removal as $Cu(OH)_2$ with rising pH. Saturation with respect to crystalline copper ferrite was indicated by the PHREEQE saturation index calculations at about pH 3,

Figure 4.21 Logarithmic plot of observed and simulation concentrations of copper and iron in the neutralization titration versus pH.

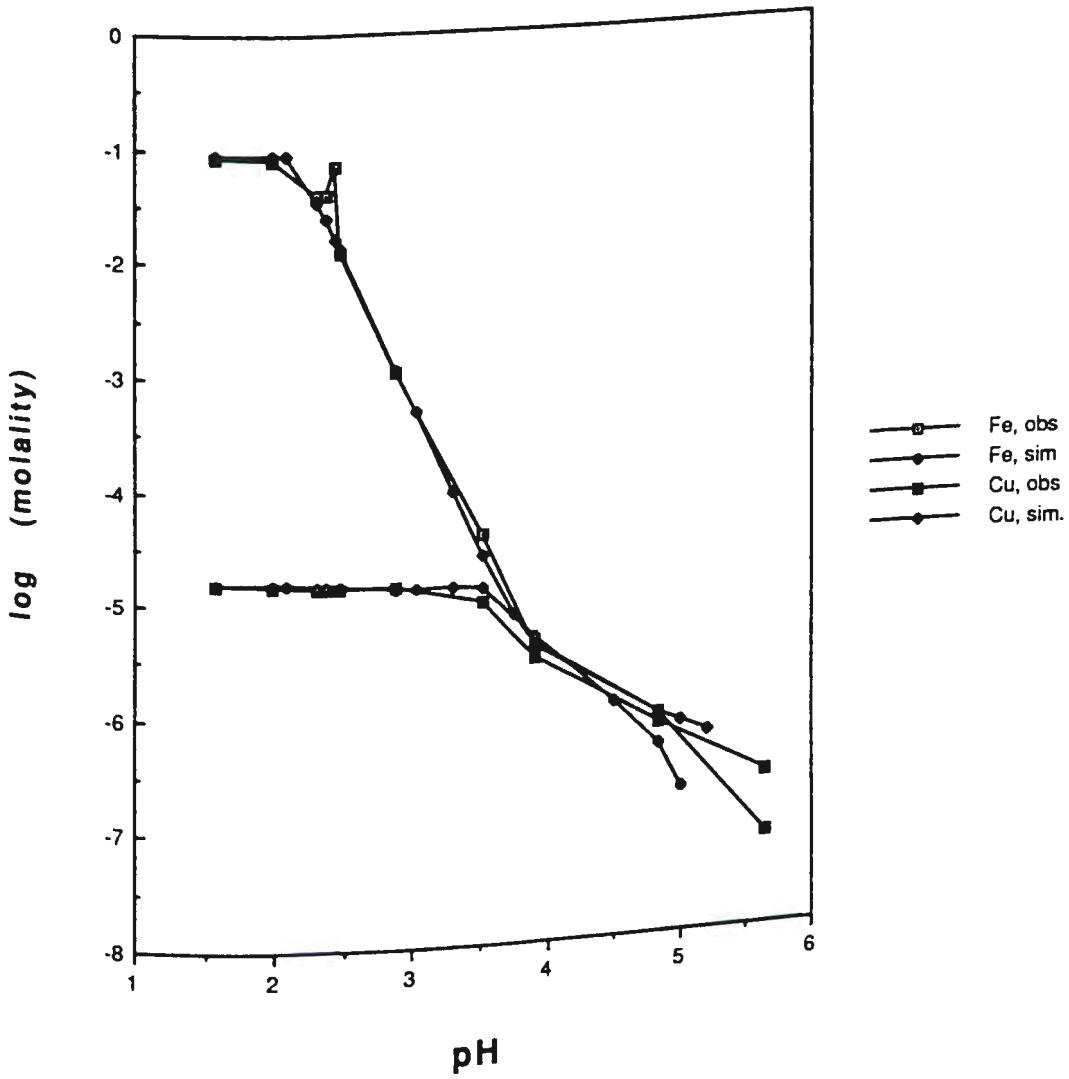

well before significant removal of copper by coprecipitation with iron. However, $CuFe_2O_{4(cr)}$ is not expected to form quickly in an aqueous system at room temperature.

The lead data, both observed and simulated, are presented in Figure 4.22, superimposed on the iron data. The simulation data only roughly approximates that of the experimental work, due to the noise and uncertainty of the latter. The simulation did approximate the highest lead concentrations of the early samples, the pH range of significant removal of lead, and the average concentrations found in the last few samples.

It should be noted that the pH range found in this study of lead removal from synthetic coal leachate during neutralization with sodium bicarbonate contrasts with results obtained with lead in other systems. Baes and Mesmer 1976, show 10^{-5} molal lead(II) to be soluble up to pH 9.5 in a simple aqueous system with solubility limited by PbO. The hydrous ferric oxide surface complexation model of Dzombak and Morel 1990, predicts the removal of lead in the pH range of 4 to 5. However, Buffle 1988, summarizing data on the adsorption edges of metal ions on oxide surfaces, indicates the removal of 1.25×10^{-4} molar lead by Fe(III) oxyhydroxide gel (where total iron was 0.093 molar) to occur between pH 2 and 4.

Figure 4.22 Logarithmic plot of observed and simulation concentrations of lead and iron in the neutralization titration versus pH.

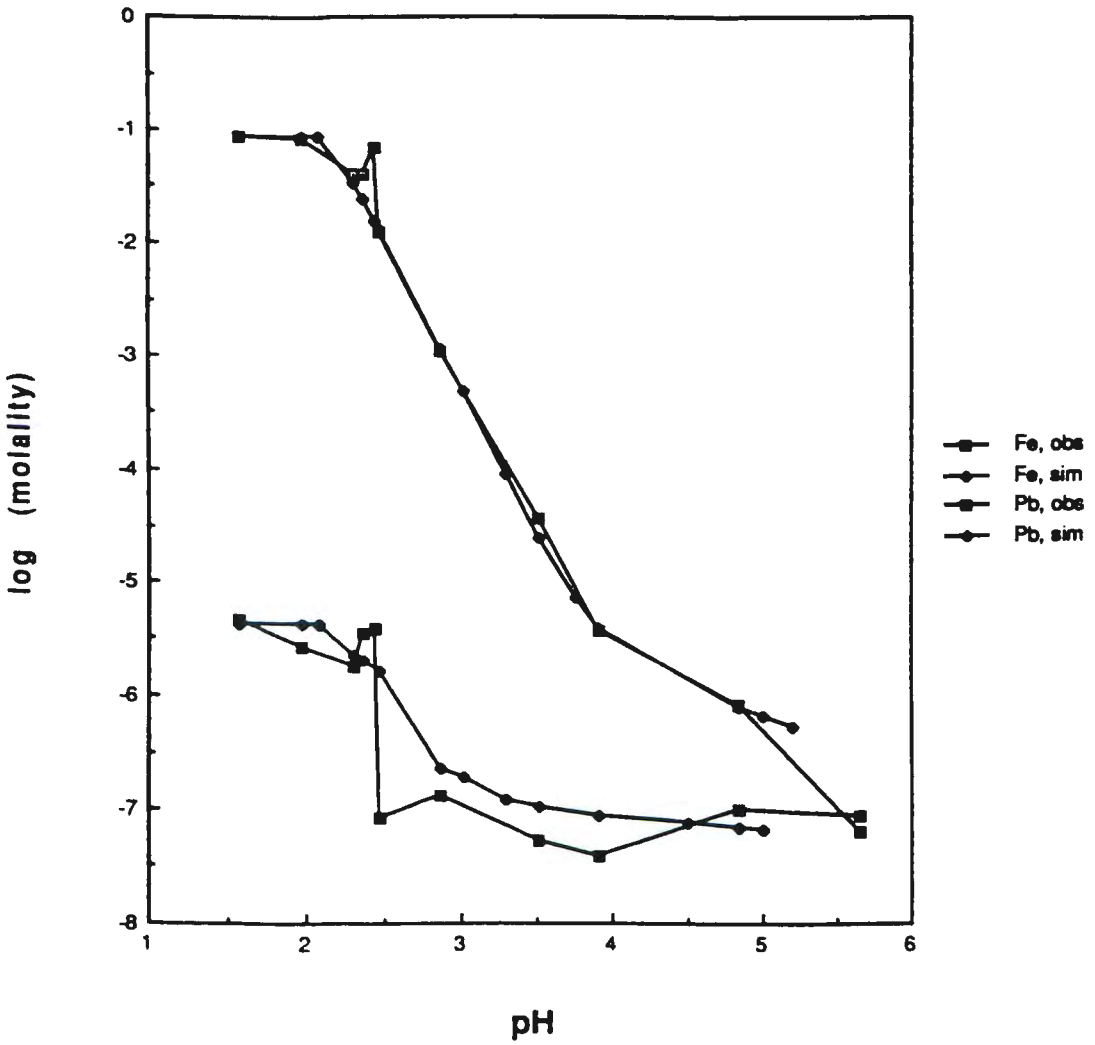

Compared to the experimental data from the neutralization, the plot of data from this simulation gives a smoother curve that better fits the expected sigmoid shape for removal of metal ions from solution by sorption/coprecipitation processes.

4.3.2 Application of the model to West Squaw Creek data

Filipek, Nordstrom, and Ficklin 1987, reported a study of the interaction of acid mine drainage with West Squaw Creek in northern California. The North Fork is largely uncontaminated. The South Fork receives drainage from several mines containing massive sulfide deposits. The site of greatest contamination of the entire West Squaw Creek was found just upstream of the junction of these forks. Below this junction were found two more small, uncontaminated tributaries that joined West Squaw Creek before it emptied into Shasta Lake. This system was selected as a good test for the application of our computer model to field data where acid mine drainage contaminated with trace metals and containing high concentrations of iron and sulfur was being diluted and neutralized by tributary waters of pH 5.5 to 6. Table 4.4 summarizes data from Filipek et al. 1987, that are the basis for this simulation/test.

Table 4.4 West Squaw Creek: Field Data,* after Filipek et al. 1987.

Site:	24	25	26	27	28	29	30	31
pH	2.70	5.55	2.70	5.25	2.75	2.95	6.10	3.00
Ca	-3.40	-3.60	-3.46	-3.90	-3.49	-3.52	-3.17	-3.49
Mg	-3.31	-4.02	-3.48	-4.18	-3.47	-3.49	-3.92	-3.52
Na	-3.70	-3.70	-3.69	-4.08	-3.70	-3.68	-3.51	-3.67
K	-5.14	-5.69	-5.31	-5.42	-5.29	-5.07	-5.99	-5.23
Fe	-2.89	-7.0	-3.13	-6.8	-3.24	-3.67	-6.47	-3.71
Mn	-4.78	<-6.7	-5.00	<-6.7	-5.00	-5.06	<-6.7	-5.09
Al	-3.25	-6.5	-3.48	-5.97	-3.48	-3.43	-6.25	-3.47
Si	-3.16	-3.50	-3.35	-3.70	-3.33	-3.33	-3.40	-3.32
Cl	-4.19	-4.8	-4.47	-5.1	-4.9	-4.8	-4.32	-4.9
C	<-4.8	-3.53	<-4.8	<-4.8	<-4.8	<-4.8	-3.11	<-4.8
SO_4	-2.40	-3.87	-2.52	-3.94	-2.608	-2.731	-3.25	-2.673
F	-4.51	-5.4	-4.88	-5.8	-5.00	-4.96	-4.96	-5.13
Zn	-3.725	-7.2	-3.96	-6.81	-3.96	-4.04	-7.3	-4.08
Cu	-3.742	<-6.8	-4.00	<-6.8	-3.99	-4.10	<-6.8	-4.12

*Note: All concentrations are log(molality).

The water analysis for site 24, about one-half mile below the site of greatest contamination, and just above the junction of the South Fork with the North Fork, was chosen as the starting data for a computer simulation that would test our model's ability to predict the composition of the stream water below each confluence. Site 25 provided the data for the North Fork waters just above the junction, and site 26 provided data on the composition soon after the waters mixed. About one-half mile downstream, the first small, uncontaminated tributary empties into Squaw Creek. Its composition was determined by samples from site 27; while site 28 data described the system just after these two had mixed.

There followed an 0.8 mile stretch of Squaw Creek having no known tributaries before its junction with Mary's Fork, the second known source of dilution by uncontaminated water. Site 29 data described Squaw Creek just above this junction, site 30 data described Mary's Fork water, and site 31 data describes the composition of the creek water about one-tenth of a mile below the junction. The observed data (from Table 4.4) for pH and the elements to be studied in this simulation are plotted in Figure 4.23; and the results of the simulation (from Table 4.5) are plotted in Figure 4.24. (Note that both plots only show data for sites along the flow path of the contaminated stream, and not for the tributaries.) As

Table 4.5 West Squaw Creek: Simulation results*

Site:	26	28	29	31
pH	2.85	2.77	2.85	2.98
Ca	-3.47	-3.47	-3.50	-3.49
Mg	-3.48	-3.48	-3.55	-3.51
Na	-3.70	-3.70	-3.70	-3.67
K	-5.29	-5.29	-5.35	-5.10
Fe	-3.13	-3.25	-3.35	-3.70
Mn	-5.00	-5.00	-5.10	-5.09
Al	-3.48	-3.49	-3.58	-3.46
Si	-3.26	-3.27	-3.31	-3.34
Cl	-4.35	-4.36	-4.42	-4.72
C	-4.95	-4.95	-4.95	-4.95
SO_4	-2.61	-2.62	-2.71	-2.75
F	-4.69	-4.70	-4.77	-4.96
Zn	-3.95	-3.96	-4.05	-4.08
Cu	-3.96	-3.97	-4.07	-4.13

*Note: All concentrations are log(molality).

will be seen in subsequent figures, the model closely approximates the field data through site 28, but the predictions for site 29 diverge from the observed data.

During the 0.8 mile stretch between sites 28 and 29, the investigators did not find identifiable sources of dilution or neutralization. However, they did note among the elements thought to be conserved in the system, a change of stream composition that could be accounted for by a 20% dilution of the main stream by undetected base flow or seeps of uncontaminated water (such as reported for sites 27 and 30 that were immediately above and below this section).

Figure 4.23 Logarithmic plot of observed pH and concentrations of selected elements in West Squaw Creek, West Shasta, California.

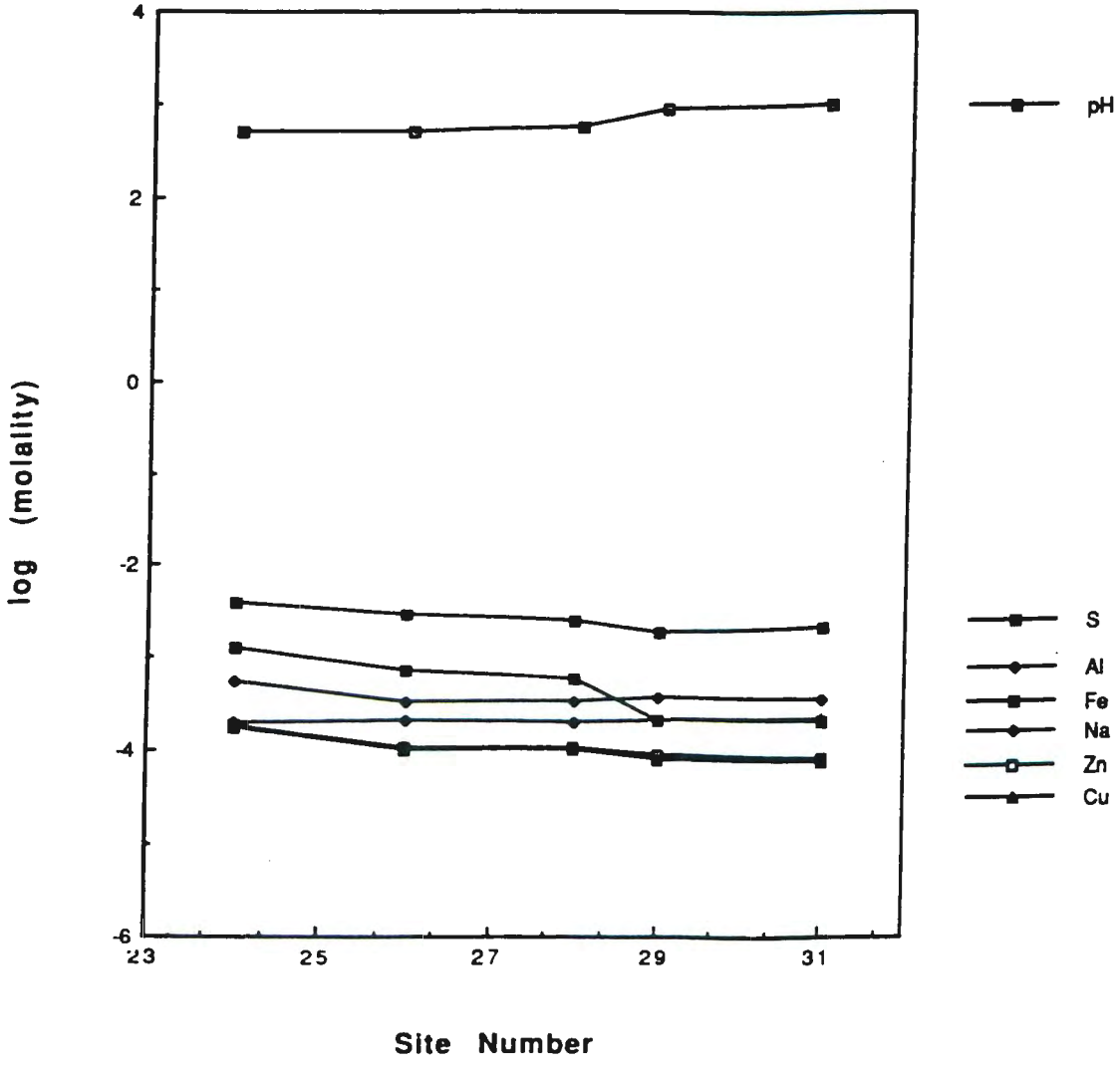

Note: Concentrations are log(molal) except for pH, which is plotted in terms of pH units.

Figure 4.24 Logarithmic plot of simulation pH and concentrations of selected elements for West Squaw Creek, West Shasta, California

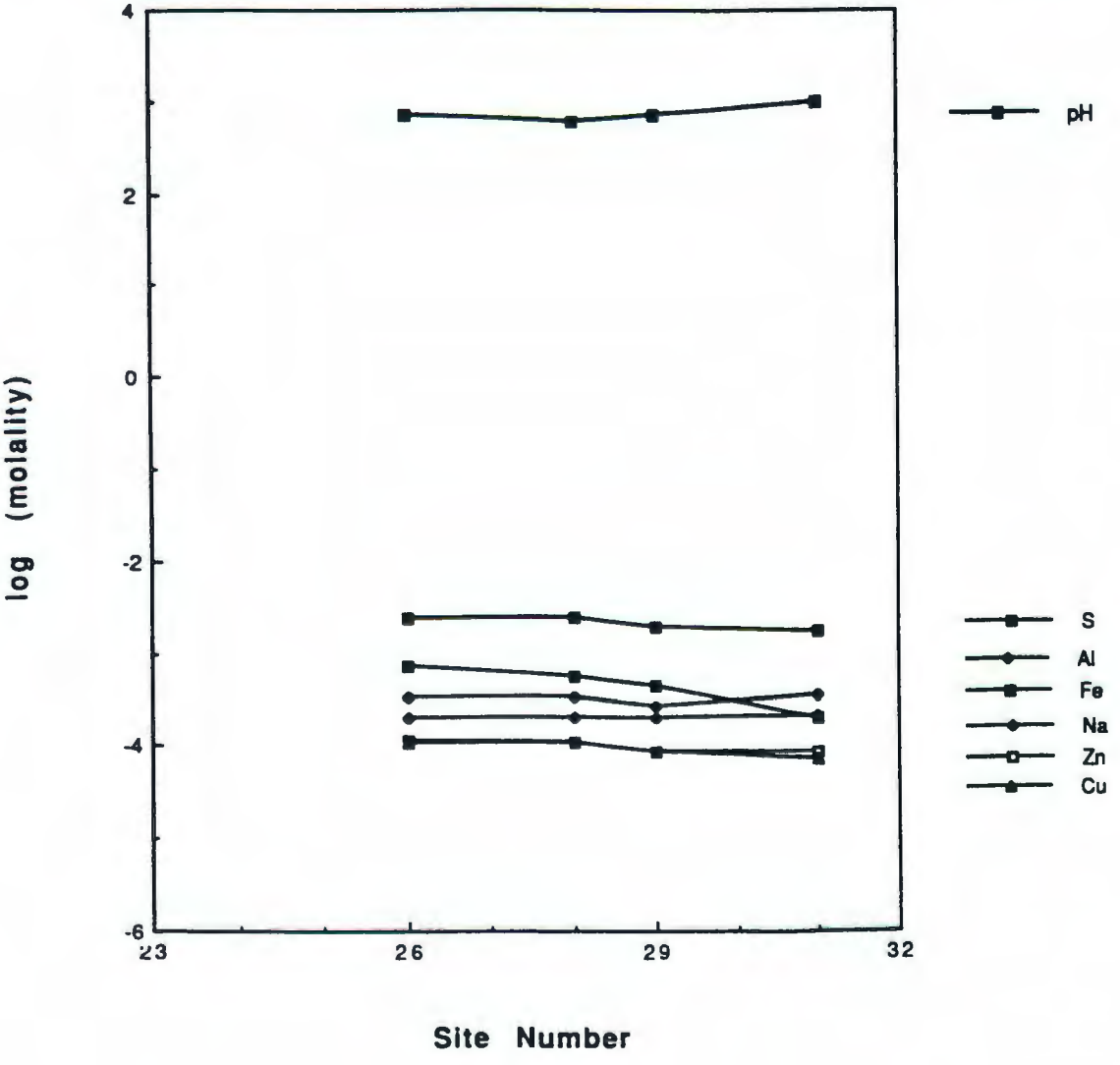

Note: Concentrations are log molal except for pH, which is plotted in terms of pH units.

Without quantitative data, it was impossible to obtain a good prediction of the stream composition at site 29, (and therefore of site 31 as well). Thus, the simulation results for site 31 were calculated from input of observed data from sites 29 and 30.

Figure 4.25 shows both the observed and simulation data for pH and filterable sulfur and iron. The authors of the study calculate that the South Fork:North Fork mixing ratio was approximately 60:40 of waters that were pH 2.70 and 5.55 respectively. They explained the absence of pH increase just below the confluence (site 26 also had pH 2.70) to be the result of continued oxidation of Fe^{2+} to Fe^{3+} and hydrolysis, and (or) the oxidation of any remaining sulfide. In the simulation, 5.1% of the total iron was precipitated as $Fe(OH)_3$ in order to obtain reasonably good fits of both pH and iron to the observed data. However, the system was still supersaturated with respect to $Fe_{16}O_{16}(OH)_{12}(SO_4)_2$, for which a saturation index of +16.0710 was calculated, (which corresponds to +1.0044 per iron atom).

Again after the first tributary (site 27) diluted Squaw Creek slightly, (approximately 2%), both the predicted pH and iron concentrations were significantly higher than observed at site 28, suggesting that some precipitation of iron had continued after site 26.

Figure 4.25 Logarithmic plot of observed and simulation pH, sulphate, and iron for W. Squaw Creek.

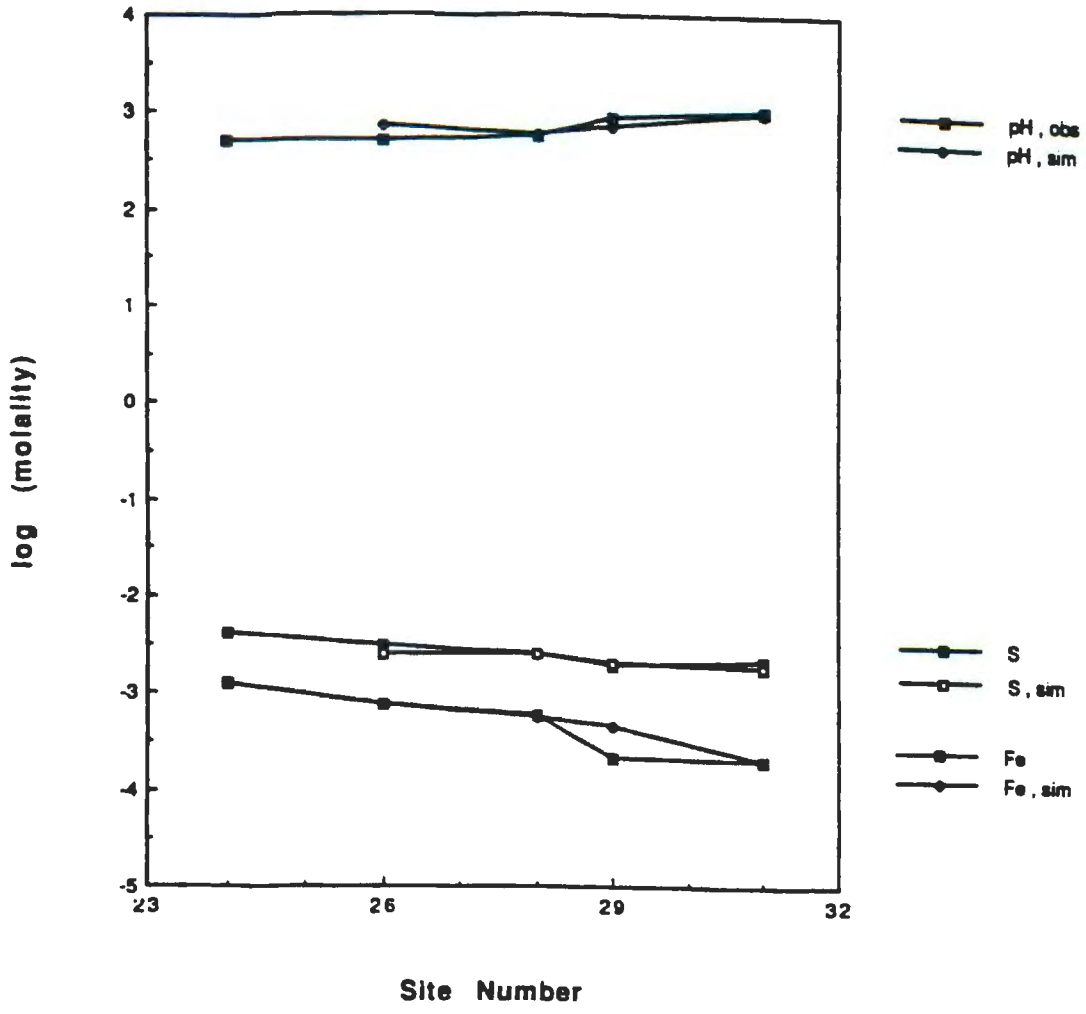

Note: Concentrations are log(molal) except for pH, which is plotted in pH units.

This time 22.5% of the iron calculated to be still in the system was precipitated as $Fe(OH)_3$, yet the system was still supersaturated with respect to soil-$Fe(OH)_3$ by one order of magnitude, (and $Fe_{16}O_{16}(OH)_{12}(SO_4)_2$ by +0.6888 log units per iron atom).

To approximate the prediction of the creek composition at site 29, the stream was diluted by 20% with "base flow" like that of site 25 (chosen because these North Fork waters were of intermediate composition between those of the other uncontaminated waters in the region, analyzed for sites 27 and 30). The pH was predicted to be 2.85 (2.95 was observed) and the predicted total iron was double the observed concentration of 2.15×10^{-4} molal. The authors estimated that from 53% to 62% of the dissolved iron of site 28 precipitated before site 29, citing evidence of iron precipitation on the stream boulders and all along its banks in this stretch. Since precipitation of more iron would have increased the error in the predicted pH and thrown off subsequent calculations for the other metals in the system, the simulation was interrupted at this point and restarted using the observed site 29 data as input, as mentioned above. The resulting concentrations calculated for site 31 were in very good agreement with those observed.

The filterable sulfur observed at site 26 was higher that the model predicted based on simple dilution of the site 24 sulfur concentration. The stream, with its burden of leachates from sulfidic mines, almost certainly was not yet in equilibrium with atmospheric oxygen by the time the water reached site 26. Continued oxidation of suspended sulfidic material rendering it water soluble could explain the excess sulfur and iron found in the filtered samples at site 26.

The sulfur concentrations predicted for subsequent sites fit the observations quite well, except for site 31 which is 9.5% below the measured value. The authors did not discuss this stream junction and minerals and evidence for reaction, although they did flag the data for sodium, sulfur, and SiO_2 as being higher for site 31 than for either of the contributing streams. Their data also indicates higher ferrous iron concentration at site 31 than at site 29, despite a slight decrease in total iron. This suggests the possibility that there was an undetected source of sulfide that was being oxidized to soluble sulfate by ferric iron in solution, which in turn was reduced to ferrous iron. The counter ion for the sulfide is unknown, as it is assumed that the excess sodium was associated with a silicate being dissolved.

Figure 4.26 shows both the observed and simulation data for aluminum and zinc; (pH is included for reference). The predicted concentrations show excellent agreement with those observed, except for aluminum at site 29. In their discussion of the data, the authors suggest that dissolution of Al minerals, possibly clays, may occur along this stretch. This would tend to minimize the lowering of pH with the precipitation of iron, and could produce the observed increase of aluminum concentration even in the face of the estimated dilution by base flow. Without quantitative data, these effects of the suggested dissolving of Al minerals could not be modeled, so the site 29 observed aluminum was input for the last part of the simulation, as previously mentioned.

The simulation results for zinc concentrations all along West Squaw Creek show excellent agreement with the observed concentrations, as do the simulation results for sodium and copper, (shown in Figure 4.27). Since no zinc removal mechanisms were incorporated in the model (which performs simulations of dilution and neutralization of aqueous systems between pH 1.5 and 5.0); since sodium is generally expected to be conserved in solution (unless significantly involved in precipitation/dissolution of

Figure 4.26 Logarithmic plot of observed and simulation pH, aluminum, and zinc for W. Squaw Creek.

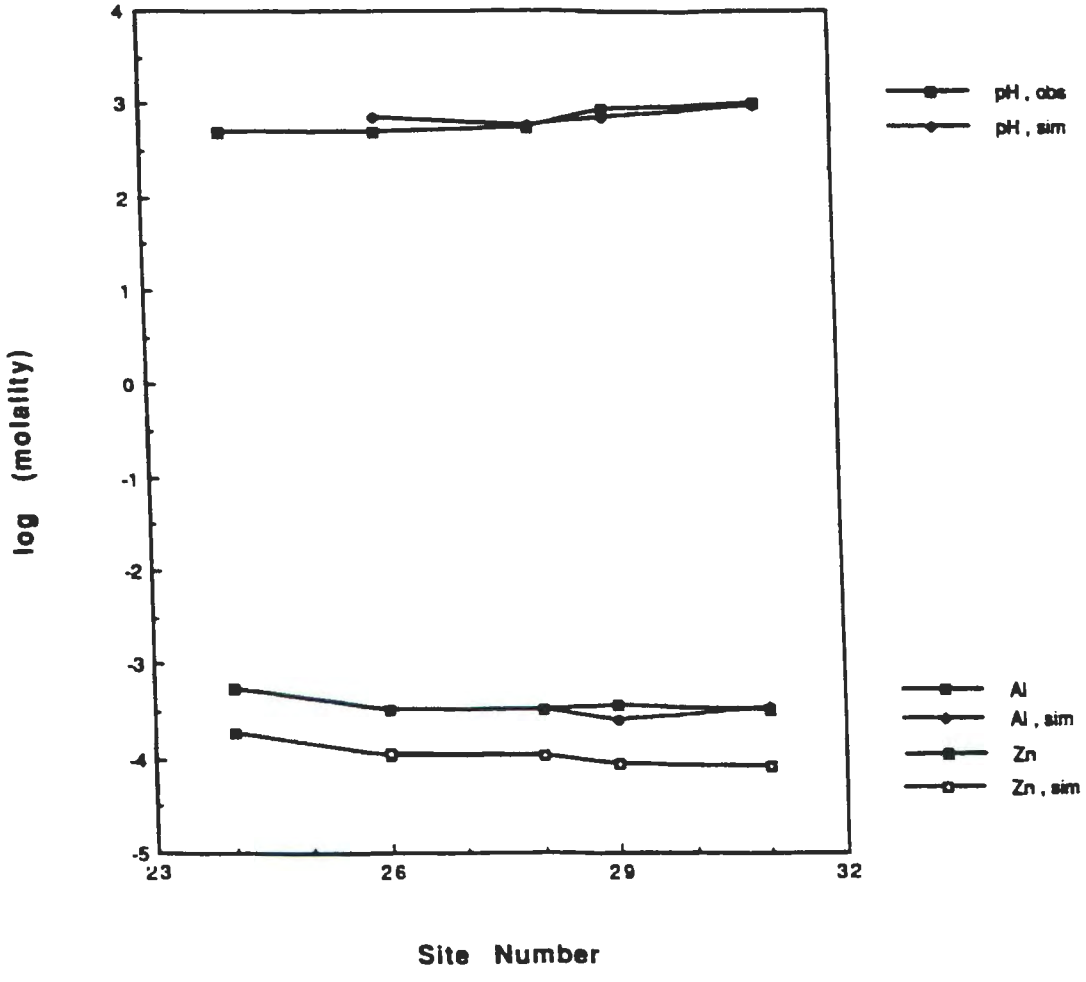

Note: Concentrations are log(molal) except for pH, which is plotted in pH units.

Figure 4.27 Logarithmic plot of observed and simulation pH, sodium, and copper for West Squaw Creek.

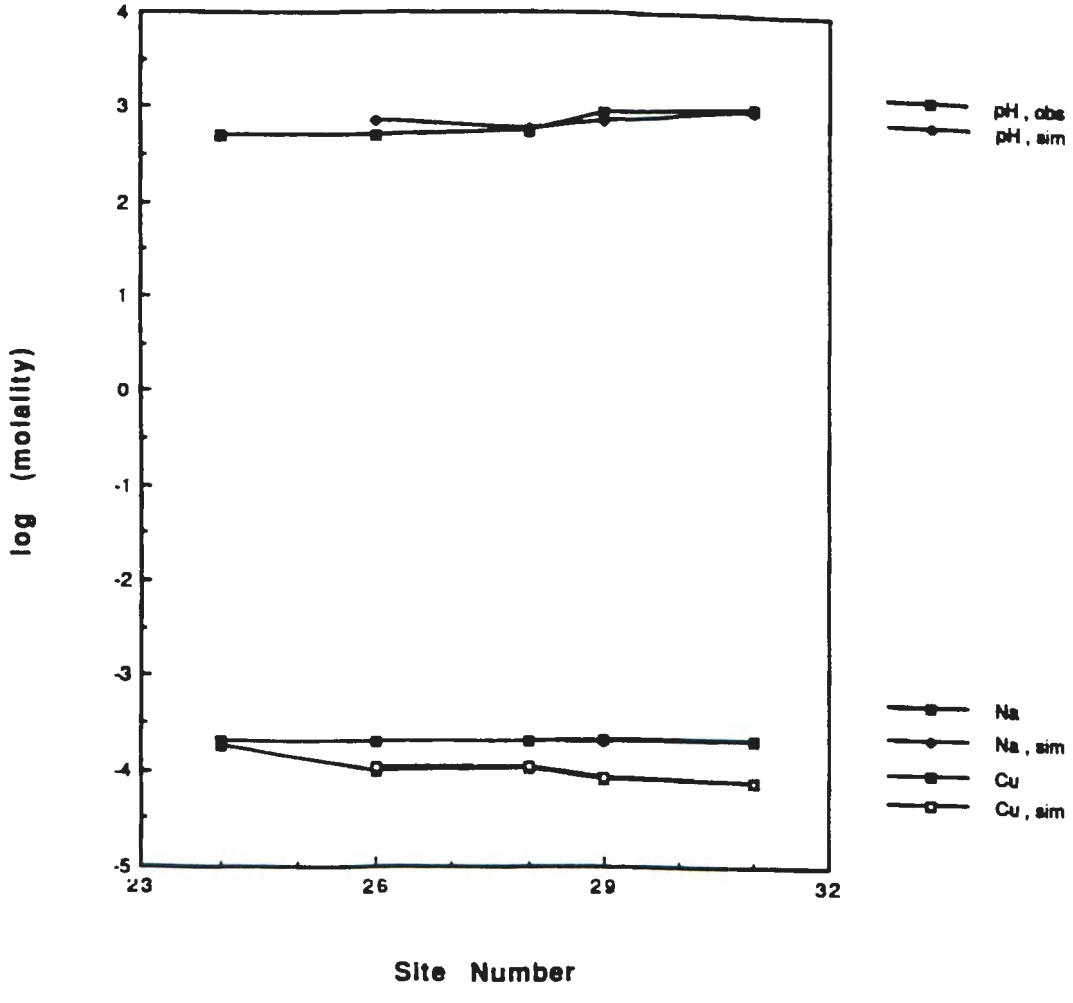

Note: Concentrations are log(molal) except for pH, which is plotted in pH units.

sodium silicates, alunite, and/or jarosites); and since the system pH never exceeded pH 3.00 (above which the model would be expected to simulate the coprecipitation of copper with iron oxyhydroxysulfate): then the excellent agreement of the simulation results with the observed data may be understood to indicate that the creek system is essentially undergoing dilution without significant chemical interactions of these trace elements with pure precipitates or other solid phases.

4.3.3 Strengths and Weaknesses of the Model

The major strength of the model lies in its adaptability to different chemical systems and environments. The data base for the PHREEQE program is completely user-defined, which allows for updating the equilibrium constants for each reaction, for adding or deleting elements and adding/modifying/deleting the reactions that define the interactions of any element with the chemical system being investigated. Thus, one may begin with a very simple system and develop a geochemical model piece-meal. Or one may investigate the effects of varying equilibrium constants, the reactions included in the model, or even the addition of more components each of which may include a set (small or large) of defining equilibria.

The versatility of PHREEQE is greatly enhanced by its acceptance of segmented input. One may define a

relatively simple initial problem, obtain the results, and then redefine the problem, elaborate on the system, add equilibration with additional phases, add reagents, mix solutions, initiate reactions, define segmented additions and temperature changes, or even combinations of these factors. Furthermore, the output from each program segment may be retained for use in the next step of the simulation, or ignored while altering the treatment given the previous output. Thus, a multistep process combining various streams of reactants and processes and conditions can be modeled, and adjustments of even individual factors can be followed as to their predicted effects on the immediate solution and the ultimate products.

PHREEQE solves even large sets of interactive equilibria within a few minutes and to a high degree of reproducibility by invoking two methods of successive approximations which seek to maximize convergence to an internally consistent set of solutions for all the equilibria involved. However, such a large, complex, variable, and interactive program has weaknesses that affect its performance in some cases, and/or limit is application to some problems. There follows a summary of the assumptions, weaknesses, and limitations found to affect the application of PHREEQE to modeling trace element behaviour in acidic leachates from coal and sulfidic ore

mines that undergo neutralization with bicarbonate and/or dilution and neutralization with carbonate-bearing streams.

Convergence problems that result in failure of the program have sometimes been encountered: when attempting to achieve electroneutrality within a solution by having the program adjust the concentration of a highly interactive element, (e.g. when PHREEQE attempts to adjust total iron to obtain charge balance in 0.1 molar iron solutions); when simulating the mixing of very different solutions, (e.g. near neutral, low ionic strength, and saturated with carbon dioxide mixed with acidic, high ionic strength, and unequilibrated with gases); when combining program options, (e.g. mixing solutions while requiring equilibration of the entire system with gases and solid phases); when polynuclear species were included which led to large factors in their equilibrium expression, (e.g. $Fe_{12}(OH)_{34}^{2+}$); when attempting to model solutions with high concentrations of elements with large numbers of equilibria of interacting species, (e.g. 0.05 molar ferric sulfate solution with several trace elements that each form 1 to 3 complexes with sulfate and bisulfate ions); and, when higher order and/or composite functions which have multiple local minima and maxima are incorporated into the PHREEQE program code, (e.g. the

copper coprecipitation function derived using a third order polynomial fit to obtain a relation from estimated copper data).

The most obvious impact of these convergence problems has been to limit the application of the model to the pH range 1.5 to 5. Convergence of systems including the trace elements and the coprecipitation functions rarely could be obtained above pH 5. An important factor in that occurrence seemed to be the low concentrations of hydrogen and hydroxide ions in near-neutral solutions, such that small oscillations in the successive approximations to solving the equilibrium system caused unmanageable gyrations of the H^+ and/or OH^- concentrations.

Assumptions built into the model and/or program code may limit its applicability in some cases and/or may introduce systematic error into the calculated results. By design PHREEQE assumes simultaneous equilibrium between all the components defined for a system. Phreeqe also lacks any provision to include kinetic information, including rates of reactions and rate limiting steps. But equilibration of real systems requires time, and sometimes great lengths of time, so that use of the model to simulate a real environment may be unrealistic. (e.g. Simulation of natural drainage and ground waters which flow through different assemblages of minerals, sands, clays, and muds, and may well not have enough surface

contact or time to reach equilibrium.) Furthermore, any solution of interacting equilibria is affected by the equilibrium constant for every reaction, so that the solution of every particular equation is critically dependent on the quality of each and every other reaction and constant. Obviously, natural systems are not fully known as to chemical inputs, minerals, clays, solubilities, and kinetics, let alone the effects of the living organisms that interact with the system.

Factors that are recognized as important to the control of trace element mobility, but were not incorporated into the model developed in this study include particle size and surface area of the precipitates, as well as surface adsorption and colloidal effects. Nor were any organic species investigated or modeled, although organic complexation and chelation are important factors and are surely significant in many if not most natural aqueous systems.

4.3.4 Comparison with Other Computer Models

The computer program GEOCHEM (Mattigod and Sposito 1979) was adapted from REDEQL2 for application to soil solutions. In addition to including thermodynamic data for several hundred soluble complexes and solids of relevance to trace metal equilibria in soil, it contained

a subroutine for cation exchange on constant charge surfaces and a subroutine for the estimation of single-ion activity coefficients at ionic strengths up to 3 molar. In comparison, the PC-executable version of PHREEQE can include up to 220 complexes and 200 solids. It also calculates activity coefficients for each ion or complex at ionic strengths at least up to that of seawater.

PHREEQE does not include adsorption equilibria, though the defining equations of an adsorption model could easily be added to its data base. Programs that do take adsorption processes into account include REDEQL2, (McDuff and Morel 1973), and MINEQL, (Westall et al. 1976). They can model the adsorption of major and trace metals by solid oxides and hydroxides such as silica, alumina, MnO_2, and goethite. The BASIC computer program ADSORP, (Alain Bourg 1982), introduces the adsorption of trace element complexes.

Complete chemical equilibrium is assumed by PHREEQE. Bernard Chapman 1982, modified MINEQL to include a physical transport submodel to model one-dimensional movement of solutes undergoing adsorption and precipitation as well as dissociation and redissolution in a stream.

Jenke et al. 1983, report the modification of the aqueous chemical equilibrium program REDEQL·EPAK to allow modeling a high volume mixing process for three influents

with the simultaneous addition of chemical reagents. PHREEQE allows the mixing of two influent streams, or the addition of a chemical, but not simultaneously.

Davis and Runnels 1987, used the MINTEQ computer model (Felmy et al, 1983) to simulate reactions between acidic tailings fluid and bedrock. They modeled aluminum behavior using $AlOHSO_4$ in acid conditions, and assumed an aluminum hydroxide solubility limit above pH 5.7. Our model uses jurbanite and microcrystalline gibbsite for acidic and near neutral conditions; but it incorporates a brief series of stable, pure solid phases to control the solubility of aluminum in the pH range 4 to 5; (see discussion in section 4.2.4).

Davis and Runnels modeled iron behavior by the precipitation of an amorphous ferric hydroxide, for which they found the log(K) to be in the range +8.5 to +4.4. We found the iron compound $Fe_{16}O_{16}(OH)_{12}(SO_4)_2$ to simulate our neutralization data better, and we used a value for log(K) that approximated the stability of soil-$Fe(OH)_3$, as defined by Lindsay 1979. Davis and Runnels (1987) were also able to use the MINTEQ triple-layer sorption algorithm for zinc, assuming the amorphous ferric hydroxide phase to be the sorbent. We were foiled in our attempts to model zinc by the failure of PHREEQE to converge past pH 5 once coprecipitation models for chro-

mium, copper, and lead had been incorporated in the program code.

The extensively revised computer program SOLMINEQ.-88, (Perkins et al. 1989), includes 80 organic aqueous species as well as 214 minerals and over 270 inorganic species. Organic species and equilibria could easily be added to the PHREEQE data base, although none are provided with the program package. SOLMINEQ.88 can also calculate the effects of boiling and partitioning of gases between water, oil, and a vapor phase. It also includes an option for ion exchange and another option for ion adsorption, both of which can be added to PHREEQE by modifying its data base of species and equilibria. SOLMINEQ.88 even includes the option of using the Pitzer activity coefficient model, which is not available in PHREEQE, but is the basis for the related program PHRQ-PITZ.

An additional important area of computer model development for aqueous chemical systems is the incorporation of kinetic factors and the ability to handle oxidation-reduction processes. PHREEQE accepts redox couples and reactions, but includes no provision for kinetic factors. K. W. Bladh 1978, simulated the oxidation of sulfide minerals in aqueous solution. Liddell and Bautista 1981, incorporated a kinetic equation for dissolution of chalcopyrite by O_2. Jaynes et al. 1984,

simulated long term oxidation of pyrite and subsequent leaching of reaction products with a model featuring several kinetic factors, including: gas diffusion of oxygen, independent rates for direct oxidation of pyrite by oxygen and by Fe^{3+}, calculation of bacterial activity, and the effects of particle size. EQ6, of the EQ3/6 software package (Wolery et al. 1989), computes reaction path models of both equilibrium step processes and kinetic reaction processes, for closed as well as relatively simple open systems.

Finally, Dzombak and Morel have published (1990) a major effort to compile, evaluate, and select data on complexation on the hydrous ferric oxide surface. They have applied computer programs to extract intrinsic surface complexation constants from each data set and to estimate the best overall sorption constants. They present the equations used to model the surface complexation reactions, including a system of equations to model surface precipitation (or dissolution).

4.4 NEUTRALIZATION OF SYNTHETIC ACIDIC COAL LEACHATE

4.4.1 Reaction Progress

The plot of pH vs percent neutralized (Figure 4.28) reveals this to be the neutralization of a buffered acid. Initially the pH rises steadily as excess acid in the system is neutralized by added base. The plateau represents that portion of the reaction during which the system pH is buffered by the hydrolysis of iron which regenerates H^+ ions. The slightly elevated pH measured at 29% neutralized is indicative of supersaturation with respect to hydrolysis of iron. (See Dousma et al. 1978.) Khoe and Robins 1989, obtained similar results in their study of the hydrolysis and polymerization of iron(III) in the presence of sulfate. Past this point they observed a pH relaxation to occur after each injection of titrant as the iron underwent hydrolysis. They noted the same increasing deep red-brown color of solution and subsequent increased turbidity that were observed in this experiment. These were cited as evidence of polymerization and precipitation. For this sample, PHREEQE calculated a saturation index of +0.9181 for $Fe(OH)_{3(soil)}$, and +13.36 for $Fe_{16}O_{16}(OH)_{12}(SO_4)_2$ (which corresponds to +0.835 for the formula $FeO(OH)_{.75}(SO_4)_{.125}$ and which can be compared to the saturation index of each $Fe(OH)_3$ compound).

Figure 4.28 pH of the neutralization titration as a function of reaction progress expressed as percent neutralized.

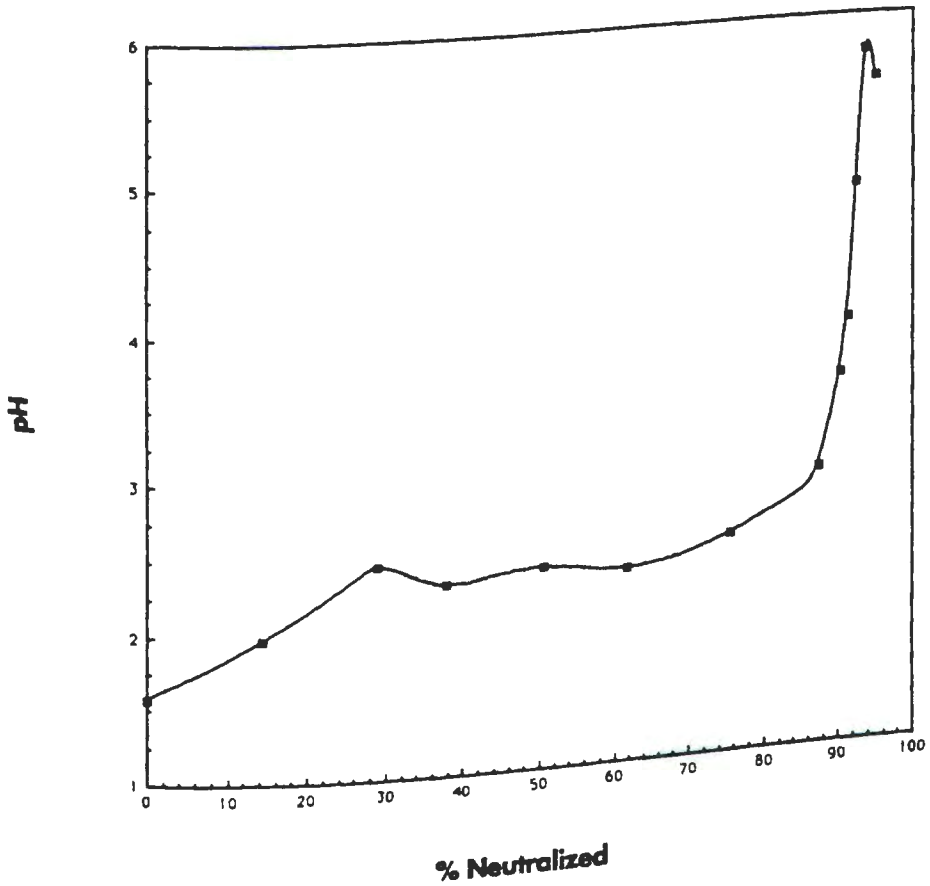

Note: The curve is smoothed by interpolation between data points.

indicating supersaturation with respect to this phase by almost one order of magnitude. The saturation index for amorphous ferric hydroxide was -1.2729, indicating undersaturation. The SI calculated for goethite was +4.6198, which indicates a very high degree of supersaturation with respect to this most stable form of iron oxyhydroxide. However, goethite forms very slowly at room temperature, often taking weeks or months. (See Atkinson et al. 1968, Flynn Jr. 1984, Schneider 1984, and Bryson 1986.) Throughout the rest of the experiment, the calculated SI for the "$FeO(OH)_{.75}(SO_4)_{.125}$" ranged from -0.06 to +0.45 and averaged +0.13, suggesting that the solution was in contact (if not equilibrium) with a solid iron oxyhydroxysulfate phase that controlled the solubility of iron(III).

As noted before, the source of the fluctuations in SI for the solid hydroxy-compounds is traceable to the variations in the pH measured in each sample filtrate. The variation in the pH of samples 3 through 7 (along the pH plateau) are thought to be real, and not just due to analytical error and uncertainty. Sylva 1972, stated that precipitation of hydrolysed iron(III) does not involve only the deposition of ionic units upon a growing crystal nucleus. As a result of work done using a reactor not unlike the one used in this experiment, Dousma and deBruyn proposed four stages (previously listed) in

the iron(III) hydrolysis process. Schneider 1984, also used neutralization with sodium bicarbonate to study the hydrolysis of iron(III). He concluded that nucleation occurs at the inlet of base solution within the time of intermixing with the bulk solution.

Taken together, these ideas support the explanation that each injection of base resulted in the hydrolysis of dissolved iron(III) to monomers, dimers, and the nucleation of small polymers, rather than significant growth of the more mature, but slowly reacting large polymers. Thus, the extent of pH relaxation observed after each base injection depends to a degree on the number (concentration) of new nuclei formed, their initial extent of hydrolysis, and the ability of the bulk solution to fuel further hydrolysis and growth of these new particles. The hydrolysis stalls and the pH appears to stabilize when the solution reaches equilibrium with these metastable particles.

Given sufficient time, the higher energy ions and particles will undergo rearrangement, or dissolve and reprecipitate forming the structure of the thermodynamically stable end products appropriate to the system (e.g. goethite or one of the jarosites). Then a truly stable pH would be observed. In this experiment however, often less than 24 hours elapsed between base injection and pH measurement; thus the pH value is believed to have been

relatively accurate for the time of sampling; but the variation from sample to sample indicates significant variation in the relative stability of the system as a whole.

The above explanation of the formation of fresh polymeric material with each base injection also accounts for the passage of excess iron into each filtrate. If the hydrolyzing iron only built up existing particles, then they would grow in size and soon be removed efficiently by the filters.

By the time sample 8 was collected, the neutralization was over 87% complete, and about 99% of the original dissolved iron had precipitated. Thus the buffer capacity of the system was nearly exhausted, and the pH rose dramatically with each new addition of base. To the end, each titration episode was followed by pH relaxation with time, and the next to the last sample was apparently taken when the system was not yet equilibrated.

Figure 4.29 shows the adjusted (for charge balance) concentration of iron in solution as a function of pH. It clearly shows the dramatic removal of iron from solution by pH 2.5. It also indicates that the third sample was supersatured with iron for the pH that was observed.

Figure 4.29 Iron in solution as a function of pH during the neutralization titration.

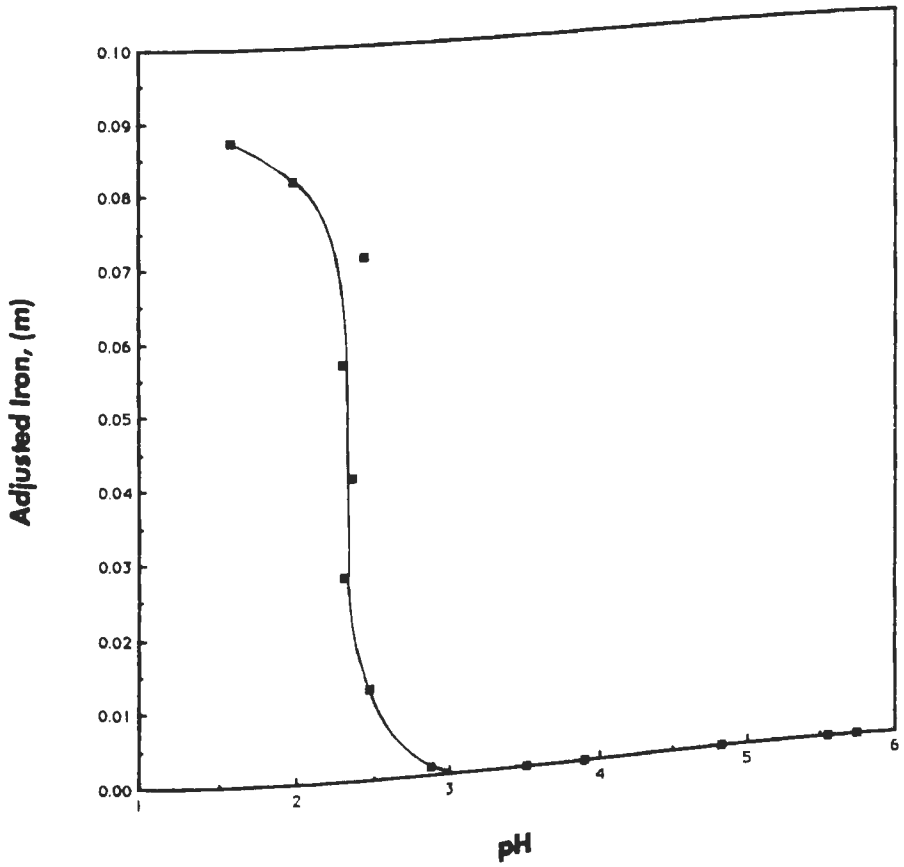

Notes: Concentrations are molal and are for total iron in solution after adjustment to obtain charge balance. The smooth curve is an "eyeball" fit to the data points. It was drawn ignoring the value for sample 3, which is believed to represent supersaturation of the solution with iron at that pH.

Both Figures 4.30 and 4.31 are plots of the total measured and adjusted iron concentrations throughout the neutralization. Figure 4.30 uses a linear concentration scale and shows the relative adjustment of iron necessary in the data for each sample to achieve charge balance. This plot also gives indication that sample 3 was super-saturated with iron. Figure 4.31 uses a logarithmic concentration scale to show the rapid decline of iron concentration after the system was 87% neutralized (sample 8 with pH 2.87). This plot also indicates that the values obtained for iron in the last two samples were erroneous. The computer program aborted with each effort to model that data until the iron inputs were reduced to the levels shown.

Figure 4.32 shows total iron and all of the major iron species as modeled by PHREEQE. The logarithmic plot sacrifices detail for the individual species, but it shows the overall importance and behavior of each one plotted. Only a few points were plotted for $FeH_2AsO_4^{2+}$ because it was not reported to be of significance in the remaining solutions as modeled.

Figure 4.30 Iron in solution (as measured and as adjusted to obtain charge balance) as a function of reaction progress (expressed as percent neutralized).

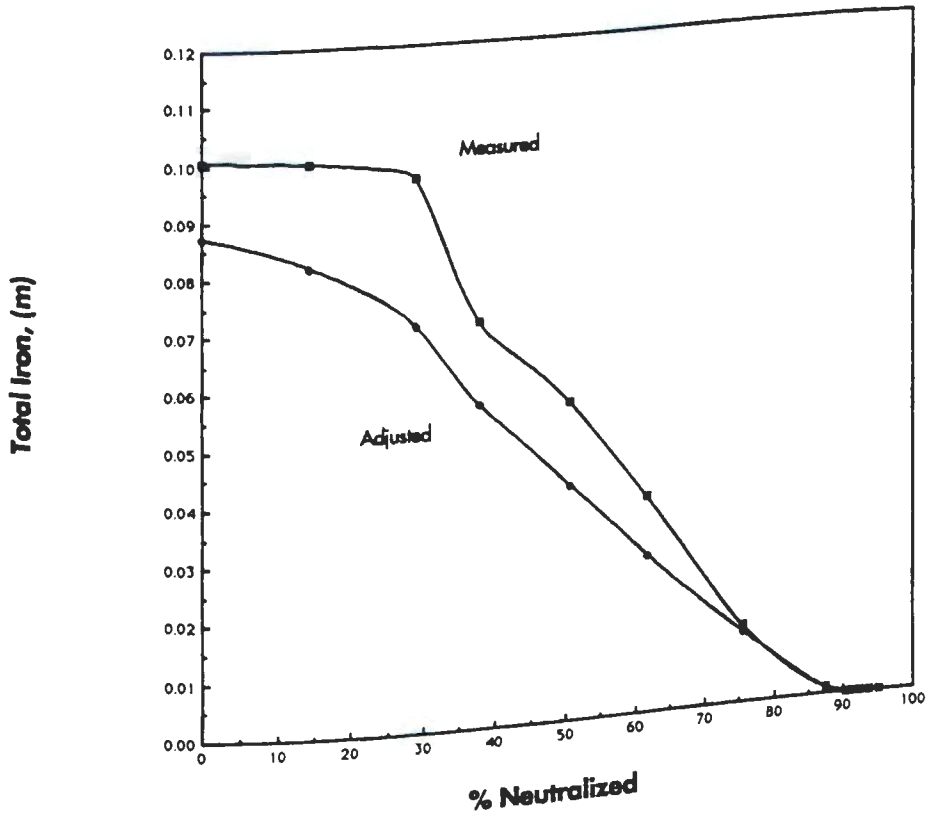

Notes: Concentrations are molal, and the scale is linear. Both curves were smoothed by interpolation between data points.

Figure 4.31 Logarithmic plot of iron in solution (as measured and as adjusted to obtain charge balance), as a function of reaction progress (expressed as percent neutralized).

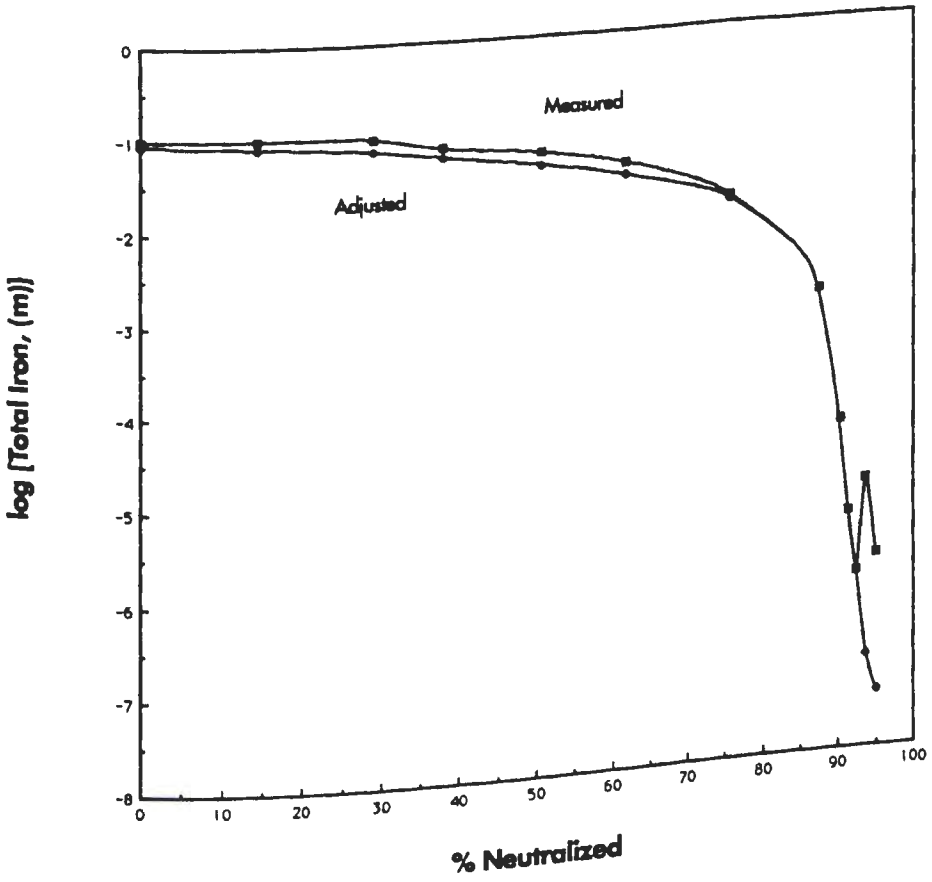

Notes: Concentrations are log(molal). Both curves were smoothed by interpolation. The last two "measured" values are considered erroneously high for their samples (pH > 5.5). The last two "adjusted" values were arbitrarily reduced until the computer program PHREEQE would process the data.

Figure 4.32 Logarithmic plot of total molal iron concentration in solution and all major iron species (as modeled by the computer program PHREEQE) for each sample taken from the neutralization titration.

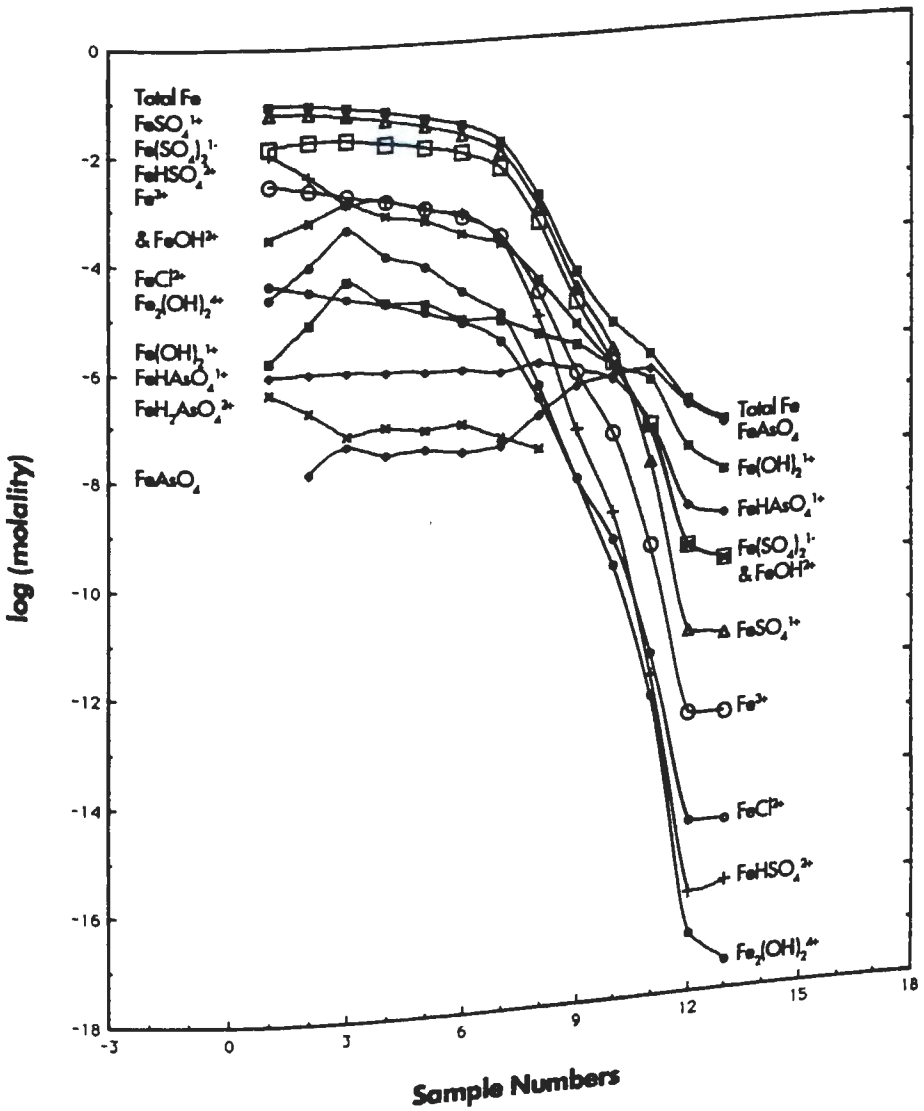

Notes: Concentrations are log(molal) for total iron (adjusted to obtain charge balance) and the major iron species in solution. The curves are all smoothed by interpolation between data points. The iron in the last two samples are arbitrary concentrations used because they did not cause the computer program (PHREEQE) to crash.

The next two figures show subsets of related iron species and their relative importance during the period that significant concentrations of iron remained in solution. Note that the scale of the vertical axis changes with each plot. Figure 4.33 shows the sulfate complexes of iron. Comparison with Figure 4.32 indicates that the double-sulfate complex becomes much more important than the mono-sulfate at higher pH. Also note that the bisulfate complex is always of minor importance among the sulfate complexes of iron, at least as modeled in this system.

Figure 4.34 shows the simple iron(III) ion and the hydroxide species. Note that Fe^{3+} is the most important of this group of species while the system is less than 80% neutralized (pH approximately 2.6 or 2.7). Also note that the dimer was never of much significance according to this model, and that the higher polycations were never reported by PHREEQE as being of significance.

Figure 4.35 shows the "colloidal Fe" (taken to be the adjustment of the iron concentration necessary to obtain charge balance in each sample) versus % neutralized. Note that the peak of this assumed colloidal iron corresponds to the peak concentrations of $Fe(OH)^{2+}$ and the dimer $Fe_2(OH)_2^{4+}$ (shown in Figure 4.34).

Figure 4.33 Concentrations of sulfate complexes of iron (as modeled by the computer program PHREEQE) in the neutralization titration solution, as a function of reaction progress (expressed as percent neutralized).

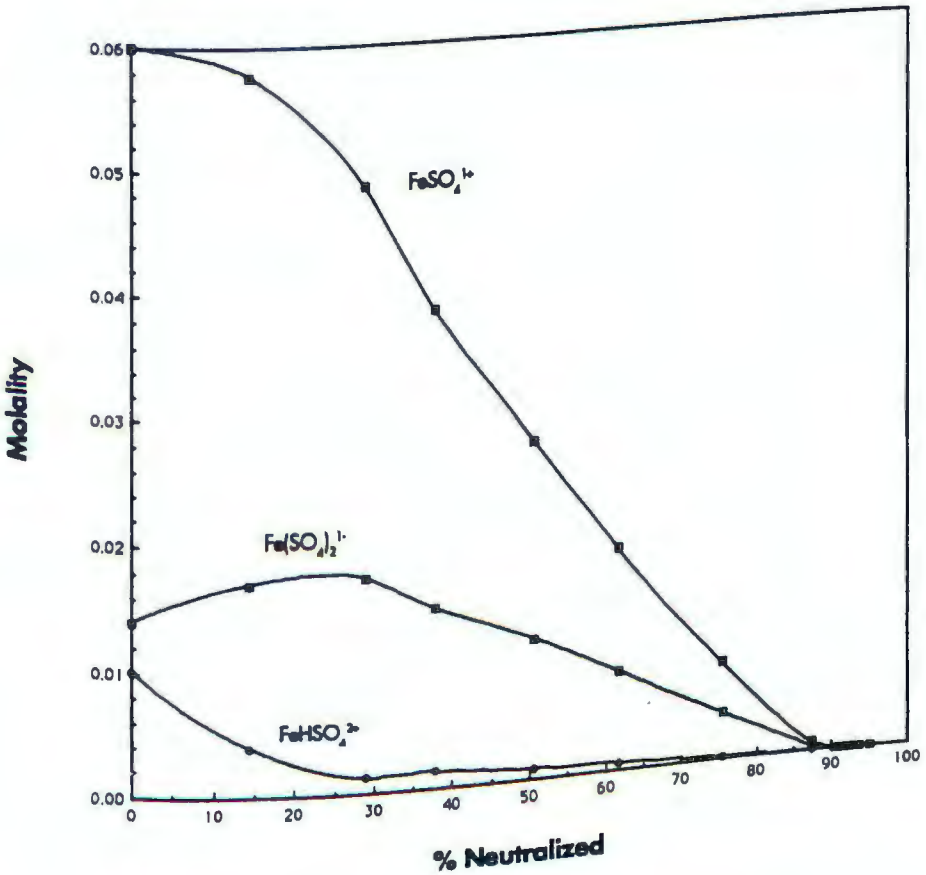

Notes: Concentrations are molality of each sulfate complex of iron (III) in solution. The curves are all smoothed by interpolation.

Figure 4.34 Concentrations of Fe^{3+} and its hydroxy complexes (as modeled by the computer program PHREEQE) in the neutralization titration solution, as a function of reaction progress (expressed as percent neutralized).

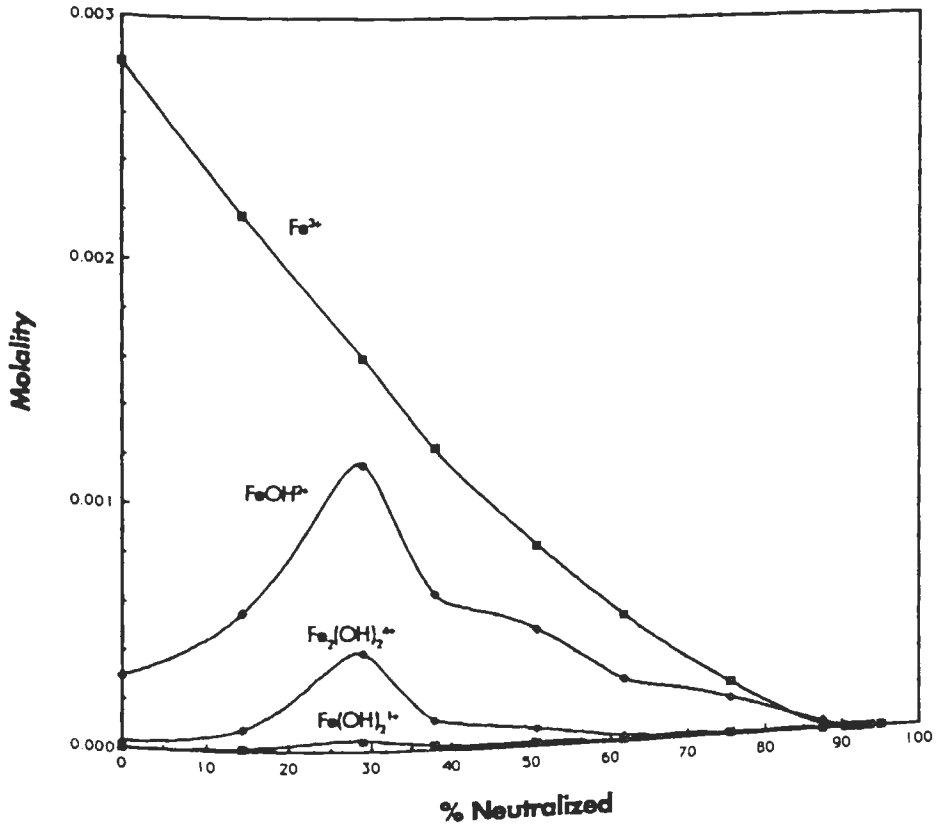

Note: Concentrations are molality of each species. The curves are smoothed by interpolation.

Figure 4.35 Colloidal Iron in the neutralization titration solution as a function of reaction progress (expressed as percent neutralized).

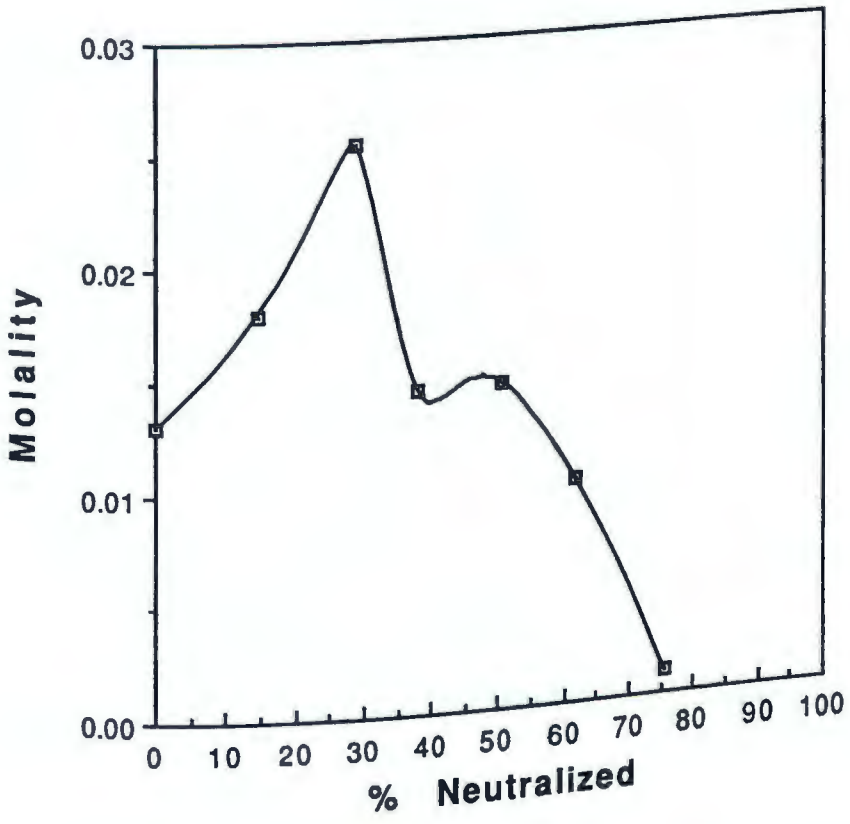

Notes: The units of molality represent the adjustment of the molal concentration of iron in each sample that was necessary to obtain charge balance for the solution. The curve is smoothed by interpolation.

Figure 4.36 shows the arsenate complexes of iron. Comparison with Figure 4.32 indicates that although the concentration of the arsenate complexes was low in these solutions, they became important in the last three samples as the pH was pushed above 4.5.

Figure 4.37 is a plot of just the most important iron species as calculated by PHREEQE for these samples from the neutralization of a synthetic acidic inorganic coal leachate. This plot shows the percent of adjusted total iron(III) in solution that is bound up in each of the most important complexes as a function of pH. The jumble of data points between pH 2.25 and 2.5 are from the samples on the buffered pH plateau of the reaction. The discontinuity of those points is a function of the fluctuation of the pH values as measured, rather than being caused by fluctuations of the individual species. Compare the smoothness of the individual plots in Figures 4.33, 4.34, and 4.36. Note that, according to this model for this system, below pH 4 the mono-sulfate complex is of greatest importance, followed by the di-sulfate complex. However, above pH 4.25 the neutral arsenate complex becomes of greatest importance with the dihydroxy complex of secondary importance.

Figure 4.36 Concentrations of arsenate complexes of iron (as modeled by the computer program PHREEQE) in the neutralization titration solution, as a function of reaction progress (expressed as percent neutralized).

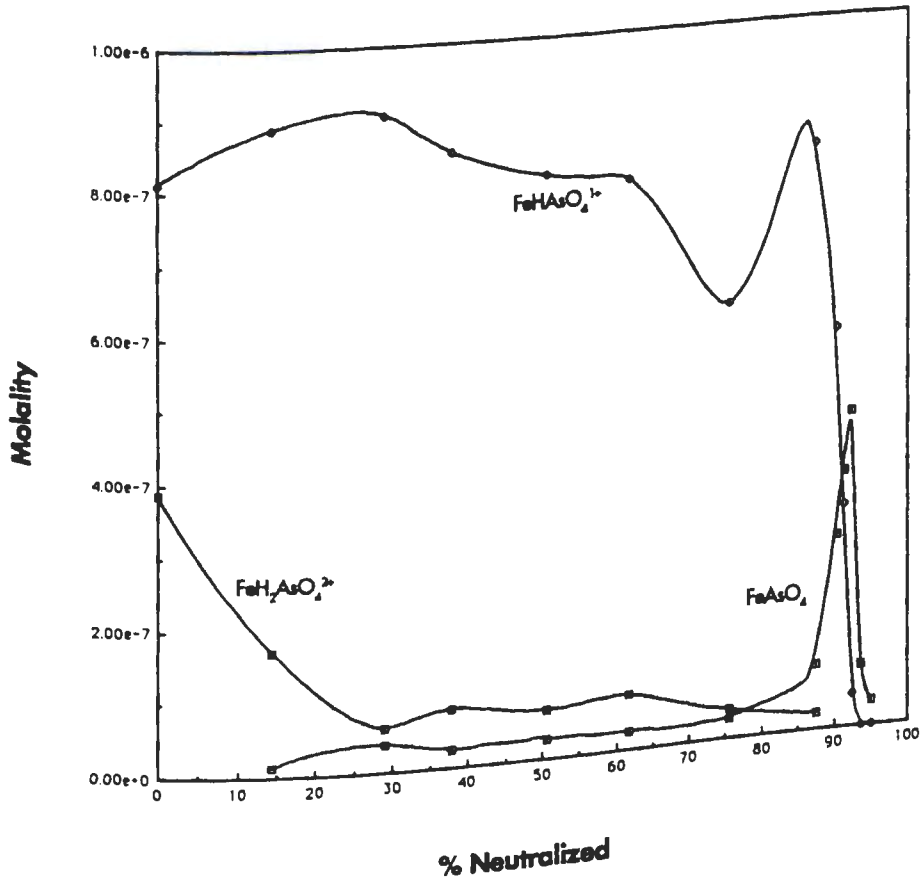

Notes: Concentration are molality of each species. The curves are smoothed by interpolation.

Figure 4.37 Relative abundance of the most important iron(III) complexes (as modeled by the computer program PHREEQE) in the neutralization titration solution, as a function of pH.

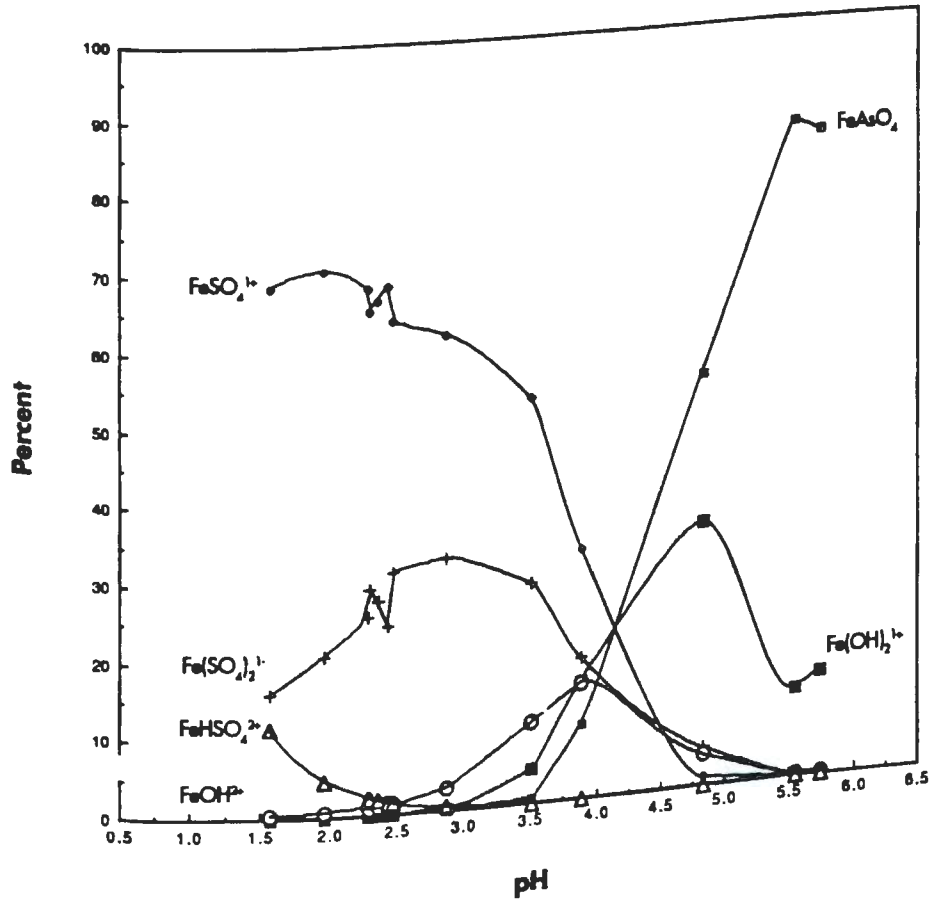

Notes: The plot indicates the percent of iron(III) in solution that is bound up in each of the most important complexes over the pH range of the neutralization experiment. The curves are smoothed by interpolation.

4.4.2 Trace Elements

In this section the chemical behavior of the trace elements included in the neutralization will be discussed. Recall that aluminum, zinc, chromium, copper, cadmium, lead, arsenic, and selenium were doped into an acidic ferric sulfate solution to make a synthetic inorganic leachate (see Table 2.5). This solution was titrated stepwise with the slow addition of sodium bicarbonate. Samples were filtered and analyzed for the concentration of each trace element. They will be considered in order from highest to lowest concentration in the filtrates.

Tables 4.6 through 4.11 contain representative data summarized from the computer output of PHREEQE for three of the neutralization samples: #2 was selected because the titration had just begun and no precipitates were observed yet; #7 was a "middle" sample, and the last one for which charge balance could be obtained by adjusting the total iron concentration; #11 was a "late" sample, and the last one for which the experimental iron data could be processed by PHREEQE.

Table 4.6 Summary of concentration data from the computer program analysis of neutralization titration sample #2.

Ionic Strength = 0.1894 pH = 1.973 14.5% Neutralized

Element	log(molal)	Principal Species (log molality)			
Al	(-3.4126)	$Al(SO_4)_2^-$ (-3.776)	$AlSO_4^+$ (-3.807)	Al^{3+} (-4.209)	
As	(-5.9700)	$FeHAsO_4^+$ (-6.052)	$FeH_2AsO_4^{2+}$ (-6.767)	$FeAsO_4^\circ$ (-7.887)	
C	(-4.9679)	$H_2CO_3^\circ$ (-4.968)	HCO_3^- (-9.204)	CO_3^{2-} (-17.183)	
Cd	(-5.0715)	$CdSO_4^\circ$ (-5.464)	Cd^{2+} (-5.532)	$Cd(SO_4)_2^{2-}$ (-5.771)	
Cl	(-2.8161)	Cl^- (-2.825)	$FeCl^{2+}$ (-4.522)	$CdCl^+$ (-6.900)	
Cr	(-4.6796)	$CrSO_4^+$ (-4.689)	Cr^{3+} (-6.423)		
Cu	(-4.8345)	Cu^{2+} (-5.165)	$CuSO_4^\circ$ (-5.222)	$Cu(SO_4)_2^{2-}$ (-5.748)	
Fe	(-1.0877)	$FeSO_4^+$ (-1.239)	$Fe(SO_4)_2^-$ (-1.768)	$FeHSO_4^{2+}$ (-2.406)	
N	(-3.0249)	NO_3^- (-3.025)			
Na	(-1.3207)	Na^+ (-1.349)	$NaSO_4^-$ (-2.520)		
Pb	(-5.5757)	$PbSO_4^\circ$ (-5.802)	Pb^{2+} (-6.160)	$Pb(SO_4)_2^{2-}$ (-6.429)	
S	(-0.7866)	$FeSO_4^+$ (-1.239)	SO_4^{2-} (-1.343)	HSO_4^- (-1.728)	
Si	(-3.0385)	$H_4SiO_4^\circ$ (-3.038)			
Zn	(-4.6102)	Zn^{2+} (-4.964)	$ZnSO_4^\circ$ (-5.000)	$Zn(SO_4)_2^{2-}$ (-5.437)	

Table 4.7 Summary of Saturation Index data from the computer program (PHREEQE) analysis of neutralization titration sample #2.

Element	Solid Phase (Saturation Index)		
Aluminum			
	Basaluminite (-24.8885)	Bayerite (-7.5791)	Jurbanite (-1.1811)
	$Gibbsite_{(microcrystalline)}$ (-8.5191)		
Arsenic			
	Ferric $arsensate_{(am)}$ (-6.4098)		Scorodite (-3.5680)
Carbon			
	$CuCO_{3(cr)}$ (-11.8289)	$PbCO_{3(cr)}$ (-11.2192)	Malachite (-19.7297)
Cadmium			
	$CdCO_{3(cr)}$ (-9.9812)	$CdSO_{4(anhy)}$ (-7.8051)	$CdSO_4 \cdot H_2O_{(cr)}$ (-6.2566)
Chromium			
	Chromite (-28.3865)	$Cr(OH)_{3(cr)}$ (-6.2399)	
Copper			
	Copper ferrite (-2.836)	$Cu(OH)_{2(cr)}$ (-10.3008)	$Cu_2(OH)_2SO_4$ (-6.9938)
Iron			
	$Fe(OH)_{3(am)}$ (-2.5119)	$Fe(OH)_{3(soil)}$ (-0.3209)	Goethite (+3.3806)
	H^+-Jarosite (+0.9031)	HNa-Jarosit (+1.1046)	Na-Jarosite (+1.2883)
Lead			
	$Pb(OH)_{2(cr)}$ (-10.8711)	Pb-Jarosite (+4.5852)	$PbSO_{4)cr)}$ (-0.7431)
Silicon			
	Kaolinite (-11.8046)	Quartz (+0.9640)	Silica glass (0.0000)
Zinc			
	Zinc ferrite (-4.0251)	ϵ-$Zn(OH)_2$ (-13.0694)	$ZnSiO_{3(cr)}$ (-11.7543)

Table 4.8 Summary of concentration data from the computer program analysis of neutralization titration sample #7.

Ionic Strength = 0.3126 pH = 2.475 75% Neutralized

Element	log(molal)	Principal Species (log molality)			
Al	(-3.3166)	$Al(SO_4)_2^-$ (-3.554)	$AlSO_4^+$ (-3.804)	Al^{3+} (-4.340)	
As	(-6.1725)	$FeHAsO_4^+$ (-6.218)	$FeH_2AsO_4^{2+}$ (-7.406)	$FeAsO_4^\circ$ (-7.573)	
C	(-4.9801)	$H_2CO_3^\circ$ (-4.980)	HCO_3^- (-8.686)	CO_3^{2-} (-16.110)	
Cd	(-5.1107)	$CdSO_4^\circ$ (-5.566)	$Cd(SO_4)_2^{2-}$ (-5.604)	Cd^{2+} (-5.803)	
Cl	(-2.8508)	Cl^- (-2.852)	$FeCl^{2+}$ (-5.627)		
Cr	(-4.8555)	$CrSO_4^+$ (-4.897)	$HCrO_4^-$ (-5.985)	Cr^{3+} (-6.774)	
Cu	(-4.8614)	$CuSO_4^\circ$ (-5.237)	Cu^{2+} (-5.322)	$Cu(SO_4)_2^{2-}$ (-5.495)	
Fe	(-1.9089)	$FeSO_4^+$ (-2.103)	$Fe(SO_4)_2^-$ (-2.413)	Fe^{3+} (-3.659)	
N	(-3.0597)	NO_3^- (-3.060)			
Na	(-0.6390)	Na^+ (-0.685)	$NaSO_4^-$ (-1.641)		
Pb	(-7.0815)	$PbSO_4^\circ$ (-7.322)	$Pb(SO_4)_2^{2-}$ (-7.680)	Pb^{2+} (-7.850)	
S	(-0.8536)	SO_4^{2-} (-1.042)	$NaSO_4^-$ (-1.641)	HSO_4^- (-2.002)	
Si	(-3.0519)	$H_4SiO_4^\circ$ (-3.052)			
Zn	(-4.4881)	$ZnSO_4^\circ$ (-4.884)	Zn^{2+} (-4.977)	$Zn(SO_4)_2^{2-}$ (-5.052)	

Table 4.9 Summary of Saturation Index data from the computer program (PHREEQE) analysis of neutralization titration sample #7.

Element	Solid Phase (Saturation Index)		
Aluminum			
	Basaluminite (-20.5685)	Bayerite (-6.3036)	Jurbanite (-0.6876)
	$Gibbsite_{(microcrystalline)}$ (-7.2436)		
Arsenic			
	$Ferric\ arsensate_{(am)}$ (-6.0836)		Scorodite (-3.2438)
Carbon			
	$CuCO_{3(cr)}$ (-11.0490)	$PbCO_{3(cr)}$ (-11.9442)	Malachite (-18.1710)
Cadmium			
	$CdCO_{3(cr)}$ (-9.2877)	$CdSO_{4(anhy)}$ (-7.8946)	$CdSO_4 \cdot H_2O_{(cr)}$ (-6.3472)
Chromium			
	Chromite (-25.8445)	$Cr(OH)_{3(cr)}$ (-5.1408)	
Copper			
	Copper ferrite (-1.237)	$Cu(OH)_{2(cr)}$ (-9.5220)	$Cu_2(OH)_2SO_4$ (-6.4105)
Iron			
	$Fe(OH)_{3(am)}$ (-2.1035)	$Fe(OH)_{3(soil)}$ (+0.0875)	Goethite (+3.7901)
	H^+-Jarosite (+0.5646)	HNa-Jarosit (+1.0522)	Na-Jarosite (+2.1007)
Lead			
	$Pb(OH)_{2(cr)}$ (-11.5971)	Pb-Jarosite (+3.1821)	$PbSO_{4)cr)}$ (-2.2511)
Silicon			
	Kaolinite (-9.2505)	Quartz (+0.9650)	Silica glass (0.0000)
Zinc			
	Zinc ferrite (-2.2933)	ϵ-$Zn(OH)_2$ (-12.1587)	$ZnSiO_{3(cr)}$ (-10.8415)

Table 4.10 Summary of concentration data from the computer program analysis of neutralization titration sample #11.

Ionic Strength = 0.3726 pH = 4.83 92% neutralized

Element	log(molal)	Principal Species (log molality)			
Al	(-3.8854)	$Al(SO_4)_2^-$ (-4.168)	$AlSO_4^+$ (-4.480)	$AlOHSO_4^\circ$ (-4.753)	
As	(-6.2165)	$FeAsO_4^\circ$ (-6.356)	$H_2AsO_4^-$ (-6.928)	$FeHAsO_4^+$ (-7.347)	
C	(-4.9655)	$H_2CO_3^\circ$ (-4.986)	HCO_3^- (-6.327)	CO_3^{2-} (-11.379)	
Cd	(-5.0695)	$Cd(SO_4)_2^{2-}$ (-5.524)	$CdSO_4^\circ$ (-5.560)	Cd^{2+} (-5.850)	
Cl	(-2.8317)	Cl^- (-2.832)			
Cr	(-6.2948)	$HCrO_4^-$ (-6.336)	CrO_4^{2-} (-7.579)	$NaCrO_4^-$ (-7.718)	
Cu	(-6.1676)	$CuSO_4^\circ$ (-6.551)	Cu^{2+} (-6.670)	$Cu(SO_4)_2^{2-}$ (-6.734)	
Fe	(-6.0870)	$FeAsO_4^\circ$ (-6.356)	$Fe(OH)_2^+$ (-6.551)	$FeHAsO_4^+$ (-7.347)	
N	(-3.0405)	NO_3^- (-3.041)			
Na	(-0.5328)	Na^+ (-0.585)	$NaSO_4^-$ (-1.480)		
Pb	(-7.0042)	$PbSO_4^\circ$ (-7.257)	$Pb(SO_4)_2^{2-}$ (-7.540)	Pb^{2+} (-7.836)	
S	(-0.8366)	SO_4^{2-} (-0.950)	$NaSO_4^-$ (-1.480)	$Al(SO_4)_2^-$ (-4.168)	
Si	(-3.0583)	$H_4SiO_4^\circ$ (-3.058)			
Zn	(-4.7786)	$ZnSO_4^\circ$ (-5.187)	$Zn(SO_4)_2^{2-}$ (-5.281)	Zn^{2+} (-5.310)	

Table 4.11 Summary of Saturation Index data from the computer program (PHREEQE) analysis of neutralization titration sample #11.

Element	Solid Phase (Saturation Index)		
Aluminum			
	Basaluminite (+0.0584)	Bayerite (+0.0136)	Jurbanite (+0.9876)
	$Gibbsite_{(microcrystalline)}$ (-0.9264)		
Arsenic			
	Ferric $arsensate_{(am)}$ (-4.8606)		Scorodite (-2.0217)
Carbon			
	$CuCO_{3(cr)}$ (-7.7140)	$PbCO_{3(cr)}$ (-7.2300)	Malachite (-11.5014)
Cadmium			
	$CdCO_{3(cr)}$ (-4.6336)	$CdSO_{4(anhy)}$ (-7.8830)	$CdSO_4 \cdot H_2O_{(cr)}$ (-6.3360)
Chromium			
	Chromite (-30.2331)	$Cr(OH)_{3(cr)}$ (+0.4094)	
Copper			
	Copper ferrit (+4.1395)	$Cu(OH)_{2(cr)}$ (-6.1874)	$Cu_2(OH)_2SO_4$ (-4.2364)
Iron			
	$Fe(OH)_{3(am)}$ (-1.0836)	$Fe(OH)_{3(soil)}$ (+1.1074)	Goethite (+4.8104)
	H^+-Jarosite (-5.6600)	HNa-Jarosit (-4.5609)	Na-Jarosite (-1.6754)
Lead			
	$Pb(OH)_{2(cr)}$ (-6.8834)	Pb-Jarosite (-4.5533)	$PbSO_{4)cr)}$ (-2.1794)
Silicon			
	Kaolinite (+3.3853)	Quartz (+0.9654)	Silica glass (0.0000)
Zinc			
	Zinc ferrite (+4.0933)	ϵ-$Zn(OH)_2$ (-7.8136)	$ZnSiO_{3(cr)}$ (-6.4955)

Aluminum

Aluminum concentrations varied from 590 μM down to 130 μM. Figure 4.38 shows the log of the aluminum and iron concentrations plotted against reaction progress expressed as percent neutralized. Total aluminum appears to be conserved in solution through sample 8 when the pH was 2.87 and the system was 87% neutralized. About 81% of the filterable aluminum was removed from solution by the time the system pH was driven up to 3.90, (91% neutralized). However, the change in iron concentration over the same period was 2.4 times larger. Saturation index calculations indicated that amorphous aluminum hydroxide was undersaturated by 5 to 7 order of magnitude, and that gibbsite was undersaturated by 2 to 5 orders of magnitude in these solutions. The SI calculated for crystalline jurbanite ($AlOHSO_4$) in sample 8 was -0.2166, for sample 9 it was +0.0140, and for sample 10 it was +0.1642. The calculated speciation for the dissolved aluminum indicates that the neutral species $AlOHSO_4^\circ$ rises rapidly after this point to become the dominant form of aluminum in solution. Taken together, these ideas suggest the formation of a jurbanite-like solid as the likely sink for aluminum being removed from solution. It is not likely that crystalline jurbanite would form in solution under these conditions, and X-ray

Figure 4.38 Logarithmic plot of aluminum and iron in the neutralization titration solution, as a function of reaction progress (expressed as percent neutralized).

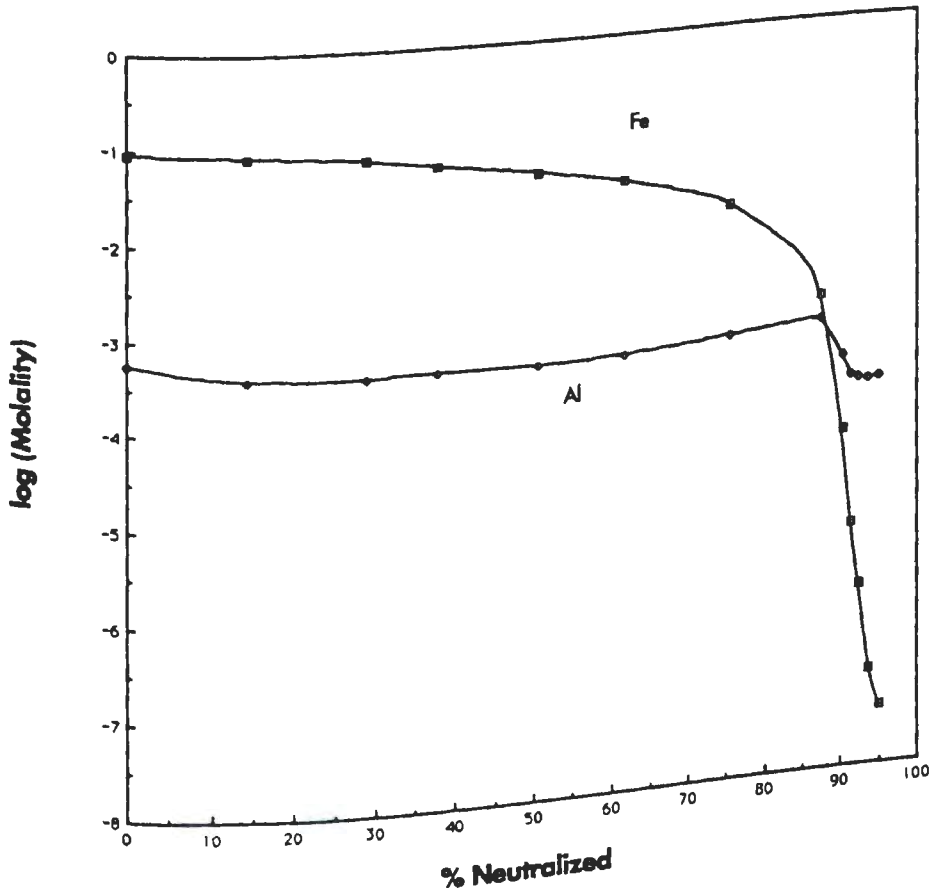

Notes: Concentrations are log(molal). The curves are smoothed by interpolation.

diffraction of the solids filtered out of sample 13 did not indicate the presence of crystalline jurbanite.

Zinc

Zinc concentrations in the filtrates ranged from 36 μM down to 3 μM. Figure 4.39 shows the log concentrations of iron and zinc in these samples versus percent neutralization in the titration. The zinc appears to be conserved in solution at least through 90% neutralization (pH 3.51). By this time more than 99.9% of the original iron had been removed from solution. But the zinc concentration fell rapidly as the pH was pushed above 3.9, resulting in the loss of over 90% of the original dissolved zinc before the last sample (pH 5.55). From sample 9 (90% neutralized) onward, SI calculations for $ZnO \cdot Fe_2O_3$ indicate supersaturation with respect to this solid. The crystalline form is not expected to form in solution under the conditions of this experiment, especially given the trace amount of zinc available. Kinniburgh and Jackson 1982, showed the adsorption by iron hydrous oxide gel of 10^{-5} M zinc to run from about pH 4 to 6 with 50% of the zinc sorbed by about pH 5.1. Thus, the removal of zinc from solution is thought to be by adsorption onto the suspended particles of precipitated hydrous ferric oxyhydroxides.

Figure 4.39 *Logarithmic plot of zinc and iron in the neutralization titration solution, as a function of reaction progress (expressed as percent neutralized).*

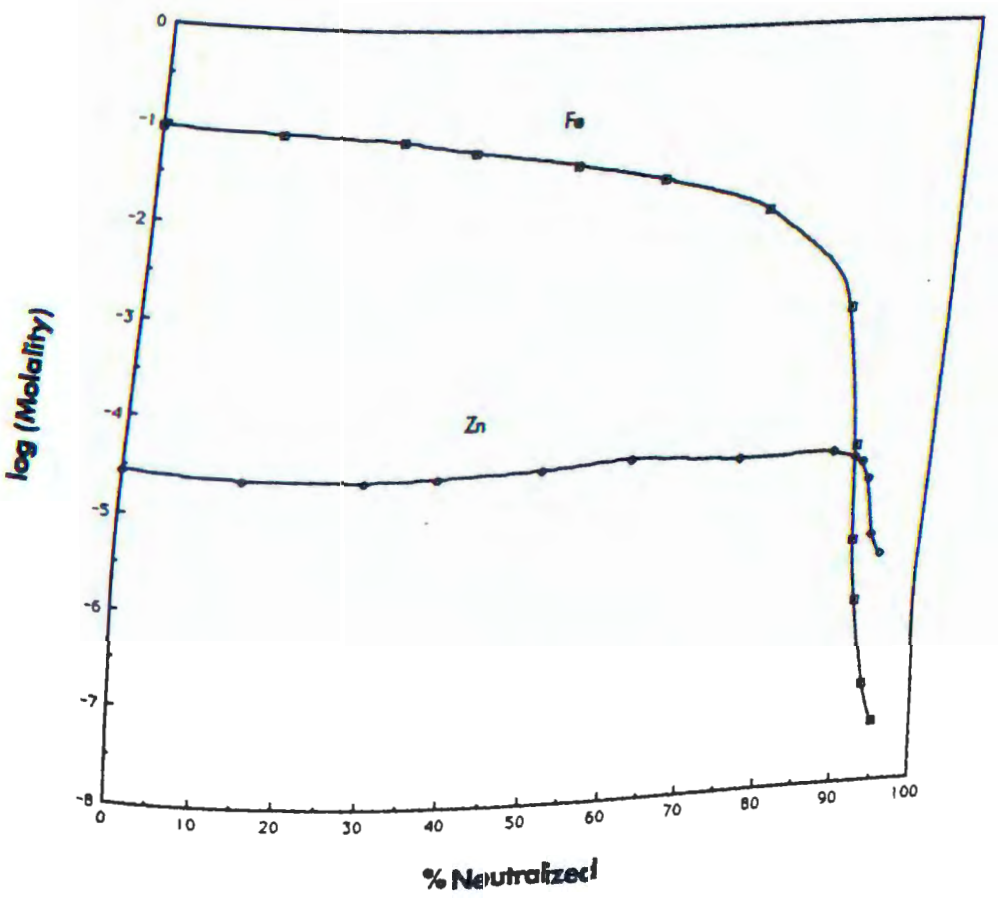

Notes: Concentrations are log(molal). The curves are smoothed by interpolation.

Chromium

Chromium concentrations in the filtrates ranged from 15.1 μM down to the detection limit. Figure 4.40 shows the log concentration of iron and chromium versus percent neutralization. They appear to be removed from solution together. Figure 4.41 is a plot of log concentration of iron and chromium versus pH. It shows that the concentrations of iron and chromium converged as the neutralization proceeded. This suggests that as iron precipitated from solution, the solid had a higher Fe/Cr ratio than did the bulk solution. In this way, iron would be removed from solution faster than chromium and their concentrations would converge.

Sass and Rai (1987) investigated the solubility of amorphous chromium(III)-iron(III) hydroxide solid solutions and developed a general relationship that can be used to calculate the mole fractions of chromium and iron in the solid solution. Their work suggests that the Fe/Cr ratio in precipitates from our synthetic leachate may be enriched in iron relative to the solution composition by factors greater than 10^{+5}.

PHREEQE was used to calculate the redox distribution of chromium(III) and (VI) in equilibrium with the air saturated solution of synthetic leachate for each sample collected during the neutralization titration.

Figure 4.40 Logarithmic plot of chromium and iron in the neutralization titration solution, as a function of reaction progress (expressed as percent neutralized).

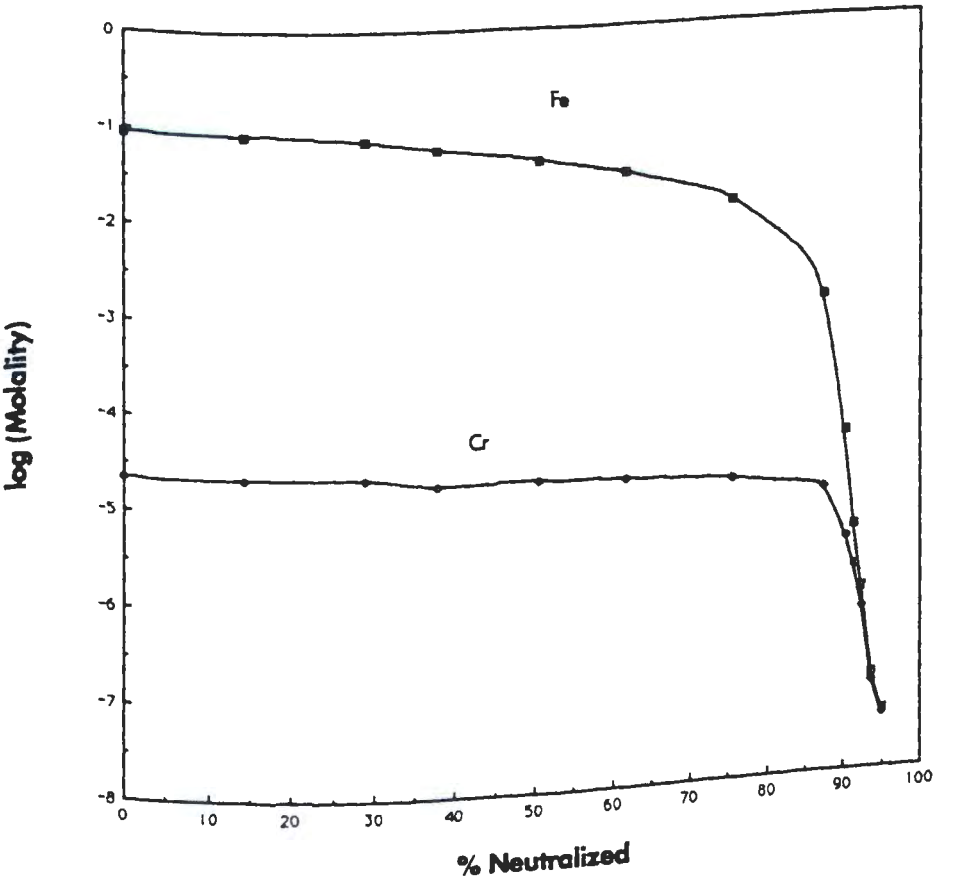

Notes: Concentrations are log(molal). The curves are smoothed by interpolation.

Figure 4.41 Logarithmic plot of chromium and iron in the neutralization titration solution, as a function of pH.

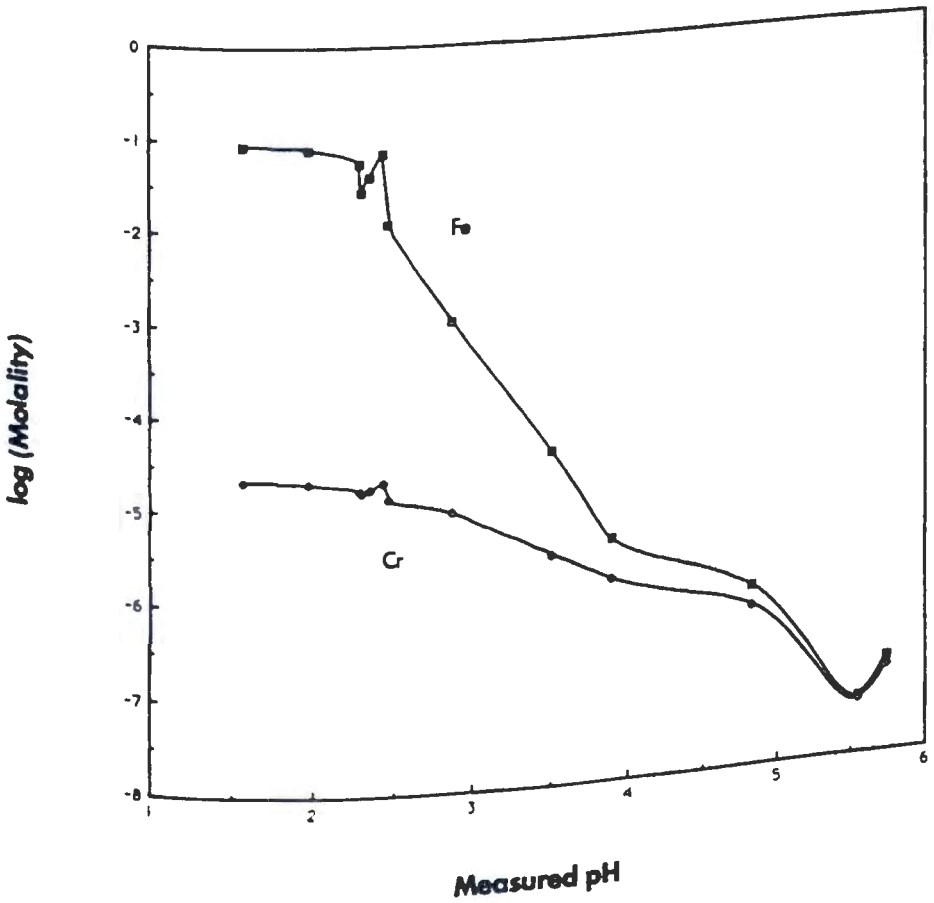

Notes: Concentrations are log(molal). The curves are smoothed by interpolation.

The resultant speciation indicated that 90% or more of the chromium in solution should exist as $CrSO_4^{1+}$ at least through pH 2.475 (75% neutralized), and thereafter shift to Cr(VI) species, primarily $HCrO_4^{1-}$. (However, note that under acidic conditions, the oxidation of Cr(III) to Cr(VI) is extremely slow.)

Chromium (VI) is adsorbed onto hydrous ferric oxide surfaces, but solution sulfate competes for the sorption sites, and cosorption of sulfate reduces chromate adsorption by as much as 80%, (Zachara et al. 1987). Thus, it is thought that chromium is removed from solution with ferric iron solids; and that the substance is enriched in iron relative to the solution composition, so that iron is removed from solution faster than chromi um, resulting in convergence of their concentrations.

Copper

Copper concentrations in the filtrates ranged from 15.1 μM down to 0.21 μM. Figure 4.42 shows the log concentrations of iron and copper in these samples versus percent neutralization. Total filterable copper appears to be conserved through 87% neutralization (pH 2.87). But over 98% of the copper initially in the system is removed by the time the system is 94% neutralized (a pH of 5.75 was measured). Saturation index calculations

Figure 4.42 Logarithmic plot of copper and iron in the neutralization titration solution, as a function of reaction progress (expressed as percent neutralized).

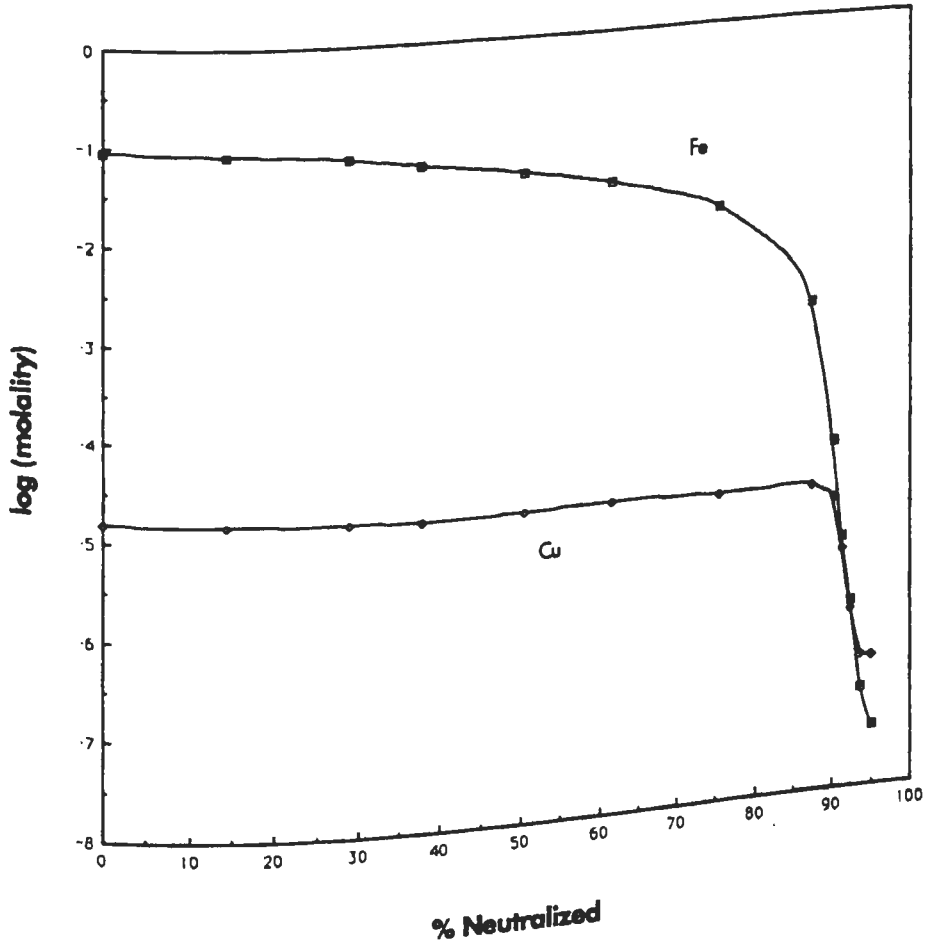

Notes: Concentrations are log(molal). The curves are smoothed by interpolation.

indicate near saturation (SI = -0.2769) with copper ferrite ($CuFe_2O_4$) in sample 8 and supersaturation in the rest of the samples. Although it is doubtful that the crystalline solid formed in these samples, this does suggest that precipitation of copper with ferric iron accounts for the removal of copper from these sample solutions.

Cadmium

Cadmium concentrations in the filtrates ranged from 9.2 μM down to 5.0 μM. Figure 4.43 shows the log concentrations of iron and cadmium versus percent neutralization. Filterable cadmium appears to be conserved in the samples until the last two samples, where almost half of the initial cadmium was lost from solution. None of the ten cadmium solids monitored by saturation index calculations ever approached saturation. Dzombak and Morel 1990, present data on the surface complexation reactions of cadmium with hydrous ferric oxide. The pH range of sorption for $2x10^{-6}$ M Cd commences about pH 6, is almost complete by pH 7.5, and 50% adsorption occurs about pH 6.75. At higher concentrations the sorption edge for cadmium runs from about pH 4.5 through 7, (Kinniburgh et al. 1976). It is tentatively proposed that the loss of cadmium in the last two samples was due to adsorption on

Figure 4.43 Logarithmic plot of cadmium and iron in the neutralization titration solution, as a function of reaction progress (expressed as percent neutralized).

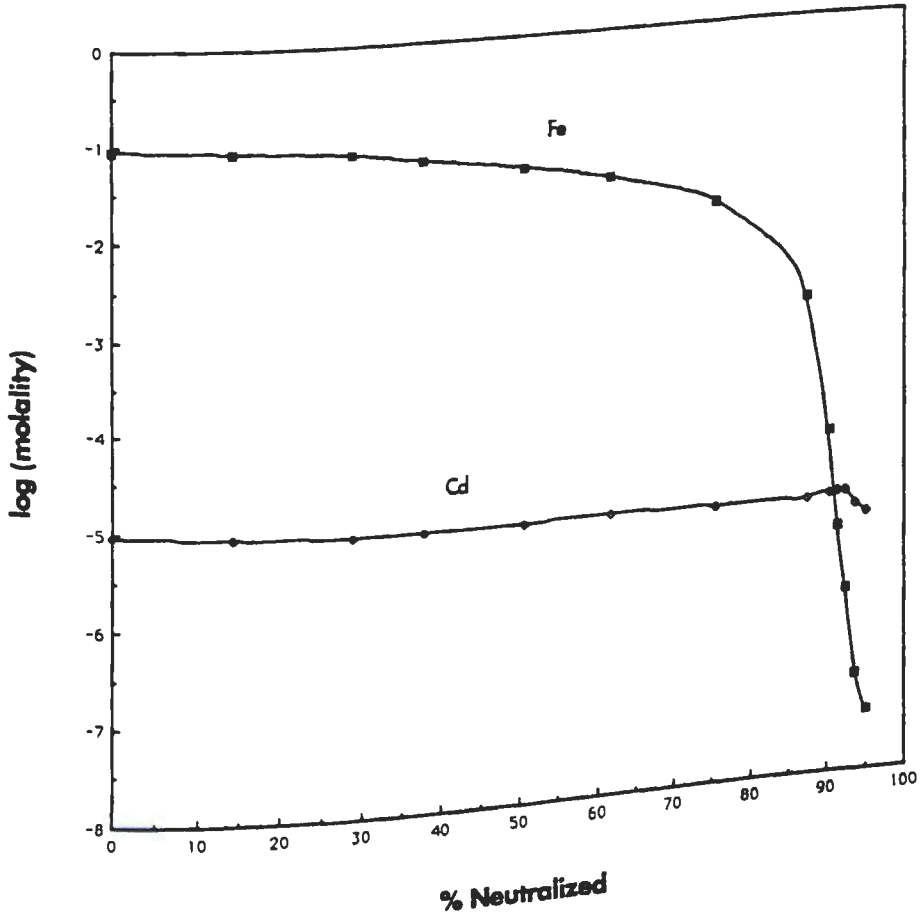

Notes: Concentrations are log(molal). The curves are smoothed by interpolation.

the surfaces of suspended hydrous ferric oxyhydroxide particles. Though it should be noted that some doubt exists as to how to interpret any observations limited to the last two samples whose iron data was clearly erroneous, and for which at least one of the pH values seems questionable.

Lead

Lead concentrations in the filtrate ranged from 4.7 μM down to the detection limit. Figure 4.44 shows the log concentration of iron and lead versus percent neutralization. Lead appears to be conserved in solution through 50% neutralization (pH 2.36). But by 75% neutralization (pH 2.47) almost 98% of the initial lead concentration had been removed from solution.

Lindsay 1979, indicates that in soils below pH 6, anglesite ($PbSO_4$) is more likely to be stable. The saturation index for anglesite hovered around -0.600 through the first five samples, but as lead disappeared from the filtrates, the SI plunged to -2.21, indicating that lead was being removed by a mechanism other than precipitation with sulfate. The saturation index for lead jarosite indicated supersaturation by orders of magnitude at least through 75% neutralization (pH 2.47). At 90% neutralization (pH 3.51) the SI was -0.2829, and

Figure 4.44 Logarithmic plot of lead and iron in the neutralization titration solution, as a function of reaction progress (expressed as percent neutralized).

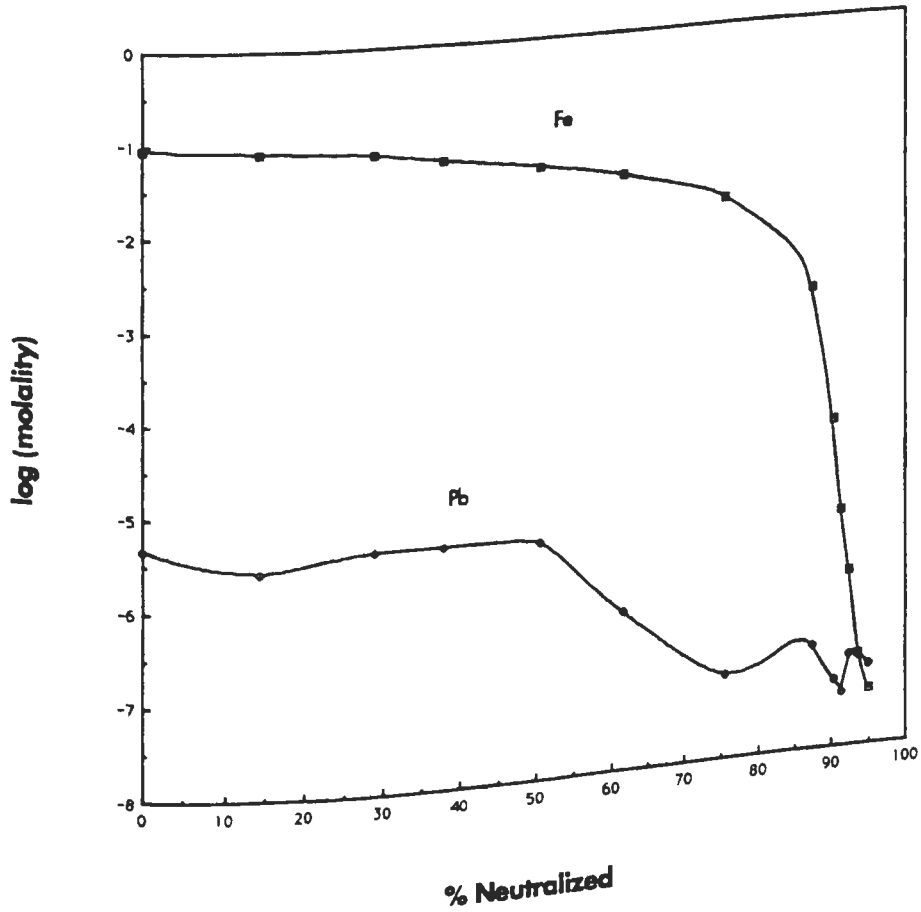

Notes: Concentrations are log(molal). The curves are smoothed by interpolation.

thereafter the solutions are undersaturated by orders of magnitude. Thus, the model indicates that lead is not forming a pure lead jarosite phase.

Dzombak and Morel 1990, present data gathered from Benjamin 1978, and Leckie et al. 1980, for the adsorption of $5x10^{-6}$ M Pb onto hydrous ferric oxide. The process commences by pH 3.5 and is not complete until about pH 6.5; 50% adsorption is achieved about pH 4.5. Frimmel and Geywitz 1987, evaluated differential pulse polarography for recording the coprecipitation of metal ions with ferric hydroxide from solutions 0.1 millimolar in total iron. Their data suggest the removal of 3 micromolar lead between pH 4.2 and 7.3. This does not explain the observed loss of lead from our solutions by pH 2.5, nor has a satisfactory explanation been found in the literature. However, the relative success of modeling lead removal by forming a solid solution with precipitating ferric iron suggests that this mechanism may account for my lead data.

Arsenic

Arsenic concentrations in the filtrates were all near the limit of quantitation and ranged from near 1.2 μM down to about 0.7 μM. Figure 4.45 shows the log concentration of iron and arsenic versus percent neutralization. Arsenic was rather well conserved in the solution

Figure 4.45 Logarithmic plot of arsenic and iron in the neutralization titration solution, as a function of reaction progress (expressed as percent neutralized).

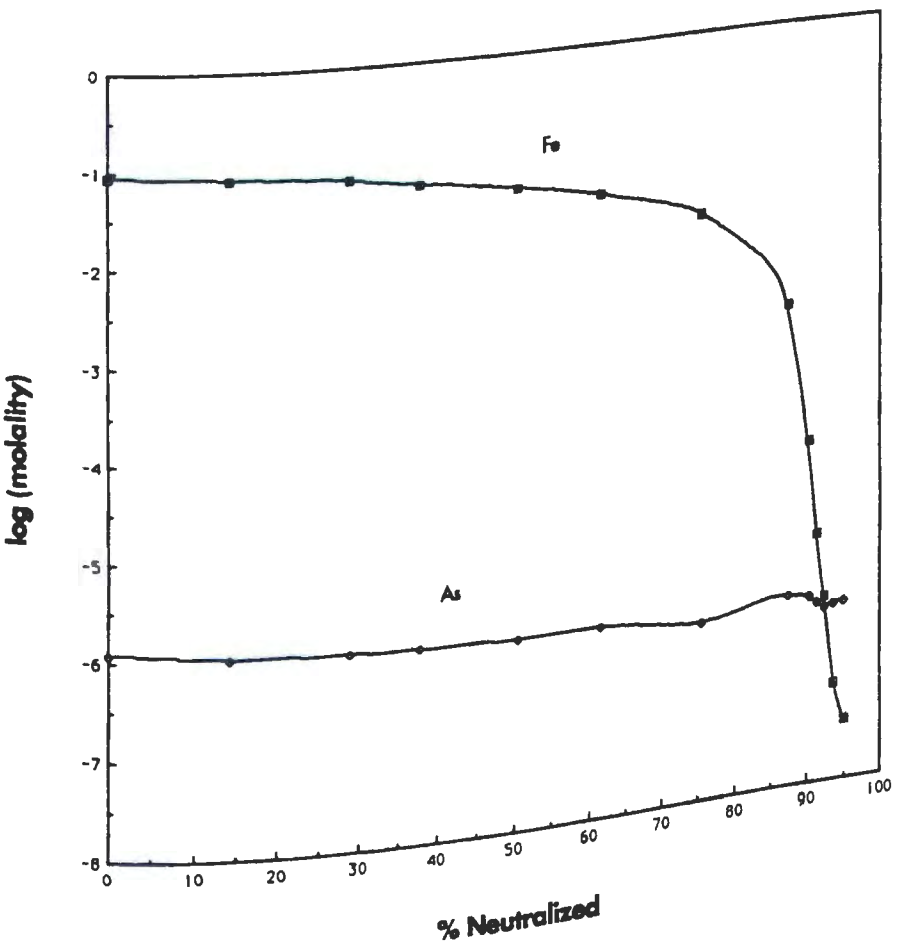

Notes: Concentrations are log(molal). The curves are smoothed by interpolation.

throughout the experiment, though there appears to have been some loss after about 90% neutralization (pH 3.5).

The samples were all found to be undersaturated by 2 to 4 orders of magnitude with respect to scorodite, $FeAsO_4 \cdot 2H_2O$, which is the most stable arsenate in acidic iron solutions, (Davis and Ashenberg, 1989). The pH dependence of arsenate concentration in contact with solid ferric hydroxide is indicated by the equation:

$$H_xAsO_4^{X-3} + Fe(OH)_{3(s)} = \qquad \text{Eqn. 4.45}$$

$$FeAsO_{4(s)} + XH_2O + (3-X)OH^-$$

According to this reaction, one would expect the concentration of dissolved arsenate to increase as pH increases. But the opposite was observed during our neutralization titration.

Figure 4.46, a plot of the log molal concentrations of arsenic and iron vs pH, does not indicate that arsenic coprecipitated significantly with iron over the pH range studied. The arsenic plots do not track those of iron, nor do they exhibit the shape characteristics of chromium, copper, and lead, which were successfully modeled as coprecipitationg with iron.

Pierce and Moore 1982, investigated the adsorption of arsenate and arsenite on amorphous iron hydroxide. They found the adsorption capacity for arsenic to be extremely high, with arsenate adsorbing to a greater

Figure 4.46 Logarithmic plot of arsenic and iron in the neutralization titration solution, as a function of pH.

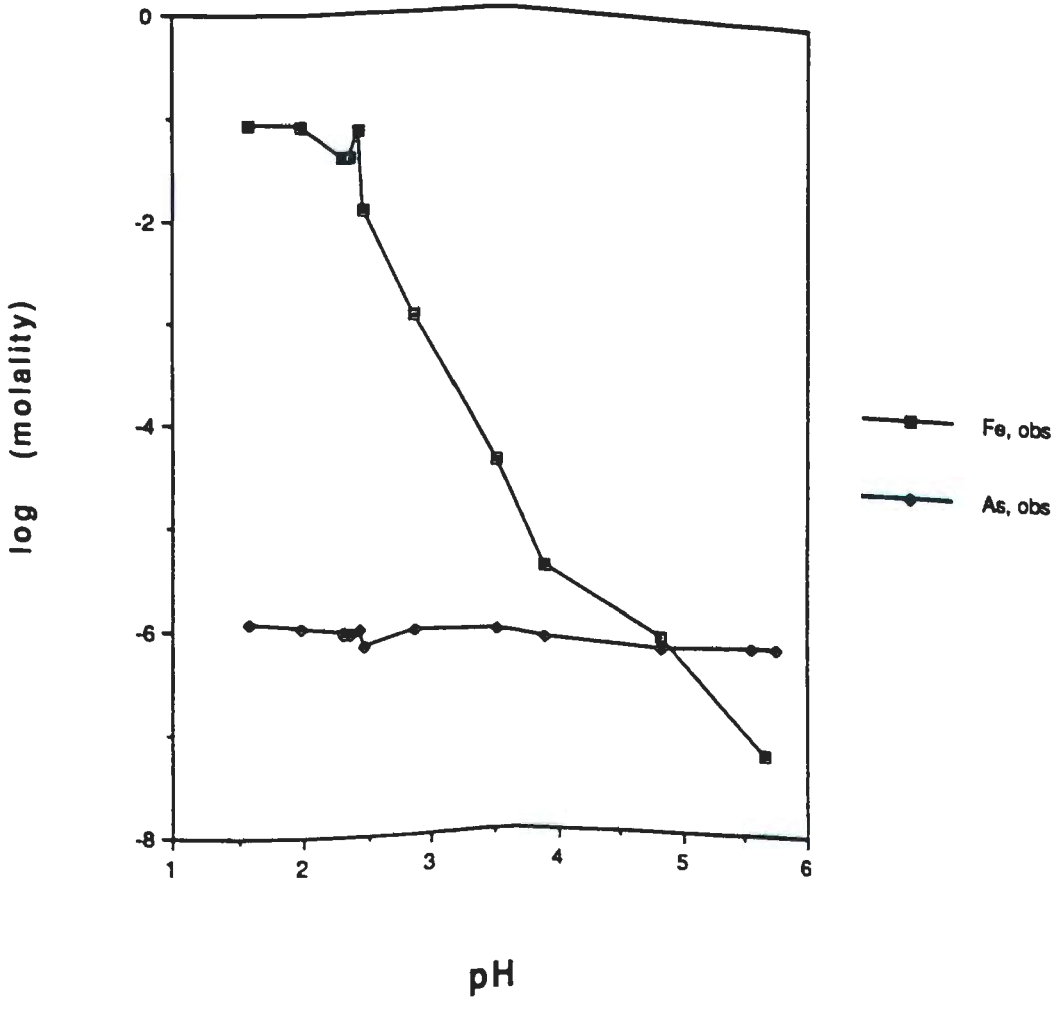

Note: Concentrations are log(molal).

extent than arsenite, and at optimum pH of 4 and 7 respectively. However, desorption occurred with increasing pH; and they also found a significant decrease of adsorption of arsenic at low concentrations in the presence of sulfate.

The model for surface complexation on hydrous ferric oxide developed by Dzombak and Morel 1990, is not consistent with our arsenic data. Their model predicts 100% sorption of $1x10^{-6}$ molar arsenate clear up through pH 9 in a system with $1x10^{-3}$ molar total iron. Desorption is predicted to reach about 50% at pH 11. Even if the model were adapted to account for the significant decrease in adsorption of arsenic at low concentrations in the presence of sulfate observed by Pierce and Moore (1982), it still would not predict the decrease of arsenic concentrations in solution.

The possibility was investigated that this gradual, rather steady decline of concentration was the result of removal of some arsenic with each sample and dilution of the rest with each addition of titrant. The total sulfate concentration of each sample was estimated from the initial sulfate in the system as adjusted for sample withdrawal, dilution, and evaporation. The same concentration adjustments were applied proportionately to the arsenic concentration of the first sample, in order to estimate the arsenic concentrations in the rest of the

samples assuming it was being conserved in solution. The results are plotted with the observed arsenic concentrations in Figure 4.47, which indicates that this scheme does not account for all of the lost arsenic. It is assumed that the uncertainties of the data and resulting estimates are not greater than ten percent; nevertheless, the calculations were repeated with a 20% increase in the estimated loss of arsenic from sample to sample due to sampling and dilution. Figure 4.48 allows the comparison of the observed arsenic concentrations with a constant concentration, the estimated conserved arsenic concentrations, and the 20% extra loss estimates. Clearly the observed decline of arsenic during this experiment was much more than can be explained by the factors of sample removal and dilution by added titrant.

Thus, no suitable basis was found with which to explain or model the removal of arsenic from acidic leachates containing high levels of total iron and sulfate during neutralization. However, the speciation model calculations for these samples indicate that $FeAsO_4^\circ$ becomes an important species for arsenic as pH rises above 3, and it becomes the most important species for iron after 92% neutralization (pH 4.8). Thus, some surface complexation of arsenate on the suspended hydrous ferric oxyhydroxysulfate particles is the suspected cause

Figure 4.47 Logarithmic plot of arsenic and sulfate in the neutralization titration solution versus sample number.

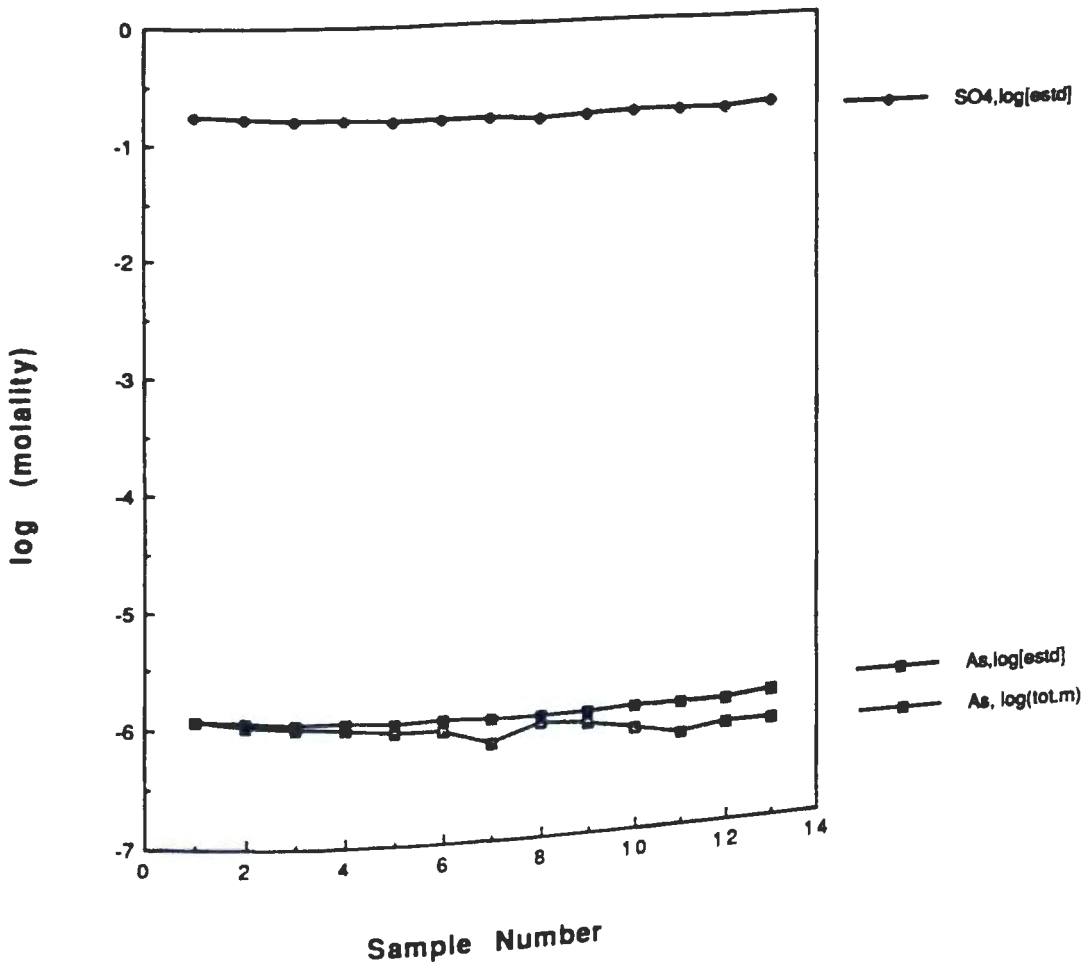

Note: The estimated sulfate and estimated arsenic concentrations were calculated assuming conservation in solution and accounting for sample removal, evaporation, and dilution by added titrant.

Figure 4.48 Molal concentration of arsenic (as measured and estimated) in the neutralization titration solution versus sample number.

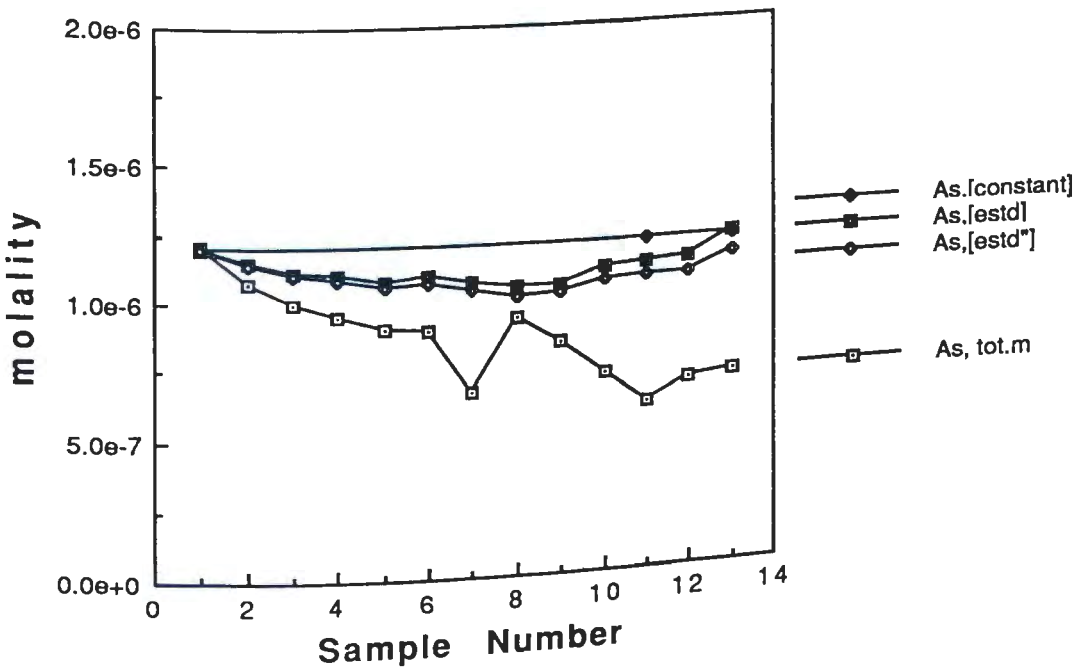

Notes: The straight line represents the initial concentration of arsenic held constant. The estimated arsenic was calculated assuming conservation in solution and accounting for sample removal, evaporation, and dilution. The second estimation of arsenic supposed a 20% increase in the amount of arsenic removed with each sample.

for removal of a fraction of the arsenic from solution. This hypothesis is supported by work done in both fresh and saline waters, (see Johnson and Thornton 1987).

CHAPTER 5 SUMMARY AND SYNTHESIS

5.1 BATCH OXIDATION EXPERIMENT

During this first experiment we observed characteristics of the oxidation of submerged whole coal, including: immediate initial acidity due to very soluble prior oxidation products; sulfate concentrations are much higher than iron as long as system pH is greater than 2.5; there is a dramatic increase in the rate of sulfate production followed by a dramatic increase in the rate of iron release when the pH drops below 2.5; the concentrations of filterable sulfate and iron rise rapidly and the sulfate to iron ratio approaches 3:2 as the pH is driven below 2.

The relative concentrations of selected solutes in the bulk solution were: SO_4 > Fe >> Al >> Zn > Cu >> As & Cr > Cd > Pb. Iron, copper, and probably arsenic tracked the production of sulfate while aluminum, zinc, chromium, and cadmium concentrations were stable to slightly rising during the experiment. Arsenic and chromium were enriched in the 1.0 molar magnesium chloride washes, but cadmium was enriched in the filtrate relative to the distribution of iron between the two solutions.

5.2 NEUTRALIZATION OF SYNTHETIC LEACHATE

The reaction proceeded as a pH 2.5 buffered acidic system while filterable iron was removed by precipitation. Each new injection of $NaHCO_3$ stimulated new nucleation and precipitation of iron from solution, with the hydrolysis resulting in pH relaxation. System pH rose rapidly after the relative exhaustion of dissolved iron.

Computer modeling of the solution samples aided in the interpretation of the analytical data for the major and trace elements studied. Excess positive charge in the solution compositions was deemed to be due to the passage of colloidal iron particles through the filters and subsequent dissolution in the acidified samples. Excess negative charge was deemed to be due to the assumption that iron precipitated as a pure phase, without any contamination by sulfate. The speciation of iron and the trace metals was dominated by complexes with sulfate. Iron was precipitated from solution as a ferric oxyhydroxy-sulfate of approximate composition $Fe_{16}O_{16}(OH)_{12}(SO_4)_2$ and holding iron solubility intermediate between those established by amorphous and crystalline $Fe(OH)_3$.

It was hypothesized that: aluminum was removed from solution as an $Al(OH)SO_4$ phase like jurbanite; zinc (and probably cadmium as well) was adsorbed onto suspended particles of hydrous ferric oxyhydroxysulfate; chromium was removed by formation of a solid solution with the

precipitating ferric iron that was enriched in iron relative to the solution composition; copper precipitates with ferric iron and its solubility is similar to that of ferrite; and, arsenic was removed at pH > 5 perhaps by surface complexation of arsenate on suspended hydrous ferric oxyhydroxysulfate particles. No literature-based explanation was found that satisfactorily accounted for the lead data. However, its removal from a synthetic leachate was rather successfully modeled by formation of a solid solution with the precipitating ferric iron.

5.3 COMPUTER MODELING

5.3.1 Equilibrium model for inorganic acidic leachates

A thermodynamic equilibrium model has been developed based on the aqueous chemical equilibrium computer program PHREEQE. The model simulates the dilution and/or neutralization of oxygenated inorganic acidic leachates from coal or related acid mine drainage when interacting with neutral or slightly basic waters and bicarbonates.

The model assumes that equilibration with air determines the partial pressures of oxygen and carbon dioxide in solution. The concentration of dissolved silica is controlled by equilibrium with silica glass. Sodium, when introduced with bicarbonate or another source, is assumed to be conserved in solution. Sulfur in the

oxidized leachate or drainage is assumed to exist as sulfate and is largely conserved in solution. However, it may be removed when precipitates of jurbanite ($Al(OH)SO_4 \cdot 5H_2O$) or jarosites ($MFe_3(OH)_6(SO_4)_2$) form, and to some extent as a ferric oxyhydroxysulfate. There was no evidence detected that any of the jarosites formed during the 2 1/2 week duration of the neutralization experiment. The only evidence from this study for the formation of a jurbanite phase is that its saturation index was near zero throughout the pH 2.87 - 3.90 range.

Iron is the major hydrolyzing cation in these systems. Its removal during neutralization is modeled by formation of the compound $Fe_{16}O_{16}(OH)_{12}(SO_4)_2$ which also removed the apparent excess (based on solution charge imbalance) of dissolved sulfate. The solubility of this ferric oxyhydroxysulfate was defined to be intermediate between goethite (α-FeOOH), and amorphous ferric hydroxide.

Although physical evidence is lacking to confirm the controls of aluminum solubility, the results of the neutralization titration were best modeled using a series of pure solid Al-containing phases. On this basis it is hypothesized that aluminum solubility is limited by jurbanite below pH 4, and by microcrystalline gibbsite above pH 5. Bayerite (α-$Al(OH)_3$), and basaluminite ($Al_4(OH)_{10}SO_4 \cdot 5H_2O$) limit the solubility of aluminum between pH 4 - 5.

Chromium loss from solution was modeled by the formation of a solid solution with precipitating ferric oxyhydroxysulfate. The removal of copper and lead from solution were modeled in the same way.

The failure of the PHREEQE simultaneous-equation solving subroutines to converge past pH 5 precluded the modeling of zinc and cadmium losses from solution. And no suitable theoretical model was found on which to base the removal of arsenic from these solutions.

The model predicted very well the concentrations of these elements in an acidic synthetic leachate undergoing episodic neutralization with sodium bicarbonate that drove the pH of the system from below 2 up to 5. The model was tested on field data from a creek system where acid sulfate mine drainage contaminated streams mixed with uncontaminated tributaries of pH 5 to 6. The model simulated the natural system quite well, considering the information available (and that which wasn't available). However, the simulation indicated that the iron solution chemistry over the course of at least a mile was not in equilibrium with iron solids observed as precipitates in the stream bed. It also indicated that the trace elements of the study and included in the model (Al, Zn, and Cu) were largely conserved in solution with only dilution affecting their concentrations. This was no doubt largely due to the limited range of pH observed in the contam-

inated stream over its course, 2.70 to 3.00, even though the uncontaminated tributaries ranged in pH from 5.25 to 6.10.

5.3.2 Predictive modeling of reactions and fates of solutes in coal leachates and acid mine drainage

Dilution and neutralization occur when contaminated, acidic drainage from coal storage areas and mines is mixed with natural waters of near neutral pH. A HCO_3^- concentration of approximately 0.002 molar may be carried by stream and river waters, principally due to contact with limestone and other mineral carbonates. A dilution ratio of 10 to 1 may be sufficient to initiate hydrolysis of the major metal contaminant, ferric iron.

The solution chemistry, including speciation, dilution, neutralization, hydrolysis, precipitation, coprecipitation, and pH, may be predicted using the modified geochemical equilibrium model that has been developed from the PHREEQE computer program and data base. However, the coagulation and actual removal of the primary precipitate, iron oxyhydroxysulfate, will not be instantaneous and may require some distance in the turbulent flow of a stream. (These kinetic and hydrodynamic factors have not been included in the model.) During this time, there is ample opportunity for interaction of other solutes with the colloidal particles resulting in adsorp-

tion to the hydrous ferric oxyhydroxysulfate surfaces. This may also be included in the model by adding the appropriate equilibria to the data base. Eventually, flocculation and settling will remove the precipitate with its coprecipitate(s) and adsorbate(s).

During the period of iron hydrolysis, the system will be buffered near pH 2.5, and the precipitation of other pure phases is not likely. Continued dilution and/or neutralization will reduce the dissolved iron concentration below 0.001 molar and exhaust the buffer capacity of the system. Thereafter, aluminum will precipitate with rising pH, as will other slightly soluble trace elements. These reactions for aluminum, arsenic, cadmium, chromium, copper, lead, and zinc, have also been included in the computer code, although its practical limit of application so far has been up to pH 5.

Spatially, close to the acid drainage source where acidity, iron, aluminum, and sulfate concentrations are the highest, jarosite precipitates have been reported (Nordstrom et al. 1979, Chapman et al. 1983), as well as saturation with respect to jurbanite or a basic aluminum sulfate of composition $Al(OH)SO_4$ (Chapman et al. 1983, Davis and Runnells 1987, Filipek et al. 1987). Farther downstream are found the hydrous ferric oxides followed by hydrous aluminum oxides. The other contaminants are expected to be present in trace amounts, and will inter-

act with these precipitates by surface complexation and adsorption processes. Even farther downstream will be encountered other exposed minerals and solids. Carbonates may be expected to dissolve and release their cations while further neutralizing the stream. Goethite and other oxides will provide additional sites for surface complexation and adsorption. Clays and clay minerals will provide a reservoir of silica and many sites for ion exchange, which may alter the profile of trace elements in solution. All of these features may be incorporated in the model by adding the appropriate equilibria and thermodynamic constants to the PHREEQE database.

The stepwise evolution of a contaminated effluent or stream may be simulated in segments by using the PHREEQE input program to build a sequence of geochemical problems. In this application, each segment "inherits" the output from the previous segment and alters it in accordance with a new set of conditions encountered by the flowing stream. In this manner, one can independently test individual changes in the system, such as temperature, alkalinity and/or composition of tributary waters, contact with different minerals and solid phases (one at a time or in combinations), or even test the effects of different equilibrium constants for the same reaction.

5.3.3 Predictive modeling of the generation of coal leachates and acid mine drainage

The acid generating capacity of a coal is largely determined by its iron pyrite content, and may be moderated by the presence of carbonates such as limestone. In order to predict the composition of coal leachates or acid mine drainage, a great deal must be known about the system. Important factors would include its mineralogy (qualitative, quantitative, and degree of subdivision), its chemical composition (of soluble organic complexing agents as well as inorganic compounds and trace elements), and its system dynamics (including flushing water composition, frequency, and amounts, as well as particle sizes and porosity).

Careful construction of the chemical model would be necessary to obtain all of the important equilibria and applicable thermodynamic equilibrium constants. Kinetic factors would also have to be incorporated into the model, including: diffusion coefficients, reaction rates, the dynamics of microbial colony growth and activity, and the effects of temperature on all physical, chemical, and biological aspects of the system.

Taken together, these appear to be more than can be adequately managed within one program. For the near future it is expected that technicians will analyze and monitor the drainage from coal piles and mines, and then

use computer models to anticipate the fate of dissolved solids in the effluents. They could investigate the effects of various neutralization and clean-up treatments, predict the concentrations of dissolved solutes and trace contaminants in the treated effluents, and then predict the ultimate fate of these substances after release into a stream or river.

APPENDIX A

Graphite Furnace Atomic Absorption Spectrophotometry

(Instrument parameters and analytical conditions used with the Perkin-Elmer model 2380 Atomic Absorption spectrophotometer with HGA-300 Graphite Furnace and the AS-40 Autosampler for the analyses of iron, aluminum, arsenic, cadmium, chromium, copper, lead, selenium, and zinc in the filtered samples from the batch oxidation and neutralization titration experiments.)

IRON in the neutralization samples.

Instrument:
- Fe hollow cathode lamp
- 248.3 nm line
- 0.2 nm slits
- D_2-arc background correction
- Absorbance mode
- 10 sec peak area integration

Atomizer:
- Pyrolytically coated graphite tube
- Massive pyrolytic L'Vov platform
- Argon purge gas

Program:	Drying		Char	Atomize	Purge
Temp, °C	80	120	1400	2500	2700
Ramp, sec	1	50	13	0	1
Hold, sec	0	0	30	10	5
Gas flow				stop	

Solutions:
- Matrix Mod: 20 µL of 2.5 g/L Mg in 1% HNO_3
- Stock Std: 1000. ppm Fe in 2.5% Ultrex HNO_3
- Working Stds: 20 µL of 1, 5, 10, 20, 40, 60, 80, and 100 ppb in 0.2% Ultrex HNO_3
- Best range: 5 - 60 ppb
- Samples: diluted 1:100,000 with 0.2% Ultrex HNO_3 autopipette 20 µL aliquots

ALUMINUM

Instrument: Al hollow cathode lamp
309.3 nm line (or 308.2 is less sensitive)
0.7 nm slits
D_2-arc background correction
Absorbance mode
10 sec peak area integration

Atomizer: Pyrolytically coated graphite tube
Massive pyrolytic L'Vov platform
Argon purge gas

Program:*	Drying		Charring		Atomize	Purge
Temp, °C	90	130	400	1750	2550	2700
Ramp, sec	1	50	26	14	0	1
Hold, sec	8	10	9	20	10	5
Gas flow					stop	

Solutions:
Matrix Mod: 20 µL of 2.5 g/L Mg in 1% HNO_3
Stock Std: 1002. ppm Fe in 3% Ultrex HNO_3
Working Stds: 20 µL of 1, 9, 25, 40, 60, 80, and 100 ppb in 0.2% Ultrex HNO_3
Best range: 5 - 40 ppb (or 5 - 80 at 308.2 nm)
Samples: diluted 1:1000 with 0.2% Ultrex HNO_3 autopipette 20 µL aliquots (or 10 µL if signal is beyond linear range).

* Differences for analysis of the Neutralization samples:

Program:	Drying		Char	Atomize	Purge
Temp, °C	80	130	1750	2550	2700
Ramp, sec	1	75	17	0	1
Hold, sec	0	0	25	10	5
Gas flow				stop	

Samples were diluted 1:100 with 0.2% HNO_3

ARSENIC

Instrument: As hollow cathode lamp
193.7 nm line
0.7 nm slits
D_2-arc background correction
Absorbance mode
10 sec peak area integration

Atomizer: Pyrolytically coated graphite tube
Massive pyrolytic L'Vov platform
(both pre-coated with Mo:
10 x 100 µL of 1 g/L Mo)
Argon purge gas

Program:*	Drying		Charring		Atomize	Purge
Temp, °C	90	140	300	1400	2100	2650
Ramp, sec	1	50	1	1	0	1
Hold, sec	9	0	0	30	10	5
Gas flow					stop	

Solutions:
Matrix Mod: 20 µL of 1 g/L Ni as the nitrate, & 100 mg/L Mo, & 0.24% Pt, & 1 g/L H_2SO_4, in 1.3% chloride and 2.2% nitrate solution.
Stock Std: 1000. ppm As in 1% Ultrex HNO_3.
Working Stds: 20 µL of 5, 10, 20, 40, 60, 80, and 100 ppb in 0.2% Ultrex HNO_3.
Best range: 10 - 80 ppb
Samples: diluted 1:10 with 0.2% Ultrex HNO_3
autopipette 20 µL aliquots

* Differences for analysis of the Neutralization samples:
Drying step: 30 sec. ramp to 130 °C.
Charring step: 1 sec. to 1400 °C and hold 20 sec.

CADMIUM

Instrument:
Cd hollow cathode lamp
228.8 nm line
0.7 nm slits
D_2-arc background correction
Absorbance mode
5 sec peak area integration

Atomizer:
Pyrolytically coated graphite tube
Massive pyrolytic L'Vov platform
Argon purge gas

Program:*	Drying		Charring		Atomize	Purge
Temp, °C	90	140	400	700	1400	2650
Ramp, sec	1	50	26	7	0	1
Hold, sec	5	10	9	20	5	5
Gas flow					stop	

Solutions:
Matrix Mod: 20 µL of 10. g/L $NH_4H_2PO_4$ and 0.50 g/L Mg in 0.2% Ultrex HNO_3.
Stock Std: 998. ppm Cd in 1% HCl.
Working Stds: 20 µL of 1, 3, 6, 10, 15, and 20 ppb in 0.2% Ultrex HNO_3.
Best range: 1 - 10 ppb
Samples: diluted 1:10 with 0.2% Ultrex HNO_3
autopipette 20 µL aliquots

* Differences for analysis of the Neutralization samples:

Program:	Drying		Char	Atomize	Purge
Temp, °C	80	130	700	1400	2650
Ramp, sec	1	75	7	0	1
Hold, sec	0	0	25	5	5
Gas flow				stop	

Used 10 µL of all samples and standards.

CHROMIUM

Instrument: Cr hollow cathode lamp
357.9 nm line
0.7 nm slits
Absorbance mode
5 sec peak area integration

Atomizer: Pyrolytically coated graphite tube
Massive pyrolytic L'Vov platform
Argon purge gas

Program:*	Drying		Charring		Atomize	Purge
Temp, °C	80	140	400	1600	2550	2700
Ramp, sec	1	60	26	12	0	1
Hold, sec	0	0	9	25	5	5
Gas flow					stop	

Solutions:
Matrix Modifiers (also for matrix matching):
For Standards: 20 µL of std. plus 20 µL of 0.03 M $MgCl_2$ & 170. ppm Fe & 5.0 ppm Al in 0.5% HNO_3 & 0.015% HCl.
For Filtrates: 20 µL of sample plus 20 µL of 0.03 M $MgCl_2$ & 100 ppm Fe in 0.32% HNO_3.
For Washes: 10 µL of sample plus 30 µL of 100 ppm Fe & 3.0 ppm Al in 0.28% HNO_3 & 0.01% HCl.
Stock Std: 1000. ppm Cr in Milli-Q water.
Working Stds: 20 µL of 1, 9, 20, and 40 ppb in 0.2% Ultrex HNO_3.
Best range: 5 - 40 ppb
Samples: diluted 1:10 with 0.2% Ultrex HNO_3 autopipette aliquots as above.

* Differences for analysis of the Neutralization samples:

Use 20 µL each standards, samples and matrix modifier.
Matrix modifier = 2.5 g/L Mg in 1% HNO_3.
Use slower drying step: 75 sec ramp to 130 °C.

COPPER

Instrument:
Cu hollow cathode lamp
324.8 nm line
0.7 nm slits
D_2-arc background correction
Absorbance mode
10 sec peak area integration

Atomizer:
Pyrolytically coated graphite tube
Massive pyrolytic L'Vov platform
Argon purge gas

Program:*	Drying		Charring		Atomize	Purge
Temp, °C	90	140	400	1200	2200	2650
Ramp, sec	1	50	26	10	0	1
Hold, sec	5	10	9	20	10	5
Gas flow					stop	

Solutions:
Matrix Mod: 20 µL of 2.5 g/L Mg in 1% HNO_3.
Stock Std: 1000. ppm Cu in 1% HNO_3.
Working Stds: 20 µL of 1, 5, 10, 15, 20, 25, 30, 40, and 50 ppb in 0.2% Ultrex HNO_3.
Best range: 5 - 40 ppb
Samples: diluted 1:100 with 0.2% Ultrex HNO_3
autopipette 20 µL aliquots

* Differences for analysis of the Neutralization samples:

Program:	Drying		Char	Atomize	Purge
Temp, °C	80	120	1200	2200	2650
Ramp, sec	1	60	12	0	1
Hold, sec	0	0	25	10	5
Gas flow				stop	

And used slower drying step for wash samples (high salts): 75 second ramp to 130 °C.

LEAD

Instrument:
Pb hollow cathode lamp
283.3 nm line
0.7 nm slits
D_2-arc background correction
Absorbance mode
5 sec peak area integration

Atomizer:
Pyrolytically coated graphite tube
Massive pyrolytic L'Vov platform
Argon purge gas

Program:*	Drying		Charring		Atomize	Purge
Temp, °C	90	140	400	900	1750	2650
Ramp, sec	1	50	26	10	0	1
Hold, sec	5	10	9	20	5	5
Gas flow					stop	

Solutions:
Matrix Mod: 20 µL of 10.0 g/L $NH_4H_2PO_4$ and 0.50 g/L Mg in 0.2% Ultrex HNO_3.
Stock Std: 1000. ppm Pb in 1% HNO_3.
Working Stds: 20 µL of 1, 3, 9, 25, 50, and 80 ppb in 0.2% Ultrex HNO_3.
Best range: 5 - 40 ppb
Samples: diluted 1:10 with 0.2% Ultrex HNO_3
autopipette 20 µL aliquots

* Differences for analysis of the Neutralization samples:

Program:*	Drying		Charring		Atomize	Purge
Temp, °C	90	140	400	900	1750	2650
Ramp, sec	1	55	26	5	0	1
Hold, sec	0	7	9	25	5	5
Gas flow					stop	

SELENIUM

Instrument: Se hollow cathode lamp
196.0 nm line
0.7 nm slits
D_2-arc background correction
Absorbance mode
5 sec peak area integration

Atomizer: Pyrolytically coated graphite tube
Massive pyrolytic L'Vov platform
(both pre-coated with Mo:
10 x 100 µL of 1 g/L Mo)
Argon purge gas

Program:*	Drying		Charring		Atomize	Purge
Temp, °C	90	140	300	1000	2100	2650
Ramp, sec	1	50	1	1	0	1
Hold, sec	9	10	10	30	5	5
Gas flow					stop	

Solutions:
Matrix Mod: 20 µL of 0.5 g/L Cu, & 0.2 g/L Mg, & 100 mg/L Mo, & 0.24% Pt, & 1 g/L H_2SO_4 in 1.3% chloride solution.
Stock Std: 1020. ppm Se in 10% HCl.
Working Stds: 20 µL of 5, 10, 20, 40, 60, and 80 ppb in 0.2% Ultrex HNO_3.
Best range: 20 - 80 ppb
Samples: diluted 1:10 with 0.2% Ultrex HNO_3
autopipette 20 µL aliquots

* Differences for analysis of the Neutralization samples:

Program:*	Drying		Charring		Atomize	Purge
Temp, °C	90	130	300	1000	2100	2650
Ramp, sec	1	30	1	1	0	1
Hold, sec	9	0	5	20	5	5
Gas flow					stop	

Used 10 µL aliquots of matrix modifier

ZINC

Instrument: Zn hollow cathode lamp
213.9 nm line
0.7 nm slits
D_2-arc background correction
Absorbance mode
5 sec peak area integration

Atomizer: Pyrolytically coated graphite tube
Massive pyrolytic L'Vov platform
Argon purge gas

Program:*	Drying		Charring		Atomize	Purge
Temp, °C	90	140	400	700	1800	2650
Ramp, sec	1	50	26	3	0	1
Hold, sec	9	0	9	25	5	5
Gas flow					stop	

Solutions:
Matrix Mod: 24 µL of 0.25 g/L Mg in 0.2% HNO_3.
Stock Std: 1000. ppm Zn in 1% HCl.
Working Stds: 20 µL of 0.2, 1, 3, 6, 9, 12, and 15 ppb in 0.2% Ultrex HNO_3.
Best range: 1 - 8 ppb
Samples: diluted 1:100 or 1:1000 with 0.2% Ultrex HNO_3.
autopipette 20 µL aliquots

* Differences for analysis of the Neutralization samples:

Program:	Drying		Char	Atomize	Purge
Temp, °C	80	130	700	1800	2650
Ramp, sec	1	75	7	0	1
Hold, sec	0	0	25	5	5
Gas flow				stop	

And used 10 µL aliquots of samples and standards.

APPENDIX B

Chemical Equilibria and Constants

The following pages list the chemical equilibria used in the data file for the geochemical computer program PHREEQE (Parkhurst et al. 1980, revised August, 1990), which was used for the computer modeling in this study.

Also listed is the logarithm of the equilibrium constant corresponding to each reaction, and a number designating the reference(s) upon which the information is based. Below is the key to these references, for which complete literature citations may be found in the References section that follows this appendix.

1. Plummer and Tisaranni 1990
2. Alpers and Brimhall 1989
3. Alpers et al. 1989
4. Davis and Ashenberg 1989
5. Hem and Roberson 1989
6. Nordstrom et al. 1989
7. Parkhurst 1989
8. Smith and Martell 1989
9. Karathanasis et al. 1988
10. Khoe and Robins 1988
11. Krause and Ettel 1987
12. Rai et al. 1987
13. Bard et al. 1985
14. Brown et al. 1985
15. Driscoll et al. 1984
16. Plummer et al. 1984
17. Chapman et al. 1983
18. Nordstrom 1982b
19. Smith and Martell 1982
20. Wagman et al. 1982
21. Turner et al. 1981
22. Leckie and Davis 1979
23. Lindsay 1979
24. May et al. 1979
25. Sunda and Hanson 1979
26. Sylva and Davidson 1979
27. Baes and Mesmer 1976
28. Smith and Martell 1976
29. Naumov et al. 1974
30. Zirino and Yamamoto 1972

Notes: (*) = "Based on", (+) = "Adapted from"

Equilibrium Equations for Species:	Log(K)	Ref's
$H_2O = H^+ + OH^-$	-14.000	6
$H^+ + F^- = HF^o$	+3.18	6
$H^+ + 2F^- = HF_2^-$	+3.76	6
$H_4SiO_4 + 4H^+ + 6F^- = SiF_6^{2-} + 4H_2O$	+30.18	6
$H_4SiO_4 = SiO_3^{2-} + H_2O + 2H^+$	-22.	17*
$H_4SiO_4 = H_3SiO_4^- + H^+$	-9.83	6
$H_4SiO_4 = H_2SiO_4^{2-} + 2H^+$	-23.0	6
$CO_3^{2-} + H^+ = HCO_3^-$	+10.329	6
$CO_3^{2-} + 2H^+ = CO_{2(aq)} + H_2O$	+16.681	6
$CO_{2(aq)} = CO_{2(g)}$	+1.468	6
$SO_4^{2-} + H^+ = HSO_4^{1-}$	+1.988	6,8
$Al^{3+} + H_2O = AlOH^{2+} + H^+$	-5.00	6,9,23
$Al^{3+} + 2H_2O = Al(OH)_2^+ + 2H^+$	-10.1	5,6,9
$Al^{3+} + 3H_2O = Al(OH)_3^o + 3H^+$	-16.9	6
$Al^{3+} + 4H_2O = Al(OH)_4^- + 4H^+$	-22.7	5,6
$2Al^{3+} + 2H_2O = Al_2(OH)_2^{4+} + 2H^+$	-8.2	6*,14+,27+
$3Al^{3+} + 4H_2O = Al_3(OH)_4^{5+} + 4H^+$	-15.6	6*,14+,27+
$13Al^{3+} + 32H_2O = Al_{13}(OH)_{32}^{7+} + 32H^+$	-107.4	6*,14+,27+
$2Al^{3+} + 2H_2O + CO_3^{2-} = Al_2(OH)_2CO_3^{2+} + 2H^+$	+2.46	8*
$3Al^{3+} + 4H_2O + CO_3^{2-} = Al_3(OH)_4HCO_3^{4+} + 3H^+$	+0.13	8*
$Al^{3+} + H_2O + SO_4^{2-} = AlOHSO_4^o + H^+$	-1.903	13
$Al^{3+} + H^+ + SO_4^{2-} = AlHSO_4^{2+}$	+2.448	6
$Al^{3+} + SO_4^{2-} = AlSO_4^+$	+3.02	6
$Al^{3+} + 2SO_4^{2-} = Al(SO_4)_2^-$	+4.92	6
$2Al^{3+} + 3SO_4^{2-} = Al_2(SO_4)_3^o$	-1.88	23

$Al^{3+} + F^- = AlF^{2+}$	+7.0	6,15,23
$Al^{3+} + 2F^- = AlF_2^+$	+12.7	6,15,23
$Al^{3+} + 3F^- = AlF_3^\circ$	+16.8	6,15,23
$Al^{3+} + 4F^- = AlF_4^-$	+19.4	6
$Al^{3+} + 5F^- = AlF_5^{2-}$	+20.6	6
$Al^{3+} + 6F^- = AlF_6^{3-}$	+20.6	6
$Al^{3+} + 3NO_3^- = Al(NO_3)_3^\circ$	+0.12	23
$AsO_4^{3-} + 2e^- + 4H^+ = H_2AsO_3^- + H_2O$	+30.805	4,20
$AsO_4^{3-} + 2e^- + 5H^+ = H_3AsO_3^\circ + H_2O$	+40.03	4,20
$AsO_4^{3-} + H^+ = HAsO_4^{2-}$	+11.595	4,20
$AsO_4^{3-} + 2H^+ = H_2AsO_4^-$	+18.35	4,11,20
$AsO_4^{3-} + 3H^+ = H_3AsO_4^\circ$	+20.60	4,11,20
$Ca^{2+} + H_2O = CaOH^+ + H^+$	-12.78	6
$Ca^{2+} + CO_3^{2-} = CaCO_3^\circ$	+3.224	6
$Ca^{2+} + CO_3^{2-} + H^+ = CaHCO_3^+$	+11.435	6
$Ca^{2+} + F^- = CaF^+$	+0.94	6
$Ca^{2+} + SO_4^{2-} = CaSO_4^\circ$	+2.30	6
$Cd^{2+} + H_2O = CdOH^+ + H^+$	-10.08	7,21,27
$Cd^{2+} + 2H_2O = Cd(OH)_2^\circ + 2H^+$	-20.35	7,21,27
$Cd^{2+} + 3H_2O = Cd(OH)_3^- + 3H^+$	-33.3	7,21,27
$Cd^{2+} + 4H_2O = Cd(OH)_4^{2-} + 4H^+$	-47.35	7,21,27
$2Cd^{2+} + H_2O = Cd_2OH^{3+} + H^+$	-9.39	7,27
$4Cd^{2+} + 4H_2O = Cd_4(OH)_4^{4+} + 4H^+$	-32.85	27
$Cd^{2+} + H_2O + Cl^- = CdOHCl^\circ$	-7.40	7,20
$Cd^{2+} + Cl^- = CdCl^+$	+1.98	7,21,23
$Cd^{2+} + 2Cl^- = CdCl_2^\circ$	+2.6	7,21,23

$Cd^{2+} + 3Cl^- = CdCl_3^-$	+2.4	7,21,23
$Cd^{2+} + CO_3^{2-} = CdCO_3^o$	+4.09	23
$Cd^{2+} + H^+ + CO_3^{2-} = CdHCO_3^+$	+12.42	23
$Cd^{2+} + 2CO_3^{2-} = Cd(CO_3)_2^{2-}$	+7.	8
$Cd^{2+} + NO_3^- = CdNO_3^+$	+0.31	23
$Cd^{2+} + 2NO_3^- = Cd(NO_3)_2^o$	+0.00	23
$Cd^{2+} + SO_4^{2-} = CdSO_4^o$	+2.46	7,19,21
$Cd^{2+} + 2SO_4^{2-} = Cd(SO_4)_2^{2-}$	+3.50	7
$Cd^{2+} + 3SO_4^{2-} = Cd(SO_4)_3^{4-}$	+3.09	21
$Cr^{3+} + H_2O = CrOH^{2+} + H^+$	-3.2	12*
$Cr^{3+} + 2H_2O = Cr(OH)_2^+ + 2H^+$	-9.5	12*
$Cr^{3+} + 3H_2O = Cr(OH)_3^o + 3H^+$	-16.0	12*
$Cr^{3+} + 4H_2O = Cr(OH)_4^- + 4H^+$	-27.3	12*
$2Cr^{3+} + 2H_2O = Cr_2(OH)_2^{4+} + 2H^+$	-4.3	12*
$3Cr^{3+} + 4H_2O = Cr_3(OH)_4^{5+} + 4H^+$	-9.7	12*
$4Cr^{3+} + 6H_2O = Cr_4(OH)_6^{6+} + 6H^+$	-15.2	12*
$Cr^{3+} + SO_4^{2-} = CrSO_4^+$	+2.2	12*
$Cr^{3+} + H_2O + SO_4^{2-} = CrOHSO_4^o$	-2.45	12*
$Cr^{3+} + Cl^- = CrCl^{2+}$	+0.62	21
$Cu^{2+} + H_2O = CuOH^+ + H^+$	-8.00	7,21,22
$Cu^{2+} + 2H_2O = Cu(OH)_2^o + 2H^+$	-13.68	7,22
$2Cu^{2+} + 2H_2O = Cu_2(OH)_2^{2+} + 2H^+$	-10.36	7,27
$3Cu^{2+} + 4H_2O = Cu_3(OH)_4^{2+} + 4H^+$	-18.	26+
$Cu^{2+} + CO_3^{2-} = CuCO_3^o$	+6.77	8
$Cu^{2+} + H^+ + CO_3^{2-} = CuHCO_3^+$	+12.13	8
$Cu^{2+} + 2CO_3^{2-} = Cu(CO_3)_2^{2-}$	+10.2	8,25

$Cu^{2+} + Cl^- = CuCl^+$	+0.43	7,20
$Cu^{2+} + 2Cl^- = CuCl_2^\circ$	+0.16	7,20
$Cu^{2+} + 3Cl^- = CuCl_3^-$	-2.29	7,20
$Cu^{2+} + NO_3^- = CuNO_3^+$	+0.5	19,23
$Cu^{2+} + 2NO_3^- = Cu(NO_3)_2^\circ$	-0.4	19,23
$Cu^{2+} + SO_4^{2-} = CuSO_4^\circ$	+2.31	7,20,22
$Cu^{2+} + 2SO_4^{2-} = Cu(SO_4)_2^{2-}$	+3.13	7
$Fe^{2+} + H_2O = FeOH^+ + H^+$	-9.5	6
$Fe^{2+} + 2H_2O = Fe(OH)_2^\circ$	-18.8	29
$Fe^{2+} + CO_{32-} = FeCO_3^\circ$	+4.38	6
$Fe^{2+} + H^+ + CO_3^{2-} = FeHCO_3^+$	+12.329	6
$Fe^{2+} + SO_4^{2-} = FeSO_4^\circ$	+2.25	6
$Fe^{2+} + H^+ + SO_4^{2-} = FeHSO_4^+$	+3.068	6
$Fe^{2+} + F^- = FeF^+$	+1.0	6
$Fe^{2+} + Cl^- = FeCl^+$	+0.14	6
$Fe^{2+} + 2Cl^- = FeCl_2^\circ$	-10.93	20
$Fe^{2+} = Fe^{3+} + e^-$	-13.02	6
$Fe^{2+} + H_2O = FeOH^{2+} + H^+ + e^-$	-15.21	6,9
$Fe^{2+} + 2H_2O = Fe(OH)_2^+ + 2H^+ + e^-$	-18.69	6
$Fe^{2+} + 3H_2O = Fe(OH)_3^\circ + 3H^+ + e^-$	-25.58	6
$Fe^{2+} + 4H_2O = Fe(OH)_4^- + 4H^+ + e^-$	-34.62	6
$2Fe^{2+} + 2H_2O = Fe_2(OH)_2^{4+} + 2H^+ + 2e^-$	-28.99	6
$3Fe^{2+} + 4H_2O = Fe_3(OH)_4^{5+} + 4H^+ + 3e^-$	-45.36	6
$4Fe^{2+} + 6H_2O = Fe_4(OH)_6^{6+} + 6H^+ + 4e^-$	-61.46	6^+
$Fe^{2+} + F^- = FeF^{2+} + e^-$	-6.82	6
$Fe^{2+} + 2F^- = FeF_2^+ + e^-$	-2.22	6

$Fe^{2+} + 3F^- = FeF_3^\circ + e^-$	+0.98	6
$Fe^{2+} + Cl^- = FeCl^{2+} + e^-$	-11.54	6
$Fe^{2+} + 2Cl^- = FeCl_2^+ + e^-$	-10.89	6
$Fe^{2+} + 3Cl^- = FeCl_3^\circ + e^-$	-11.89	6
$Fe^{2+} + SO_4^{2-} = FeSO_4^+ + e^-$	-8.98	6,8
$Fe^{2+} + H^+ + SO_4^{2-} = FeHSO_4^{2+} + e^-$	-8.552	6
$Fe^{2+} + 2SO_4^{2-} = Fe(SO_4)_2^- + e^-$	-7.64	6
$3Fe^{2+} + 4H_2O + SO_4^{2-} = Fe_3(OH)_4SO_4^{3+} + 3e^-$	-41.7	10*
$Fe^{2+} + e^- + AsO_4^{3-} + 4H^+ = FeH_2AsO_3^{2+} + H_2O$	+22.673	4
$Fe^{2+} + 3e^- + 2AsO_4^{3-} + 8H^+ = Fe(H_2AsO_3)_2^+ + 2H_2O$	+54.58	4
$Fe^{2+} + AsO_4^{3-} = FeAsO_4^\circ + e^-$	+7.087	4
$Fe^{2+} + H^+ + AsO_4^{3-} = FeHAsO_4^+ + e^-$	+10.75	4
$Fe^{2+} + 2H^+ + AsO_4^{3-} = FeH_2AsO_4^{+2} + e^-$	+11.63	4
$K^+ + H_2O = KOH^\circ + H^+$	-14.46	6
$K^+ + SO_4^{2-} = KSO_4^-$	+0.85	6,8
$Mg^{2+} + F^- = MgF^+$	+1.82	6
$Mg^{2+} + H_2O = MgOH^+ + H^+$	-11.44	6
$Mg^{2+} + CO_3^{2-} = MgCO_3^\circ$	+2.98	6
$Mg^{2+} + H^+ + CO_3^{2-} = MgHCO_3^+$	+11.399	6
$Mg^{2+} + SO_4^{2-} = MgSO_4^\circ$	+2.37	6
$Mn^{2+} + H_2O = MnOH^+ + H^+$	-10.59	6
$Mn^{2+} + CO_3^{2-} = MnCO_3^\circ$	+4.90	6
$Mn^{2+} + H^+ + CO_3^{2-} = MnHCO_3^+$	+12.279	6
$Mn^{2+} + SO_4^{2-} = MnSO_4^\circ$	+2.25	6
$Mn^{2+} + 2NO_3^- = Mn(NO_3)_2^\circ$	+0.6	1
$Mn^{2+} + F^- = MnF^+$	+0.84	6

$Mn^{2+} + Cl^- = MnCl^+$	+0.61	6
$Mn^{2+} + 2Cl^- = MnCl_2^\circ$	+0.25	6
$Mn^{2+} + 3Cl^- = MnCl_3^-$	-0.31	6
$Mn^{2+} = Mn^{3+} + e^-$	-25.51	6
$Na^+ + H_2O = NaOH^\circ + H^+$	-14.18	6
$Na^+ + CO_3^{2-} = NaCO_3^-$	+1.27	6
$Na^+ + H^+ + CO_3^{2-} = NaHCO_3^\circ$	+10.079	6
$Na^+ + SO_4^{2-} = NaSO_4^-$	+0.70	6,8
$Na^+ + F^- = NaF^\circ$	-0.24	6
$Pb^{2+} + H_2O = PbOH^+ + H^+$	-7.71	7,21,23
$Pb^{2+} + 2H_2O = Pb(OH)_2^\circ + 2H^+$	-17.12	7,21,27
$Pb^{2+} + 3H_2O = Pb(OH)_3^- + 3H^+$	-28.06	7,20,21
$Pb^{2+} + 4H_2O = Pb(OH)_4^{2-} + 4H^+$	-39.7	7
$2Pb^{2+} + H_2O = Pb_2OH^{3+} + H^+$	-6.36	7,27
$3Pb^{2+} + 4H_2O = Pb_3(OH)_4^{2+} + 4H^+$	-23.88	7,23,27
$4Pb^{2+} + 4H_2O = Pb_4(OH)_4^{4+} + 4H^+$	-20.88	23,27
$6Pb^{2+} + 8H_2O = Pb_6(OH)_8^{4+} + 8H^+$	-43.6	23,27
$Pb^{2+} + Cl^- = PbCl^+$	+1.6	7,20,23
$Pb^{2+} + 2Cl^- = PbCl_2^\circ$	+1.8	7,20
$Pb^{2+} + 3Cl^- = PbCl_3^-$	+1.7	7,21,23
$Pb^{2+} + 4Cl^- = PbCl_4^{2-}$	+1.38	7,23
$Pb^{2+} + CO_3^{2-} = PbCO_3^\circ$	+7.24	21,30
$Pb^{2+} + 2CO_3^{2-} = Pb(CO_3)_2^{2-}$	+10.64	7
$Pb^{2+} + H^+ + CO_3^{2-} = PbHCO_3^+$	+13.2	30
$Pb^{2+} + SO_4^{2-} = PbSO_4^\circ$	+2.75	21
$Pb^{2+} + 2SO_4^{2-} = Pb(SO_4)_2^{2-}$	+3.47	23

$Pb^{2+} + NO_3^- = PbNO_3^+$	+1.17	23
$Pb^{2+} + 2NO_3^- = Pb(NO_3)_2^\circ$	1.40	23
$Zn^{2+} + H_2O = ZnOH^+ + H^+$	-9.6	7,20
$Zn^{2+} + 2H_2O = Zn(OH)_2^\circ + 2H^+$	-16.9	7,21,27
$Zn^{2+} + 3H_2O = Zn(OH)_3^- + 3H^+$	-28.4	7,21,27
$Zn^{2+} + 4H_2O = Zn(OH)_4^{2-} + 4H^+$	-41.2	7,21,27
$2Zn^{2+} + H_2O = Zn_2OH^{3+} + H^+$	-9.0	27
$2Zn^{2+} + 6H_2O = Zn_2(OH)_6^{2-} + 6H^+$	-57.8	27
$Zn^{2+} + H_2O + Cl^- = ZnOHCl^\circ$	-7.48	7,20
$Zn^{2+} + Cl^- = ZnCl^+$	+0.43	7
$Zn^{2+} + 2Cl^- = ZnCl_2^\circ$	+0.45	7
$Zn^{2+} + 3Cl^- = ZnCl_3^-$	+0.50	7,21,23
$Zn^{2+} + 4Cl^- = ZnCl_4^{2-}$	+0.20	7,21,23
$Zn^{2+} + CO_3^{2-} = ZnCO_3^\circ$	+5.1	8
$Zn^{2+} + H^+ + CO_3^{2-} = ZnHCO_3^+$	+11.03	8
$Zn^{2+} + SO_4^{2-} = ZnSO_4^\circ$	+2.37	7,21
$Zn^{2+} + 2SO_4^{2-} = Zn(SO_4)_2^{2-}$	+3.28	7
$Zn^{2+} + NO_3^- = ZnNO_3^+$	+0.40	23

Mineral Dissociation Equilibria:

$SiO_{2(am)} + 2H_2O = H_4SiO_4^\circ$	-2.71	6
$SiO_2 \cdot H_2O_{(glass)} + H_2O = H_4SiO_4^\circ$	-3.0183	6
$SiO_{2(quartz)} + 2H_2O = H_4SiO_4^\circ$	-3.98	6

Mineral Dissociation Equilibria (continued):	Log(K)	Ref's
$Al(OH)_{3(gibbsite)} + 3H^+ = Al^{3+} + 3H_2O$	+8.11	6,9,15
$Al(OH)_{3(B\text{-}gibbsite)} + 3H^+ = Al^{3+} + 3H_2O$	+9.35	6,9,15
$Al(OH)_{3(bayerite)} + 3H^+ = Al^{3+} + 3H_2O$	+8.41	5
$Al(OH)_{3(am)} + 3H^+ = Al^{3+} + 3H_2O$	+10.8	6,15
$AlOHSO_{4(jurbanite)} + H^+ = Al^{3+} + SO_4^{2-} + H_2O$	-3.8	9,15,17
$Al_4SO_4(OH)_{10(basaluminite)} + 10H^+ = 4Al^{3+} + SO_4^{2-} + 10H_2O$	+22.4	9,18
$NaAl_3(SO_4)_2(OH)_{6(sodium\ alunite)} + 6H^+ = Na^+ + 3Al^{3+} + 2SO_4^{2-} + 6H_2O$	+0.02	17
$Al_2Si_2O_5(OH)_{4(kaolinite)} + 6H^+ = 2Al^{3+} + 2H_4SiO_4 + H_2O$	+7.435	6,9,20
$Na(AlSi_3)O_{8(albite)} + 8H_2O = Na^+ + Al(OH)_4^- + 3H_4SiO_4$	-18.000	1
$NaAlSi_2O_6{\cdot}H_2O_{(analcime)} + 5H_2O = Na^+ + Al(OH)_4^- + 2H_4SiO_4$	-12.7	16
$Al_2Si_2O_5(OH)_{4(halloysite)} + 7H_2O = 2H^+ + 2Al(OH)_4^- + 2H_4SiO_4$	-32.82	16
$Al_2Si_4O_{10}(OH)_{2(pyrophyllite)} + 12H_2O = 2H^+ + 2Al(OH)_4^- + 4H_4SiO_4$	-42.43	16
$NaAl_7Si_{11}O_{30}(OH)_{6(beidellite)} + 22H^+ + 8H_2O = Na^+ + 7Al^{3+} + 11H_4SiO_4$	+21.	16
$CdCO_{3(cr)} = Cd^{2+} + CO_3^{2-}$	-13.74	1
$CdSO_{4(cr)} = Cd^{2+} + SO_4^{2-}$	-0.10	20
$CdSiO_{3(cr)} + 2H^+ + H_2O = Cd^{2+} + H_4SiO_4$	+9.06	20

$Cr_2O_3 \cdot FeO_{(chromite)} + 8H^+ = Fe^{2+} + 2Cr^{3+} + 4H_2O$	+19.89	12,13,20
$Cr(OH)_{3(precipitate)} + 3H^+ = Cr^{3+} + 3H_2O$	+9.	12*
$Cu(SO_4)_{0.25}(OH)_{1.5(cr)} + 1.5H^+ = Cu^{2+} + 0.25(SO_4)^{2-} + 1.5H_2O$	+3.84	28
$CuO \cdot Fe_2O_{3(cupric\ ferrite)} + 8H^+ = Cu^{2+} + 2Fe^{3+} + 4H_2O$	+5.90	20
$Fe(OH)_{3(am)} + 3H^+ = Fe^{3+} + 3H_2O$	+4.891	6
$Fe(OH)_{3(soil)} + 3H^+ = Fe^{3+} + 3H_2O$	+2.70	23
$FeO(OH)_{(goethite)} + 3H^+ = Fe^{3+} + 2H_2O$	-1.0	6
$FeAsO_4 \cdot 2H_2O_{(scorodite)} = Fe^{3+} + AsO_4^{3-} + 2H_2O$	-24.41	11
$Fe_3(SO_4)_2(OH)_{5(carphosiderite)} + 5H^+ = 3Fe^{3+} + 2SO_4^{2-} + 5H_2O$	-5.39	17
$NaFe_3(SO_4)_2(OH)_{6(natrojarosite)} + 6H^+ = Na^+ + 3Fe^{3+} + 2SO_4^{2-} + 6H_2O$	-5.28	17
$[(H_3O)_{.75}Na_{.25}]Fe_3(SO_4)_2(OH)_{6(HNa\text{-}jarosite)} + 5.25H^+ = 0.25Na^+ + 3Fe^{3+} + 2SO_4^{2-} + 6.75H_2O$	-5.47	3+,17+
$PbFe_6(SO_4)_4(OH)_{12(plumbojarosite)} + 12H^+ = Pb^{2+} + 6Fe^{3+} + 4SO_4^{2-} + 12H_2O$	-16.28	17
$PbSO_{4(anglesite)} = Pb^{2+} + SO_4^{2-}$	-7.79	8,23
$PbSO_4 \cdot PbO_{(cr)} + 2H^+ = 2Pb^{2+} + SO_4^{2-} + H_2O$	-0.277	20
$ZnO \cdot Fe_2O_{3(cr)} + 8H^+ = Zn^{2+} + 2Fe^{3+} + 4H_2O$	+7.25	20
$ZnSiO_{3(cr)} + 2H^+ + H_2O = Zn^{2+} + H_4SiO_4$	+7.2	17*,20*

GLOSSARY OF MINERALS

Mineral	Chemical Formula	Mineral	Chemical Formula
Albite	$NaAlSi_3O_8$	Chromite	$FeO{\cdot}Cr_2O_3$
Alkali feldspar	$(Na,K)AlSi_3O_8$	Copper ferrite	α-$CuFe_2O_4$
Alunite	$KAl_3(OH)_6(SO_4)_2$	Dolomite	$CaMg(CO_3)_2$
Alunogen	$Al_2(SO_4)_3{\cdot}17H_2O$	Ferrihydrite	$Fe(OH)_3$
Ankerite	$CaFe(CO_3)_2$	Galena	PbS
Apatite	$Ca_5(OH,F,Cl)(PO_4)_3$	Gibbsite	γ-$Al(OH)_3$
Barite	$BaSO_4$	Goethite	α-FeO(OH)
Basaluminite	$Al_4(OH)_{10}SO_4{\cdot}5H_2O$	Gypsum	$CaSO_4{\cdot}2H_2O$
Bayerite	α-$Al(OH)_3$	Hydronium jarosite	(see Carphosiderite)
Calcite	$CaCO_3$	Illite	$K_{0.6}Mg_{0.25}Al_{2.5}Si_{3.5}O_{10}(OH)_2$
Carphosiderite	$H_3O^+Fe_3(OH)_6(SO_4)_2$	Jarosite	$KFe_3(OH)_6(SO_4)_2$
Chalcopyrite	$CuFeS_2$	Jurbanite	$AlOHSO_4{\cdot}5H_2O$
Chlorite	$(Mg_5Al)Si_3AlO_{10}(OH)_8$	Kaolinite	$Al_2Si_2O_5(OH)_4$

Mineral	Chemical Formula
Lead jarosite	(see Plumbojarosite)
Malachite	$Cu_2(OH)_2CO_3$
Marcasite	FeS_2
Mixed layer clays	Mg,Al silicates
Montmorillonite	$Ca_{0.165}Al_{2.33}Si_{3.67}O_{10}(OH)_2$
Muscovite	$KAl_2Si_3AlO_{10}(OH)_2$
Natrojarosite	$NaFe_3(OH)_6(SO_4)_2$
Plagioclase feldspar	$(NaSi,CaAl)Si_2AlO_8$
Plumbojarosite	$PbFe_6(OH)_{12}(SO_4)_4$
Potassium jarosite	(see Jarosite)
Pyrite	FeS_2
Quartz	SiO_2
Scorodite	$FeAsO_4 \cdot 2H_2O$
Siderite	$FeCO_3$
Sodium jarosite	(see Natrojarosite)
Sphalerite	ZnS
Tourmaline	$Na(Mg,Fe,Li)_3Al_6(OH)_4B_3O_9Si_6O_{18}$
Zircon	$ZrSiO_4$

REFERENCES

Alpers C. N. and Brimhall G. H. (1989) Paleohydrologic Evolution and Geochemical Dynamics of Cumulative Supergene Metal Enrichment at La Escondida, Atacama Desert, Northern Chile. Economic Geology. **84**,(2), pp. 229-253.

Alpers C. N., Nordstrom D. K. and Ball J. W. (1989) Solubility of Jarosite Solid Solutions Precipitated From Acid Mine Waters, Iron Mountain, California, U.S.A. Sciences Geologiques, Bulletin. **42**,(4), pp. 281-298.

American Society for Testing and Materials (1986) Powder Diffraction File, Inorganic Phases Search Manual, Hanawalt Method. International Centre for Diffraction Data, Swarthmore, Pennsylvania.

American Society for Testing and Materials (1985) Standard Method of Sieve Analysis of Coal. In Annual Book of ASTM Standards, Vol. 05.05, Standard Designation E 11. International Standards Organization.

American Society for Testing and Materials (1985) Standard Test Methods for Analysis of Metals in Refuse-Derived Fuel by Atomic Absorption Spectrophotometry. Annual Book of ASTM Standards. Vol. 11:04, Standard E 885, pp. 410-444.

Anderson W. C., ASCE M. and Youngstrom M. P. (1976) Coal Pile Leachate--Quantity and Quality Characteristics. Journal of the Environmental Engineering Division. **102**, pp. 1239-1253.

Atkinson R. J., Posner A. M. and Quirk J. P. (1968) Crystal Nucleation in Fe(III) Solutions and Hydroxide Gels. Journal Inorganic and Nuclear Chemistry. **30**, pp. 2371-2381.

Baes C. P. and Mesmer R. E. (1976) Hydrolysis of Cations. John Wiley & Sons.

Ball J. W. and Nordstrom D. K. (1985) Major and Trace-Element Analyses of Acid Mine Waters in the Leviathan Mine Drainage Basin, California/Nevada--October 1981 to October 1982. U. S. Geological Survey. WRI Report 85-4169.

Bard A. J., Parsons R. and Jordan J. (1985) Standard Potentials in Aqueous Solution. International Union of Pure and Applied Chemistry.

Bartlett R. J. and James B. R. (1988) Mobility and Bioavailability of Chromium in Soils. In Chromium in the Natural and Human Environments, Chap. 10, pp. 267-301. Wiley.

Bassett R. L. and Melchior D. C. (1989) Chemical Modeling of Aqueous Systems, An Overview. In Chemical Modeling of Aqueous Systems, II (eds. D.C. Melchior and R.L. Bassett) Chap. 1, pp. 1-14. American Chemical Society.

Bauslaugh J., Radziuk B., Saeed K., and Thomassen Y. (1984) Reduction of Effects of Structured Non-specific Absorption in the Determination of Arsenic and Selenium by Electrothermal Atomic Absorption Spectrometry. Analytica Chimica Acta, **165**, 149-157.

Biesecker J. E. and George J. R. (1966) Stream Quality in Appalachia as Related to Coal-Mine Drainage, 1965. USGS, Geological Survey Circular 526.

Bigham J. M., Schwertmann U., Carlson L. and Murand E. (1990) A poorly crystallized Oxyhydroxysulfate of Iron Formed by Bacterial Oxidation of Fe(II) in Acid Mine Waters. Geochimica et Cosmochimica Acta. **54**, 2743-2758.

Bladh K. W. (1982) The Formation of Goethite, Jarosite, and Alunite During Weathering of the Sulfide-Bearing Felsic Rocks. Economic Geology. 77, 176-184.

Bladh K. W. (1978) The Weathering of Sulfide-bearing Rocks Associated with Porphyry-type Copper Deposits. Ph.D. dissertation, Univ. of Arizona.

Bourg Alain C. M. (1982) ADSORP, A Chemical Equilibria Computer Program Accounting for Adsorption Processes in Aquatic Systems. Environmental Technology Letters, 3, 305-310.

Brady G. W., Kurkjian C. R., Lyden E. F. X., Robin M. B., Saltman P., Spiro T. and Terzis A. (1968) The Structure of An Iron Core Analog of Ferritin. Biochemistry. 7,(6), 2185-2192.

Brady K. S., Bigham J. M., Jaynes W. F. and Logan T. J. (1986) Influence of Sulfate on Fe-Oxide Formation: Comparisons with a Stream Receiving Acid Mine Drainage. Clays and Clay Minerals. 34,(3), 266-274.

Brown J. B. (1970) A Chemical Study of Some Synthetic Potassium-Hydronium Jarosites. Canadian Mineralogist. 10, 696-703.

Brown P. L., Sylva R. N., Batley G. E., and Ellis J. (1985) The Hydrolysis of Metal Ions. Part 8: Aluminium(III). Journal of the Chemical Society Dalton Transactions. 1967-1970.

Bryson A. W. (1986) Factors That Effect the Kinetics of Nucleation and Growth and the Purity of Goethite Precipitates Produced From Sulphate Solutions. In Iron Control in Hydrometallurgy (eds. J. E. Dutrizac and A. J. Monhemius), Chap. 18, pp. 377-389. John Wiley.

Buffle J. (1988) Complexation Reactions in Aquatic Systems. John Wiley & Sons.

Buffle J. and Nembrini G. (1977) Study of the Mechanism of the electrochemical Reduction of Hydrolysed Iron(III) Species, in Connection With Their Colloidal Properties. Journal of Electroanalytical Chemistry. 76, 101-119.

Chapman Bernard M. (1982) Numerical Simulation of the Transport and Speciation of Nonconservative Chemical Reactants in Rivers. Water Resources Research, 18,1, 155-167.

Chapman B. M., Jones D. R., and Jung R. F. (1983) Processes Controlling Metal Ion Attenuation in Acid Mine Drainage Streams. Geochimica Cosmochimica Acta. 47, 1957-1973.

Ciavatta L. and Grimaldi M. (1975) On the Hydrolysis of the Iron(III) Ion, Fe^{3+}, In Perchlorate Media. Journal of Inorganic Nuclear Chemistry. 37, 163-169.

Coward N. A. and Horton J. W. (1980) Static Coal Storage--Chemical Effects on the Aquatic Environment. USEPA 60/3-80-083A.

Davis Andy and Ashenberg Daniel (1989) The Aqueous Geochemistry of the Berkeley Pit, Butte, Montana, U.S.A. Applied Geochemistry. Vol 4, pp. 23-36.

Davis E. C. and Boegly W. J., Jr. (1981a) Coal Pile Leachate Quality. Journal of the Environmental Engineering Division, Proceedings of the American Society of Civil Engineers, ASCE. **107**,(EE2), April, 399-417.

Davis E. C. and Boegly W. J., Jr. (1981b) A Review of Water Quality Issues Associated with Coal Storage. Journal of Environ. Qual. **10**,(2), 127-132.

Davis E. C. and Boegly W. J., Jr. (1978) A Review of the Literature on Leachates From Coal Storage Piles. Oak Ridge National Laboratory.

Davis A. and Runnells D. D. (1987) Geochemical Interactions Between Acidic Tailings Fluid and Bedrock: Use of the Computer Model MINTEQ. Applied Geochemistry. **2**, 231-241.

Dousma J.and de Bruyn P. L. (1979) Hydrolysis-Precipitation Studies of Iron Solutions--III. Application of Growth Models to the Formation of Colloidal aFeOOH from Acid Solutions. Journal of Colloid and Interface Science. **72**,(2), 314-320.

Dousma J.and de Bruyn P. L. (1978) Hydrolysis-Precipitation Studies of Iron Solutions--II. Aging Studies and the Model for Precipitation from Fe(III) Nitrate Solutions. Journal of Colloid and Interface Science. **64**,(1), 154-171.

Dousma J.and de Bruyn P. L. (1976) Hydrolysis-Precipitation Studies of Iron Solutions--I. Model for Hydrolysis and Precipitation From Fe(III) Nitrate Solutions. Journal Colloid Interface Science. **56**, 527.

Dousma J., den Ottelander D. and de Bruyn P. L. (1979) The Influence of Sulfate Ions on the Formation of Iron(III) Oxides. Journal of Inorganic and Nuclear Chemistry. **41**, 1565-1568.

Drever J. I. (1982) The Geochemistry of Natural Waters. Prentice Hall.

Driscoll C. T., Baker J. P., Bisogni J. J., and Schofield C. L. (1984) Aluminum Speciation and Equilibria in Dilute Acidic Surface Waters of the Adirondack Region of New York State. In Geological Aspects of Acid Deposition (ed. Owen P. Bricker) Acid Precipitation Series, Vol. 7, Chap. 4, pp. 55-75. Ann Arbor Science.

Dzombak D. A. and Morel F. M. M. (1990) Surface Complexation Modeling, Hydrous Ferric Oxide. Wiley.

Erickson P. M., Ladwig K. J., and Kleinmann R. L. P. (1984) Acid Mine Drainage From Inactive Eastern Coal Operations. Symposium on the Reclamation of Lands Disturbed by Surface Mining (ed. W. T. Plass), American Society for Surface Mining and Reclamation.

Felmy A. R., Girvin D. C., and Jenne E. A. (1983) MINTEQ--A Computer Program for Calculating Aqueous Geochemical Equilibria. Final Project Report, EPA Contract 68-03-3089. U.S. Environmental Protection Agency.

Fendinger N. J., Radway J. C., Tuttle J. H. and Means, J. C. (1989) Characterization of Organic Material Leached From Coal by Simulated Rainfall. Environ. Sci. Technol. **23**,(2), 170-177.

Fernandez F. J. and Giddings R., (1982) Elimination of Spectral Interferences Using Zeeman Effect Background Correction. Atomic Spectroscopy, **3**,(3), 61-65.

Filipek L. H., Nordstrom D. K. and Ficklin W. H. (1987) Interaction of Acid Mine Drainage with Waters and Sediments of West Squaw Creek in the West Shasta Mining District, California. Environmental Science and Technology. April, 388-396.

Florence T. M. and Batley G. E. (1980) Chemical Speciation in Natural Waters. In Critical Reviews in Analytical Chemistry. **9**, 219-296. Chemical Rubber Co, Cleveland.

Flynn C. M., Jr. (1984) Hydrolysis of Inorganic Iron(III) Salts. Chem. Rev. **84**, 31-41.

Forstner U. and Wittmann G. T. W. (1979) Metal Pollution in the Aquatic Environment. Springer-Verlag.

Frimmel F. H. and Geywitz J. (1987) Direct Polarographic Recording of Metal Elimination From Aquatic Samples by Coprecipitation with Ferric Hydroxide. The Science of the Total Environment. **60**, 57-65.

Garrels R. M. and Christ C. L. (1965) Solution, Minerals, and Equilibria. Harper & Row, N.Y.

Garrels R. M. and Thompson M. E. (1960) Oxidation of Pyrite by Iron Sulfate Solutions. American Journal of Science, Bradley Volume, **258A**, 57-67.

Gluskoter H. J., Ruch R. R., Miller W. G., Cahill R. A., Dreher G. B. and Kuhn J. K. (1977) Trace Elements in Coal: Occurrence and Distribution. Illinois State Geological Survey (Circular 499).

Goldhaber M. B. (1983) Experimental Study of Metastable Sulfur Oxyanion Formation During Pyrite Oxidation at pH 6-9 and 30°C. American Journal of Science. **283**, March, 193-217.

Gottschlich D. E., Greenfield P. F. and Bell P. R. F. (1987) Treatment Requirements for Acid Drainage From Coal Storage Heaps. Journal of Environmental Engineering. **113**,(2), April, 260-277.

Griffin R. A., Schuller R. M., Suloway J. J., Shimp N. F., Childers W. F. and Shiley R. H. (1980) Chemical and Biological Characterization of Leachates From Coal Solid Wastes. Illinois State Geological Survey Division.

Hall L. W., Jr. and Burton D. T. (1982) Effects of Power Plant Coal Pile and Coal Waste Runoff and Leachate on Aquatic Biota: An Overview with Research Recommendations. Critical Reviews in Toxicology. **10**,(4) 287-301.

Harris Daniel C. (1991) Quantitative Chemical Analysis, 3rd Edition. W. H. Freeman & Co., N.Y.

Heaton R. C., Williams J. M., Bertino J. P., Wangen L. E., Nyitray A. M., Jones M. M., Wanek P. L. and Wagner P. (1982) Leaching Behaviors of High-Sulfur Coal Wastes From Two Appalachian Coal Preparation Plants. Report LA-9356-MS (Order No. DE82 019488).

Helz G. R., Dai J. H., Kijak P. J., Fendinger N. J. and Radway, J. C. (1987) Processes Controlling the Composition of Acid Sulfate Solutions Evolved From Coal. Applied Geochemistry, **2**, pp. 427-436.

Hem J. D. and Roberson C. E. (1989) Aluminum Hydrolysis Reactions and Products in Mildly Acidic Aqueous Systems. In Chemical Modeling of Aqueous Systems II. (eds. D. C. Melchior and R. L. Basset), ACS Symposium Series No. 416. Chap. 33, pp. 429-446. American Chemical Society

Henn E. L., (1977) Use of Molybdenum in eliminating Matrix Interferences in Flameless Atomic Absorption. In Flameless Atomic Absorption Analysis: An Update, ASTM STP 618, pp 54-64. American Society for Testing and Materials.

Henn E. L., (1975) Determination of Selenium in Water and Industrial Effluents by Flameless Atomic Absorption. Analytical Chemistry, 47,(3), 428-432.

Hoffmann M. R., Faust B. C., Panda F. A., Koo H. H. and Tsuchiya H. M. (1981) Kinetics of the Removal of Iron Pyrite from Coal by Microbial Catalysis. Applied and Environmental Microbiology.

Hong-Xiao T. and Stumm W. (1987) The Coagulating Behaviors of Fe(III) Polymeric Species--I. Water Research. 21,(1), 115-121.

Jaynes D. B., Pionke H. B. and Rogowski A. S. (1984) Acid Mine Drainage From Reclaimed Coal Strip Mines, 2. Simulation Results of Model. Water Resources Research, 20,(2), 243-250.

Jenke D. R., Pagenkopf G. K., and Diebold F. E. (1983) Chemical Changes in Concentrated, Acidic, Metal-bearing Wastewaters when treated with Lime. Environmental Science and Technology. 17,4, 217-223.

Jenne E. A. and Luoma S. N. (1977) Forms of Trace Elements in Soils, Sediments, and Associated Waters: An Overview of Their Determination and Biological Availability. Biological Implications of Metals in the Environment, 15th Annual Hanford Life Sciences Symposium. 110-124.

Johnson C. A. and Thornton I. (1987) Hydrological and Chemical Factors Controlling the Concentrations of Fe, CU, Zn, and As in a River System Contaminated by Acid Mine Drainage. Wat. Res. 21,(3), 359-365.

Karathanasis A. D., Evangelou V. P. and Thompson Y. L. (1988) Aluminum and Iron Equilibria in Soil Solutions and Surface Waters of Acid Mine Watersheds. Journal of Environmental Quality. 17(4), 534-43.

Kashkay C. M., Borovskaya Y. B. and Babazade M. A. (1975) Determination of G^{o}_{f298} of Synthetic Jarosite and its Sulfate Analogues. Geochemistry International. 12,(3), 115-121.

Khoe G. H. and Robins R. G. (1989) Polymerization Reactions in Hydrolyzed Iron(III) Solutions. Journal of Colloid and Interface Science. **133**,(1), 244-252.

Khoe G. H. and Robins R. G. (1988) The Complexation of Iron (III) With Sulphate, Phosphate, or Arsenate Ion in Sodium Nitrate Medium at 25°C. J. Chem. Soc. Dalton Trans., pp. 2015-2021.

Kinniburgh D. G. and Jackson M. L. (1982) Concentration and pH Dependence of Calcium and Zinc Adsorption by Iron Hydrous Oxide Gel. Soil Sci. Soc. Am. J. **46**, 56-61.

Kinniburgh D. G., Jackson M. L., and Syers J. K. (1976) Adsorption of Alkaline Earth, Transition, and Heavy Metal Cations by Hydrous Oxide Gels of Iron and Aluminum. Soil Sci. Soc. Am. J. **40**, 796-799.

Kleinmann R. L. P. and Crerar D. A. (1979) Thiobacillus ferrooxidans and the Formation of Acidity in Simulated Coal Mine Environments. Geomicrobiology Journal. **1**,(4), 373-388.

Kleinmann R. L. P., Crerar D. A. and Pacellil R. R. (1981) Biogeochemistry of Acid Mine Drainage and a Method to Control Acid Formation. Mining Engineering. **March**, 300-305.

Krause E. and Ettel V. A. (1987) Solubilities and Stabilities of Ferric Arsenates. In Crystallization and Precipitation. (eds. G. L. Strathdee, M. O. Klein, and L. A. Melis) Proceedings of the International Symposium, Saskatoon, Saskatchewan, Canada, 5-7 Oct. 1987. pp. 195-210.

Kuhn J. K., Fiene F. L., Cahill R. A., Gluskoter H. J. and Shimp, N. F. (1980) Abundance of Trace and Minor Elements in Organic and Mineral Fractions of Coal. Illinois Institute of Natural Resources, State Geological Survey Division, Urbana.

Kuznetsov S. I., Ivanov M. V. and Lyalikova N. N. (1962) The Biogenic Oxidation of Sulfide Deposits. In Introduction to Geological Microbiology, (International Series in the Earth Sciences) Chap. 8, pp. 124-164. McGraw-Hill, 1963.

Langmuir Donald L. and Whittemore Donald O. (1971) Variations in the Stability of Precipitated Ferric Oxyhydroxides. Nonequilibrium Systems in Natural Water Chemistry. (Advances in Chemistry Series, No. 106), American Chemical Society. pp. 209-234.

Lazaroff N., Sigal W. and Wasserman A. (1982) Iron Oxidation and Precipitation of Ferric Hydroxysulfates by Resting Thiobacillus ferrooxidans Cells. Applied Environmental Microbiology. **43**, 924-938.

Leckie J. O. and Davis (III) J. A. (1979) Aqueous Environmental Chemistry of Copper. In Copper in the Environment, Part I. (ed. Jerome O. Nriagu) Chap. 5, pp. 89-121. John Wiley and Sons, Inc.

Liddell K. C. and Bautista R. G. (1983) A Partial Equilibrium Model to Characterize the Precipitation of Ferric Ion During the Leaching of Chalcopyrite with Ferric Sulfate. Metallurgical Transactions B. **14B**, 5-15.

Liddell K. C. and Bautista R. G. (1981) A Partial Equilibrium Chemical Model for the Dump Leaching of Chalcopyrite. Metallurgical Transactions B. **12B**, 627-637.

Lindsay W. L. (1979) Chemical Equilibria In Soils. John Wiley & Sons.

Lowson, R. T. (1982) Aqueous Oxidation of Pyrite by Molecular Oxygen. Chemical Reviews **82**,(5), 461-497.

Mance G. (1987) Pollution Threat of Heavy Metals in Aquatic Environments. Elsevier Applied Science.

Mattigod S. V. and Sposito G. (1979) Chemical Modeling of Trace Metal Equilibria in Contaminated Soil Solutions Using the Computer Program GEOCHEM. In Chemical Modeling in Aqueous Systems (ed. E. A. Jenne) Chap. 37, 837-856. American Chemical Society.

May H. M., Helmke P. A., and Jackson M. L. (1979) Gibbsite Solubility and Thermodynamic Properties of Hydroxy-aluminum Ions in Aqueous Solution at 25°C. Geochim. et Cosmochim. Acta **43**, 861-868.

McAndrew R. T., Wong S. S. and Brown W. R. (1975) Precipitation of Iron Compounds from Sulphuric Acid Leach Solutions. Hydrometallurgy, (CIM Bulletin). January, 1975, pp. 101-110.

McDuff R. E. and Morel F. M. M. (1973) Description and Use of the Chemical Equilibrium Program REDEQL2. Keck Laboratory Technical Report EQ-73-02. California Institute of Technology, Pasadena, CA. (Cited in Nordstrom et al, 1979b).

Means J. C., Tuttle J. H. Helz G. R., Radway J. C., and Fendinger N. J. (1987) Chemical and Microbiological Factors Influencing the Leaching of Trace Metals and Trace Organics From Coal. Report to: Power Plant Research Program, Maryland Department of Natural Resources, Annapolis, Maryland.

Myerson A. S. (1981) Oxygen Mass Transfer Requirements During the Growth of Thiobacillus ferrooxidans on Iron Pyrite. Biotech. Bioeng. 23,(6), 1413-1416.

Naumov G. B., Ryzhenko B. N. and Khodakovsky I. L. (1974) Handbook of Thermodynamic Data (USGS-WRD-74-001) U.S. Geological Survey, Water Resources Division, Menlo Park, CA.

Nicholson R. V., Gillham R. W., Cherry J. A. and Reardon E. J. (1989) Reduction of Acid Generation in Mine Tailings Through the Use of Moisture-Retaining Cover Layers as Oxygen Barriers. Can. Geotech. J. 26.

Nordstrom D. K. (1982a) Aqueous Pyrite Oxidation and the Consequent Formation of Secondary Iron Minerals. In Acid Sulfate Weathering, (eds. Hossaer, Kettrick, and Faming), Chap. 3, pp. 37-56. 1982 Soil Science Society of America.

Nordstrom D. K. (1982b) The Effect of Sulfate on Aluminum Concentrations in Natural Waters: Some Stability Relations in the System Al_2O_3 - SO_3 -H_2O at 298K. Geochimica et. Cosmochimica Acta. 46, 681-692.

Nordstrom D. K. and Ball J. W. (1986) The Geochemical Behavior of Aluminum in Acidified Surface Waters. Science. 232, 54-56.

Nordstrom D. K., Jenne E. A. and Ball J. W. (1979) Redox Equilibria of Iron in Acid Mine Waters. In Chemical Modeling in Aqueous Systems. Speciation, Sorption, Solubility, and Kinetics (ACS Symposium Series 93) (ed. E. A. Jenne) pp. 51-79. American Chemical Society.

Nordstrom D. K., Plummer L. N., Langmuir D., Busenberg E., May H. M., Jones B. F. and Parkhurst, D. L. (1989) Revised Chemical Equilibrium Data for Major Water-Mineral Reactions and Their Limitations. In Chemical Modeling of Aqueous Systems, II (eds. Melchior and Bassett), Chap. 31, pp. 398-413. American Chemical Society.

Nordstrom D. K., Plummer L. N., Wigley T. M. L., Wolery T. J., Ball J. W., Jenne E. A., Bassett R. L., Crerar D. A., Florence T. M., Fritz B., Hoffman M., Holdren G. R. Jr., LaFon G. M., Mattigod S. V., McDuff R. E., Morel F., Reddy M. M., Sposito G., and Thrailkill J. (1979b) A Comparison of Computerized Chemical Models for Equilibrium Calculations in Aqueous Aqueous Systems. In Chemical Modeling in Aqueous Systems (ed. E. A. Jenne). Chap. 38, pp. 857-892. American Chemical Society.

Nriagu J. O. (1980) Cadmium in the Environment Part I. Wiley.

Olem H., (1982) Coal and Coal Mine Drainage. Journal of the Water Pollution Control Federation. 54,(6), 717-723.

Paciorek K. J. L., Kratzer R. H., Kimble P. F., Toben W. A. and Vatasescu A. L. (1981) Degradation of Massive Pyrite: Physical, Chemical, and Bacterial Effects. Geomicrobiology Journal. 2,(4), 363-375.

Parkhurst, D. L. (1989) Ion-Association Models and Mean Activity Coefficients of Various Salts. In Chemical Modeling of Aqueous Systems, II (eds. Melchior and Bassett), Chap. 3, pp. 30-43. American Chemical Society.

Parkhurst D. L. Thorstenson D. C. and Plummer L. N. (1980) PHREEQE - A Computer Program for Geochemical Calculations. U. S. Geological Survey (Water-Resources Investigations 80-96).

Perkins E. H., Kharaka Y. K., Gunter W. D., DeBraal J. D. (1989) Geochemical Modeling of Water-Rock Interactions Using SOLMINEQ.88. In Chemical Modeling in Aqueous Systems, II (eds. D. C. Melchior and R. L. Bassett) Chap. 9, pp. 117-127. American Chemical Society.

Phillips W. R. and Griffen D. T. (1981) Optical Mineralogy, The Nonopaque Minerals. W. H. Freeman & Co.

Pierce M. L. and Moore C. B. (1982) Adsorption of Arsenite and Arsenate on Amorphous Iron Hydroxide. Water Res. **16**, 1247-1253.

Plummer L.N. and Tisaranni J. V. (1990) Personal Communication (Disc Documentation that Accompanied Summer '90 Version of PHREEQE). U.S. Geological Survey, National Center. Reston Virginia.

Plummer L. N., Jones B. F. and Truesdell A. H. (1984) WATEQF - A FORTRAN IV Version of WATEQ. A Computer Program for Calculating Chemical Equilibrim of Natural Waters. (Report WRI-76-13, 1984 revision) U.S. Geological Survey, Water Resources Division, Reston, VA.

Rai Dhanpat, Sass Bruce M. and Moore Dean A. (1987) Chromium (III) Hydrolysis Constants and Solubility of Chromium (III) Hydroxide. Inorganic Chemistry, **23**,3, 345-349.

Reardon E. J. and Beckie R. D. (1987) Modeling Chemical Equilibria of Acid Mine-drainage: The $FeSO_4$-H_2SO_4-H_2O System. Geochimica et Cosmochimica Acta. **51** 2355-2368.

Rengasamy P. and Oades J. M. (1977) Interaction of Monomeric and Polymeric Species of Metal Ions with Clay Surfaces. I. Adsorption of Iron(III) Species. Australian Journal of Soil Research.**15**, 221-233.

Riley K. W., (1982) Spectral Interference by Aluminum in the Determination of Arsenic Using the Graphite Furnace: Choice of Resonance Lines. Atomic Spectroscopy. **3**,(4), 120-121.

Sass B. M. and Rai D. (1987) Solubility of Amorphous Chromium(III)--Iron(III) Hydroxide Solid Solutions. Inorganic Chemistry. **26**, 2228-2232.

Schneider W. (1984) Hydrolysis of Iron(III)--Chaotic Olation Versus Nucleation. Comments Inorganic Chemistry. **3**,(4), 205-223.

Schneider W. and Schwyn B. (1987) The Hydrolysis of Iron in Synthetic, Biological, and Aquatic Media. In Aquatic Surface Chemistry (ed. W. Stumm), Chap. 7, pp. 167-197.

Schubert J. P. and Prodan P. F. (1981) Groundwater Pollution Resulting From Disposal of Pyritic Coal Wastes. In quality of groundwater (Studies in Environmental Science, No. 17) (eds. W. von Duijvenbooden, P. Glasbergen, H. von Lelyveld), Chap. 1. Elsevier.

Schwertmann U. and Taylor R. M. (1977) Minerals in Soil Environments. Soil Sci. Soc. of Amer.

Silverman M. P. (1967) Mechanism of Bacterial Pyrite Oxidation. Journal of Bacteriology, **Oct 1967**, 1046-1051.

Singer P. C. and Stumm W. (1970) Acid Mine Drainage: The Rate Determining Step. Science **167**, 1121-1123.

Slavin Walter (1984) Graphite Furnace AAS, A Source Book. Perkin-Elmer Corporation, Norwalk, CT.

Smith R. M. and Martell A. E. (1989) Critical Stability Constants. Vol. 6 (2nd Supplement). Plenum Press.

Smith R. M. and Martell A. E. (1982) Critical Stability Constants. Vol. 5 (1st Supplement). Plenum Press.

Smith R. M. and Martell A. E. (1976) Critical stability Constants. Vol. 4. Plenum Press.

Spiro T. G., Allerton S. E., Renner J., Terzis A., Bils R. and Saltman P. (1966) The Hydrolytic Polymerization of Iron(III). Journal of American Chemical Society. **88**,(12), 2721-2726.

Stahl R. G., Jr. and Davis E. M. (1984) The Quality of Runoff from Model Coal Piles. American Society for Testing and Materials. 163-170.

Stumm, W. and Morgan J. (1981) Aquatic Chemistry. 2nd Edition. Wiley.

Stumm, W. and Singer P. C. (1970) Acid Mine Drainage: The rate Determining Step. Science. **167**, 1121-1123.

Sunda W. G. and Hanson P. J. (1979) Chemical Speciation of Copper in River Water, Effect of Total Copper, pH, Carbonate, and Dissolved Organic Matter. In Chemical Modeling in Aqueous Systems (ed. E. A. Jenne) Chap. 8.

Swift M. C. (1982) Effects of Coal Pile Runoff on Stream Quality and Macro-Invertebrate Communities. Water Resources Research Center.

Sylva R. N. and Davidson M. R. (1979) The Hydrolysis of Metal Ions, Part 1. Copper (II). J. Chem. Soc. Dalton Trans. 232-235.

Sylva R. N. (1972) The Hydrolysis of Iron(III). Rev. Pure and Appl. Chem. **22**, 115-132.

Taylor B. E., Wheeler M. C., and Nordstrom D. K. (1984) Stable Isotope Geochemistry of Acid Mine Drainage: Experimental Oxidation of Pyrite. Geochimica et Cosmochimica Acta. **48**, 2669-2678.

Temple K. L. and Delchamps E. W. (1953) Autotrophic Bacteria and the Formation of Acid in Bituminous Coal Mines. Applied Microbiology, **1**, 255-258.

Torrey S. (1978) Trace Contaminants From Coal. (NDC Pollution Technology Review No. 50) Noyes Data Corp.

Truesdell A. H., and Jones B. F. (1973) WATEQ, A Computer Program for Calculating Chemical Equilibria of Natural Waters. NTIS PBZ-20464.

Tsalev D. L. (1984) Atomic Absorption Spectrometry in Occupational and Environmental Health Practice. Vol II: Determination of Individual Elements, pp. 167-180. C.R.C. Press, Inc., Boca Raton, FL.

Turner D. R., Whitfield M. and Dickson, A. G. (1981) The Equilibrium Speciation of Dissolved Components in Freshwater and Seawater at 25°C and 1 atm pressure. Geochimica et Cosmochimica Acta. **45**, 855-881

United States Environmental Protection Agency (1976, July) Quality Criteria for Water Report EPA-440/9-76-023, U.S. Environmental Protection Agency, Washington, D.C.

Valette-Silver N. J. and Helz G. R. (1989) Behavior of Dissolved Al, Cu, Be, and Cr During Simulated Dilution of Acidic Coal Leachates with Alkaline Surface Waters. Maryland Power Plant Research Program.

Vlek P. L. G., Blom T. J. M., Beek J. and Lindsay W. L. (1974) Determination of the Solubility Product of Various Iron Hydroxides and Jarosite by the Chelation Method. Soil Science Society of America, Proceedings. **38**, 429-432.

Wachter R. A. and Blackwood T. R. (1978) Source Assessment: Water Pollutants From Coal Storage Areas. U.S. Environmental Protection Agency. Report No. EPA-600/2-78-004M.

Wagman D. D., Evans W. H., Parker V. B., Schumm R. H., Halow I., Bailey S. M., Churney K. L. and Nuttall R. L. (1982) The NBS Tables of Chemical Thermodynamic Properties. Journal of Physical and Chemical Reference Data, **11**,(2).

Wangen L. E. and Jones M. M. (1984) The Attenuation of Chemical Elements in Acidic Leachates from Coal Mineral Wastes by Soils. Environ. Geol. Water Sci., **6**,(3), 161-170.

Welz B. and Schlemmer G., (1986) Determination of Arsenic, Selenium and Cadmium in Marine Biological Tissue Samples Using a Stabilised Temperature Platform Furnace and Comparing Deuterium Arc with Zeeman-effect Background Correction Atomic Absorption Spectrometry. Journal of Analytical Atomic Spectrometry. **1**, 119-124.

Westall J. C., Zachary J. L., and Morel F. M. M. (1976) MINEQL, A Computer Program for the Calculation of Chemical Equilibrium Composition of Aqueous Systems. Technical Note 18, Department of Civil Engineering, Massachusetts Institute of Technology, Cambridge, MA. (Cited in Nordstrom et al, 1979b).

Wewerka E. M., Williams J. M. and Wagner P. (1982) The Use Of Multimedia Environmental Goals to Evaluate Potentially Hazardous Trace Elements in the Drainage From High Sulfur Coal Preparation Wastes. Report No. LA-9189-MS, NTIS No. DE82 014115.

Wolery T. J, Jackson K. J., Bourcier W. L., Bruton C. J., Viani B. E., Knauss K. G., and Delany J. M. (1989) Current Status of the EQ3/6 Software Package for Geochemical Modeling. In Chemical Modeling in Aqueous Systems, II (eds. D. C. Melchior and R. L. Bassett) Chap. 8, pp. 104-116. American Chemical Society.

Woods T. L. and Garrels R. M. (1987) Thermodynamic Values at Low Temperature For Natural Inorganic Materials: An Uncritical Summary. Oxford University Press.

Zachara J. M., Girvin D. C., Schmidt R. L. and Resch C. T. (1987) Chromate Adsorption on Amorphous Iron Oxyhydroxide in the Presence of Major Groundwater Ions. Environ. Sci. Technol. 21, 589-594.

Zirino A, and Yamamoto S. (1972) A pH-Dependent Model for the Chemical Speciation of Copper, Zinc, Cadmium, and Lead in Seawater. Limnology and Oceanography. 17,5, 661-671.

Zotov A. V., Mironova G. D. and Rusinov V. L. (1973) Determination of the Gibbs Free Energy G^{o}_{f298} of Jarosite Synthesized From a Natural Solution. Geokhimiya. (5), 739-745.